SYNTHESIS AND ANTISCHISTOSOMAL STRUCTURE-ACTIVITY RELATIONSHIP PROFILING OF *N*-PYRIDAZIN-3-YLBENZAMIDES

BY

HARRISON BANDA

A dissertation submitted to the University of Zambia in partial fulfilment of the requirements for the award of the degree of

Master of Science in Chemistry

THE UNIVERSITY OF ZAMBIA

LUSAKA

2024

DECLARATION

I, **Harrison Banda**, do this day hereby solemnly declare that this Master of Science in Chemistry dissertation, entitled '**Synthesis and Antischistosomal Structure-Activity Relationship Profiling of *N*-Pyridazin-3-ylbenzamides**', is my own original work.

I affirm that:

1. I know the meaning of plagiarism and that plagiarism is wrong. Plagiarism is to use another's work and pretend that it is one's own.

2. I have used the citation and referencing convention of the journal *Medicinal Chemistry Letters* of the American Chemical Society *(ACS Med. Chem. Lett.),* as per discipline.[1]

3. Each significant contribution to, and quotation in, this dissertation from the works of others has been cited and referenced. Use of particular registered trademarks (®/ ™) does not endorse them but is for repeatability/ reproducibility; and to the best of my knowledge, does not breach laws relating to defamation, libel and copyright.

4. This dissertation has solely been composed by myself, both in concept and execution, apart from the normal guidance of the supervisors; and neither this dissertation nor part of this work has previously been, is being or is intended to be submitted for award of any degree, diploma or other qualification at this or any other university.

5. I have not allowed, and will not allow, anyone to copy my work with the intention of passing it off as his/her work. My findings are part of two Elsevier,[2] one Springer and one Wiley journal article manuscripts and several conference abstracts (see publications list Appendices D and E) and the publication of the findings herein does not violate any copyright policies[3,4]. I hereby grant the University of Zambia a non-exclusive free licence to deposit it in its repository or the right to impose an embargo.

Candidate's Signature: _____ Date: 21/05/2025

[1] The University of Zambia. *Regulations and Guidelines for Postgraduate Studies.* Directorate of Research, Innovation and Development: Lusaka. **2024.** Section 23.4 and Appendix A.
[2] with CRediT authorship contribution statement: Harrison Banda: Writing – review & editing, Writing – original draft, Methodology, Investigation, Formal analysis, Data curation
[3] https://scientific-publishing.webshop.elsevier.com/publication-process/how-to-write-a-journal-article-from-a-thesis/ (accessed 2025-01-15).
[4] https://www.springer.com/gp/authors-editors/journal-author/frequently-asked-questions/3832 (accessed 2025-02-15)

SUPERVISORS' CERTIFICATE OF COMPLETION

The supervisors of **Harrison Banda**'s research work do hereby certify that he has completed his research work and dissertation for the award of the degree of Master of Science in Chemistry of the University of Zambia.

Principal Supervisor

Name: Dr Peter Mubanga Chewka

Signature: _____ Date: 21/05/2025

Co-Supervisor

Name: Dr Evelyn Funjika

Signature: _____ Date: 21/05/2025

CERTIFICATE OF APPROVAL

This dissertation, by **Harrison Banda**, has been approved as partial fulfilment of the requirements for the award of the degree of Master of Science in Chemistry of the University of Zambia.

Examiner 1

Name: DR JAMES MYIRENDA

Signature: _____ Date: 6/6/2025

Examiner 2

Name: DR FRANCIS KAMPAMBA

Signature: _____ Date: 06/06/2025

Examiner 3

Name: DR ANGELA CHOMBOLOLA

Signature: _____ Date: 11/06/2025

Chairperson – Board of Examiners

Name: DR. SYDNEY MALAMA

Signature: _____ Date: 11/06/2025

ABSTRACT

Schistosomiasis is a neglected tropical disease and the second most fatal tropical disease. The 2024 World Health Organization (WHO) report indicates global mortality rates of 130,000 and 150,000 schistosomiasis deaths attributed to the causative agents *Schistosoma mansoni* and *S. haematobium,* respectively, both of which species are endemic to Zambia. Although praziquantel (PZQ) remains the almost exclusive standard of care drug, it has some shortcomings including ineffectiveness against immature parasites, challenges in paediatric dosing, a high adult dose and has shown drug resistance. Therefore, there remains an unmet medical need to develop other treatment options with different modes of action to circumvent the now well-known mechanism of resistance. This study was based on Medicines for Malaria Venture's compound **MMV687807**, which was preliminarily shown to possess promising *in vitro* antischistosomal activity but whose extensive structure-activity exploration was not undertaken yet. The study was also inspired by the desire to design analogues with better physicochemical properties such as logarithms of partition coefficient or distribution (Log*P* or Log*D*) and solubility. Accordingly, the study introduced an *N*-pyridazin-3-yl heterocyclic ring *in lieu* of the *N*-phenyl carbocyclic ring thereby editing the *N*-phenylbenzamide (*N*-PhBA) scaffold of **MMV687807**, **MK1-11**, etc., to the *N*-pyridazin-3-ylbenzamides (*N*-PdzBAs) seeing that *N*-PhBAs had high hydrophobicity (e.g. **MMV687807**: Log*D* = 5.14; **MK1-11**: Log*D* = 4.36) and hence possessed low aqueous solubility (e.g. **MK1-11**: S_{aq} = 13.3 μM). Six target compounds were successfully synthesized by EDCI-mediated amide coupling to the required purity i.e. ≥ 95 %. Liquid chromatography – mass spectrometry (LC-MS) was used as the ultimate criterion of purity and to profile retention time (t_R) while ultraviolet-visible (UV-Vis), infrared (IR), proton (^{1}H) and carbon-13 (^{13}C) nuclear magnetic resonance (NMR) spectroscopic methods were used for characterization. Compared to the first-generation *N*-PhBAs (e.g. **MK1-11**), *N*-PdzBAs showed much lower *in vitro* activity (severity score ≤ 1) on *S. mansoni* adult worms but favourably lower *in vitro* cytotoxicity (CC_{50} > 20 μM) on the HEK293 cell line (an experimental result which also agreed with *in silico* predictions), favourably higher estimated aqueous solubility (S_{aq} > 100 μM) and lower hydrophobicity (cLog*P* ≤ 4). Therefore, although inferior activity-wise, the new pyridazinic analogues possess favourable physicochemical properties and could still find utility against other diseases.

KEY WORDS: *EDCI-mediated amide coupling,* N-*pyridazin-3-ylbenzamide*, S. mansoni *antischistosomal activity, HEK293 cytotoxicity, hydrophobicity, aqueous solubility*

DEDICATION

TO THE LADIES OF MY FAMILY

To ma moyo ***Martha*** *(my 'Shonammite' 'mother'), I hope this thesis could repay us for time we didn't spend together, hugs on arrivals, tears on departures and homesickness.* Tatenda *for the subfusc,* UNZA moma (Proverbs 18:22; 2 Kings 4:8–37; 3 John 2)!

To ***Mum****, the teacher of English. See your 'comparatives'/ 'superlatives' and 'budgets' produced bookkeepers and now a don; suits and now coats and gowns* (John 19:26,27).

Kwa malemu mlongo wanga, ***Peggy Addie Banda*** *as we emulate your hospitality!*

To my sister ***Maggie*** *as you account for Pounds, audit your electronic transactions not my electronic transitions; your government bonds/ Euro bonds not my chemical bonds.*

To my niece ***Faith****, may you be faithful in life!*

TO THE MEN OF MY FAMILY

To my son Master ***Newton Banda,*** *"And further, by these, my son, be admonished: of making many books there is no end; and much study is a weariness of the flesh"* (Ecclesiastes 12:12 KJV).

To my nephew ***Blessings****, the A student of 'books', "study to shew thyself approved" like Solomon the 'jobby' who "spake of trees, from the cedar tree that is in Lebanon, hyssop, beasts, fowl, creeping things and fishes"* (2 Timothy 2:15; 1 Kings 4:33 KJV).

Allan *my cousin, your love is inexplicable* (John 15:13).

Kwa malemu bambo anga, ***Mr Banda (Snr),*** *you wisely supported your wife to college. You should have lived to see her graduate as a* magna cum laude *university graduate decades on. They say when you educate a girl child; you educate the world.*

TO THE OMNISCIENT GOD

"From the minutest ***atom*** *to the greatest world, all things, animate and inanimate, in their unshadowed beauty and perfect joy, declare that* ***God*** *is love"* (Ellen Gould-White in Great Controversy pp 677, 8).

ACKNOWLEDGEMENTS

Firstly, I gratefully acknowledge my Principal Supervisor, Dr Peter Mubanga Cheuka, PhD, MACS (Senior Lecturer and Researcher; Lab Head – Medicinal Chemistry & Drug Discovery (MCDD) Group; and Head of Department (HoD) – Department of Pure & Applied Chemistry, UNZA); and my Co-Supervisor, Dr Evelyn Funjika, PhD (Lecturer and Researcher; former HoD), who patiently and passionately mentored me into a researcher. I also gratefully acknowledge the study sponsor, Ministry of Higher Education (MoHE) of the Government of the Republic of Zambia (GRZ) for the Science & Technology Postgraduate Scholarship; and the MCDD Group sponsor, Merck KGaA (Germany) for the Schistosomiasis Research Grant. Special thanks go to the collaborating lab heads for *gratis* hosting of the respective analyses/assays: Prof Kelly Chibale, Holistic Drug Discovery and Development (H3D) Centre and Department of Chemistry, University of Cape Town (UCT); and Prof Conor R. Caffrey, University of California San Diego (UCSD). Thanks to collaborators Christabel N. Hikaambo and Dr Godfrey W. Mayoka both of UCT, (for LC-MS and NMR experiments); Robert Singogo, UNZA (for helping me with UV-Vis experiments); Simoonga Mulunda, Yash Life Sciences (for IR experiments); Mai Shingyoji and Dr Thaiz R. Teixeira, all of UCSD (adult *S. mansoni* and cytotoxicity assays). Thanks to MCDD Group colleagues: Ameera M. Dawoodjee, Chilufya Lengwe (A/Chief Scientist), John Sichinga, Masebe Kanyanta and Steve N. Mbaya. Thanks to Dr Dickson Mambwe for the insights in the Research Group meetings.

Secondly, thanks to the following for free courses/workshops: Coursera, Ersilia, International Society for the Study of Xenobiotics (ISSX), Wellcome Centre for Anti-Infectives Research (WCAIR)/ University of Dundee and US National Institutes of Health. Thanks to Anna Adams (Medicines for Malaria Venture) for the updates on **MMV687807**. Thanks to European Laboratory Research and Innovation Group (ELRIG), H3D, ISSX, Royal Society of Chemistry (RSC) and WCAIR for the conference travel bursaries. American Chemical Society, American Society of Tropical Medicine & Hygiene, ISSX and RSC are thanked for low-income country membership waivers and Chemical Society of Zambia (CSZ) for full membership. CSZ and ISSX are thanked for my nomination to their Strategic Plan Committee and Africa Chapter Steering Committee, respectively. Choonzo Chiyumba is thanked for my RSC reference.

Lastly, profound gratitude goes to my parents, Mr Ponsilio Banda and Mrs Maggie Banda (née Kaulu), for life, upbringing and giving me the best education head start. I will not forget my wife Mrs Martha Banda (née Mache) not forgetting my only surviving sibling, Maggie. Last but not the least, thanks to the LORD God Almighty for the gift of life and health.

TABLE OF CONTENTS

LIST OF FIGURES

LIST OF TABLES

LIST OF EQUATIONS

LIST OF ABBREVIATIONS AND ACRONYMS

ABC	ATP-binding cassette
AD	Ameera Dawoodjee
ADME(T)	Absorption, distribution, metabolism, excretion (and toxicity)
AI/ML	Artificial intelligence/machine learning
API	Active pharmaceutical ingredient
ATP	Adenosine triphosphate
ATPase	Adenosine triphosphatase (adenosine triphosphate hydrolase)
ATR	Attenuated total reflectance
BBB	Blood-brain barrier
(br)	Broad
Bz	Benzoyl
Caco-2	Colon carcinoma cell line 2 enterocyte
CAS	Chemical Abstracts Service
CHI	Chromatographic hydrophobicity index
CNS	Central nervous system
Compd	Compound
COSY	Correlation spectroscopy
COVID-19	Corona virus disease 2019
CR	Cure rate
CYP	Cytochrome P450
d	Doublet
dd	Doublet of doublets
DAD (FS)	Diode array detector (fixed slit)
DCM	Dichloromethane
DHA	Dihydroartemisinin
DMAP	4-Dimethylaminopyridine
DMPK	Drug metabolism and pharmacokinetics
DMSO	Dimethyl sulfoxide
dt	Doublet of triplets
EDCI	1-Ethyl-(3-(3-dimethylamino) propyl)-carbodiimide
EDG	Electron donating group
EMA	European Medicines Agency
ERR	Egg reduction rate
ESI	Electrospray ionization
EWG	Electron withdrawing group
FG	Functional group
FT	Fourier transform
H2L	Hit-to-lead
H3D	Holistic Drug Discovery and Development Centre
HB	Harrison Banda
HBA	Hydrogen bond acceptor
HBD	Hydrogen bond donor
HEK293	Human embryonic kidney cell line
HepG2	Hepatocellular carcinoma cell line
HPLC	High performance liquid chromatography
ID	Internal diameter
IR	Infrared
LC	Liquid chromatography
m	Medium

m	*Meta*
m	Multiplet
MCDD	Medicinal Chemistry and Drug Discovery Research Group at UNZA
MDA	Mass drug administration
MK	Masebe Kanyanta
MMV	Medicines for Malaria Venture
MMP	Matched molecular pair
MOA	Mode of action
MOE	Molecular operating environment
MS	Mass spectrometry
***N*-ArBA**	*N*-arylbenzamide
NMR	Nuclear magnetic resonance
***N*-PdzBA**	*N*-pyridazinylbenzamide
***N*-PhBA**	*N*-phenylbenzamide
NTD	Neglected tropical disease
NTS	Newly transformed schistosomula
o	*Ortho*
p	*Para*
p	Pentate
Pdz	Pyridazine/ pyridazinyl
Ph	Phenyl
Praziquantel	**Pyraz**inyl**i**so**qu**inoline **ant**i**hel**mintic
pSAR	Proposed structure-activity relationship
Py	Pyridine
PZQ	Praziquantel
Ro5	Rule of 5
RP	Reverse phase
(s)	Sharp
s	Singlet
S	Strong
SAR	Structure-activity relationship
SCH	Schistosomiasis
Sh	*Schistosoma haematobium*
Sj	*Schistosoma japonicum*
Sm	*Schistosoma mansoni*
SMILES	Simplified molecular input line entry system
SPR	Structure-property relationship
t	Triplet
td	Triplet of doublets
TFM	Trifluoromethyl group
TLC	Thin layer chromatography
TPSA	Topological polar surface area
UCSD	University of California San Diego
UCT	University of Cape Town
UNZA	University of Zambia
UoD	University of Dundee
UPLC	Ultra-performance liquid chromatography
UV-Vis	Ultraviolet-visible
WHO	World Health Organization
w	Weak

LIST OF SYMBOLS AND UNITS

Å	Angström
°C	Degrees Celsius
%	Percent
δ	Delta: chemical shift
δ_C	Delta C: carbon-13 chemical shift
δ_H	Delta H: proton chemical shift
$\varepsilon_{(max)}$	Epsilon: molar absorptivity (at wavelength of maximum absorption)
$\lambda_{(max)}$	Lambda: wavelength (of maximum absorption)
μ	Mu: micro
$\tilde{\nu}$	Nu bar: wave number
π	Pi: substituent hydrophobicity constant; also pi bond
σ	Sigma: Hammett substituent constant
AU	Absorbance unit
C18	Octadecylsilane
CC_{50}	50% cytotoxic concentration
CHI-Log*D*	CHI logarithm of distribution coefficient
ChromLog*D*	Chromatographic logarithm of distribution coefficient
CL	Clearance
cLog*P*	Calculated logarithm of partition coefficient
D	Distribution coefficient
DMSO-d_6	Deuterated dimethyl sulfoxide
EC_{50}	50% effective concentration
eq	Equivalent
f_u	Fraction unbound
g	Gram
Hz	Hertz
IC_{50}	50% inhibitory concentration
J	Coupling constant
L	Litre
Log*D*	Common logarithm (base 10) of distribution coefficient
Log*P*	(Experimental) logarithm of partition coefficient
M	Molar
MeOH	Methanol
$[M+H]^+$	Pseudo molecular ion
min	Minute
mol	Mole
m/z	Mass to charge ratio
N-	Nitrogen bonded
O-	Oxygen bonded
P	Partition coefficient
Ppm	Parts per million
R_f	Retardation factor
$S_{(aq)}$	(Aqueous) solubility
%T	Percentage transmittance
T_m	Melting point
t_R	Retention time
ZnSe	Zinc selenide

CHAPTER 1

INTRODUCTION

1.1 Chapter Overview

Africa is home to about one billion of the 1.6 billion people globally affected by neglected tropical diseases (NTDs). NTDs perpetuate poverty and limit economic growth in the very countries that are always grappling with food insecurity, lack of sanitation infrastructure, poor healthcare and foreign aid dependence. These NTDs are co-endemic with other tropical diseases such as malaria, etc.[1,2] This introductory chapter provides a background of schistosomiasis in terms of its terminology, history, pathogens, prevalence, aetiology, pathology and diagnosis. This is followed by treatment in terms of antischistosomal agents of clinical significance, drug mode of action and praziquantel resistance mechanisms. Finally, it highlights the statement of the problem, significance of the study, aim, objectives and research questions.

1.2 Schistosomiasis

1.2.1 Etymology, History and Human Pathogenic Species

'Schistosomiasis' comes from the union of two Greek roots: '*schistos*' meaning 'split' and '*soma*' meaning 'body'.[1] The name was proposed by David Friedrich Weinland (1858) because of the male worm's split body morphology.[2] Schistosomiasis (SCH), or snail fever, is a water-borne helminthiasis type of parasitic disease caused by trematodes (flatworms) of the genus *Schistosoma*. The human medically relevant species (in alphabetical order and year of discovery) are: *S. guineensis* (1972), *S. haematobium* (1852), *S. intercalatum* (1934), *S. japonicum* (1904), *S. mansoni* (1907) and *S. mekongi* (1978). There exist several other species of veterinary relevance and many other non-medical wildtype species and hybrid species.[1,2]

Earlier in 1851, Dr Theodor Bilharz, a German physician discovered the disease, coined it 'bilharzia' which term was later adapted to 'bilharziasis'/ 'bilharziosis'. He also described *S. haematobium* (also spelt *hematobium*). *S. haematobium (Sh), S. mansoni (Sm)* and *S. japonicum (Sj)* account for the highest disease burden among the six *Schistosoma* species that infect humans, and the diseases are named according to the species as schistosomiasis haematobium, mansoni and japonica, etc, respectively.[1–4] Katayama syndrome is acute schistosomiasis, especially schistosomiasis japonica, discovered by Katsurada in 1904.[4,5]

1.2.2 Epidemiology and Medical Geography: World, Africa, Zambia and Lusaka

WHO reports published in 2023 and 2024 indicate that 253.8 million people globally required antischistosomal preventative chemotherapy in 2023, a decrease of 10.9 million from 2022 when it was 264.7 million. Additionally, more than 700 million people were either living with the disease or at risk of infection especially in developing countries with a mortality rate of more than 280,000 deaths per annum. Of these deaths, over 150, 000 and 130, 000 deaths per annum were due to *S. haematobium* and *S. mansoni* infections, respectively. After malaria, it is the second most prevalent, virulent and fatal tropical disease.[6–8]

Figure 1 below shows its global distribution typical of the tropics and subtropics.[5]

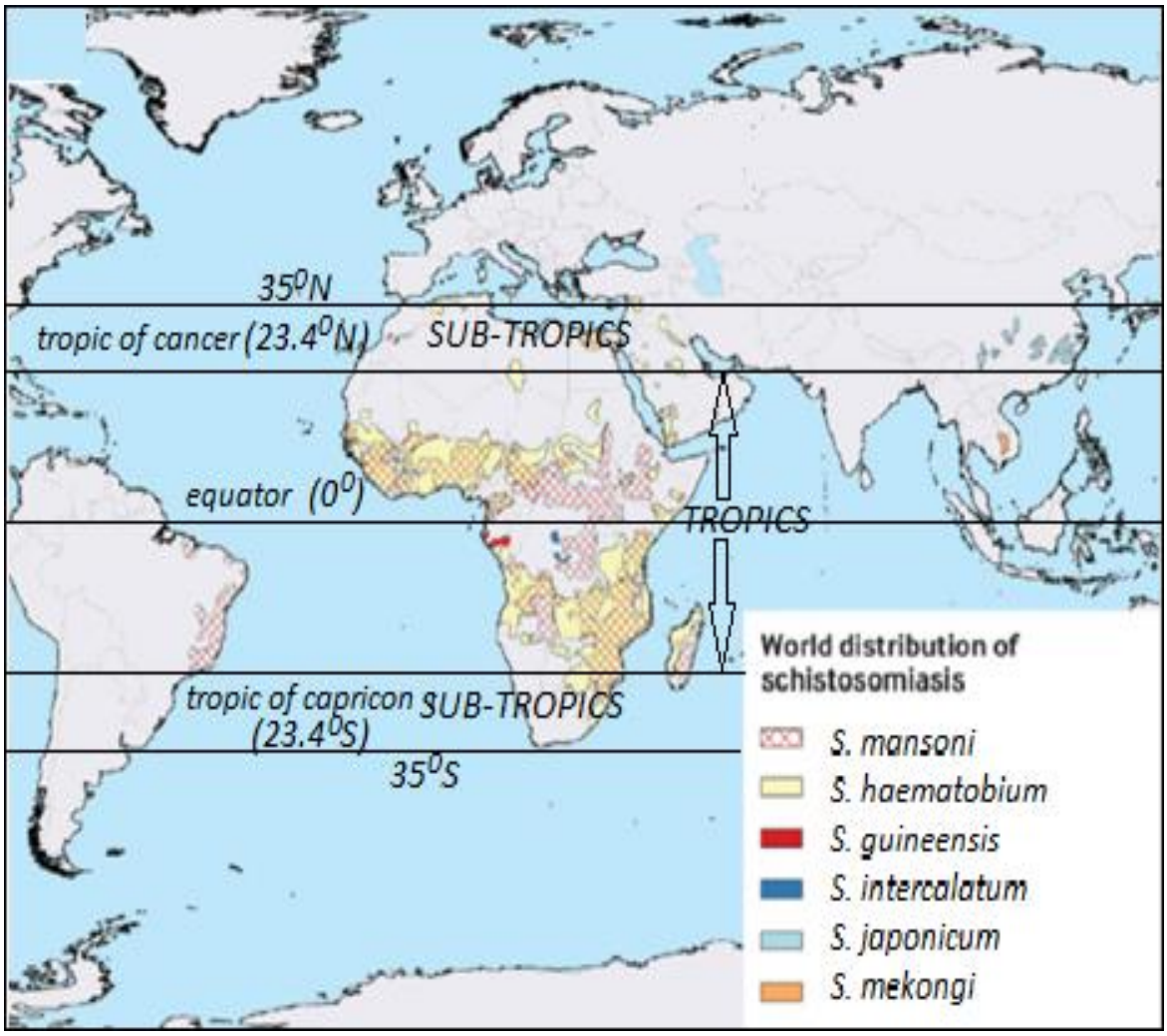

Figure 1: World map showing human schistosomiasis prevalence.[5]

In Africa, the latest WHO estimates show that at least 218 million people required preventative chemotherapy for schistosomiasis i.e. 90% of global cases (Figure 2).[5,9–11]

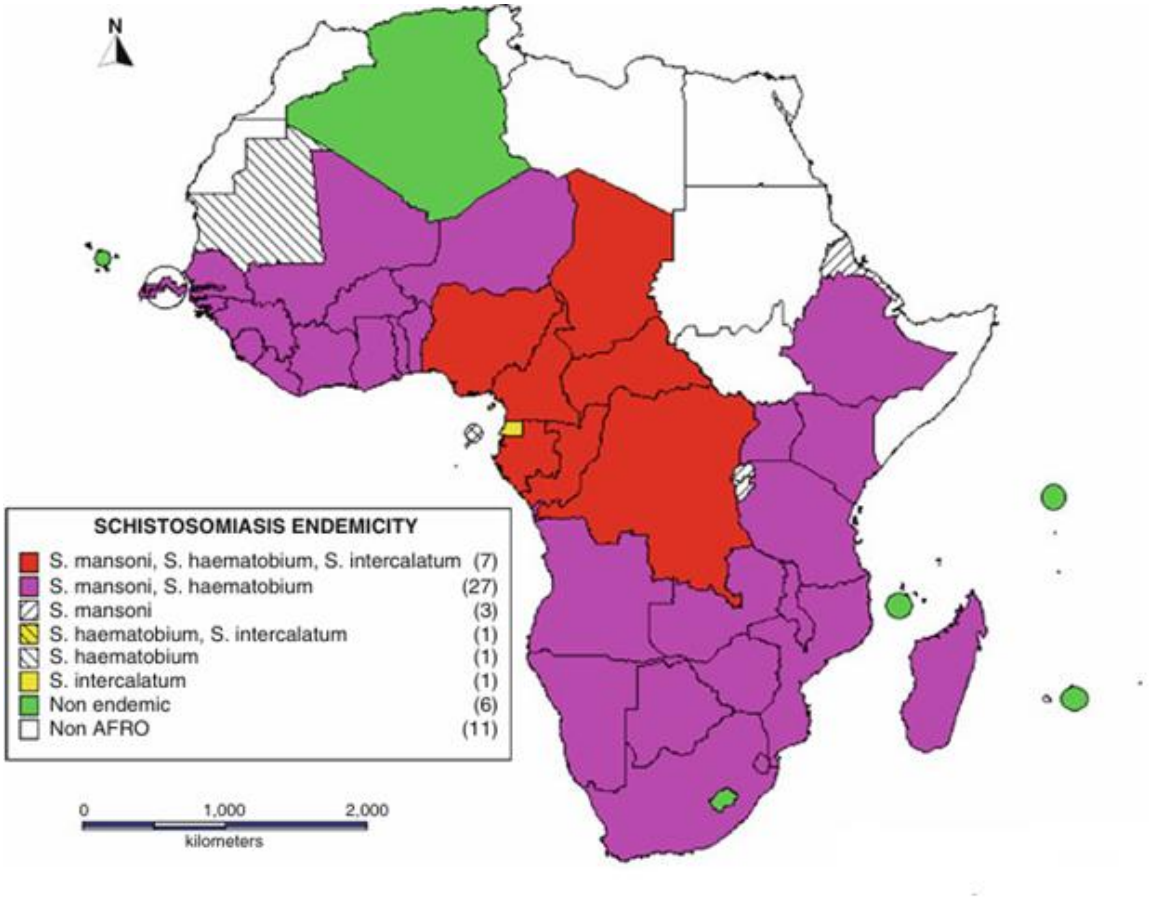

Figure 2: Map of Africa showing prevalence of human schistosome infection by species.[5]

In Zambia, the prevalence is approximately 26.6%, with an estimated 2.39 million individuals infected and an additional 3 million at risk which are due to *S. haematobium* and *S. mansoni* (Figure 3).[12]

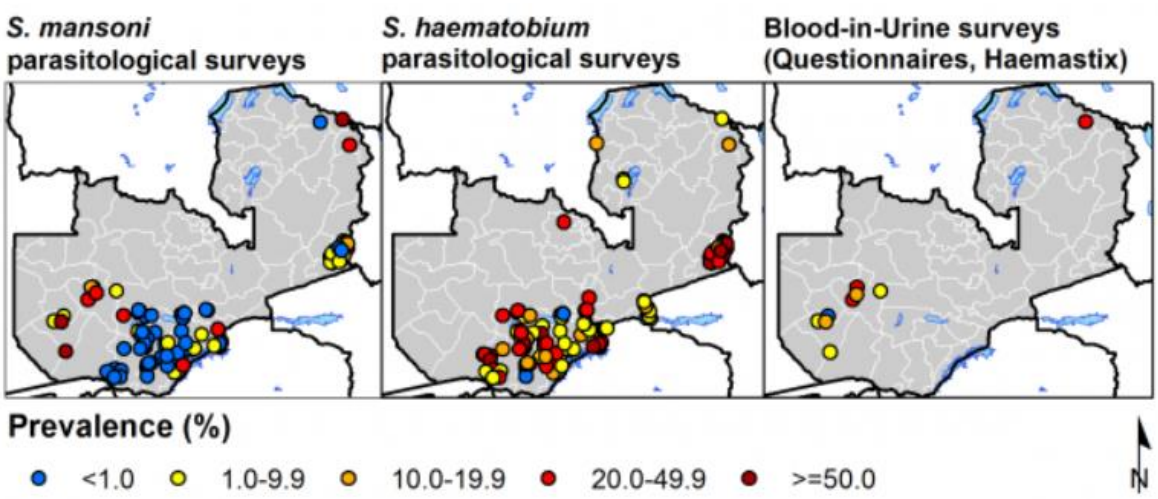

Figure 3: Maps of Zambia showing *S. mansoni* and *S. haematobium* surveys.[13]

The former species is the more common and is endemic in all the ten provinces of Zambia. Generally, the disease is prevalent in rural areas close to the lakes or rivers but also slum urban areas which lack water supply and sanitation infrastructure.[13–21] (A study outside Zambia found that the reduction of schistosomiasis new infections and child mortality decreased by 77% and 55%, respectively, with improved water supply and sanitation.)[22]

Lusaka province has the highest prevalence among Zambian provinces (Figure 4).[14]

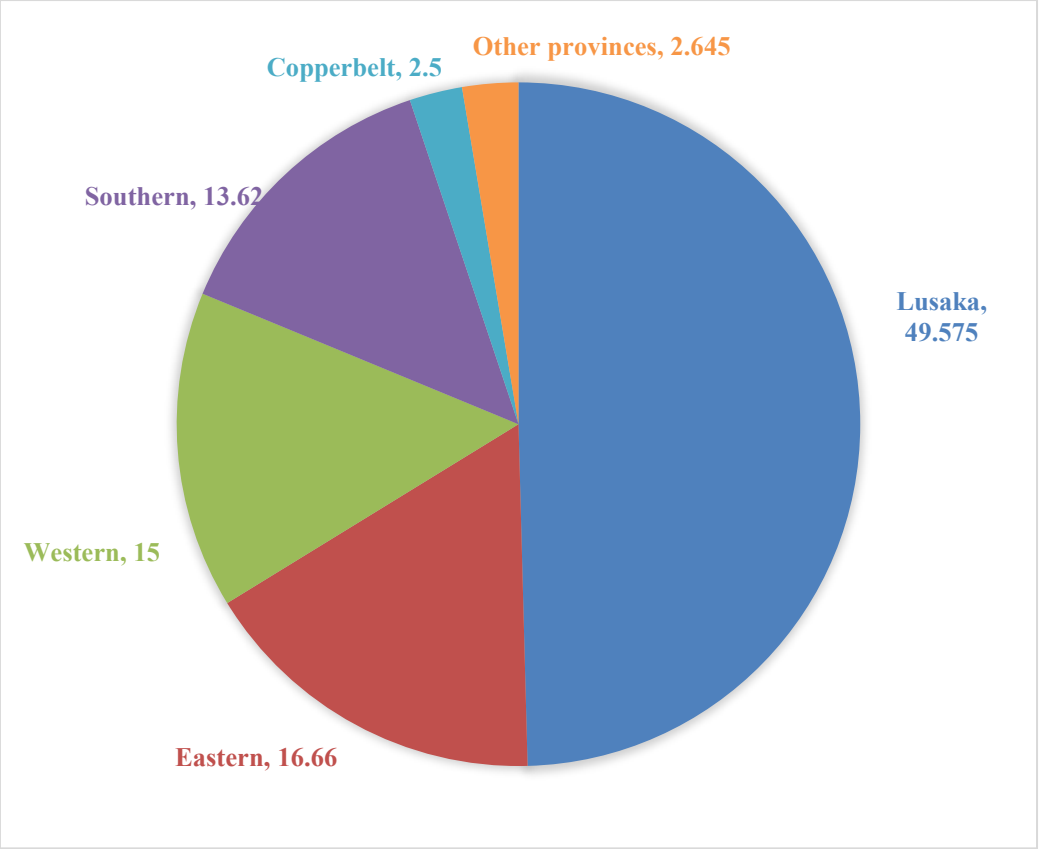

Figure 4: Pie chart showing provincial schistosomiasis prevalence percentages in Zambia.[14]

Urinary schistosomiasis is common among children in some parts of Lusaka province where water contact activity is high and sanitation is poor e.g. Ng'ombe township, a shanty compound in Lusaka urban district and Chongwe district as in Figure 5.[15–18,23]

Figure 5: Schistosomiasis exposure in Chongwe district of Lusaka province[31] (a) boys swimming (b) girls holding containers of their respective haematuric urine.

1.2.3 Parasitology, Aetiology and Pathology

Schistosomes are parasitic with a digenetic life cycle alternating between a snail- and a vertebral host. *S. haematobium* and *S. mansoni* miracidia infect *Bulinus*[5] (e.g. *B. globosus*) and *Biomphalaria* (e.g. *B. glabrata, B. pfeifferi, B. sudanica*) snail vectors, respectively (Figure 6).[10,24–29]

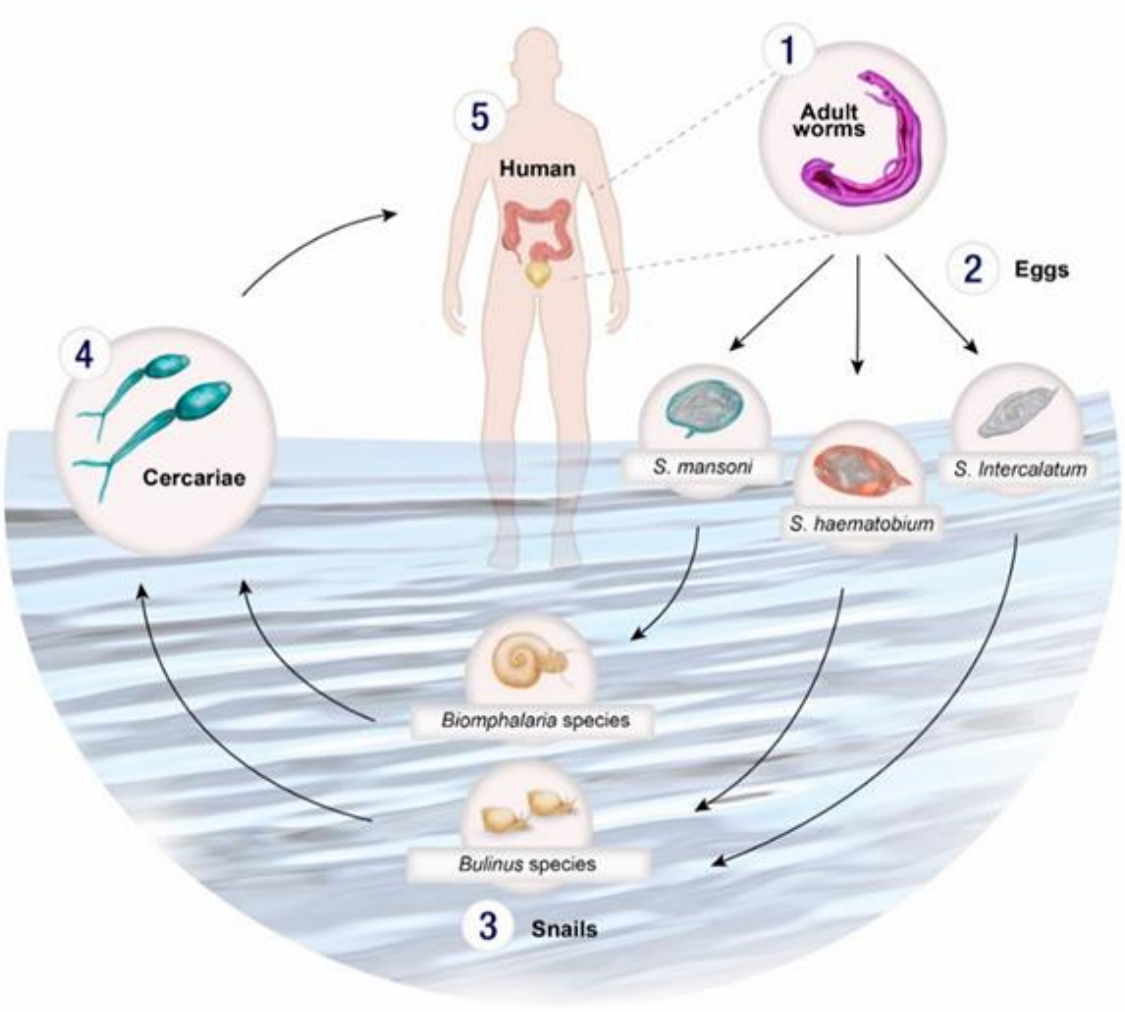

Figure 6: Life cycle and transmission of schistosomes highlighting snail host specificity.[10]

Generally, the most pathogenic species have a similar life cycle. Adult worms living in the blood venules lay about 300 eggs daily, which are released on defecation/ micturition. In water eggs hatch into miracidia, and these locate then infect snails, change into sporocysts ultimately yielding infective cercariae. Cercariae lose their tails during percutaneous penetration of the human host's skin and become larvae which are called newly-transformed schistosomula (NTS). NTS migrate to the hepatic portal veins where they mature into adult worms. Adult

[5] Also spelt as '*Bolinus*'[5,29]

male and female worms pair up, copulate, and then travel to the intestines/ bladder. Under experiment, permissive vertebral hosts are rodents (mice/ rats/ hamsters).[30,31]

Urogenital and intestinal schistosomiasis (due to *S. haematobium* and *S. mansoni* infections, respectively) are the main disease forms, whose infection is divided into the acute, established active and late chronic, with slightly different symptomatology mainly fever, lethargy and malaise but may also be asymptomatic.[30,31] *Sh* exacerbates HIV transmission, while *Sm* and pulmonary arterial hypertension are comorbities.[32,33] In Zambia, *Sh* exposure and *Sm* hepatosplenic schistosomiasis or HSS (Figure 7) have each been found among HIV/AIDS patients co-infected with hepatitis B virus.[5,34–38]

Figure 7: A boy with *S. mansoni* HSS-induced hepatosplenomegaly.[5]

Medico-geographically, schistosomiasis (*Sh* and *Sm*) and malaria (*Plasmodium falciparum*) known to be largely co-endemic as tropical diseases have shown co-infection commonly associated with anaemia namely in Nigeria and Ghana, among other tropical countries.[39,40]

1.2.4 Diagnostic Methods and Mechanisms of Detection

There are three main clinical methods (Table 1) and several others under validation.[4,41–44]

Table 1: Schistosomiasis diagnostic methods and their mechanisms of detection.[a]

Diagnostic method	Mechanism of detection
Microscopic detection	Egg counting from urine[b] or feces[c] (Kato-Katz coprology)[4,41–43]
Immuno/ lateral flow	Circulating cathodic antigen (CCA)/ antibody: active infection/ past infection[4,41–43]
Molecular diagnostic	Nucleic acid amplification test (NAAT): active infection[4,44]

[a]**Source**: Adapted (with modification) from Weber *et al*, **2019**. See Ref **4**. [b]especially *Sh*; [c]especially *Sm*

1.3 Treatment, Management, Control and Prevention

1.3.1 Chemotherapy: Composition, Enantiomerism, Names and Dosages

Praziquantel, oxamniquine and metrifonate are the international nonproprietary names (INNs) of active pharmaceutical ingredients (APIs) of antischistosomal drugs used extensively, with the latter two drugs having now largely been withdrawn.[45–48] The INNs have stems which can be used to decipher the key moieties in the API molecules (Figure 8).[49]

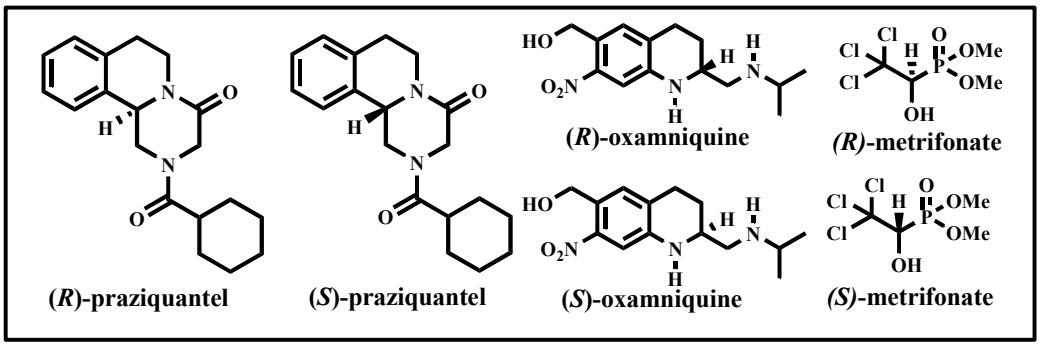

Figure 8: Structures of enantiomers of praziquantel, oxamniquine and metrifonate.[45–48]

Note: Key to stems (roots/prefixes/suffixes) in drug international non-proprietary names (INNs): praz = pyrazine; iqu = isoquinoline; antel = anthelminthic; ox = oxygen (O); am = amine (NR_3); ni = nitro ($-NO_2$); me = methyl (Me/CH_3); fon = phosphonate $PO(OR)_2$; ate = ester[49]

'Praziquantel' (PZQ), the standard of care, is a contraction of '***py raz***inyl***i***so***qu***inoline ***ant***ih***el***mintic' which comes from the main scaffold in the full name 2-(cyclohexylcarbonyl)-1,2,3,6,7,11*b*-hexahydro-4*H*-pyrazino[2,1-*a*]isoquinolin-4-one.[49–51] It is usually manufactured as a racemate, dispensed at WHO recommended dose of 40 mg/kg. However, only the *R*-PZQ enantiomer is active i.e. L-PZQ/ (-)-PZQ, whereas the *S*-enantiomer being inactive is mostly responsible for the bitter taste. The enantiomerism connotes drug-drug interactions.[50–55]

Besides, PZQ's drug metabolism pharmacokinetics (DMPK) profile is well documented.[54–56] Epigastric pain, anorexia and headache are adverse effects. Commonly branded as Biltricide®, etc., besides the API, the excipients are: corn starch, magnesium stearate, microcrystalline cellulose, povidone, sodium lauryl sulfate, polyethylene glycol, titanium dioxide and hydroxypropylmethylcellulose. These excipients (in this marketed product) and others (in research and development) are meant to optimize the solubility and stability.[57–59] It is cheap when subsidized though the annual cost is US$ 17.92 million globally; a 600 mg adult tablet ranging between US$ 0.08 and 6.60 usually donated by WHO. PZQ prophylactic mass drug administration (MDA), molluscicides, snail habitat biologic control also used.[4,5]

Oxamniquine 250 mg is commonly branded as Vansil®, etc while metrifonate 50 mg was commonly branded as Dipterex®.[4,5]

1.3.2 Targets and Modes of Action of Selected Clinically Approved Drugs

Although PZQ has been the main treatment for many years, its precise mode of action had not been fully elucidated.[46,52] The disrupted calcium ion (Ca^{2+}) homeostasis observed upon administration of PZQ had been postulated to be due to an altered function of the voltage operated Ca^{2+} channels which causes contraction of the worm muscle fibres by causing Ca^{2+} influx. The transient receptor potential (TRP) channels had drawn the attention of parasitologists by 2016 who highlighted the eight TRP families in metazoans as: TRPC, TRPV, TRPA, TRPM (melastatin), TRPML, TRPP, TRPN and TRPVL. In 2019, a schistosome Ca^{2+}-permeable *S. mansoni* TRPM channel activated by PZQ was indeed identified, genetically mapped as *Sm*.$TRPM_{PZQ}$, *Smp_246790.5*, chromosome 3; molecularly docked with PZQ (Figure 9), which was confirmed by further studies in 2021 and 2023.[50,60–65]

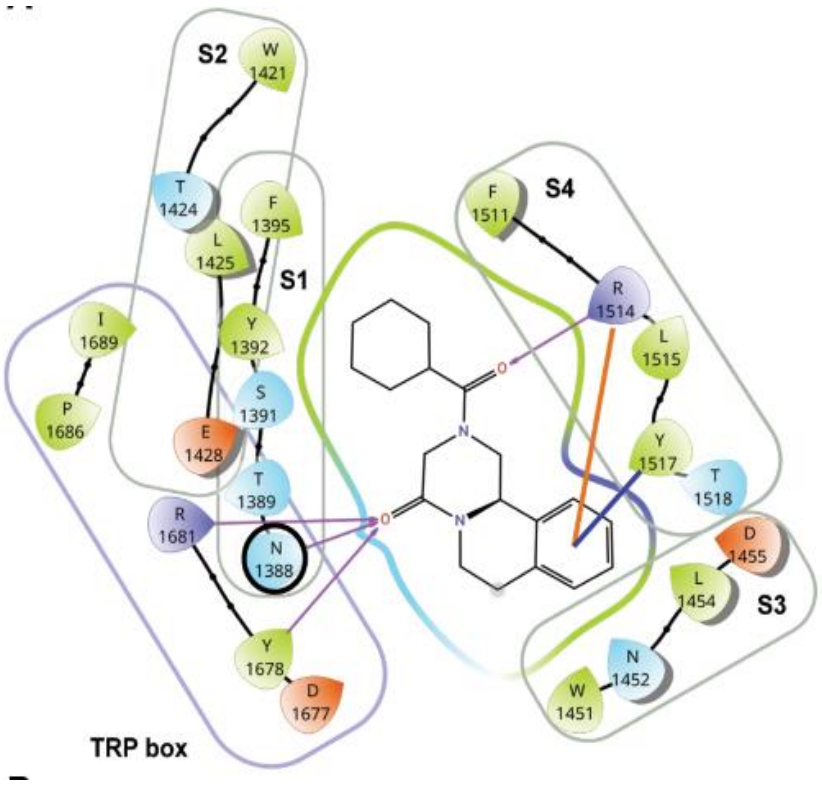

KEY
TRP: transient receptor potential
S1 to **S4**: transmembrane helices;
Amino acid single letter symbols:
D: aspartate;
E: glutamate;
F: phenylalanine;
I: isoleucine;
L: leucine;
N: asparagine;
P: proline;
R: arginine;
S: serine;
T: threonine;
W: tryptophan;
Y: tyrosine;
R1514/ R1681: Arginine on the 1514th and 1681st position, respectively in the 1° polypeptide structure, etc. from the amino end

Figure 9: PZQ docked onto *S. mansoni* TRP_{PZQ} target (Schrödinger Maestro™ software).[63]

Note: Two carbonyl oxygens of PZQ act as hydrogen bond acceptors (HBAs) to amide, phenoxyl and guanidino hydrogens of arginine (R), tyrosine (Y) and asparagine (N) amino acid residue side chains (hydrogen bond donors i.e. HBDs). Also notable are hydrophobic interactions between the phenyl group of PZQ to both Y and R.[66]

Arachidonic acid metabolism is a PZQ target in *S. mekongi*.[67] Oxamniquine inhibits nucleic acid synthesis while metrifonate alters cholinesterase activity.[47,48]

1.3.3 Mechanisms of Resistance against PZQ

The efficacy of PZQ on each of the major species i.e. *S. haematobium, S. mansoni* and *S. japonicum* was established by the clinical trials initially conducted in Zambia, Brazil and Philippines, respectively.[68–70] Indeed, 50% effective concentration (EC_{50}) values for PZQ were 0.1 μg/mL at 4 h, 0.05 μg/mL at 72 h in one follow-up study and 0.1 μM at 72 h in another.[55] However, of late PZQ resistance has been reported in Kenya among other countries potentially fuelled by MDA in such jurisdictions. The resistance mechanisms in *S. mansoni* are explained mainly using two postulates: adenosine triphosphate-binding cassettes (ABCs) and sarcoplasmic/ endoplasmic reticulum calcium ATPases (SERCAs). Adult *S. mansoni* worms with reduced PZQ susceptibility, have been found to have higher levels of ABCs e.g. P-glycoprotein, suggesting that they remove PZQ. Calmodulin kinase II activation followed by nuclear activated factor kappa B activation, is linked to SERCA in *S. mansoni* was shown to have PZQ sensitivity reduction.[50,71–75]

1.4 Statement of the Problem

PZQ has been the almost exclusive standard of care since 1977, whose downside include resistance, paediatric dosing challenges, adverse effects and a short shelf life. Besides, it is also ineffective on younger life cycle stages which may trigger re-infections by failure to stop transmission, necessitating repetitive administration. In fact, little has been done into developing new antischistosomal drugs or vaccines.[45–47]

Therefore, there remains an unmet medical need to develop other treatment options with different modes of action to circumvent the now well-known Ca^{2+} channel-mediated mechanism of resistance against PZQ's pyrazino-isoquinoline core scaffold. Even with WHO donations, Zambia still failed to reach the 75% threshold national coverage in preventative chemotherapy in school-aged children in 2023 unlike the neighbours, Democratic Republic of the Congo and Malawi, among other African countries.[6]

In fact resistance is also already of concern even in the most promising antimalarial repurposed antischistosomal candidates in clinical development globally since the responsible parasites are co-endemic in tropical and sub-tropical regions (section 2.3) especially in their co-infection cases (subsection 1.2.3).[39,40] Advisedly, the use of such drugs should be restricted to areas outside those where there is any trace of malaria transmission.[76,77] Besides, poor solubility and related properties as well as severe cytotoxicity and target organ toxicity have made several

good antischistosomal drug candidates discovered, even those more potent than PZQ, not reach the market (section 2.5 and Table 4).[78–82]

1.5 Significance of the Study

This study has contributed insights into medicinal chemistry optimization of a new class of compounds, which future researchers could exploit in the pursuit of novel antischistosomal treatments in terms of a less hydrophobic, more water soluble, less cytotoxic, cheaper and orally active candidate since higher aqueous solubility (S_{aq}) *in vitro* translates into higher blood solubility and bioavailability *in vivo.* Besides, an orally administrable drug would not require injections and refrigerators for low temperature and the constant care of health workers hence would be cheaper to administer by MDA even to the poor. Structure-activity relationships (SARs) are key in drug discovery as a drug-like molecule is taken to consist of a pharmacophore, a metabophore and a toxicophore which are basically molecular fragments responsible for therapeutic effect, metabolism and toxicology, respectively. SAR exploration is key to hit-to-lead optimization in medicinal chemistry and drug discovery before drug development of a molecule can be considered. In addition, the study has highlighted how *in silico* computer aided drug discovery can cheaply be applied to NTDs like schistosomiasis and hence prevent wastage of chemicals and other resources by prediction of some physicochemical and drug metabolism pharmacokinetic (DMPK) properties as well as cytotoxicity using free readily available web-based databases/software such as SwissADME™, PkCSM™ and Cyto-Safe™ at design stage prior to the actual synthesis.

1.6 Aim, Objectives and Research Questions

1.6.1 Aim

The aim of this study was to synthesize *N*-pyridazin-3-ylbenzamide (*N*-PdzBA) analogues and profile their hydrophobicity, solubility, cytotoxicity and antischistosomal activity.

1.6.2 Objectives

1. To design and synthesize *N*-PdzBA target compounds via carbodiimide-mediated amide coupling.
2. To comprehensively characterize target compounds using LC-MS, UV-Vis, IR, ^{1}H- and ^{13}C-NMR spectroscopy.
3. To evaluate *in vitro* antischistosomal SARs on *S. mansoni* adult worms.
4. To profile the *N*-PdzBAs in terms of hydrophobicity, aqueous solubility (S_{aq}), cytotoxicity using *in vitro* and/or *in silico* approaches.

1.6.3 Research Questions

1. Is it possible to synthesize *N*-PdzBAs via carbodiimide-mediated amide coupling?
2. Is it feasible to characterize target compounds using LC-MS, UV-Vis, IR, ^{1}H- and ^{13}C-NMR?
3. Is there appreciable *in vitro* antischistosomal activity on *S. mansoni* adult worms exposed to *N*-PdzBA chemical insult and if yes what is the SAR?
4. What are the calculated Log*P* (cLog*P*), aqueous solubility, cytotoxicity (on HEK293 cells) profiles of the *N*-PdzBAs, as determined using *in vitro* and/or *in silico* approaches?

1.7 References

(1) da Silva Emery, F.; Chibale, K. Forging a Future Free from Neglected Tropical Diseases. *ACS Med. Chem. Lett.* **2024**, *15* (3), 314–315.

(2) Folahan, F. F. Neglected Tropical Diseases: Progress and Expectations. *Lancet. Microbe.* **2023**, *4*, 137–138.

(3) Villamizar-Monsalve, M.; López-Abán, J; Vicente, B.; Peláez, R.; Muro, A. Current Drug Strategies for the Treatment and Control of Schistosomiasis. *Expert Opin. Pharmacother.* **2024**, *25* (4), 409–420.

(4) Weber, C. J.; Hargan-Calvopiña, J.; Graef, K. M.; Manner, C. K.; Dent, J. WIPO Re:Search – A Platform for Product-centered Cross-Sector Partnerships for the Elimination of Schistosomiasis. *Trop. Med. Infect. Dis.* **2019**, *4* (1), 11.

(5) Danso-Appiah, T. *Neglected Tropical Diseases: Sub-Saharan Africa;* Springer International Publishing, **2016**, pp 251–288.

(6) World Health Organization. Schistosomiasis and Soil-Transmitted Helminthiases: Progress Report, 2023. *WHO Weekly Epidemiological Record.* **2024**, *99* (48), 707–717. https://www.eliminateschisto.org/sites/gsa/files/content/attachments/2024-12-18/WER9948-707-717.pdf (accessed 2024-12-19).

(7) World Health Organization. *Global Report on Neglected Tropical Diseases 2023.* World Health Organization, **2023**. https://iris.who.int/bitstream/handle/10665/365729/9789240067295-eng.pdf?sequence=1 (accessed 2024-02-29).

(8) World Health Organization. *WHO International: Schistosomiasis (Bilharzia)*. World Health Organization. https://www.who.int/health-topics/schistosomiasis#tab=tab_1 (accessed 2024-03-19).

(9) World Health Organization. *WHO Africa Region: Schistosomiasis (Bilharzia)*. World Health Organization. https://www.afro.who.int/health-topics/schistosomiasis-bilharzia (accessed 2024-03-19).

(10) Aula, O. P.; McManus, D. P.; Jones, M. K.; Gordon, C. A. Schistosomiasis with a Focus on Africa. *Trop. Med. Infect. Dis*. **2021**, *6* (3), 109.

(11) Hikaambo, C. N.; Shakela, N.; Woodland, J. G.; Wicht, K. J.; Chibale, K. Drug Discovery in Africa Tackles Zoonotic and Related Infections. *Sci. Transl. Med.* **2023**, *15* (718), eadj0035.

(12) Chimfwembe, K.; Mutesu, L. M. Predicting *Schistosoma haematobium* Risk Distribution in Zambia Using Geographic Information System (GIS) And Remote Sensing (RS) Technologies. *Asian J. Heal. Res.* **2024**, *3* (3), 233–243.

(13) Global Atlas of Helminth Infections. *This Wormy World.* www.thiswormyworld.org (accessed 2023-08-25).

(14) Kalinda, C.; Chimbari, M. J.; Mukaratirwa, S. Schistosomiasis in Zambia: A Systematic Review of Past and Present Experiences. *Infect. Dis. Poverty.* **2018**, *7* (1), 41.

(15) Tembo, R.; Muleya, W.; Yabe, J.; Kainga, H.; Nalubamba, K. S.; Zulu, M.; Mwaba, F.; Saad, S. A.; Kamwela, M.; Mukubesa, A. N.; Monde, N.; Kallu, S. A.; Mbewe, N.; Phiri, A. M. Prevalence and Molecular Identification of *Schistosoma haematobium* among Children in Lusaka and Siavonga Districts, Zambia. *Trop. Med. Infect. Dis.* **2022**, *7* (9), 239.

(16) Simoonga, C.; Kazembe, L. N.; Kristensen, T. K.; Olsen, A.; Appleton, C. C.; Mubita, P.; Mubila, L. The Epidemiology and Small-scale Spatial Heterogeneity of Urinary Schistosomiasis in Lusaka Province, Zambia. *Geospat. Health.* **2008**, *3* (1), 57–67.

(17) Agnew-Blais, J.; Carnevale, J.; Gropper, A.; Shilika, E.; Bail, R.; Ngoma, M. Schistosomiasis Haematobium Prevalence and Risk Factors in a School-age Population of Peri-urban Lusaka, Zambia. *J. Trop. Pediatr.* **2009**, *56* (4), 247–253.

(18) Kalungwana, N.; Ng'andwe, K.; Mwakazanga, D.; Mwansa, J.; Mutengo, M. M.; Siziya, S. Prevalence and Factors Associated with Schistosomiasis in Ng'ombe Township of Lusaka Urban District. *J. Biol. Sci.* **2012**, *1* (1), 7–11.

(19) Mutengo, M. M.; Mwansa, J. C. L.; Mduluza, T.; Sianongo, S.; Chipeta, J. High *Schistosoma mansoni* Disease Burden in a Rural District of Western Zambia. *Am. J. Trop. Med. Hyg.* **2014**, *91* (5), 965–972.

(20) Shehata, M.; Chama, M.; Funjika, E. Prevalence and Intensity of *Schistosoma haematobium* Infection among School Children in Central Zambia before and after Mass Treatment with a Single Dose of Praziquantel. *Trop. Parasitol.* **2018**, *8* (1), 12–17.

(21) Sandema, C.; Daka, V.; Syapiila, P.; Tembo, M.; Sikalima, J.; Patel, S.; Mudenda, S.; Mfune, R. L.; Mutanekelwa, I.; Zyambo, C.; Mwanakasale, V. Prevalence and Correlates of *Schistosoma haematobium* Infections among School-going Children Aged 5 to 17 Years in Kawama, Ndola, Zambia. *Pan Afr. Med. J.* **2023**, *45*, 170.

(22) Grimes, J. E. T.; Croll, D.; Harrison, W. E.; Utzinger, J.; Freeman, M. C.; Templeton, M. R. The Roles of Water, Sanitation and Hygiene in Reducing Schistosomiasis: A Review. *Parasit. Vectors.* **2015**, *8* (156), 1–16.

(23) la Camp, M. *Schistosomiasis*. Virtual Doctors. www.virtualdoctors.org (accessed 2023-08-25).

(24) Nelwan, M. L. Schistosomiasis: Life Cycle, Diagnosis, and Control. *Curr. Ther. Res.* **2019**, *91* (24), 5–9.

(25) Shebel, H. M.; Elsayes, K. M.; Abou El Atta, H. M.; Elguindy, Y. M.; El-Diasty, T. A. Genitourinary Schistosomiasis: Life Cycle and Radiologic-pathologic Findings. *Radiographics.* **2012**, *32* (4), 1031–1046.

(26) Rollinson, D.; Stothard, J. R.; Southgate, V. R. Interactions between Intermediate Snail Hosts of the Genus *Bulinus* and Schistosomes of the *Schistosoma haematobium* Group. *Parasitol*. **2001**, *123* (7), 245–260.

(27) Monde, C.; Syampungani, S.; van den Brink, P. J. Natural and Human-induced Factors Influencing the Abundance of *Schistosoma* Host Snails in Zambia. *Environ. Monit. Assess.* **2016**, *188* (6), 1–14.

(28) Dejong, R. J.; Morgan, J. A. T.; Wilson, W. D.; Al-Jaser, M. H.; Appleton, C. C.; Coulibaly, G.; d'Andrea, P. S.; Doenhoff, M. J.; Haas, W.; Idris, M. A.; Magalhães, L. A.; Moné, H.; Mouahid, G.; Mubila, L.; Pointier, J. P.; Webster, J. P.; Zanotti-Magalhães, E. M.; Paraense, W. L.; Mkoji, G. M.; Loker, E. S. Phylogeography of *Biomphalaria glabrata* and *B. pfeifferi*, Important Intermediate Hosts of *Schistosoma mansoni* in the New and Old World Tropics. *Mol. Ecol.* **2003**, *12* (11), 3041–3056.

(29) Stensgaard, A. S.; Utzinger, J.; Vounatsou, P.; Hürlimann, E.; Schur, N.; Saarnak, C. F. L.; Simoonga, C.; Mubita, P.; Kabatereine, N. B.; Tchuem Tchuenté, L. A.; Rahbek, C.; Kristensen, T. K. Large-scale Determinants of Intestinal Schistosomiasis and Intermediate Host Snail Distribution across Africa: Does Climate Matter? *Acta. Trop.* **2013**, *128* (2), 378–390.

(30) Elbaz, T.; Esmat, G. Hepatic and Intestinal Schistosomiasis: Review. *J. Adv. Res*. **2013**, *45* (1), 445–452.

(31) Tan, W. P.; Bs, T. H.; Park, J.; Elterman, L. *Schistosoma hematobium*: A Delayed Cause of Hematuria. *Urology.* **2017**, *100* (107), e7–e8.

(32) Sibomana, J. P.; Campeche, A.; Carvalho-Filho, R. J.; Correa, R. A.; Duani, H.; Pacheco Guimaraes, V.; Hilton, J. F.; Kassa, B.; Kumar, R.; Lee, M. H.; Loureiro, C. M. C.; Mazimba, S.; Mickael, C.; Oliveira, R. K. F.; Ota-Arakaki, J. S.; Rezende, C. F.; Silva, L. C. S.; Sinkala, E.; Ahmed, H. Y.; Graham, B. B. Schistosomiasis Pulmonary Arterial Hypertension. *Front. Immunol*. **2020**, *11*, 608883.

(33) Yegorov, S.; Joag, V.; Galiwango, R. M.; Good, S. V.; Mpendo, J.; Tannich, E.; Boggild, A. K.; Kiwanuka, N.; Bagaya, B. S.; Kaul, R. *Schistosoma mansoni* Treatment Reduces HIV Entry into Cervical $CD4^+$ T Cells and Induces IFN-I Pathways. *Nat. Commun.* **2019**, *10* (1), 1–12.

(34) Kaonga, P.; Kaimoyo, E.; Besa, E.; Zyambo, K.; Sinkala, E.; Kelly, P. Direct Biomarkers of Microbial Translocation Correlate with Immune Activation in Adult Zambians with Environmental Enteropathy and Hepatosplenic Schistosomiasis. *Am. J. Trop. Med. Hyg.* **2017**, *97* (5), 1603–1610.

(35) Mutengo, M. M.; Mduluza, T.; Kelly, P.; Mwansa, J. C. L.; Kwenda, G.; Musonda, P.; Chipeta, J. Low IL-6, IL-10, and TNF-α and IL-13 Cytokine Levels are Associated with Severe Hepatic Fibrosis in *Schistosoma mansoni* Chronically Exposed Individuals. *J. Parasitol. Res.* **2018**, *2018* (1), 9754060.

(36) Sinkala, E.; Vinikoor, M.; Siyunda, M. A.; Zyambo, K.; Besa, E.; Nsokolo, B.; Wandeler, G.; Foster, G. R.; Kelly, P. Hepatosplenic Schistosomiasis in Zambian Adults is

Characterized by Increased Liver Stiffness: A Nested Case-control Study. *Heliyon.* **2020**, *6* (7), e04534.

(37) Shanaube, K.; Ndubani, R.; Kelly, H.; Webb, E. L.; Mayaud, P.; Lamberti, O.; Fitzpatrick, J.; Kasese, N.; Sturt, A.; van Lieshout, L.; van Dam, G. J.; Corstjens, P. L. A. M.; Kosloff, B.; Bond, V.; Hayes, R.; Terris-Prestholt, F.; Webster, B.; Vwalika, B.; Hansingo, I.; Ayles, H.; Bustinduy, A. L. The Zipime-Weka-Schista Study Protocol: A Longitudinal Cohort Study and Economic Evaluation of a Home-based Approach for Genital Multi-screening in Women, Including Female Genital Schistosomiasis, Trichomonas and HIV in Zambia. *B. M. J. Open.* **2024**, *14* (6), e080395.

(38) Chisenga, C.; Sinkala, E.; Chilengi, R.; Chitundu, H.; Zyambo, Z.; Wandeler, G.; Vinikoor, M. Prevalence and Clinical Significance of Schistosomiasis – Chronic Hepatitis B Virus Co-infection in Zambia. *B. M. J. Glob. Health.* **2017**, *2* (2), A8.3–A9.

(39) Muhammed, H.; Balogun, J. B.; Dogara, M. M.; Adewale, B.; Ibrahim, A. A.; Okolugbo, C. B.; Jackson, G. Co-infection of Urogenital Schistosomiasis and Malaria and Its Association with Anaemia and Malnutrition amongst Schoolchildren in Dutse, Nigeria. *S. Afr. J. Sci.* **2023**, *119* (7/8), 1–12.

(40) Dassah, S. D.; Nyaah, K. E.; Senoo, D. K.; Ziem, Z. B.; Aniweh, Y.; Amenga-Etego, L.; Awandare, G. A.; Abugri, J. Co-infection of *Plasmodium falciparum* and *Schistosoma mansoni* is Associated with Anaemia. *Malar. J.* **2023**, *22* (1), 272.

(41) Vaillant, M. T.; Philippy, F.; Neven, A.; Barré, J.; Bulaev, D.; Olliaro, P. L.; Utzinger, J.; Keiser, J.; Garba, A. T. Diagnostic Tests for Human *Schistosoma mansoni* and *Schistosoma haematobium* Infection: A Systematic Review and Meta-analysis. *Lancet Microbe.* **2024**, *5* (4), e366–78.

(42) Lodh, N.; Mwansa, J. C. L.; Mutengo, M. M.; Shiff, C. J. Diagnosis of *Schistosoma mansoni* without the Stool: Comparison of Three Diagnostic Tests to Detect *Schistosoma mansoni* Infection from Filtered Urine in Zambia. *Am. J. Trop. Med. Hyg.* **2013**, *89* (1), 46–50.

(43) Yin, X.; N'Goran, E. K.; Ouattara, M.; Aka, N. A. D.; Diakité, N. R.; Bassa, F. K.; Kourany-Lefoll, E.; Tappert, A.; Yalkinoglu, Ö.; Huber, E.; Bezuidenhout, D.; Bagchus, W. M.; Hayward, B. Comparison of POC-CCA with Kato-Katz in Diagnosing *Schistosoma mansoni* Infection in a Pediatric L-Praziquantel Clinical Trial. *Front. Trop. Dis.* **2021**, *2*, 686288.

(44) Mcmanus, D. P.; Gordon, C.; Weerakoon, K. G. A. D. Testing of Water Samples for Environmental DNA as a Surveillance Tool to Assess Risk of Schistosome Infection in a Locality. *Int. J. Infect. Dis.* **2018**, *76*, 128–129.

(45) Lago, E. M.; Xavier, R. P.; Teixeira, T. R.; Silva, L. M.; da Silva Filho, A. A.; de Moraes, J. Antischistosomal Agents: State of Art and Perspectives. *Future Med. Chem*. **2018**, *10* (1), 89–120.

(46) Dziwornu, G. A.; Attram, H. D.; Gachuhi, S.; Chibale, K. Chemotherapy for Human Schistosomiasis: How Far Have We Come? What's New? Where Do We Go from Here? *RSC Med. Chem.* **2020**, *11* (4), 455–490.

(47) da Silva, V. B. R.; Campos, B. R. K. L.; de Oliveira, J. F.; Decout, J.; de Lima, M. do D. A. Medicinal Chemistry of Antischistosomal Drugs: Praziquantel and Oxamniquine. *Bioorg. Med. Chem*. **2017**, *25* (13), 3259–3277.

(48) Taylor, A. B.; Picca-Mattoccia, L.; Polcaro, C. M.; Donati, E.; Cao, X.; Basso, A.; Guidi, A.; Rugel, A. R.; Holloway, S. P.; Anderson, T. J. C.; Hart, P. J.; Cioli, D.; LoVerde, P. T. Structural and Functional Characterization of the Enantiomers of the Antischistosomal Drug Oxamniquine. *PLoS Negl. Trop. Dis*. **2015**, *9* (10), e0004132.

(49) World Health Organization. *The Use of Stems in The Selection of International Nonproprietary Names (INN) For Pharmaceutical Substances.* World Health Organization, **2018**.

(50) Banda, H.; Abere, A. Navigating the Challenge of Praziquantel Resistance in Schistosomiasis: Molecular Mechanisms and Future Directions. *Discover. Med.* **2025**, *2* (105).

(51) Spangenberg, T. Learnings in Schistosomiasis Drug Discovery. In: *Proceedings of the Drug Discovery Africa Conference*, Accra, March **2025** (DDAC25). https://d1ssu070pg2v9i.cloudfront.net/pex/wcair/2025/02/27202655/Drug-Discovery-Africa-Abstract-Book.pdf (accessed 2025-03-14)

(52) Cezanne, B.; Harder, A.; Maillard, D.; Sun, R.; Waechtler, A.; Wang, J.; Wang, S. Praziquantel – 50 Years of Research. *Chem. Med. Chem.* **2023**, *18* (12), e202300154.

(53) Meyer, T.; Sekljic, H.; Fuchs, S.; Bothe, H.; Schollmeyer, D.; Miculka, C. Taste, a New Incentive to Switch to *(R)*-Praziquantel in Schistosomiasis Treatment. *PLoS Negl. Trop. Dis.* **2009**, *3* (1), e357.

(54) Mutiti, C. S.; Kapungu, N. N.; Kanji, C. R.; Stadler, N.; Stingl, J.; Nhachi, C.; Hakim, J.; Masimirembwa, C.; Thelingwani, R. S. Clinically Relevant Enantiomer Specific *R*- and *S*-Praziquantel Pharmacokinetic Drug-drug Interactions with Efavirenz and Ritonavir. *Pharmacol. Res. Perspect.* **2021**, *9* (3), e00769.

(55) Meister, I.; Ingram-Sieber, K.; Cowan, N.; Todd, M.; Robertson, M. N.; Meli, C., Patra, M.; Gasser, G.; Keiser, J. Activity of Praziquantel Enantiomers and Main Metabolites against *Schistosoma mansoni. Antimicrob. Agent. Chemother.* **2014**, *58* (9), 5466–5472.

(56) Zdesenko, G.; Mutapi, F. Drug Metabolism and Pharmacokinetics of Praziquantel: A Review of Variable Drug Exposure during Schistosomiasis Treatment in Human Hosts and Experimental Models. *PLoS Negl. Trop. Dis*. **2020**, *14* (9), e0008649.

(57) Garrido, C. C.; Vandooren, M.; Robeyns, K.; Debecker, D. P.; Luis, P.; Leyssens, T. Combining a Drug and a Neutraceutical: A New Co-crystal of Praziquantel and Curcumin. *Crystals.* **2024**, *14* (2), 181.

(58) Špehar, T. K.; Pocrnić, M.; Klarić, D.; Bertoša, B.; Čikoš, A.; Jug, M.; Padovan, J.; Dragojević, S.; Galić, N. Investigation of Praziquantel/Cyclodextrin Inclusion Complexation by NMR and LC-HRMS/MS: Mechanism, Solubility, Chemical Stability and Degradation Products. *Mol. Pharm.* **2021**, *18* (11), 4210–4223.

(59) D'Abbrunzo, I.; Gigli, L.; Demitri, N.; Sabena, C.; Nervi, C.; Chierotti, M. R.; Bertoni, S.; Škorić, I.; Häberli, C.; Keiser, J.; Hasa, D.; Perissutti, B. Higher-order Multicomponent Crystals as a Strategy to Decrease the IC_{50} Parameter: the Case of

Praziquantel, Niclosamide and Acetic Acid. *J. Drug Deliv. Sci. Technol.* **2025**, *109*, 106974.

(60) Bais, S.; Greenberg, R. M. TRP Channels in Schistosomes. *Int. J. Parasitol.: Drugs Drug Resist*. **2016**, *6* (3), 335–342.

(61) Park, S. K.; Sprague, D. J.; Rohr, C. M.; Chulkov, E. G.; Petrow, I.; Kumar, S.; Marchant, J. S. The Anthelmintic Meclonazepam Activates a Schistosome Transient Receptor Potential Channel. *J. Biol. Chem*. **2024**, *300* (1), 105528.

(62) Park, S. K.; Gunaratne, G. S.; Chulkov, E. G.; Moehring, F.; McCusker, P.; Dosa, P. I.; Chan, J. D.; Stucky, C. L.; Marchant, J. S. The Anthelmintic Drug Praziquantel Activates a Schistosome Transient Receptor Potential Channel. *J. Biol. Chem.* **2019**, *294* (49), 18873–18880.

(63) Park, S. K.; Friedrich, L.; Yahya, N. A.; Rohr, C.; Chulkov, E. G.; Maillard, D.; Rippmann, F.; Spangenberg, T.; Marchant, J. S. Mechanism of Praziquantel Action at a Parasitic Flatworm Ion Channel. *Sci. Transl. Med.* **2021**, *13* (625), eabj5832.

(64) le Clec'h, W.; Chevalier, F. D.; Carolina, A.; Mattos, A.; Strickland, A.; Diaz, R.; Mcdew-White, M.; Rohr, C. M.; Kinung'hi, S.; Allan, F.; Webster, B. L.; Webster, J. P.; Emery, A. M.; Rollinson, D.; Djirmay, A. G.; Al Mashikhi, K. M.; Al Yafae, S.; Idris, M. A.; Moné, H.; Mouahid, G.; Loverde, P.; Marchant, J. S.; Anderson, T. J. C. Genetic Analysis of Praziquantel Response in Schistosome Parasites Implicates a Transient Receptor Potential Channel. *Sci. Transl. Med.* **2021**, *13* (625), eabj9114.

(65) Chevalier, F. D.; le Clec'h, W.; Berriman, M.; Anderson, T. J. C. A Single Locus Determines Praziquantel Response in *Schistosoma mansoni*. *Antimicrob. Agents Chemother.* **2024,** *68* (3), e0143223.

(66) Patrick, G. L. *An Introduction to Medicinal Chemistry*, 7th ed.; Oxford University Press, **2023**.

(67) Chienwichai, P.; Tipthara, P.; Tarning, J.; Limpanont, Y.; Chusongsang, P.; Chusongsang, Y.; Adisakwattana, P.; Reamtong, O. Metabolomics Reveal Alterations in Arachidonic Acid Metabolism in *Schistosoma mekongi* after Exposure to Praziquantel. *PLoS Negl. Trop. Dis.* **2021**, *15* (9), e0009706.

(68) Davis, A.; Biles, J. E.; Ulrich, A. M. Initial Experiences with Praziquantel in the Treatment of Human Infections Due to *Schistosoma haematobium*. *Bull. World Health Organ.* **1979**, *57* (5), 773–779.

(69) Katz, N.; Rocha, R.; Chaves, A.; Rachou, R.; Horizonte, B. Preliminary Trials with Praziquantel in Human Infections Due to *Schistosoma mansoni*. *Bull. World Health Organ.* **1979**, *57* (5), 781–785.

(70) Santos, A. T.; Blas, B. L.; Nosenas, J. S.; Portillo, G. P.; Ortega, O. M.; Hayashi, M.; Boehme, K. Preliminary Clinical Trials with Praziquantel in *Schistosoma japonicum* Infections in the Philippines. *Bull. World Health Organ.* **1979**, *57* (5), 793–799.

(71) Patra, M.; Ingram, K.; Leonidova, A.; Pierroz, V.; Ferrari, S.; Robertson, M. N.; Todd, M. H.; Keiser, J.; Gasser, G. *In Vitro* Metabolic Profile and *In Vivo* Antischistosomal Activity Studies of (η(6)-Praziquantel)$Cr(CO)_3$ Derivatives. *J. Med. Chem.* **2013**, *56* (2), 9192–9198.

(72) Vale, N.; Gouveia, M. J.; Rinaldi, G.; Brindley, P. J.; Gärtner, F.; da Costab, J. M. C. Praziquantel for Schistosomiasis: Single-Drug Metabolism Revisited, Mode of Action, and Resistance. *Antimicrob. Agents Chemother.* **2017**, *61* (5), e0258216.

(73) Eastham, G.; Fausnacht, D.; Becker, M. H.; Gillen, A.; Moore, W. Praziquantel Resistance in Schistosomes: A Brief Report. *Front. Parasitol.* **2024**, *3*, 1471451.

(74) Abou-El-Naga, I. F. *Schistosoma mansoni* Sarco/Endoplasmic Reticulum Ca^{2+} ATPases (SERCA): Role in Reduced Sensitivity to Praziquantel. *J. Bioenerg. Biomembr*. **2020**, *52* (5), 397–408.

(75) Abou-El-Naga, I. F. Calcium/Calmodulin Dependent Protein Kinase II in *Schistosoma:* Relation to Praziquantel Action and Resistance. *Mol. Biochem. Parasitol*. **2025**, *263*, 111686.

(76) Muok, E. M. O.; Were, V. O.; Obonyo, C. O. Efficacy and Safety of a Single Oral Dose Artesunate plus Sulfalene-Pyrimethamine Versus Praziquantel in the Treatment of *Schistosoma mansoni* in Kenyan Children: An Open-Label, Randomized, Exploratory Trial. *Am. J. Trop. Med. Hyg.* **2024**, *110* (4), 677–680.

(77) Rosenthal, P. J.; Asua, V.; Bailey, J. A.; Conrad, M. D.; Ishengoma, D. S.; Kamya, M. R.; Rasmussen, C.; Tadesse, F. G.; Uwimana, A.; Fidock, D. A. The Emergence of Artemisinin Partial Resistance in Africa: How Do We Respond? *Lancet Infect. Dis.* **2024**, *24* (9), e591–e600.

(78) Kapale, S. S.; Chaudhari, H. K. Niclosamide and Challenges in Chemical Modifications: A Broad Review on Enhancement of Solubility. *J. Indian Chem. Soc.* **2021**, *98* (12), 100262.

(79) Gardner, J. M. F.; Mansour, N. R.; Bell, A. S.; Helmby, H.; Bickle, Q. The Discovery of a Novel Series of Compounds with Single-Dose Efficacy against Juvenile and Adult *Schistosoma* Species. *PLoS Negl. Trop. Dis.* **2021**, *15* (7), e0009490.

(80) Leas, D. A.; Keiser, J.; Charman, S. A.; Shackleford, D. M.; Jones, J. O.; Campbell, M.; Chen, G.; Katneni, K.; Patil, R.; Hu, M.; Pham, T.; Häberli, C.; Schulze, T.T.; Neville, A. J.; Wang, X.; Dong, Y.; Davis, P. H.; Vennerstrom, J. L. Single-Dose Drug Development Candidate for Schistosomiasis. *ACS Infect. Dis.* **2024,** *10* (11), 3963–3972.

(81) Ueberall, M. E.; Berchthold, M.; Häberli, C.; Lindemann, S.; Spangenberg, T.; Keiser, J.; Grevelding, C. G. Merck Open Global Health Library *In Vitro* Screening Against *Schistosoma mansoni* Identified Two New Substances with Antischistosomal Activities for Further Development. *Parasit. Vectors*. **2025**, 18 (40), 1–20.

(82) Spaulding, A.; Sharma, A.; Giardini, M. A.; Hoffman, B.; Bernatchez, J. A.; McCall, L.; Calvet, C. M.; Ackermann, J.; Souza, J. M.; Thomas, D.; Millard, C. C.; Devine, W. G.; Singh, B.; Silva, E. M.; Leed, S. E.; Roncal, N. E.; Penn, E. C.; Erath, J.; Kumar, G. Sepulveda, Y.; Garcia, A.; Rodriguez, A.; El-Sakkary, N.; Sciotti, R. J.; Campbell, R. F. Momper, J. D.; McKerrow, J. H.; Caffrey, C. R.; Siqueira-Neto, J. L. Pollastri, M. P.; Mensa-Wilmot, K.; Ferrins, L. Identification of Substituted 4-Aminocinnolines as Broad-spectum Antiparasitic Agents. *ACS Infect. Dis.* **2025**, 11 (3), 543–795.

CHAPTER 2

LITERATURE REVIEW

2.1 Chapter Overview

In its roadmap to eliminate schistosomiasis by 2030, the WHO called for the development of drugs or vaccines but due to limited incentives, very little has been done.[1–3] Thus, this chapter briefly reviews drug discovery and development approaches and then highlights the notable efforts in antischistosomal drug development at clinical and pre-clinical stages. The chapter then discusses drug repurposing efforts in the area of antischistosomal drug discovery at hit-to-lead (H2L) stage. The chapter also discusses known, albeit few, pharmacological properties of *N*-PdzBAs, a chemotype which was explored in this research work and ends with a summary of the literature search and patent search.

2.2 Approaches to Drug Discovery and Development in Brief

There are three main kinds of drug discovery approaches: phenotypic screening, target-based approach and drug repurposing/ repositioning/ rescue. Phenotypic screening is done on whole cells/ microbes while target-based approach focuses on enzymes/ receptors, etc. The latter tends to incorporate *in silico* methods which are computed-aided simulations based on artificial intelligence/ machine learning (AI/ML). Drug repurposing is the application of an existing drug to a new indication i.e. a disease for which it was not originally targeted while drug repositioning is the medicinal chemistry optimization of a known drug or drug lead to suit another disease. Drug rescue employs medicinal chemistry optimization to improve upon the properties of a drug that has been abandoned in development or withdrawn from clinical use.[3–11] In drug development, preclinical trials (i.e. in lower animals) are followed by clinical trials i.e. in humans. Phase I (1) trials are carried out on healthy volunteers while Phase II (2) trials are carried out on a few patients. Phase III (3) trials are carried out on many patients.[12]

2.3 Recent Efforts in Antischistosomal Drug Development

Recently, there have been 10 antischistosomal vaccines in development: one in Phase III, one in Phase II, three in Phase I and five in preclinical trials.[13] Besides, several natural products have been tested against schistosomes.[14–16] However, both vaccines and natural products were beyond the scope of this research work, the focus being synthetic small molecules. No new API molecule approved as an antischistosomal drug/ vaccine[17] was found to the author's best knowledge. Several efforts have involved antimalarial drug repurposing/ repositioning.[3,17,18]

2.3.1 Approval

For decades, there has been no praziquantel formulation for children aged 3 months to 6 years. Fortunately, clinical trials for such a formulation were successfully completed in 2021 now referred to as paediatric praziquantel formulation. It is a 150 mg tablet containing the bioactive *R*-PZQ enantiomer, mannitol and sucralose to improve palatability. By 2022, the formulation's regulatory submission to the European Medicines Agency (EMA) was finalized, validated for review in the same year, then received approval as a positive opinion from EMA by 2023, was added to the list of prequalified medicines by WHO in 2024 currently rolled-out in Uganda. However, this development does not add any new API molecule to the pipeline. [19–24]

2.3.2 Phase III Clinical Trials

Cheuka had argued that there was no antischistosomal in the pipeline by 2020.[25] However, this may not be accurate since Co-Arinate®, an artemisinin-based combination therapy (Figure 10) underwent a Phase III trial against *S. haematobium* in 2019.[26]

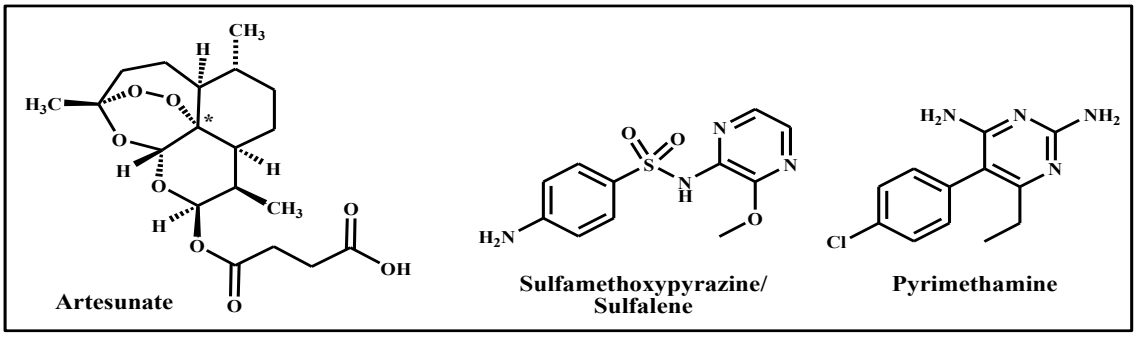

Figure 10: Structures of artesunate, sulfalene and pyrimethamine.

Actually, the first (2009) clinical trial of artesunate + sulfamethoxypyrazine + pyrimethamine against *S. haematobium* had a cure rate (CR) of 44% versus 53% for PZQ.[27] Muok and Obonyo had further shown that a single oral dose of Co-Arinate® had comparable efficacy to PZQ on *S. mansoni*-infected children.[28,29] They and others replicated this trial in 2024 with the following results. In *S. mansoni*-infected children, the CRs were 75.6%, 60.7% and 77.8%; and egg reduction rates (ERRs) were 80.1%, 85.0%, and 88.4% for PZQ, Co-Arinate, and PZQ + Co-Arinate combination, respectively, while in *S. haematobium*-infected children, the corresponding CRs were 81.4%, 71.1% and 82.2%; and ERRs were 95.6%, 97.1% and 97.7%, respectively.[30,31] Unfortunately, co-endemic malaria is resistant to artemisinin and pyrimethamine.[3,24,32–34]

2.3.3 Phase II Clinical Trials

Artesunate + mefloquine has just undergone a phase II trial proving to be non-inferior to PZQ (CR: 59.6% vs 62.1% for PZQ).[35] Moxidectin, Synriam® (piperaquine + arterolane

combination) and Synriam® + PZQ combination (Figure 11) first underwent Phase II trials against *Sh* and *Sm* in 2016 with better ERRs on *Sm*.[24,36,37]

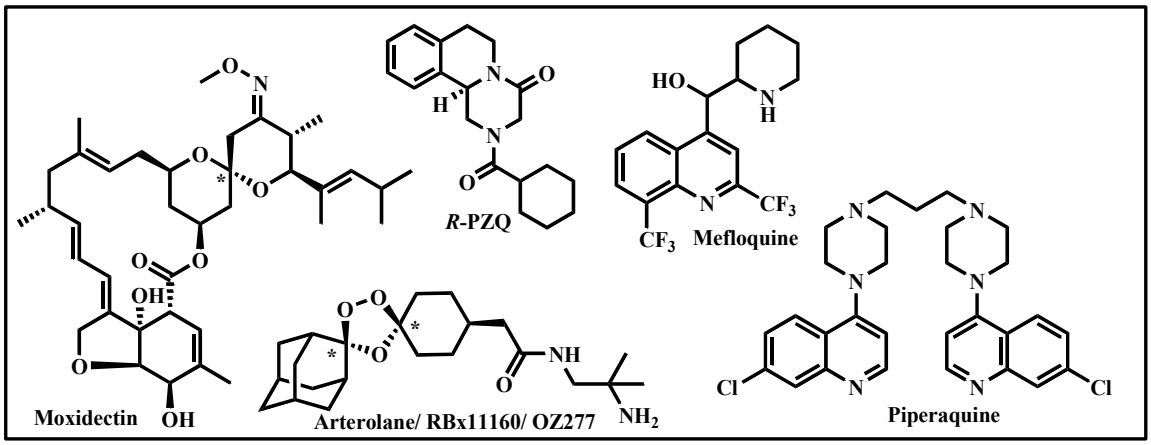

Figure 11: Structures of moxidectin, arterolane, piperaquine, mefloquine and *R*-PZQ.

Similarly, resistance to piperaquine by malaria from which they are repurposed is well-known taking into account co-infection which also affects artesunate since a common metabolite of all artemisinins/ derivatives which is dihydroartemisinin (DHA) has also shown resistance.[38]

2.3.4 Phase I Clinical Trials

No antischistosomal candidate undergoing phase I clinical trials was found at press time in this literature search to the best of the author's knowledge.

2.3.5 Pre-clinical Trials

A series of imidazopyrazines (active on both the adult and juvenile stages) is undergoing preclinical trials after being derivatized to prodrugs having initially faced solubility issues. These molecules patented under WO2018130853 were discovered by London School of Hygiene and Tropical Medine in collaboration with Salvensis and have since been adopted by Merck. The most notable molecule is **LSHTM-3642** which was a lead optimized from the hit **LSHTM-1945** from Medicines for Malaria Venture (MMV) as shown in Figure 12.[24,39–41]

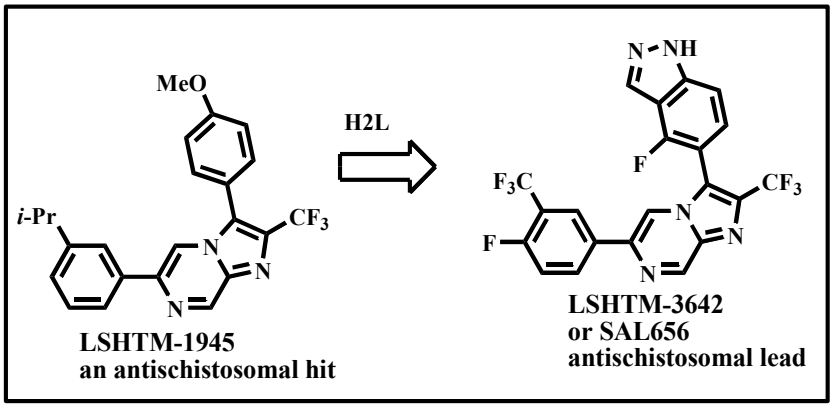

Figure 12: H2L optimization of **LSHTM-1945** to **LSTMH-3642/SAL656.**

Roche's **Ro15–5458** (Figure 13) in 2020 showed efficacy in several animal models against most schistosome species inhibiting gene expression. Its effect is similar to that of PZQ though has different binding sites and also affects the immature stages better than PZQ.[42,43] Miltefosine (Figure 13), a repurposed antileishmanial drug, in 2015 underwent preclinical trials in mice after showing significant activity against various stages of *S. mansoni in vitro*.[24,27]

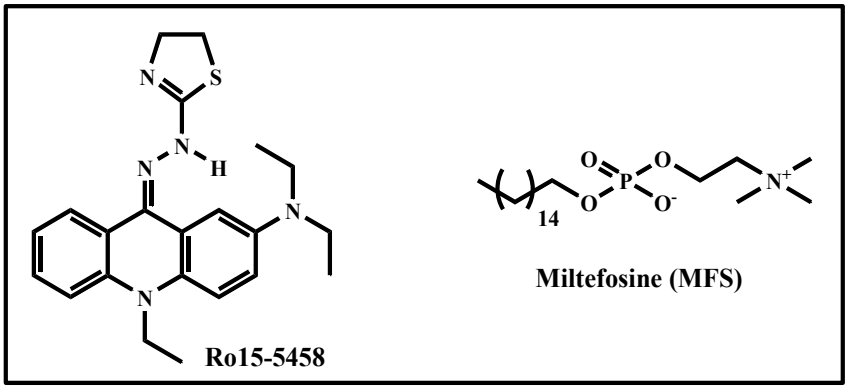

Figure 13: Structures of **Ro15-5458** and miltefosine.

2.4 Antimalarial Drug Repositioning at Hit-to-Lead Drug Discovery Stage

Schistosoma and *Plasmodium* spp (schistosomiasis and malaria pathogens, respectively) are both blood-feeding parasites and have evolved heme detoxification mechanisms as can also be inferred in their synergistic anaemic effects in co-infection.[44–47] Several drug hit compounds have originated from compound libraries, such as the MMV Malaria-, Pathogen-, etc. compound libraries so called Boxes.[48–53] SAR exploration of **MMV665852**, an *N,N*'-diphenyl urea from the Malaria Box, by Cowan *et al* and Ingram-Sieber *et al*, led to compound **35** which is an *N*-phenylbenzamide (Figure 14).[24,49,50]

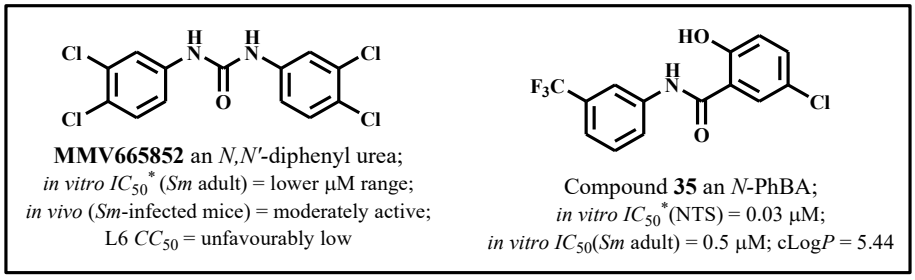

Figure 14: Structures and pharmacological data for **MMV665852** and Compound **35.**[49,50]

Compounds from the Pathogen Box were first screened *in vitro* on *S. mansoni* NTS from which 43 hits were further tested against adult worms by Pasche *et al*. From this secondary screen, 11 hits were identified and tested for albumin-binding and *in vitro* activity on adult *S.*

haematobium. **MMV687807** (Figure 15), was identified as one of the promising hits. On *in vitro* evaluation against *S. mansoni* NTS after 24 h, it showed an IC_{50} = 0.3 μM and 0.2 μM at 24 h and 72 h, respectively. (The so called 'IC_{50}' values should strictly be called *'EC_{50}'* since they are based on whole-cell screening.) On adult worms, it showed IC_{50} values of 9.7 μM, 2.6 μM, 2.2 μM, 2.3 μM and 2.1 μM at 1 h, 16 h, 24 h, 48 h and 72 h post-incubation, respectively. In the presence of albumin, IC_{50} values of 5.7 μM, 5.5 μM and 5.6 μM were reported at 24 h, 48 h and 72 h post-incubation, respectively. This hit compound was lethal on screening *in vitro* at 10 μM against adult *Sh* worms at 24 h, 48 h and 72 h post-incubation.[51] MMV has since reported its chromatographic Log*D* (ChromLog*D*) as 5.14 higher than the Lipinski's Rule of 5 cut-off (5) and 20% cytotoxic concentration on human hepatoma cells (HepG2 CC_{20}) as 0.658 μM (<< 80 μM cut-off).[24,51,52]

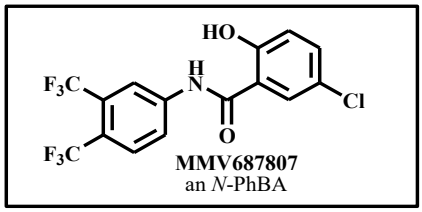

Figure 15: Structure of **MMV687807.**

Table 2 shows rat *in vivo* DMPK data for **MMV687807**.[51,52]

Table 2: Rat* *in vivo* DMPK data for **MMV687807.**[51,52]

Route/*Dose* (mg/kg)	T_{max} (h)	C^0/C_{max} (ng/mL)	AUC_{last} (ng.h/mL)	AUC_{inf} (ng.h/mL)	*CL* (mL/min/kg)	V_{dss} (L/kg)	$T_{1/2}$ (h)	*% F*
IV/*1*	N/A	640	108	110	151	16.5	2.58	-
PO/*5*#	0.625	20	29.8	33.2#	N/A	N/A	1.78#	6

Notes: *Sprague Dawley male rat; #data for n = 1 animal; *C* = concentration; T_{max} = time to maximum *C*; C^0 = initial *C*; C_{max} = maximum *C*; *AUC* = area under the curve; AUC_{last} = *AUC* up to the last data point; AUC_{inf} = *AUC* up to infinity; *CL* = clearance; V_{dss} = volume of distribution at steady state; $T_{1/2}$ = half-life; *%F* = % bioavailability; IV = intravenous; PO = oral (*per os*); N/A = non-applicable

Other parameters are also documented by MMV[51,52] but not aqueous solubility explicitly, as confirmed by email (Adam, A. (MMV). email communication, August 20, 2023). In the studies by Cowan *et al* and Pasche *et al*, trifluoromethyl (TFM) on *N*-phenyl and/ or benzoyl moieties (Figure 16) showed favourable antischistosomal activity, just as in recent **MMV687807** SAR exploration studies by Kanyanta *et al*, etc. other TFM *N*-PhBAs **MK1-11** and **MK1-09** were quite potent *in vitro* (Figure 16) which have since been repeated in this study[6].[24,49–53]

[6] Unpublished

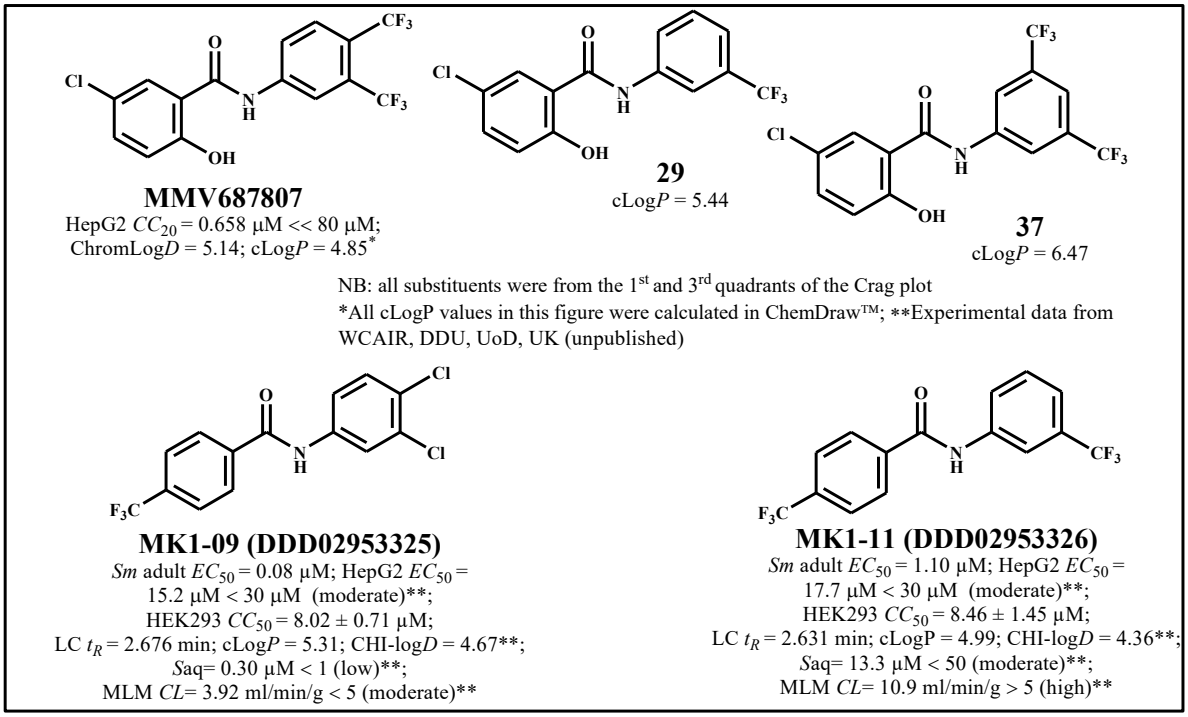

Figure 16: Structures and pharmacological data of *N*-PhBAs in Cowan *et al*, Pasche *et al* and Kanyanta *et al* studies.[49–53]

Note: CC_{20} = 20% cytotoxic concentration *(C);* CC_{50} = 50% cytotoxic *C*; Chrom = chromatographic; *CL* = clearance; cLog*P* = calculated log*P*; EC_{50} = 50% effective *C*; HEK293 = human embryonic kidney cell; HepG2 = hepatocellular carcinoma cell; LC = liquid chromatography; Log*D* = logarithm of *D*; **MK1-09** and **M1-11** (**DDD02953325** and **DDD02953326**, respectively) were first synthesized by **M**asebe **K**anyanta while DMPK studies by University of **D**undee's **D**rug **D**iscovery Unit; MLM = mouse liver microsome; S_{aq} = aqueous solubility; t_R = retention time; NB: CHI-log*D* = ChromLog*D*; HepG2 EC_{50} = HepG2 CC_{50}[41]

Like earlier studies, which unraveled compounds **29**, **35**, **37** and **MMV687807**, the studies by Kanyanta *et al* also demonstrated the importance of electron withdrawing groups (EWGs) to activity (EC_{50}) with respect to the *N*-Ph ring. 3,4-Cl was less active than 3-CF_3. This was also observed for polarity in terms of LC t_R with respect to the *N*-Ph ring. 3,4-Cl was less polar than 3-CF_3. Similar trends can be observed for cLog*P*, Log*D* and solubility (Figure 16).[49–53]

2.5 Poor Physicochemical Properties of *N*-PhBAs

In the phenotypic screens referred to above conducted by Cowan *et al*, Ingram-Siber *et al* and Pasche *et al*, measured aqueous solubilities of some of the hit compounds were low.[49–51] Niclosamide (Figure 17), an *N*-PhBA, which has undergone repositioning for schistosomiasis, etc., has not been successfully optimized due to poor solubility.[24,54–56]

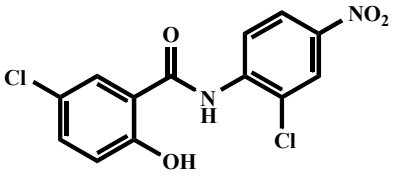

Figure 17: Niclosamide, a poorly soluble extensively repositioned *N*-PhBA.

2.6 The Pyridazine Scaffold in Medicinal Chemistry Optimization

Pyridazine (Pdz) is a six-membered aromatic heterocycle with two adjacent nitrogens. Pdz is less lipophilic, with a weak basicity, a high dipole moment and dual hydrogen-bonding capacity, which contribute to the lower Log*P* (cLog*P* = -0.58) and Log*D* as well as improved crystalline salts compared to phenyl (cLog*P* = 2.14).[57] A study concluded that about half of all drugs contain a phenyl ring which can be either substituted or not i.e. with heterocycles e.g. pyridazine, to improve physicochemical properties.[58] In another study, diazepam was derivatized to a pyridazine derivative to improve solubility (Figure 18):[57]

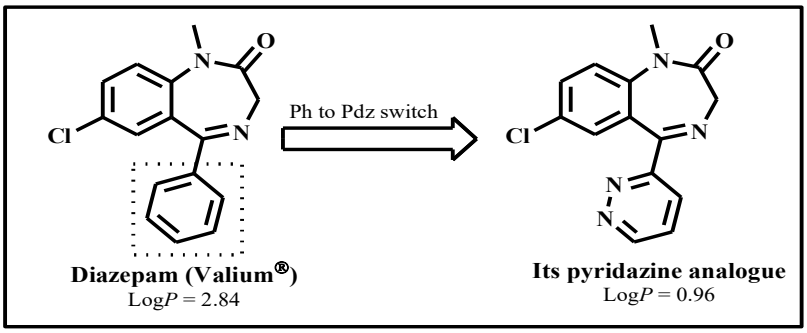

Figure 18: Attenuation of Log*P* of diazepam via a phenyl to pyridazine switch.[57]

In yet another study, minaprine was salted in as a soluble crystalline powder based on the hydrogen-bonding capacity of pyridazine – in addition to that of morpholine (Figure 19).[57]

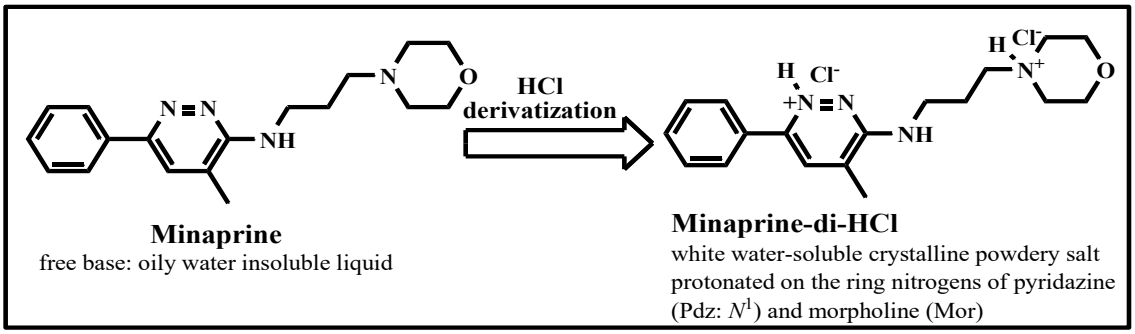

Figure 19: Solubility optimization of minaprine via a pyridazine-morpholine salting in.[57]

Although **MK1-09** and **MK1-11** have marked *in vitro* antischistosomal activity (section 2.4, a study which has been since repeated alongside the *N*-PdzBA analogues in this study[7]),[54] they have unfavourable cLog*P* values and which have indeed been confirmed by log*D* and solubility experimental values.[8] These could negatively impact other physicochemical parameters and developability profile of this earlier series of *N*-PhBAs. Hence, in this research work their *N*-phenyl ring was replaced with a pyridazine to form *N*-PdzBAs, to optimize Log*P*

[7] Unpublished
[8] Unpublished

and solubility. Studies have reported increased inhibition of cytochrome P450 (CYP), on phenyl to Pdz substitution.[58–62] Phenyl (Ph) to Pdz derivatization can increase, reduce or maintain potency.[63,64] In a survey involving replacing a Pdz with a Ph (i.e. a reverse substitution to that of this research work), etc.: 16% reduced, 47% maintained and 37% increased potency.[63] In another study, a Ph analogue, i.e. **27,** exhibited much better inhibition of phosphatidylinositol-3-kinase delta (PI3Kδ) relative to that of Pdz, i.e. **29** (Table 3).[64]

Table 3: PI3Kδ IC_{50} SAR explorations of phenyl versus 6-membered heterocycles.[64]

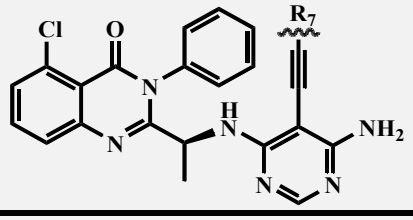

Compd code	R_7	PI3Kδ IC_{50} (nM)	Comment
27	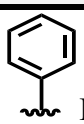 Ph	0.3	Potency in terms of the PI3Kδ IC_{50} decreases with increasing numbers on nitrogens in the R_7 aromatic ring since the lower the concentration the more potent
28	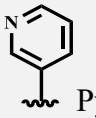 Py	0.5	
30	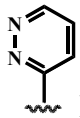 Pdz	240	

2.7 Pharmacological Properties of *N*-PdzBAs

In 2022, a study reported an *N*-PdzBA derivative as an anti-COVID19 compound where the pyridazine nitrogens were key in target binding (Figure 20).[65]

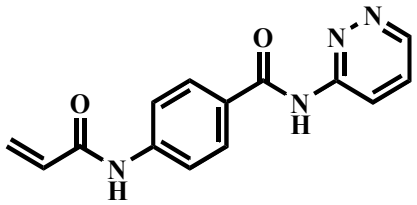

Figure 20: Structure of 4-acrylamido-*N*-pyridazin-3-ylbenzamide, an *N*-PdzBA anti-COVID19 compound

In 2019, another study reported *N*-pyridazinylbenzamides with high potencies of leucine-rich repeat kinase 2 inhibition, improved physicochemical properties with promising Parkinson's disease utility.[66] No antischistosomal *N*-PdzBAs were found in this literature search and patent search to the best of the author's knowledge (Table 4).

Table 4: Summary of literature search and patent search.

Literature	Findings	Knowledge Gap
Fortin and Jansen, **2011**;[26] Muok *et al*, **2024**;[29] Obonyo *et al,* **2024**[30]	Co-Arinate® (artesunate + sulfalene + pyrimethamine) had comparable efficacy to PZQ on *Sh* and *Sm* in Phase III trials with a cure rate (CR) of 44% (vs 53% PZQ);[26,29,30] (patented WO2007028413A1)[67]	Combinations involved drugs for co-endemic malaria: pyrimethamine (and artesunate) resistant (to the close analogue artemisinin) especially in co-infection since their common metabolite DHA has also been shown to be resistant[3,31]
Bottieau *et al,* **2024**[35]	Artesunate + mefloquine had a comparable CR (59.6%): PZQ (62.1%) on *Sh* in Phase II clinical trial[35]	Combinations involved drugs for co-endemic malaria: both mefloquine and artesunate (and its metabolite DHA) resistant especially in co-infection[3,35]
Barda *et al,* **2016**[36]	Moxidectin, Synriam® (piperaquine + arterolane), Synriam + PZQ in Phase II trial on *Sh; Sm* with better egg reduction rates (ERRs) on *Sm;*[36] (application for No. PCT/IB2021/057494)[68]	Combinations involved drugs for co-endemic malaria (piperaquine) especially in co-infection, to which it is resistant and PZQ with already known SCH resistance[38]
Pasche *et al,* **2018**[51]	**MMV687807** (*N*-PhBA): active on *Sh*, *Sm in vitro, in vivo* rats[51,52] (both spp endemic to Zambia)	Unfavourably, Log*D* was high (5.14) and aqueous solubility (S_{aq}) was low;[51,52] hence unsuitable for regular oral use
Gardner *et al,* **2021**[39,40]	**LSHTM1945** SAR study found **LSHTM3642/SAL656,** etc. imidazopyrazines 8× more potent than PZQ on *Schistosoma* spp *in vivo* mice now in pre-clinical trials (WO2018130853)[39,40]	S_{aq} was low;[39,40] this is explainable from the flat aromatic rings and polyhalogenation; unsuitable for regular oral use. This is being circumvented by the prodrug approach.[41]
Xu *et al,* **2023**;[69] Ja'afaru *et al*, **2024**[70]	PZQ SAR studies found **P96** as only active analogue *in vitro*, (PZQ has tight SAR);[69] Compd **17a** by ligand-based discovery[70]	**P96** active only on *S. japonicum (Sj)* endemic to Japan (eradicated) etc. Asia[69] not Zambia/ Africa; For compound **17a**, more wet experimental assays needed[70]
Kanyanta *et al,* **2023**[53]	**MMV687807** SAR found *N*-PhBAs potent on *Sm in vitro*: e.g. **MK1-09**, **MK1-11**, etc[53]	t_R, cLog*P*, Log*D* (and cytotoxicity) were high[53] hence their S_{aq} was low[9] like other *N*-PhBAs;[51,52] hence orally unavailable

[9] Unpublished

2.8 References

(1) Diaz, A. V.; Walker, M.; Webster, J. Reaching the World Health Organization Elimination Targets for Schistosomiasis: The Importance of a One Health Perspective. *Phil. Trans. R. Soc. B.* **2023**, *378* (1887), 20220274.

(2) Spangenberg, T. Alternatives to Praziquantel for the Prevention and Control of Schistosomiasis. *ACS Infect. Dis.* **2021**, *7* (5), 939–942.

(3) Chibale, K. *Medicinal Chemistry Approaches to Malaria and Other Tropical Diseases;* Academic Press, **2019**.

(4) Hikaambo, C. N.; Shakela, N.; Woodland, J. G.; Wicht, K. J.; Chibale, K. Drug Discovery in Africa Tackles Zoonotic and Related Infections. *Sci. Transl. Med.* **2023**, *15* (718), eadj0035.

(5) Lago, E. M.; Silva, M. P.; Queiroz, T. G.; Mazloum, S. F.; Rodrigues, V. C.; Carnaúba, P. U.; Pinto, P. L.; Rocha, J. A.; Ferreira, L. L. G.; Andricopulo, A. D.; de Moraes, J. Phenotypic Screening of Nonsteroidal Anti-Inflammatory Drugs Identified Mefenamic Acid as a Drug for the Treatment of Schistosomiasis. *EBioMedicine.* **2019**, *43*, 370–379.

(6) Roquini, V.; Mengarda, A. C.; Cajas, R. A.; Martins-da-Silva, M. F.; Godoy-Silva, J.; Santos, G. A.; Espírito-Santo, M. C. C.; Pavani, T. F. A.; Melo, V. A.; Salvadori, M. C.; Teixeira, F. S.; Rando, D. G. G.; de Moraes, J. The Existing Drug Nifuroxazide as an Antischistosomal Agent: *In Vitro, In Vivo,* and *In Silico* Studies of Macromolecular Targets. *Microbiol. Spectr.* **2023**, *11* (4), e0139323.

(7) Daina, A.; Michielin, O.; Zoete, V. SwissADME: A Free Web Tool to Evaluate Pharmacokinetics, Drug-likeness and Medicinal Chemistry Friendliness of Small Molecules. *Sci. Rep.* **2017**, *7* (1), 42717.

(8) Silva, L. M. N.; França, W. W. M.; Santos, V. H. B.; Souza, R. A. F.; Silva, A. M.; Diniz, E. G. M.; Aguiar, T. W. A.; Rocha, J. V. R.; Souza, M. A. A.; Nascimento, W. R. C.; Lima Neto, R. G.; Cruz Filho, I. J.; Ximenes, E. C. P. A.; Araújo, H. D. A.; Aires, A. L.; Albuquerque, M. C. P. A. Plumbagin: A Promising *In Vivo* Antiparasitic Candidate against *Schistosoma mansoni* and *In Silico* Pharmacokinetic Properties (ADMET). *Biomedicines.* **2023**, *11* (9), 2340.

(9) Andong, B.; Onyeka, S.; Ekemini, V.; Effiong, M.; Chinonso, J.; Udofot, A.; Ebong, A.; Esename, F.; Omotos, A.; Eseyin, O. Repurposing Sirolimus as a Single and Combination Therapy for Malaria. In: *Proceedings of the Drug Discovery Africa Conference*, Accra, March **2025** (DDAC25). https://d1ssu070pg2v9i.cloudfront.net/pex/wcair/2025/02/27202655/Drug-Discovery-Africa-Abstract-Book.pdf (accessed 2025-03-14)

(10) Mambwe, D. Repositioning Astemizole for Malaria. PhD Thesis, University of Cape Town, Cape Town, South Africa, **2021**.

(11) Hikaambo, C.; Masike, K.; Salomane, N.; Coulson, L.; Woodland, J. G.; Wicht, K. J.; Chibale, K. Repositioning the Anticancer Agent **MLN0128** as an Inhibitor of *Plasmodium* Phosphatidylinositol 4-kinase (PI4K) via a Targeted Covalent Inhibitor approach. In: *Proceedings of the Drug Discovery Africa Conference*, Accra, March **2025** (DDAC25). https://d1ssu070pg2v9i.cloudfront.net/pex/wcair/2025/02/27202655/Drug-Discovery-Africa-Abstract-Book.pdf (accessed 2025-03-14)

(12) Patrick, G. L. *An Introduction to Medicinal Chemistry*, 7th ed.; Oxford University Press, **2023**.

(12) Molehin, A. J. Schistosomiasis Vaccine Development: Update on Human Clinical Trials. *J. Biomed. Sci*. **2020**, *27* (1), 28.

(14) Mtemeli, F.; Ndlovu, J.; Mugumbate, G.; Makwikwi, T.; Shoko, R. Advances in Schistosomiasis Drug Discovery Based on Natural Products. *All Life.* **2022**, *15* (1), 608–623.

(15) Azevedo, C. M.; Meira, C. S.; da Silva, J. W.; Moura, D. M. N.; de Oliveira, S. A.; da Costa, C. J.; Santos, E. de S.; Soares, M. B. P. Therapeutic Potential of Natural Products in the Treatment of Schistosomiasis. *Molecules.* **2023**, *28* (19), 6807.

(16) Ueberall, M. E.; Berchthold, M.; Häberli, C.; Lindemann, S.; Spangenberg, T.; Keiser, J.; Grevelding, C. G. Merck Open Global Health Library *In Vitro* Screening Against *Schistosoma mansoni* Identified Two New Substances with Antischistosomal Activities for Further Development. *Parasit. Vectors*. **2025**, 18 (40), 1–20.

(17) World Health Organization. *Global Report on Neglected Tropical Diseases 2023.* World Health Organization. **2023**. https://iris.who.int/bitstream/handle/10665/365729/9789240067295-eng.pdf?sequence=1 (accessed 2024-02-29).

(18) Villamizar-Monsalve, M.; López-Abán, J; Vicente, B.; Peláez, R.; Muro, A. Current Drug Strategies for the Treatment and Control of Schistosomiasis. *Expert Opin. Pharmacother.* **2024**, *25* (4), 409–420.

(19) Al-Obaidi, I.; Krome, A. K.; Wagner, K. G.; Pfarr, K.; Kuesel, A. C.; Batchelor, H. K. Drugs for Neglected Tropical Diseases: Availability of Age-appropriate Oral Formulations for Young Children. *Parasit. Vectors*. **2022**, *15* (1), 462.

(20) N'goran, E. K.; Odiere, M. R.; Aka, R. A.; Ouattara, M.; Aka, N. A. D.; Ogutu, B.; Rawago, F.; Bagchus, W. M.; Bödding, M.; Kourany-Lefoll, E.; Tappert, A.; Yin, X.; Bezuidenhout, D.; Badenhorst, H.; Huber, E.; Dälken, B.; Haj, O.; Saflo, O. H. Efficacy, Safety, and Palatability of Arpraziquantel (L-Praziquantel) Orodispersible Tablets in Children Aged 3 Months to 6 Years Infected with *Schistosoma* in Côte d'Ivoire and Kenya: An Open-Label, Partly Randomised, Phase 3 Trial. *Lancet. Infect. Dis.* **2023**, 23 (7), 867–876.

(21) Mutapi, F.; Garba, A.; Woolhouse, M.; Kazyoba, P. Paediatric Schistosomiasis: Last Mile Preparations for Deploying Paediatric Praziquantel. *Trends Parasitol.* **2024**, *40* (8), 678–695.

(22) Stothard, J. R. Schistosomiasis Treatment in Young Children: A Welcome Step Towards Deployment of the Paediatric Praziquantel Formulation. *Int. Health*. **2025**, 0, 1–3.

(23) Bustinduy, A. L.; Edielu, A.; Ayebazibwe, G. K.; Nakyesige, R.; Anguajibi, V.; Mpooya, S.; Nassuna, J.; Adriko, M.; Elliott, A.; van Dam, G.; Corstjens, P.; Pach, S.; Wu, H.; Colt, S.; Mawa, P. A.; Muheki, E.; Kabatereine, N. B.; Webb, E. L.; Friedman, J. F. Safety and Efficacy of Praziquantel 40 mg/kg Versus 80 mg/kg in Preschool-aged Children with Intestinal Schistosomiasis in Uganda: A 2 × 2 Factorial, Double-blind, Placebo-controlled, Phase 2 Randomised Trial. *Lancet Glob. Health.* **2025**, *13*, e1091–1100.

(24) Banda, H.; Abere, A. Navigating the Challenge of Praziquantel Resistance in Schistosomiasis: Molecular Mechanisms and Future Directions. *Discover. Med.* **2025**, *2* (105).

(25) Cheuka, P. M. Drug Discovery and Target Identification against Schistosomiasis: A Reality Check on Progress and Future Prospects. *Curr. Top. Med. Chem.* **2021**, *22* (19), 1595–1610.

(26) Fortin, A.; Jansen, F. H. ACTs for the Treatment of Schistosomiasis. *Lancet. Infect. Dis*. **2011**, *11* (7), 498.

(27) Weber, C. J.; Hargan-Calvopiña, J.; Graef, K. M.; Manner, C. K.; Dent, J. WIPO Re:Search – A Platform for Product-centered Cross-sector Partnerships for the Elimination of Schistosomiasis. *Trop. Med. Infect. Dis.* **2019**, *4* (1), 11.

(28) Sissoko, M. S.; Dabo, A.; Traoré, H.; Diallo, M.; Traoré, B.; Konaté, D.; Niaré, B.; Diakité, M.; Kamaté, B.; Traoré, A.; Bathily, A.; Tapily, A.; Touré, O. B.; Cauwenbergh, S.; Jansen, H. F.; Doumbo, O. K. Efficacy of Artesunate + Sulfamethoxypyrazine/Pyrimethamine versus Praziquantel in the Treatment of *Schistosoma haematobium* in Children. *PLoS One.* **2009**, *4* (10), e6732.

(29) Muok, E. M. O.; Were, V. O.; Obonyo, C. O. Efficacy and Safety of a Single Oral Dose Artesunate plus Sulfalene-Pyrimethamine Versus Praziquantel in the Treatment of *Schistosoma mansoni* in Kenyan Children: An Open-Label, Randomized, Exploratory Trial. *Am. J. Trop. Med. Hyg.* **2024**, *110* (4), 677–680.

(30) Obonyo, C. O.; Were, V.O.; Wamae, P.; Muok, E. M. O. Efficacy and Safety of Praziquantel plus Artemisinin-based Combinations versus Praziquantel in the Treatment of Kenyan Children with *Schistosoma mansoni* Infection: Open-label, Randomized, Head-to-head, Non-inferiority Trial. *Antimicrob. Agents Chemother*. **2024**, e0073924.

(31) Guémas, E.; Coppée, R.; Ménard, S.; du Manoir, M.; Nsango, S.; Makaba Mvumbi, D.; Nakoune, E.; Eboumbou Moukoko, C. E.; Bouyou Akotet, M. K.; Mirabeau, T. Y.; Manguin, S.; Malekita Yobi, D.; Akiana, J.; Kouna, L. C.; Mawili Mboumba, D. P.; Voumbo-Matoumona, D. F.; Otam, A. L.; Rubbo, P. A.; Lombart, J. P.; Kwanai, E.; Cohen, O.; Iriart, X.; Ayong, L.; Lekana-Douki, J. B.; Ariey, F.; Berry, A. Evolution and Spread of *Plasmodium falciparum* Mutations Associated with Resistance to Sulfadoxine–Pyrimethamine in Central Africa: A Cross-Sectional Study. *Lancet. Microbe.* **2023**, *4* (24), 983–993.

(32) Cheuka, P. M.; Njaria, P.; Mayoka, G.; Funjika, E. Emerging Drug Targets for Antimalarial Drug Discovery: Validation and Insights into Molecular Mechanisms of Function. *J. Med. Chem.* **2024**, *67* (2), 838–863.

(33) Muhammed, H.; Balogun, J. B.; Dogara, M. M.; Adewale, B.; Ibrahim, A. A.; Okolugbo, C. B.; Jackson, G. Co-infection of Urogenital Schistosomiasis and Malaria and Its Association with Anaemia and Malnutrition amongst Schoolchildren in Dutse, Nigeria. *S. Afr. J. Sci.* **2023**, *119* (7/8), 1–12.

(34) Dassah, S. D.; Nyaah, K. E.; Senoo, D. K.; Ziem, Z. B.; Aniweh, Y.; Amenga-Etego, L.; Awandare, G. A.; Abugri, J. Co-infection of *Plasmodium falciparum* and *Schistosoma mansoni* is Associated with Anaemia. *Malar. J.* **2023**, *22* (1), 272.

(35) Bottieau, E.; Mbow, M.; Brosius, I.; Roucher, C.; Gueye, C. T.; Mbodj, O. T.; Faye, B. T.; De Hondt, A.; Smekens, B.; Arango, D.; Burm, C. Antimalarial Artesunate–Mefloquine versus Praziquantel in African Children with Schistosomiasis: An Open-label, Randomized Controlled Trial. *Nat. Med.* **2024**, *30* (1), 130–137.

(36) Barda, B.; Coulibaly, J. T.; Puchkov, M.; Huwyler, J.; Hattendorf, J.; Keiser, J. Efficacy and Safety of Moxidectin, Synriam, Synriam-Praziquantel versus Praziquantel against *Schistosoma haematobium* and *S. mansoni* Infections: A Randomized, Exploratory Phase 2 Trial. *PLoS Negl. Trop. Dis.* **2016**, *10* (9), e0005008.

(37) Yousof, H. A. S. A.; El-Sayed, S. H.; Elfar, E.; Khater, M. M. Repurposing of Anti-malarial Synriam and Testing Its Efficacy against Egyptian Strain of *Schistosoma haematobium*. *J. Egypt. Soc. Parasitol.* **2020**, *50* (2), 344–352.

(38) Hagenah, L. M.; Yeo, T.; Schindler, K. A.; Jeon, J. H.; Bloxham, T. S.; Small-Saunders, J. L.; Mok, S.; Fidock, D. A. *Plasmodium falciparum* African *Pf*CRT Mutant Isoforms Conducive to Piperaquine Resistance Are Infrequent and Impart a Major Fitness Cost. *J. Infect. Dis*. **2024**, jiae617.

(39) Gardner, J. M. F.; Mansour, N. R.; Bell, A. S.; Helmby, H.; Bickle, Q. The Discovery of a Novel Series of Compounds with Single-dose Efficacy against Juvenile and Adult *Schistosoma* Species. *PLoS Negl. Trop. Dis.* **2021**, *15* (7), e0009490.

(40) Caldwell, N.; Afshar, R.; Baragaña, B.; Bustinduy, A. L.; Caffrey, C. R.; Collins, J. J.; Fusco, D.; Garba, A.; Gardner, M.; Gomes, M.; Hoffmann, K. F.; Hsieh, M.; Lo, N. C.; McNamara, C. W.; Nono, J. K.; Padalino, G.; Read, K. D.; Roestenberg, M.; Spangenberg, T.; Specht, S.; Gilbert, I. H. Perspective on Schistosomiasis Drug Discovery: Highlights from a Schistosomiasis Drug Discovery Workshop at Wellcome Collection, London, September 2022. *ACS Infect. Dis.* **2023**, *9* (5), 1046–1055.

(41) Spangenberg, T. Learnings in Schistosomiasis Drug Discovery. In: *Proceedings of the Drug Discovery Africa Conference*, Accra, March **2025** (DDAC25). https://d1ssu070pg2v9i.cloudfront.net/pex/wcair/2025/02/27202655/Drug-Discovery-Africa-Abstract-Book.pdf (accessed 2025-03-14)

(42) Probst, A.; Häberli, C.; Siegel, D.; Huang, J.; Vigneron, S.; Ta, A. P.; Skinner, D. E.; El-Sakkary, N.; Momper, J. D.; Gangoiti, J.; Dong, Y.; Vennerstrom, J. L.; Charman, S. A.; Caffrey, C. R.; Keiser, J. Efficacy, Metabolism and Pharmacokinetics of **Ro 15-5458**, a Forgotten Schistosomicidal 9-Acridanone Hydrazone. *J. Antimicrob. Chemother.* **2020**, *75* (10), 2925–2932.

(43) Guirguis, F. R. Efficacy of Praziquantel and **Ro 15-5458**, a 9-Acridanone-hydrazone Derivative, against *Schistosoma hematobium*. *Drug Res.* **2003**, *53* (1), 15–5458

(44) Corrêa Soares, J. B. R.; Menezes, D.; Vannier-Santos, M. A.; Ferreira-Pereira, A.; Almeida, G. T.; Venancio, T. M.; Verjovski-Almeida, S.; Zishiri, V. K.; Kuter, D.; Hunter, R.; Egan, T. J.; Oliveira, M. F. Interference with Hemozoin Formation Represents an Important Mechanism of Schistosomicidal Action of Antimalarial Quinoline Methanols. *PLoS Negl. Trop. Dis.* **2009**, *3* (7), e477.

(45) Sun, J.; Li, C.; Wang, S. Organism-like Formation of *Schistosoma* Hemozoin and Its Function Suggest a Mechanism for Anti-malarial Action of Artemisinin. *Sci. Rep.* **2016**, *6* (1), 34463.

(46) de Villiers, K. A.; Egan, T. J. Recent Advances in the Discovery of Haem-targeting Drugs for Malaria and Schistosomiasis. *Molecules*. **2009**, *14* (8), 2868–2887.

(47) Dziwornu, G. A.; Attram, H. D.; Haberli, C.; Masike, K.; Njoroge, M.; Keiser, J. Benzimidazole Analogues Active against Adult *Schistosoma mansoni*: SAR Analyses, *In Vivo* Efficacy in Mice, and Preliminary Mechanistic Studies as Potential Inhibitors of Hemozoin Formation, *Eur. J. Med. Chem.* **2025**, *284*, 117186.

(48) Spangenberg, T.; Burrows, J. N.; Kowalczyk, P.; McDonald, S.; Wells, T. N. C.; Willis, P. The Open Access Malaria Box: A Drug Discovery Catalyst for Neglected Diseases. *PLoS One.* **2013**, *8* (6), e62906.

(49) Cowan, N.; Dätwyler, P.; Ernst, B.; Wang, C.; Vennerstrom, J. L.; Spangenberg, T.; Keiser, J. Activities of *N,N′*-Diarylurea **MMV665852** Analogs against *Schistosoma mansoni*. *Antimicrob. Agents Chemother.* **2015**, *59* (4), 1935–1941.

(50) Ingram-Sieber, K.; Cowan, N.; Panic, G.; Vargas, M.; Mansour, N. R.; Bickle, Q. D.; Wells, T. N. C.; Spangenberg, T.; Keiser, J. Orally Active Antischistosomal Early Leads Identified from the Open Access Malaria Box. *PLoS Negl. Trop. Dis.* **2014**, *8* (1), 30.

(51) Pasche, V.; Laleu, B.; Keiser, J. Early Antischistosomal Leads Identified from *In Vitro* and *In Vivo* Screening of the Medicines for Malaria Venture Pathogen Box. *ACS Infect. Dis.* **2018**, *5* (1), 102–110.

(52) Medicines for Malaria Venture. *MMV Pathogen Box Activity Biological Data SMILES Database*. Medicines for Malaria Venture, **2018**. https://www.mmv.org/sites/default/files/uploads/docs/mmv_open/Pathogen_Box_Activity_Biological_Data_Smiles.xlsx (accessed 2024-01-05).

(53) Kanyanta, M.; Lengwe, C.; Mambwe, D.; Francisco, K. R.; Liu, L. J.; Uli Sun, Y.; Amarasinghe, D. K.; Caffrey, C. R.; Cheuka, P. M. Activity of *N*-Phenylbenzamide Analogs against the Neglected Disease Pathogen, *Schistosoma mansoni*. *Bioorg. Med. Chem. Lett.* **2023**, *82*, 129164.

(54) Wu, Y. Q.; Yang, T. S.; Li, X.; Wu, J. C.; Yi, T.; Li, F. Y.; Huang, C. H.; Fan, X. L. Novel Derivatives of Niclosamide Synthesis: Its Bioactivity and Interaction with *Schistosoma japonicum* Cercariae. *Dyes Pigm.* **2011**, *88* (3), 326–332.

(55) Kapale, S. S.; Chaudhari, H. K. Niclosamide and Challenges in Chemical Modifications: A Broad Review on Enhancement of Solubility. *J. Indian Chem. Soc.* **2021**, *98* (12), 100262.

(56) D'Abbrunzo, I.; Gigli, L.; Demitri, N.; Sabena, C.; Nervi, C.; Chierotti, M. R.; Bertoni, S.; Škorić, I.; Häberli, C.; Keiser, J.; Hasa, D.; Perissutti, B. Higher-order Multicomponent Crystals as a Strategy to Decrease the IC_{50} Parameter: the Case of Praziquantel, Niclosamide and Acetic Acid. *J. Drug Deliv. Sci. Technol.* **2025**, *109*, 106974.

(57) Pharmablock Sciences. Pyridazines in Drug Discovery. *Bridging Molecules for Innovative Medicines*. **2020**. https://img01.pharmablock.com/images/guanwang/document/Resource/1583403576396 70py3v.pdf (accessed 2015-03-24)

(58) Meanwell, N. A. The Pyridazine Heterocycle in Molecular Recognition and Drug Discovery. *Med. Chem. Res.* **2023**, *32* (9), 1853–1921.

(59) Lin, S.; Liu, Z.; Hu, Y. Microwave-enhanced Efficient Synthesis of Diversified 3,6-Disubstituted Pyridazines. *J. Comb. Chem*. **2007**, 9 (5), 742–744.

(60) Taft, R. W.; Anvia, F.; Taagepera, M.; Catalan, J.; Elguero, J. Electrostatic Proximity Effects in the Relative Basicities and Acidities of Pyrazole, Imidazole, Pyridazine, and Pyrimidine. *J. Am. Chem. Soc.* **2002**, *108* (12), 3237–3239.

(61) Wermuth, C. G. Are Pyridazines Privileged Structures? *Med. Chem. Comm*. **2011**, *2* (10), 935–941.

(62) Leach, A. G.; Kidley, N. J. Quantitatively Interpreted Enhanced Inhibition of Cytochrome P450s by Heteroaromatic Rings Containing Nitrogen. *J. Chem. Inf. Model.* **2011**, *51* (5), 1048–1063.

(63) Cuozzo, A.; Daina, A.; Perez, M. A. S.; Michielin, O.; Zoete, V. SwissBioisostere 2021: Updated Structural, Bioactivity and Physicochemical Data Delivered by a Reshaped Web Interface. *Nucleic Acids Res.* **2022**, *50* (D1), D1382–D1390.

(64) Patel, L.; Chandrasekhar, J.; Evarts, J.; Haran, A. C.; Ip, C.; Kaplan, J. A.; Kim, M.; Koditek, D.; Lad, L.; Lepist, E. I.; McGrath, M. E.; Novikov, N.; Perreault, S.; Puri, K. D.; Somoza, J. R.; Steiner, B. H.; Stevens, K. L.; Therrien, J.; Treiberg, J.; Villaseñor, A. G.; Yeung, A.; Phillips, G. 2,4,6-Triaminopyrimidine as a Novel Hinge Binder in a Series of PI3Kδ Selective Inhibitors. *J. Med. Chem.* **2016**, *59* (7), 3532–3548.

(65) Sepay, N.; Chakrabarti, S.; Afzal, M.; Alarifi, A.; Mal, D. Identification of 4-Acrylamido-*N*-(Pyridazin-3yl)benzamide as Anti-COVID19 Compound: a DFTB, Molecular Docking, and Molecular Dynamics Study. *RSC Adv.* **2022**, *12* (37), 24178–24186.

(66) Ding, X.; Stasi, L. P.; Dai, X.; Long, K.; Peng, C.; Zhao, B.; Wang, H.; Sun, C.; Hu, H.; Wan, Z.; Jandu, K. S.; Philps, O. J.; Chen, Y.; Wang, L.; Liu, Q.; Edge, C.; Li, Y.; Dong, K.; Guan, X.; Tattersall, F. D.; Reith, A. D.; Ren, F. 5-Substituted-*N*-Pyridazinylbenzamides as Potent and Selective LRRK2 Inhibitors: Improved Brain Unbound Fraction Enables Efficacy. *Bioorg. Med. Chem. Lett.* **2019**, *29* (2), 212–215.

(67) Dafra Pharama NV. Artesunate/Pyrimethamine/Sulfalene. WO2007028413A1, **2005**. https://synapse.patsnap.com/drug/f00f71b43f8a49efb8c9ea0fcca82bc9#corePatent (accessed 2024-03-29)

(68) Fixed Dose Combination Drug for The Treatment of Malaria. https://patents.justia.com/patent/20220265644 (accessed 2024-03-29).

(69) Ja'afaru, S. C.; Uzairu, A.; Chandra, A.; Sallau, M. S.; Ndukwe, G. I.; Ibrahim, M. T.; Qamar, I. Ligand-based Design of Potential Schistosomiasis Inhibitors Through QSAR, Homology Modeling, Molecular Dynamics, Pharmacokinetics, and DFT Studies. *Journal of Taibah University Medical Sciences.* **2024**, *19* (2), 429–446.

(70) Xu, J.; Dong, L. L.; Sun, H.; Huang, P.; Zhang, R. Z.; Wang, X. Y.; Sun, D. Q.; Xia, C. M. Small Change, Big Difference: A Promising Praziquantel Derivative Designated **P96** with Broad-spectrum Antischistosomal Activity for Chemotherapy of Schistosomiasis Japonica. *PLoS Negl. Trop. Dis.* **2023**, *17* (7), e0011215.

CHAPTER 3

METHODOLOGY

3.1 Chapter Overview

The study was multi-centric and the materials and methods used in the design, synthesis, purification, characterization, physicochemical and pharmacological screening of target compounds are described in this chapter.

3.2 Research Design

3.2.1 Ethics Statement

All protocols, including those of the primary lab at UNZA and the IR lab at Yash Life Sciences (YLS), were in accordance with ethical approval from the Natural and Applied Sciences Research Ethics Committee (NASREC), the respective Institutional Review Board (IRB No. 00006465) Organization (IORG No. 0005376) of UNZA documented as Ref No. NASREC-2023-AUG-013 as in Appendix A. Shipment of samples between labs was done in compliance with shipment laws of various jurisdictions e.g. the United States Toxic Substance Control Act (Appendix B). Bioassays done abroad[10] at UCSD (USA) were carried out with approval by the Institutional Animal Care & Use Committee of the UCSD in accordance with protocol AN107779 which derives its authority from the US Public Health Service Policy on Humane Care & Use of Laboratory Animals, and the Animal Welfare Act & Regulations, as before.[1]

3.2.2 Screening Cascade

The research began with design and chemical synthesis. This was followed by multi-technique compound characterization protocols namely LC-MS at the UCT; UV-Vis spectroscopy at the UNZA; IR spectroscopy at YLS; and ^{1}H- and ^{13}C-NMR spectroscopy at UCT in that methodical order. This was according to the logical progression from purity determination (LC), molecule weighing (MS), chromophore determination (UV), functional group determination (IR), hydrogen atom connectivity (^{1}H-NMR) and carbon skeleton connectivity (^{13}C-NMR). This was followed by biological assays: antischistosomal adult *S. mansoni*- and *in vitro* cytotoxicity assays at UCSD and lastly physicochemical-DMPK parameters experimental and/or *in silico* methods.[1-5] Figure 21 summarizes the screening cascade.

[10] Hence no approval from the UNZA Biomedical Research Ethics Committee (BREC) (or other similar IRB) nor the National Health Research Authority (NHRA) was sought as elsewhere[2]

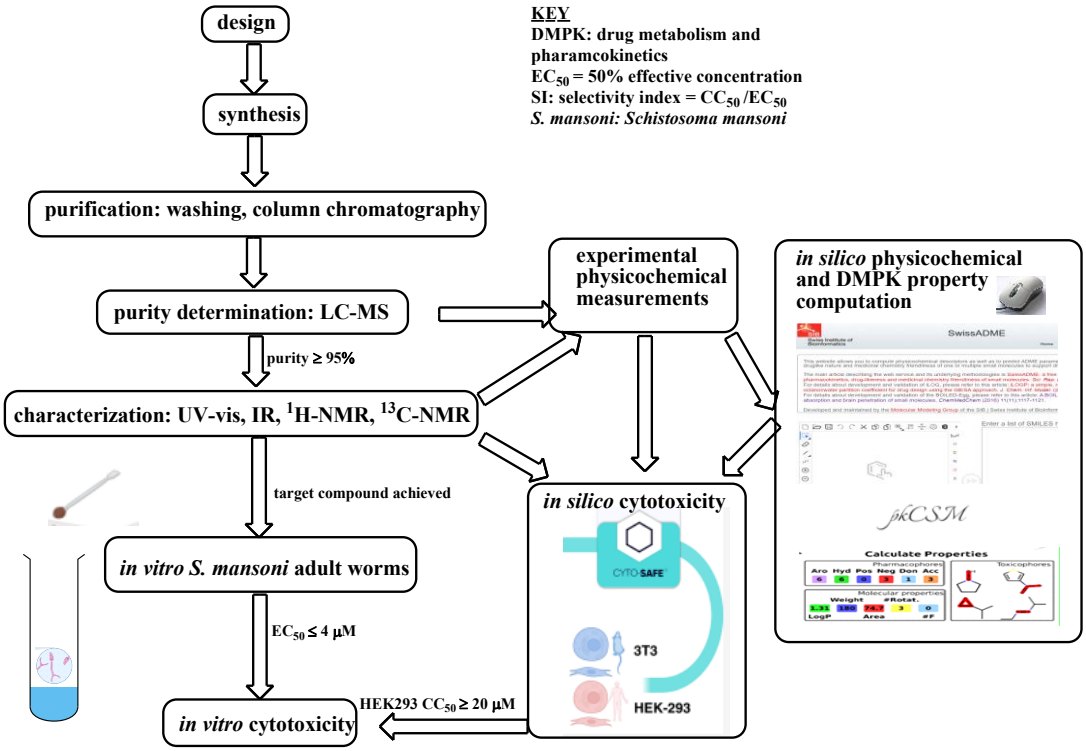

Figure 21: Screening cascade of the MSc research work.[1-5]

3.2.3 Design of Target Compounds

In this research work, a novel series of *N*-PdzBAs was designed, using the SAR exploration plan in Figure 22, replacing the *N*-phenyl ring in **MMV687807** with the *N*-pyridazin-3-yl ring.[6]

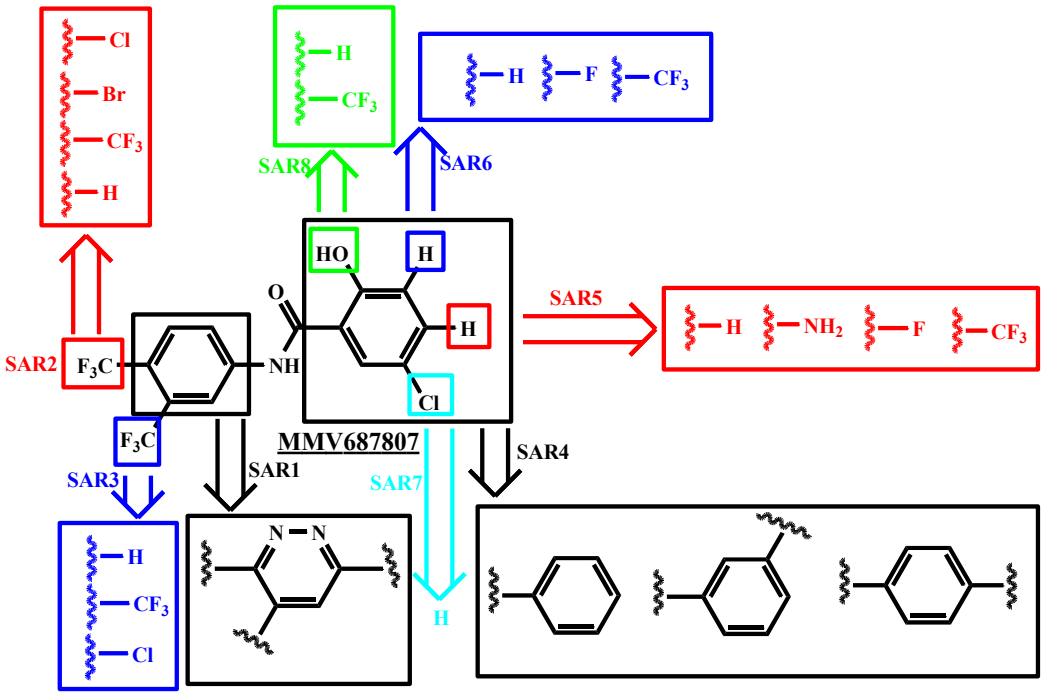

Figure 22: A graphical plan on SAR exploration on **MMV687807** to *N*-PdzBA target compounds.

The nitrogen atoms in the pyridazine scaffold were anticipated to be able to optimize physicochemical properties such as hydrophobicity, solubility and DMPK properties.[6–8] A rational quantitative SAR (QSAR) exploration approach was used in selecting which substituted analogues to synthesize. The different substituents on the *N*-PdzBA core scaffold, in this study, were selected from the Craig plot covering quadrants I and III (Figure 23).[1]

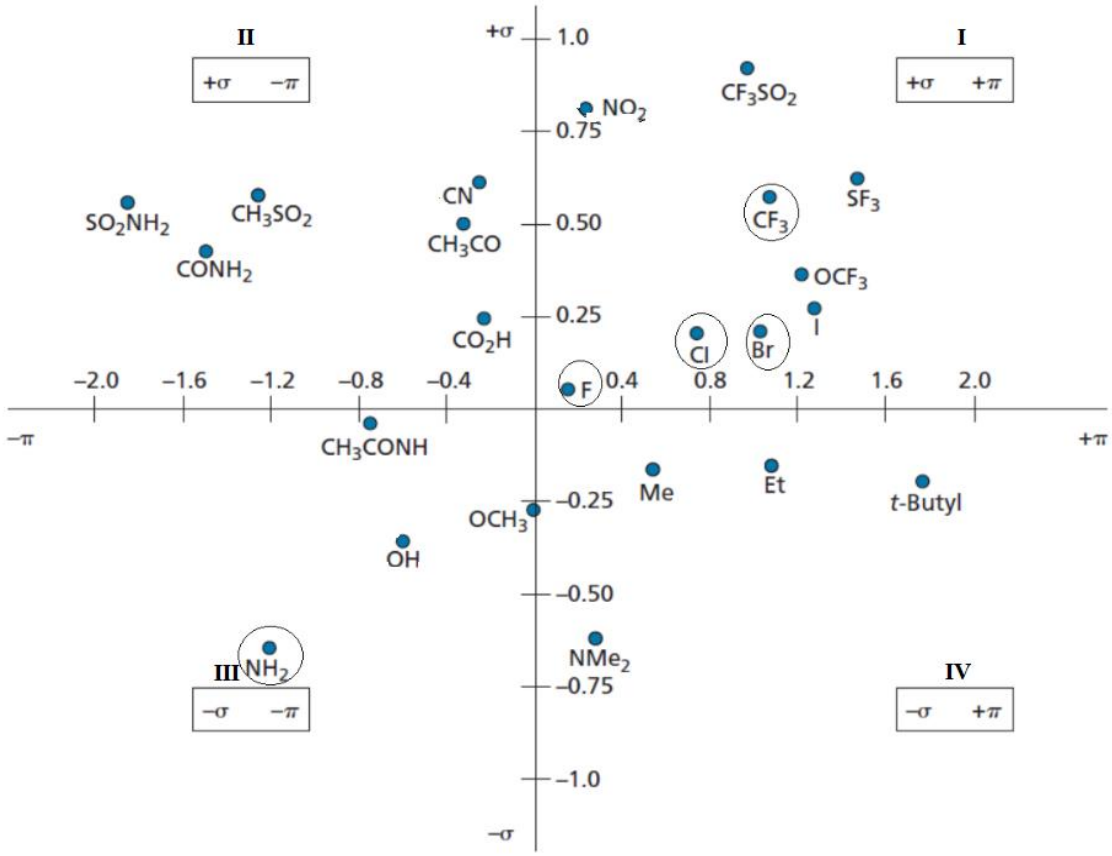

Figure 23: Craig plot highlighting substituents utilized.[a]

[a]**Source**: Adapted (with modification) from Patrick, **2023**. See Ref **9**. (Project utilized substituents encircled)

Key: π = substituent hydrophobicity (pi) constant; σ = Hammett substituent (sigma) constant; Br = bromo; CF_3 = trifluoromethyl; CF_3SO_2 = trifluoromethylsulfonyl; CH_3CO = acetyl; CH_3CONH = acetamido; CH_3SO_2 = methylsulfonyl; Cl = chloro; CN = cyano; $CONH_2$ = aminocarbonyl; CO_2H = carboxyl; Et = ethyl; F = fluoro; Me = methyl; NH_2 = amino; NMe_2 = dimethlyamino; NO_2 = nitro; OCF_3 = trifluoromethoxyl; OH = hydroxyl; SF_3 = trifluoro-λ^4-sulfanyl; SO_2NH_2 = aminosulfonyl; *t*-Butyl = tertiary butyl

This was done in order to yield the list of designed target compounds in Figure 24.[1]

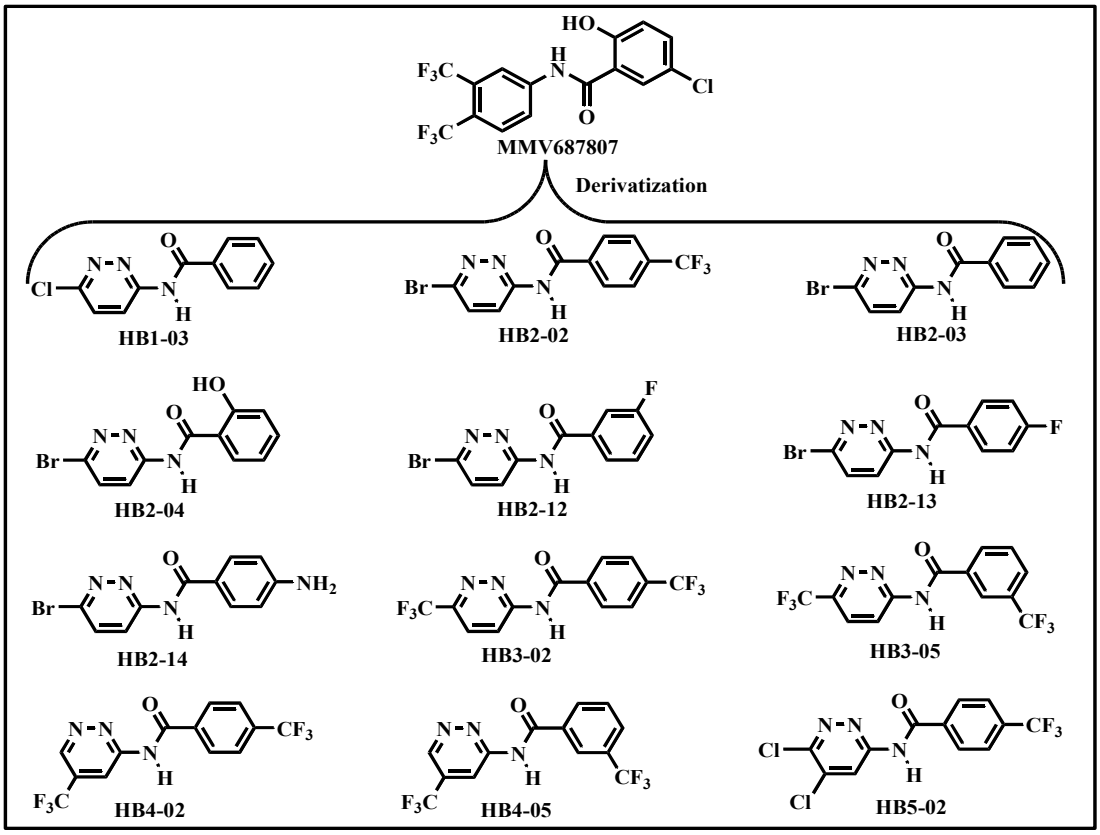

Figure 24: Structures of designed *N*-PdzBA target compounds derivatized from **MMV687807**.

Some of designed target compounds in Figure 24 were designed on an exact matched molecular pair (MMP) basis of the most potent compounds in the reference studies (Table 5) which were then collected from the UNZA MCDD chemical library and assayed alongside.[1,10]

Table 5: Comparison of *N*-PdzBAs designed on MMP basis wrt *N*-PhBAs.[1,10]

***N*-PhBA**		***N*-PdzBA[10]**	
Compd code	**Structure**	**Compd code**	**Structure**
MK1-11[1]	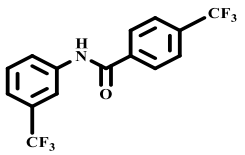	**HB4-02**	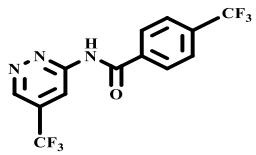
AD-3[10]	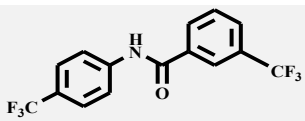	**HB3-05**	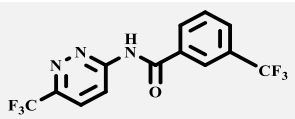
MK1-10[1]	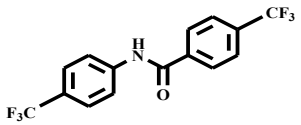	**HB3-02**	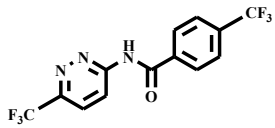
MK1-09[1]	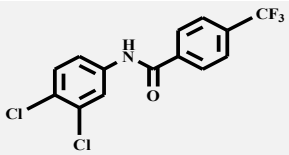	**HB5-02**	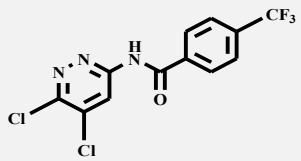

NB: Compounds on the left-hand side (LHS) were synthetized in referred to studies[1,10]

3.2.4 Adaptation of Synthetic Methods

3.2.4.1 Retrosynthetic Analysis

The disconnection approach was used in the retrosynthetic analysis shown in Figure 25.

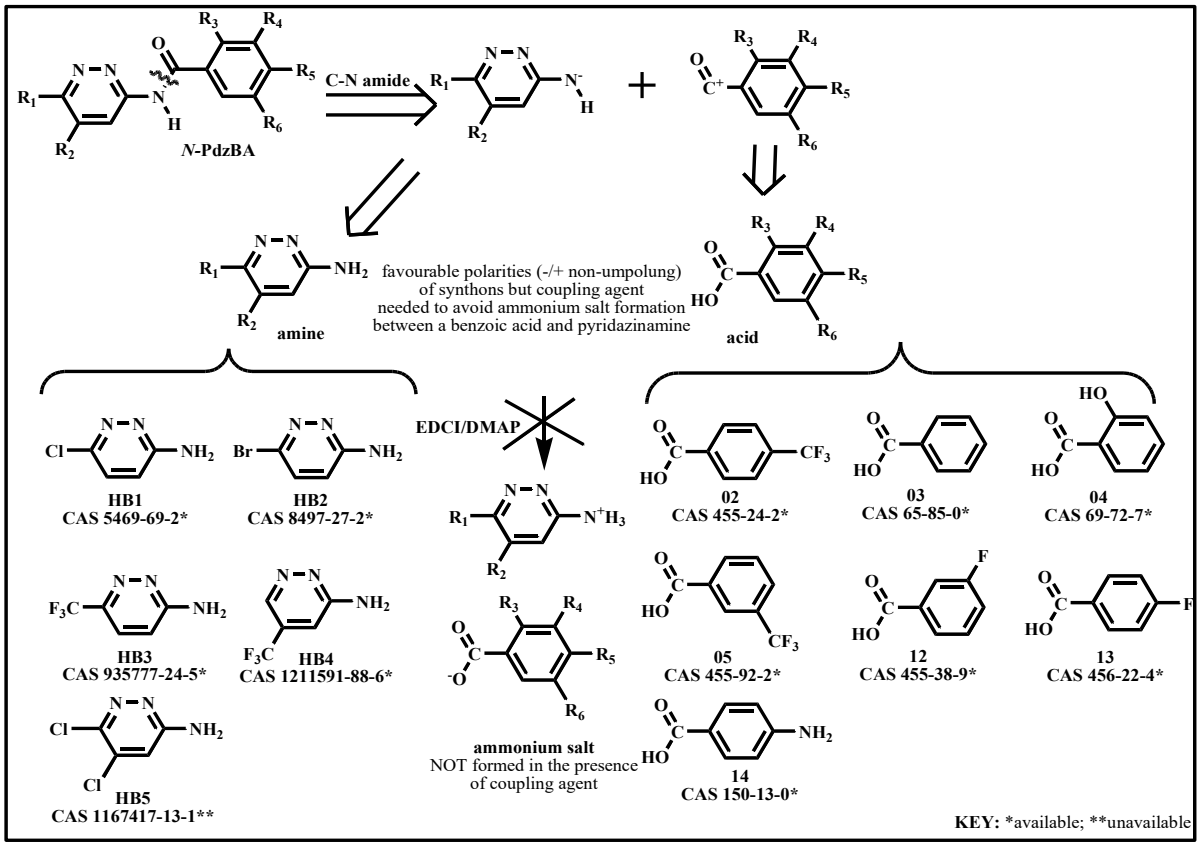

Figure 25: Retrosynthetic analysis, synthons and substrates.

3.2.4.2 Forward Synthesis: Synthetic Scheme

Figure 26 outlines the synthetic scheme adapted from those of Larsen *et al,* Prasad *et al*, Savijani *et al* and le Manach *et al,* the modification being the use of methanol (MeOH) to dissolve the 3-aminopyridazine derivative (R-Pdz-3-NH_2) *in situ*.[1,11–14]

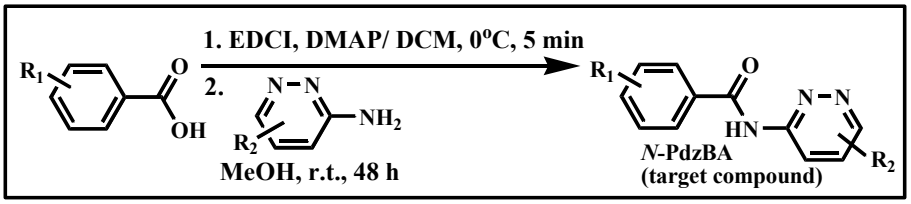

Figure 26: A one-pot generalized synthetic scheme of *N*-PdzBA analogues.[1,10]

Target compounds were realized via coupling a benzoic acid or its derivative with a R-Pdz-3-NH_2 in the presence of 1-ethyl-3-(3-dimethylaminopropyl)carbodiimide (EDCI) coupling agent and 4-dimethylaminopyridine (DMAP) catalyst in dichloromethane (DCM).[1,10]

3.3 Experimental for Chemical Synthesis

3.3.1 Materials and Equipment

The reagents and other chemicals were procured from Merck/ Sigma-Aldrich KGaA (Germany); Hi Media (India) and Chem Scene (RSA) and used without further purification.

The apparatus included Buchi Rotavapor® R-100 rotary evaporators (rotavaps), an Ohaus® Guardian™ 5000 hot plate-magnetic stirrer, Davisil® desiccators, a Marburg® UV lamp, Emil® lab thermometers (-10 – 110ºC), GallenKamp® melting point (m.p.) apparatus, a Mettler® AE100 analytical balance, a Camag TL-600® UV lamp, a Shimadzu® UV™2600i spectrophotometer in the Organic Synthesis and Drug Discovery Lab (Room 035; Figure 27, Table 6) in the Department of Pure and Applied Chemistry of the School of Natural and Applied Sciences at UNZA.

Figure 27: Buchi® rotavap components and accessories.

Table 6: Buchi® rotavap components and accessories.

Component/ Accessory	Specifications
Rotavapor	Buchi® R100
Hot bath	Buchi® B100
Recirculating chiller	Buchi® F100
Vacuum pump	Buchi® V100
Interface	Buchi® I100

Figure 28 and Figure 29 show the rest of the key apparatus in the primary and auxiliary labs at Department of Pure and Applied Chemistry at UNZA.

(a)  **(b)**  **(c)**  **(d)**  **(e)**  **(f)** 

Figure 28: Primary chemistry lab and its apparatus (a) Organic Synthesis & Drug Discovery Lab 035 (b) An Ohaus® Guardian™ 5000 stirrer (c) A Marburg® UV lamp (d) An Emil® thermometer (e) A Davisil® desiccator (f) A GallenKamp® m.p. apparatus.

Source: Pictures taken in the Department of Pure and Applied Chemistry, UNZA.

(a)  **(b)**  **(c)**  **(d)**  **(e)** 

Figure 29: Apparatus in auxiliary labs (a) A Mettler® AE100 analytical balance (Weighing Room 015) (b) An Elma® Elmasonic™ S40H sonicator (c) A Camag® TL-600 UV lamp ((b) and (c): Pharmaceutical Analysis Lab 114) (d) A Buchi® rotavap (Analytical Services/ Consulting Lab 118) (e) A Shimadzu® UV™2600i spectrophotometer (UV Lab 041).

Source: Pictures taken in the Department of Pure and Applied Chemistry, UNZA.

3.3.2 Organic Synthesis, Reaction Monitoring and Purification

3.3.2.1 General Synthetic Protocol

The following was the procedure for the synthesis of each *N*-PdzBA analogues (Figure 30). 1.5 eq of EDCI hydrochloride i.e. EDCI.HCl and 0.1 eq of DMAP were added to a 50 mL round-bottom flask containing 20 mL of ice-cooled DCM (for **HB1-03, 2-12, 2-13, 2-14, 3-02, 3-05** and **4-02**) with constant stirring on a magnetic stirrer for up to 30 min. On achieving 0°C, 1.2 eq of and appropriate benzoic acid derivative (R-BzOH) was added and allowed to continue stirring for a further 5 min. Then the mixture was removed from the ice-cold water bath and allowed to continue stirring until room temperature (r.t.) was achieved and then 1.0 eq of an aminopyridazine derivative (R-Pdz-NH_2) dissolved in 5 mL of MeOH was added to the reaction mixture. The reaction was sonicated for 5 min at 30°C and allowed to stir magnetically for 48 h at 500 rpm, while being monitored by thin layer chromatography (TLC) using 50% ethyl acetate in hexane as mobile phase.[1,10–14]

On reaction completion, the reaction mixture was taken up in 40 mL DCM; washed with water (40 mL × 3), saturated aqueous solutions of sodium bicarbonate ($NaHCO_3$: 40 mL × 4), ammonium chloride (NH_4Cl: 40 mL × 4) and finally sodium chloride (NaCl: 40 mL × 3); and dried over anhydrous sodium sulfate (Na_2SO_4). The solvent was then removed *in vacuo* on a Buchi® R100 rotavap. Since the crude products were usually very impure, they were subjected to column chromatography (EtOAc: Hex, 1: 1) and crystallized in *n*-pentane/ diethyl ether to yield the *N*-PdzBA as a solid. (*N,N*-dicyclohexylcarbodiimide (DCC) and dimethylformamide (DMF) were tried *in lieu* of EDCI and DCM, respectively, for **HB2-02**, **2-03** and **2-04** but with insufficient purities due to the water insolubility of the product and the unfavourable boiling point of DMF hence these compounds were not progressed for bioassays.)[1,10,15]

Figure 30: (a) Magnetic stirring (b) Washing (b) Column chromatography.

Source: Pictures taken in MCDD Lab 035, Department of Pure and Applied Chemistry, UNZA.

3.3.2.2 TLC, Column Chromatography and Melting Point Determination

The progress of synthetic reactions and the preparative gravity column chromatography experiments were monitored by analytical TLC. The synthesized compounds were preliminarily characterized by classical methods i.e. melting point (m.p. or T_m) and retardation factor (R_f) values before spectroscopic methods were employed. TLC Silica gel 60 F_{254} with fluorescent zinc sulfide, ZnS chromatoplates placed coated on aluminium sheets (Merck) and were visualized under UV light (λ = 256 nm). Column chromatography was used for isolation and purification. The manual glass tube column chromatography employed Hi Media silica gel at pore size 60 Å, 60-120 mesh, particle size = 74 – 250 µm for **HB1-03, HB2-02, HB2-03** and **HB2-04** and later Merck high purity grade silica gel at pore size 60 Å, 70 – 230 mesh, 63 – 200 µm for **HB2-12, HB2-13, HB2-14, HB3-02, HB3-05** and **HB4-02.** Melting points were determined in open capillary tubes with a Gallenkamp m.p. apparatus and are uncorrected.[1,10,14]

3.4 Experimental for Spectroscopic Characterization

3.4.1 LC-MS Analysis

LC-MS was used for purity determination (Figure 31,Table 7) and was strictly ultra-performance LC at ≤ 15000 psi, a pressure much higher than high performance LC (HPLC) at ≤ 6000 psi:[1,10,15]

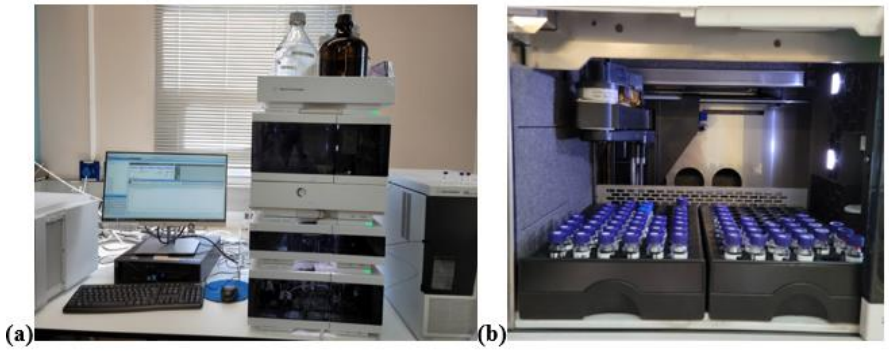

Figure 31: (a) An Agilent®1290 UPLC-Agilent®6150 MS (LC-MS) hyphenated instrument system with a controlling computer (b) Automated sampling.

Source: Pictures taken at H3D Centre, Department of Chemistry, UCT, RSA.

Table 7: LC-MS hyphenated instrument system components and accessories.[a]

Instrument	Component/ accessory	Specifications
Ultra Performance Liquid Chromatograph (UPLC: Figure 31)	Autosampler	Agilent® 1290 G7129B vial sampler
	Pump	Agilent® 1290 G7120A high speed pump
	Thermostatted column compartment (TCC)	Agilent® 1290 G1316C TCC
	Column	Kinetex® column 1.7 µm EVO® C18 100Å, 50 ID × 2.1 mm length*
	Fixed slit diode array detector (DAD FS)	Agilent® 1290 G7117A DAD FS
	Nitrogen generator	Peak Scientific® Genius™ 3010 nitrogen generator*
Mass Spectrometer (MS)	Mass analyzer	Agilent® 6150 Single Quadruple
	Ion source	Agilent® 6150 ESI^+ Jet Stream ion source

[a]**Source**: Ref **15**; *Accessory to Agilent® 1290 UPLC.
Key: C18 = octadecylsilane; ESI^+ = Electrospray Ionization (positive mode); ID = internal diameter

UPLC chromatograms are expressed as absorbance in milli-absorbance units (mAU) versus retention time (t_R) in minutes (min) having been recorded between 0 to 2.7 min. All Reverse Phase UPLC (RP-UPLC) runs were conducted using the gradient elution method in Table 8:[1,10,15]

Table 8: RP-UPLC gradient elution method parameters and conditions.*

Time (min)	Aqueous phase: 0.1% HCOOH/H_2O** A (%)	Organic phase: 0.1% HCOOH/CH_3CN B (%)	Flow rate (mL/min)
0.0	95	5	1.2
0.2	95	5	1.2
1.5	0	100	1.2
1.9	0	100	1.2
2.2	95	5	1.2
2.7	95	5	1.2

*Column temperature: 50°C; injection volume: 1 µL; **LC grade Type 1 water; **Key:** HCOOH = formic acid; H_2O = water; CH_3CN = acetonitrile

Mass spectra were recorded between 100 to 800 *m/z* expressed as percentage (%) abundance versus mass to charge ratio (*m/z*). The mass analyzer used employed electrospray ionization in the positive ionization mode i.e. ESI^+. Sample purities were established by considering the peak area on the chromatogram corresponding to the compound peak as a percentage of total peak area.[1,10,15]

3.4.2 UV-Vis Spectroscopic Analysis

One mg of each sample was dissolved in MeOH in a 10 mL measuring cylinder and the solution made to the highest mark. This was done knowing that MeOH structurally has no conjugated pi (π) electron system hence is UV-Vis inactive. Absorption spectra were recorded between 200 nm (below the 205 nm cut-off for MeOH) and 700 nm on a Shimadzu® UV™2600i spectrophotometer shown in Figure 32.[3,16]

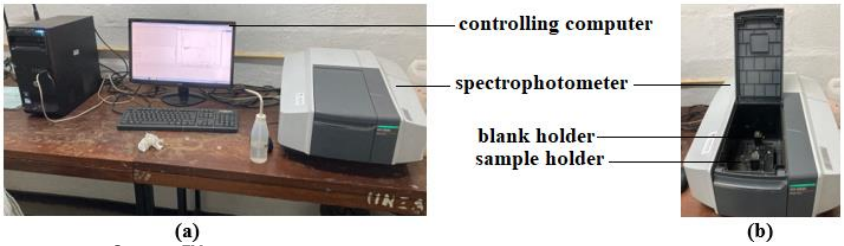

Figure 32: A Shimadzu® UV™2600i spectrophotometer and accessories (a) A spectrophotometer and a controlling computer running UVProbe®2.3 software (b) Spectrophotometer inside view.

Source: Pictures taken in the UV Lab 042 at the Department of Pure & Applied Chemistry, UNZA

The wavelength range selected was 190 - 1100 nm and were baseline-corrected, processed was via UVProbe®2.3 software expressed as absorption versus wavelength but printed from Origin®8 software.[16] The molar absorptivity *(ε_{max})* was calculated using the Beer-Lambert law (Equation 1):

$$A = \varepsilon c l$$

Equation 1: Beer-Lambert law.

Where A is absorbance, ε_{max} is molar absorptivity; ε (L mol^{-1} cm^{-1}), at the λ_{max}; c is concentration i.e. molarity (mol L^{-1}); and l is path length (cm) which, in this case, was 1 cm of the quartz cuvette.

3.4.3 IR Spectroscopic Analysis

IR measurements were done on a Shimadzu® IR™Spirit FT-IR benchtop spectrometer (Figure 33).

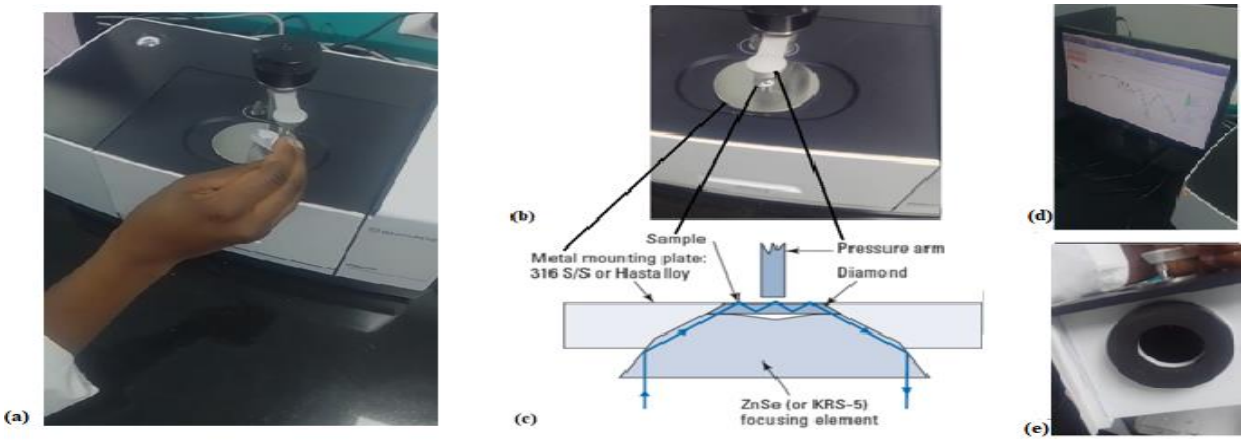

Figure 33: (a) A Shimadzu® IR-Spirit™ FT-IR spectrometer (b) QATR™-S top (c) ATR schematic diagram (d) A controlling computer running LabSolutions® software (e) QATR™-S side.

Sources: Pictures (a), (b), (d) and (e) taken during compound characterization at Yash Life Sciences (Z) Ltd, Kafue, Zambia. Image (c) reprinted from Dean *et al*, **2017**. See Ref **18**.

Each sample was loaded onto a single-reflection Attenuated Total Reflection (ATR) measurement attachment of zinc selenide (ZnSe) crystal with a diamond prism branded as a Quantum Attenuated Total Reflection™ i.e. Single reflection (QATR™-S) sample loading accessory. The IR was recorded in the wave number ($\tilde{\nu}$) range 400 – 4000 cm^{-1} at 4 cm^{-1} resolution and Happ-Genzel apodization and was converted by Fourier transformation (FT) from reflectance to percentage transmittance (%T). The IR spectra were processed using LabSolutions® software and expressed as %T versus $\tilde{\nu}$ (cm^{-1}).[17] The abbreviations used to classify intensities of absorption were: s = strong, m = medium, w = weak while those for breadth of intensity were denoted in brackets as (br) = broad, (s) = sharp and for intensity multiplicity as *d* = doublet.

3.4.4 NMR Spectroscopic Analysis

In general, both ^{1}H-NMR and ^{13}C-NMR type of NMR experiments were performed in deuterated DMSO (DMSO-d_6) using a 5 mm outer diameter sample tube inserted into a spinner. All NMR spectra were recorded at 25℃ and referenced to tetramethylsilane which was an internal standard (Figure 34).

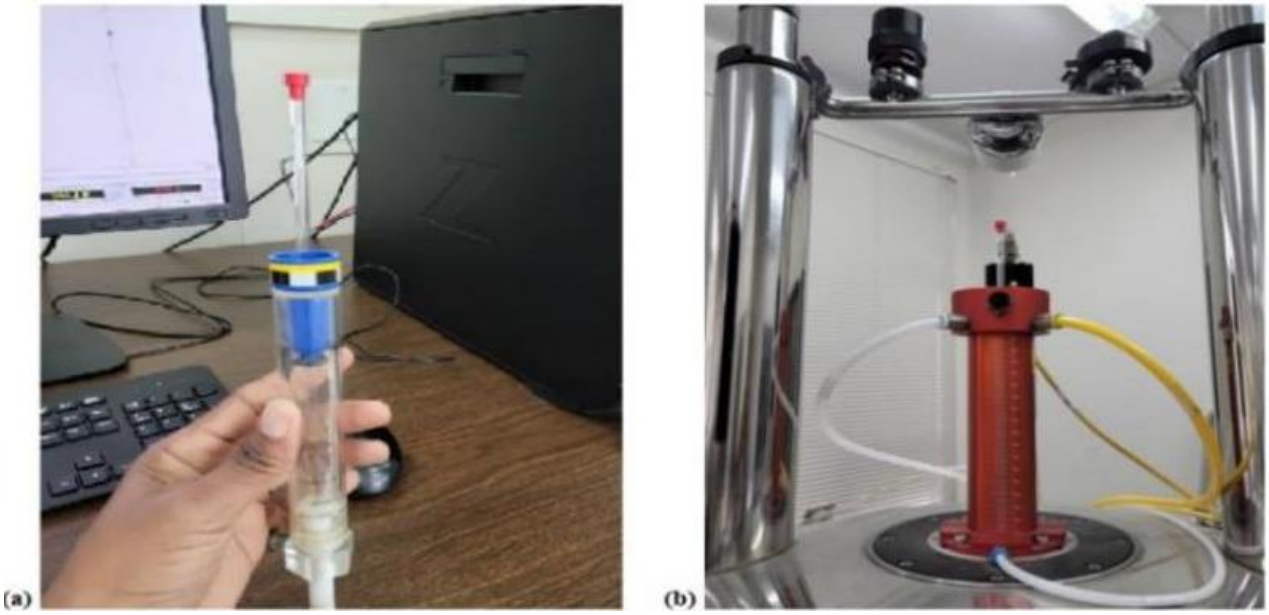

Figure 34: (a) Sample dissolution in DMSO-d_6 (b) Sample tube insertion into spinner.

Source: Pictures taken during compound characterization at H3D Centre, Department of Chemistry, UCT, RSA

Spectra were expressed as resonance intensity versus chemical shift (δ) the latter expressed as parts per million (ppm) rounded off to two decimal places. Spin-spin splitting patterns were reported using the following abbreviations: *d* = doublet, *dd* = doublet of doublets, *dt* = doublet of triplets, *m* = multiplet, *p* = pentate, *s* = singlet, *t* = triplet and *td* = triplet of doublets. Coupling constants (*J* values) were reported in hertz (Hz) to two decimal places and denoted by the number of bonds between coupling atoms (n). All NMR spectra were processed using Bruker MestRe Nova™ 14.2 Build 26256 in conjunction with ChemDraw® 15.0.[10,19–23]

3.4.4.1 ^{1}H-NMR Analysis

^{1}H-NMR spectra were acquired between -4 ppm to 16 ppm and various degeneracies on an Oxford Varian Mercury® 300 (^{1}H 300.1 MHz) NMR spectrometer run by Bruker TopSpin™ 3.7.0 (Figure 35):[51–53]

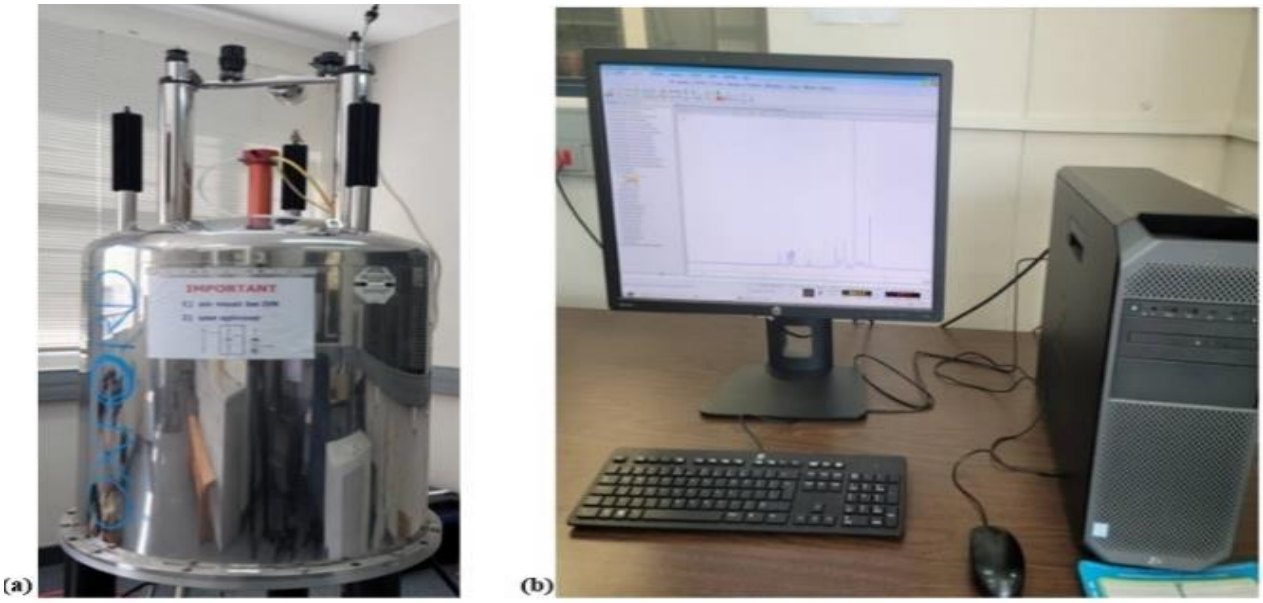

Figure 35: (a) An Oxford Varian Mercury® 300 (^{1}H 300.1 MHz) FT-NMR mononuclear spectrometer (b) A controlling computer running Bruker TopSpin™ 3.7.0 software.

Source: Pictures taken during compound characterization at H3D Centre, Department of Chemistry, UCT, RSA

Protons represented by the chemical shifts are indicated by a superscript integer (H^{n}) while the number of protons corresponding to an NMR signal is reported by an integral coefficient (nH). [21,22]

3.4.4.2 ^{13}C-NMR Analysis

^{13}C-NMR spectra were acquired between -50 ppm to 240 ppm and various degeneracies on a Bruker Ascend™ 600 (^{1}H 600.0, ^{13}C 151 MHz) multinuclear NMR spectrometer run by Bruker TopSpin™ 3.2 software (Figure 36):[23]

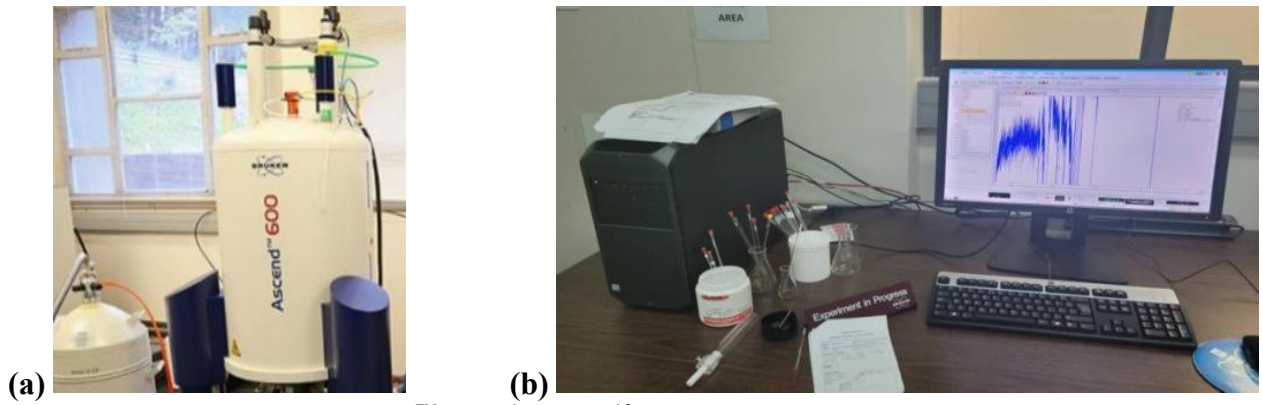

Figure 36: (a) A Bruker Ascend™ 600 (^{1}H 600, ^{13}C 151 MHz) FT-NMR multinuclear spectrometer (b) A controlling computer running Bruker TopSpin™ 3.2 software**.**

Sources: Images taken during compound characterization at H3D Centre, Department of Chemistry, UCT, RSA.

Signals for ^{13}C-NMR were obtained in the broadband proton-decoupled mode.[18,23]

3.5 Pharmacodynamic Assays

Each bioassay was performed on a sample of ≥ 95% purity whereby the *N*-PdzBAs where assayed alongside two *N*-PhBAs namely **MK1-11** and **AD-3** as known positive reference compounds.

3.5.1 *In Vitro* Adult *S. mansoni* Assays

Life cycle maintenance, preparation and co-incubation of the Naval Medical Research Institute (NMRI) isolate of *S. mansoni* adult worms (more than 42 days old) were supported in part by *Biomphalaria glabrata* intermediate snail hosts and mice definitive hosts provided by the Schistosomiasis Resource Center of the National Institute of Allergy and Infectious Diseases via Biodefense and Emerging Infections Resources Resources. Infections with *S. mansoni* were initiated by subcutaneous injections of 800 – 1000 cercariae.

3.5.1.1 Severity Score Assays on Adult *S. mansoni*

At 6 – 7 weeks post-infection, mice were euthanized with intraperitoneal injections of 50 mg/kg sodium pentobarbital and adult worms harvested by reverse perfusion of the hepatic portal system in Roswell Park Memorial Institute (RPMI) 1640 medium (Invitrogen, Carlsbad, CA). Parasite responses to chemical insult were visually recorded at 2 h, 5 h, 24 h and 48 h (Figure 37: i to iv).[1,10]

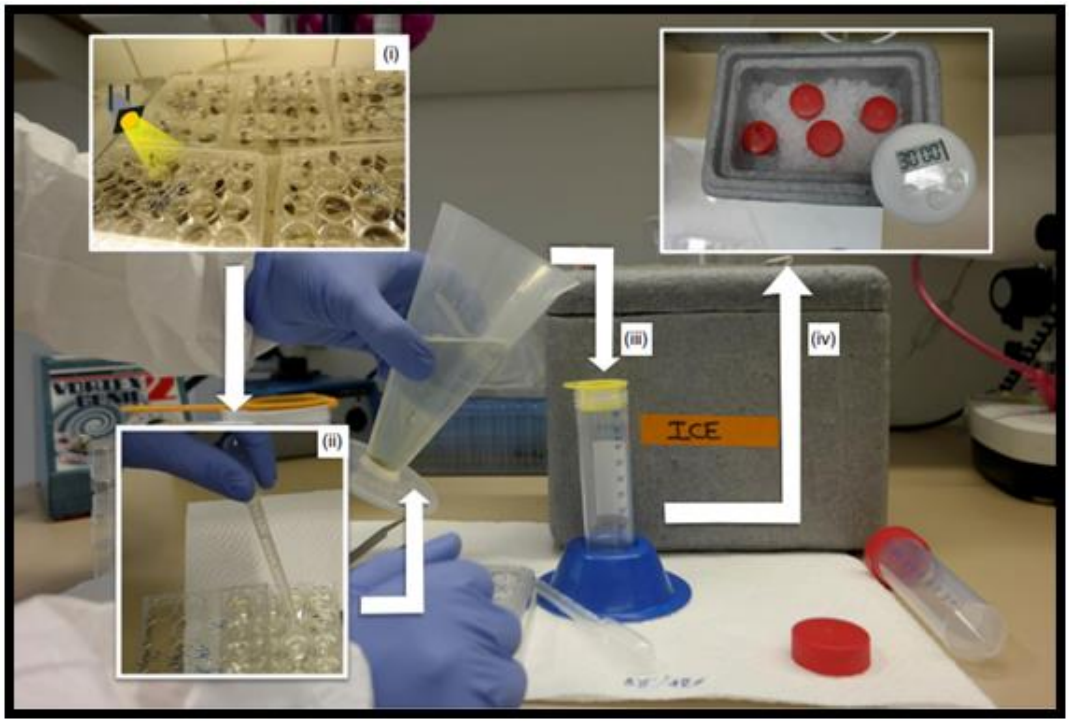

Figure 37: Severity score assay procedure.[24]

This was done sing multi-metric descriptors and severity scores from zero to 4 (maximum). Table 9 shows the phenotypic change descriptors for schistosomes on exposure to target compound.[1,10]

Table 9: Phenotypic change descriptors for schistosomes on compound exposure.*

Descriptor	Meaning	Score	Colour
	(No activity)	0	
On sides	Male worms are not adhering to dish with ventral sucker	1	
S	Slow	1	
(Slight) Shrunk	Worms are not flexing and are smaller than usual	1	
Unc	Uncoordinated movements	1	
Dark	Dark	1	
I	Immobile	2	
Deg	Degenerating	4	
Teg damage	Outer surface (tegument) of the worm is damaged	4	
D	Dead	4	

Score '**3**' coded yellow does not necessarily have an assigned descriptor so was not present on raw data but is an additive cumulative score of either any three (of five phenotypically distinct) '**1**' scores or a '**1**' plus a '**2**' cumulative score. Each compound was screen twice as a singleton.[1,10]

3.5.1.2 Motility Assays on Adult *S. mansoni*

From the severity scores obtained, the worm motility was measured (as an indicator of parasite viability on compound exposure) at 5 µM. Worm motility was measured after 24 h using a WormAssay™, a camera-based system that tracks the average motility of worms per well in an assay plate.[1,10]

3.5.2 Cytotoxicity: *In Silico* Predictions and *In Vitro* Assays

3.5.2.1 *In Silico* Predictions on HEK293

This was done using LabMol InsightAI Cyto-Safe™ web application (http://insightai.labmol.com.br/) which utilizes AI/ML techniques and is trained on a data set of approximately 90,000 compounds, evaluated against two cell lines, HEK293 and 3T3 (but in this research work only the former cell line was considered to match the planned experimental assays). This was possible by inputting a Simplified Molecular-Input Line-Entry System (SMILES) representation or sketching molecules on the molecular operating environment (MOE). [3]

3.5.2.2 *In Vitro* Assays on HEK293

Human embryonic kidney (HEK293) cells were cultured in Dulbecco's Modified Eagle's Medium (DMEM) with 10% heat-inactivated fetal bovine serum and 1% penicillin-streptomycin. Cells were grown in tissue culture flask of 175 cm^2 surface area (T175) maintained at 37 ℃ in 5% carbon dioxide (CO_2) and sub-cultured when at 60 – 80% cell confluence. Cytotoxicity in HEK293 cells was measured using the resazurin cell viability assay. Test compounds were serially diluted in DMSO and added to 96-well polystyrene assay plates to give final assay concentrations ranging from 20 μM to 0.87 nM (1 μL; 1% total DMSO). Fresh medium was added to the assay plate (49 μL/well). HEK293 cells were suspended to 4×10^5 cells/mL in DMEM and added to each well (100 μL) for a total density of 2×10^4 cells/well. Assay plates were incubated at 37°C and 5% CO_2 for 48 h, followed by addition of 20 μL 0.5 mM/well resazurin (Alfa Aesar, Cat. B21187) in phosphate-buffered saline to each well. Assay plates were incubated in the dark for 2 h at 37°C. Fluorescence was measured at 531 nm and 595 nm excitation and emission wavelengths, respectively, using a 2104 EnVision® multilabel plate reader with DMSO and bortezomib (BTZ), an α-tubulin complexing anti-tumour agent similar to cevipabulin, as negative and positive controls, respectively.[1,10]

3.6 Physicochemical Property Determinations: Experimental and *In Silico* Methods

Experimental physicochemical properties determined included the m.p., t_R, R_f and *MW*. Hydrophobicity of a drug can be measured experimentally by testing the drug's relative distribution into *n*-octanol and water in a mixture of the two solvents. This property is expressed as concentration of the drug in *n*-octanol divided by the concentration in water and is known as the partition coefficient *(P)* usually expressed as Log*P*. For ionizable drug molecules the concentration of the drug in both *n*-octanol and water represents the sum of neutral and ionized species in which case the partition coefficient is known as the distribution coefficient (Log*D*). On the other hand, if the partition experiment is carried out at a pH where the drug molecules are un-ionized, the resulting partition coefficient is usually expressed a Log*P*. While Log*P* and Log*D* are more accurately determined by experiment using, for instance the HPLC-based method, the former were calculated using SwissADME™ *in silico* chemo-informatics web tool and are reported as cLog*P*. Other drug physicochemical properties calculated include rotatable bonds (*RB*), topological polar surface area

(TPSA), and hydrogen bond donors/ acceptors (HBD/HBAs), which to affect the capacity to cross membrane barriers.[5,9,27]

Direct wet solubility *(S)* methods used in drug discovery include experimental methods such as the turbidimetric kinetic solubility and the HPLC-based DMSO, so called Dry Down thermodynamic (equilibrium) solubility methods among others, usually with a cut-off value of > 30 μM. However, algebraic methods can also be used. These include the Yalkowsky general solubility equation (GSE) and Delaney GSE-style equation among others; some e.g. Delaney and Ali GSE-style equations, being used algorithmized into the SwissADME™ *in silico* tool (by use of either SMILES or MOE) used herein hence the solubility data were reported as estimated or calculated solubility as a logarithm (Log*S*).[5,6]

3.7 Pharmacokinetic Property Determinations: *In Silico* Methods

Pharmacokinetically speaking, factors to consider are absorption, distribution, metabolism, excretion and toxicity (ADMET). Absorption-wise, orally taken drugs must cross the gut wall to reach the blood supply. Orally absorbed drugs tend to obey what is known as Lipinski's Rule of Five (Ro5), in which factors are prescribed in multiples of five. According to this rule, an oral drug must have a molecular weight *(MW)* less than 500; no more than 5 HBD groups; no more than 10 HBA groups; a cLog*P* value less than +5. Veber *et al* (2002) demonstrated that for oral activity, the requirement is ≤ 10 RBs and either a TPSA ≤ 140 Å or ≤ 12 HBDs and HBAs in total. Distribution was expressed as volume of distribution at steady-state *(V_{dss})*. Metabolism was measured in terms of CYP inhibition. BioSigLab PkCSM™, another web chemo-informatics tool utilized via either SMILES or MOE.[5,6,9]

3.8 References

(1) Kanyanta, M.; Lengwe, C.; Mambwe, D.; Francisco, K. R.; Liu, L. J.; Uli Sun, Y.; Amarasinghe, D. K.; Caffrey, C. R.; Cheuka, P. M. Activity of *N*-Phenylbenzamide Analogs against the Neglected Disease Pathogen, *Schistosoma mansoni*. *Bioorg. Med. Chem. Lett.* **2023**, *82*, 129164.

(2) Banda, P. D. Synthesis and Evaluation of Anti-hypertensive Activity of 4'-[(2,5-Disubstituted-1H-Benzimidazol-yl)methyl]biphenyl-2-carboxylic Acids. MSc Dissertation, University of Zambia, Lusaka, Zambia, **2016**.

(3) Mambwe, D. Repositioning Astemizole for Malaria. PhD Thesis, University of Cape Town, Cape Town, South Africa, **2021**.

(4) Feitosa, F. L.; Cabral, V. F.; Sanches, I. H.; Silva-Mendonca, S.; Borba, J. V. V. B.; Braga, R. C.; Andrade, C. H. Cyto-Safe: A Machine Learning Tool for Early Identification of Cytotoxic Compounds in Drug Discovery. *J. Chem. Inf. Model*. **2024**, *64* (24), 9056–9062.

(5) Daina, A.; Michielin, O.; Zoete, V. SwissADME: A Free Web Tool to Evaluate Pharmacokinetics, Drug-likeness and Medicinal Chemistry Friendliness of Small Molecules. *Sci. Rep.* **2017**, *7* (1), 42717.

(6) Pires, D. E. V.; Blundell, T. L.; Ascher, D. B. PkCSM: Predicting Small-molecule Pharmacokinetic and Toxicity Properties Using Graph-based Signatures. *J. Med. Chem.* **2015**, *58* (9), 4066–4072.

(7) Pasche, V.; Laleu, B.; Keiser, J. Early Antischistosomal Leads Identified from *In Vitro* and *In Vivo* Screening of the Medicines for Malaria Venture Pathogen Box. *ACS Infect. Dis.* **2018**, *5* (1), 102–110.

(8) Liu, Z.; Zhang, Q.; Liu, Y.; Yu, X.; Chui, R.; Zhang, L.; Zhao, B.; Ma, L. Recent Contributions of Pyridazine as a Privileged Scaffold of Anticancer Agents in Medicinal Chemistry: An Updated Review. *Bioorg. Med. Chem. Lett.* **2024**, *111*, 117847.

(9) Patrick, G. L. *An Introduction to Medicinal Chemistry*, 7th ed.; Oxford University Press, **2023**.

(10) Dawoodjee, A. M.; Sichinga, J.; Banda, H.; Mbaya, S.; Funjika, E.; Mayoka, G.; Hikaambo, C.; Francisco, K. R.; Sun, Y. U.; Liu, L. J.; Caffrey, C. R.; Cheuka, P. M. Structure Activity Relationships of Antischistosomal *N*-Phenylbenzamides by Incorporation of Electron-withdrawing Functionalities. *Results Chem.* **2024**, *12*, 101890.

(11) Larsen, B. J.; Rosano, R. J.; Ford-Hutchinson, T. A.; Reitz, A. B.; Wrobel, J. E. A Method for *C*2 Acylation of 1,3-Indandiones. *Tetrahedron.* **2018**, *74* (22), 2762–2768.

(12) Prasad, R. S.; Anderson, C. E.; Richards, C. J.; Overman, L. E. Synthesis of *Tert*-Leucine-derived Cobalt Oxazoline Palladacycles. Reversal of Palladation Diastereoselectivity and Application to the Asymmetric Rearrangement of *N*-Aryl Trifluoroacetimidates. *Organometallics.* **2005**, *24* (1), 77–81.

(13) Savjani, J. K.; Mulamkattil, S.; Variya, B.; Patel, S. Molecular Docking, Synthesis and Biological Screening of Mefenamic Acid Derivatives as Anti-Inflammatory Agents. *Eur. J. Pharmacol.* **2017**, *801*, 28–34.

(14) le Manach, C.; Gonzàlez Cabrera, D.; Douelle, F.; Nchinda, A. T.; Younis, Y.; Taylor, D.; Wiesner, L.; White, K. L.; Ryan, E.; March, C.; Duffy, S.; Avery, V. M.; Waterson, D.; Witty, M. J.; Wittlin, S.; Charman, S. A.; Street, L. J.; Chibale, K. Medicinal Chemistry Optimization of Antiplasmodial Imidazopyridazine Hits from High Throughput Screening of a SoftFocus Kinase Library. *J. Med. Chem.* **2014**, *57* (6), 2789–2798.

(15) Agilent. *Agilent® 1290 Infinity LC System Standard Autosampler User Manual.* Agilent, **2012.**

(16) Shimadzu. *UV™2600i UV-Vis Spectrophotometer Operation Manual.* Shimadzu, **2017**.

(17) Shimadzu. *Fourier Transform Infrared Spectrophotometer IR-Spirit™: Operation Manual*. Shimadzu, **2018**.

(18) Dean, J. R.; Jones, A. M.; Holmes, D.; Reed, R.; Weyers, J.; Jones, A. *Practical Skills in Chemistry*, 3rd ed.; Pearson, **2017**.

(19) Nair, M. M. The Application of Nuclear Magnetic Resonance in the Structural Elucidation of Natural Products. MSc Thesis, University of Cape Town, Cape Town, South Africa, **1994.**

(20) Schorn, C. *NMR Spectroscopy: Data Acquisition;* Wiley, **2001**.

(21) Shadbolt, S. The Use of ^{1}HNMR Analysis of Urine to Discriminate between Calcium Oxalate Kidney Patients and Healthy Controls. MSc Thesis, University of Cape Town, Cape Town, South Africa, **2001.**

(22) Abraham, R. J.; Mobli, M. *Modelling ^{1}HNMR Spectra of Organic Compounds: Theory Applications and NMR Prediction Software*; Wiley, **2008**.

(23) Harwood, J.; Mo, H. *Practical NMR Spectroscopy Laboratory Guide: Using Bruker Spectrometers*. Academic Press, **2015.**

(24) Buskes, M. J.; Clements, M.; Bachovchin, K. A.; Jalani, H. B.; Leonard, A.; Bag, S.; Klug, D. M.; Singh, B.; Campbell, R. F.; Sciotti, R. J.; El-Sakkary, N.; Caffrey, C. R.; Pollastri, M. P.; Ferrins, L. Structure-Bioactivity Relationships of Lapatinib-derived Analogs against *Schistosoma mansoni*. *ACS Med. Chem. Lett.* **2020**, *11* (3), 258–265.

(25) O'Brien, J.; Wilson, I.; Orton, T.; Pognan, F. Investigation of the Alamar Blue (Resazurin) Fluorescent Dye for the Assessment of Mammalian Cell Cytotoxicity: Resazurin as a Cytotoxicity Assay. *Eur. J. Biochem.* **2000**, *267* (17), 5421–5426.

(26) Yang, J.; Yu, Y.; Li, Y.; Yan, W.; Ye, H.; Niu, L.; Tang, M.; Wang, Z.; Yang, Z.; Pei, H.; Wei, H.; Zhao, M.; Wen, J.; Yang, L.; Ouyang, L.; Wei, Y.; Chen, Q.; Li, W.; Chen, L. Cevipabulin-Tubulin Complex Reveals a Novel Agent Binding Site on α-Tubulin with Tubulin Degradation Effect. *Sci. Adv.* **2021**, *7* (21), 4168.

(27) *Pharmaceutics: The Science of Medicine Design,* Denton, P.; Rostron, C. Ed.; Oxford University Press; **2013.**

CHAPTER 4

RESULTS AND DISCUSSION

4.1 Chapter Overview

This penultimate chapter zeroes in on the synthesis, purity and characterization data of the target compounds, their synthetic approach having been a one-pot synthesis. The bioactivity experimental data of target compounds against *S. mansoni* worms, as well as HEK293 cytotoxicity data, are then presented and discussed followed by SARs. The chapter then goes further to present and discuss physicochemical and DMPK data and draw structure-property relationships (SPRs).

4.2 Yield, Optimization, Characterization Salient Features and Reaction Mechanism

Neither the ^{1}H-NMR nor ^{13}C-NMR spectra for compounds (compds) **HB2-02, HB2-03** and **HB2-04** were acquired due to insufficient purity (≤ 95%) as a cut-off hence these four compounds were not progressed to bioassays. EDCI offered the advantage over the other even more abundant coupling agent i.e. DCC which was also initially tried, of possessing a polar amino group and being water soluble. This was advantageous during work-up unlike DCC which turned out to be problematic as in the contemporaneous projects as expected.[2-5] DCM was used in preference for DMF which was also initially tried, being a more polar solvent.[6] Poor solubility of 3-aminopyridazines in DCM affected the initial yields hence the quantities were scaled up to four times for one compound i.e. **HB1-03** and two times for the rest.[1]

For MS, the singly protonated pseudomolecular ion i.e. $[M+H]^{+}$ was detected together with its various isotopic variations of most importantly the bromine doublets. Expectedly, little or no fragmentation patterns are discernible from ESI, being soft ionization.[7] In NMR spectra, for most compounds, coupling of ^{1}H to ^{1}H and ^{1}H to ^{19}F are both considered.[8] Each raw ^{13}C-NMR spectra showed a characteristic peak upfield around a literature value of 39.5 ppm being for the ^{13}C in DMSO,[9] zoomed out to clarify the analyte peaks. This was also observed with ^{1}H-NMR spectra with characteristic peaks at literature values of 2.5 - 2.54[9–11] and 3.33 ppm[10,12] for partially protiated DMSO (CH_3)$_2$SO and H_2O impurity in DMSO-d_6, respectively, except for **HB4-02**, **2-14** and **3-02**.

The one-pot EDCI/DMAP-mediated amide coupling plausibly proceeds via the pH-dependent mechanism outlined below (Figure 38).[13,14]

Step 1 involves reversible acid-base deprotonation of the benzoic acid derivative (R_1BzOH) by EDCI.HCl salt.[14–16] Depending on pH, a reversible side reaction is possible in which the now doubly protonated coupling reagent [EDCI.H_2Cl]$^+$ cyclizes with proton exchange to a reduced pyrimidine guanidinium intermediate.[15,16] This undergoes tautomerization of the guanidino group which has repeatedly been confirmed by IR, ^{1}H-NMR, ^{13}C-NMR, nitrogen-15 (^{15}N)-NMR spectroscopy and reaction kinetics/ equilibria studies by 2007.[17–20]

Step 2 involves a nucleophilic addition of the benzoate ion (R_1BzO^-) on [EDCI.H_2Cl]$^+$ leading to an unstable *O*-acyl-isourea which is vulnerable to reversible molecular rearrangement being reactive. This could rearrange by intramolecular acyl transfer to form a stable *N*-acyl-urea.[13,14] If this occurs, the quantity of *O*-acyl-isourea available for further attack could be low and hence affect the product yield.[13,15] That explains why the benzoic acid derivative is added to EDCI.HCl at 0°C.[20]

Step 3 involves competitive nucleophilic acyl addition of DMAP catalyst, a sterically hindered basic nucleophile, to the *O*-acyl-isourea in a kinetically-controlled reversible but faster 5 minutes reaction producing an unstable tetrahedral intermediate, favoured by the low temperature.[15,16] This reaction occurs in preference to the thermodynamically controlled reversible but slower *O*-acyl-isourea intramolecular rearrangement side reaction. In this case, DMAP prevents this unwanted side reaction.[15,16]

In step 4 the unstable tetrahedral intermediate undergoes an intramolecular bimolecular nucleophilic substitution (S_N2) to yield a reactive intermediate and a urea intermediate which is resonance stabilized.[14,15] In step 5 the benzoate-DMAP amide intermediate undergoes nucleophilic acyl addition with the aminopyridazine leading to the formation of another tetrahedral intermediate.[13–15] Step 6 is DMAP catalyst restoration by an intramolecular S_N2 reaction.[14]

Finally, in step 7 an acid-base deprotonation drives the reaction towards the *N*-PdzBA target compound and a soluble urea by-product.[13,14,16]

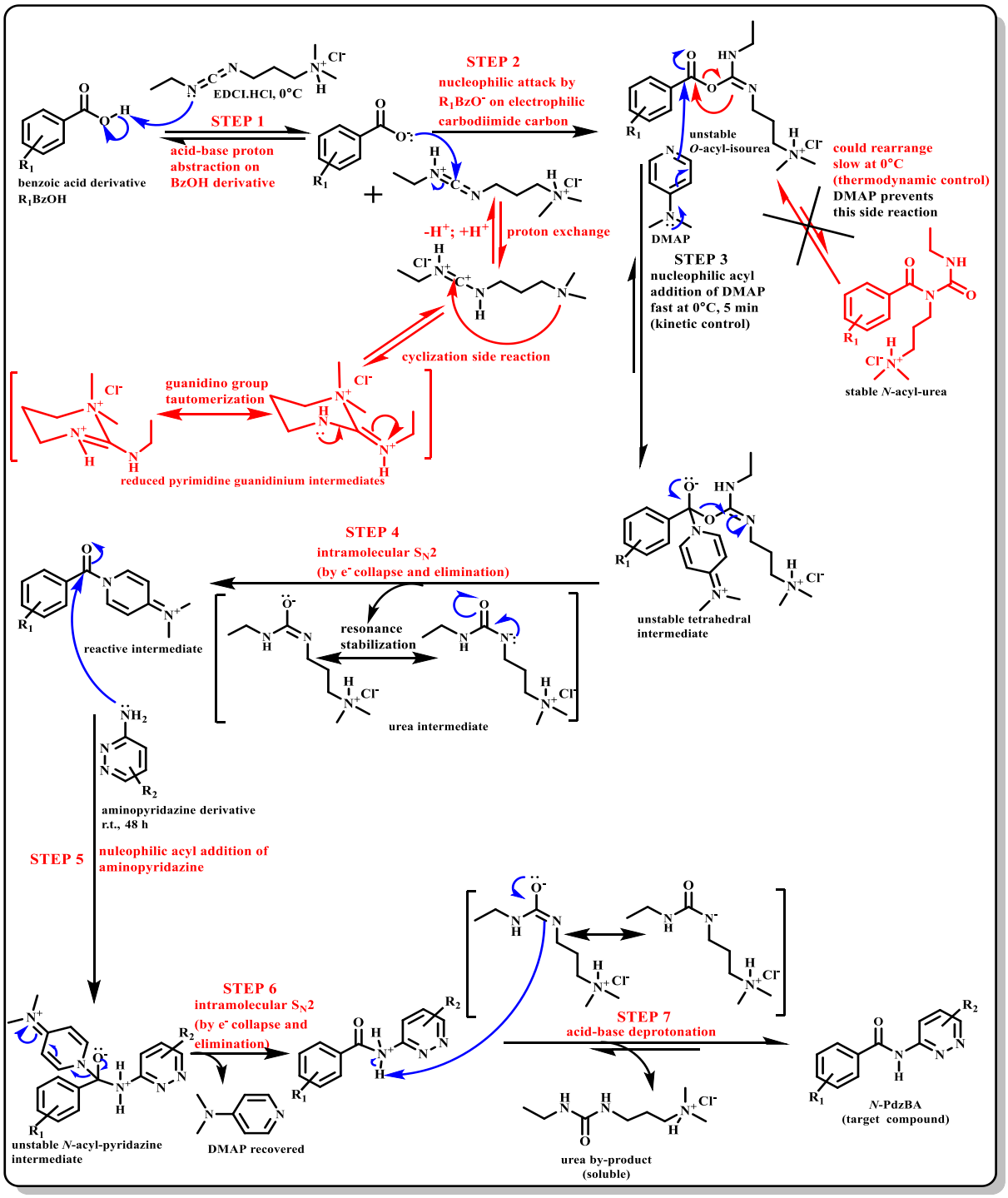

Figure 38: A plausible reaction mechanism of EDCI/DMAP-mediated amide coupling.

Synthesis of ten designed target compounds was attempted as summarized in Table 10.[1]

Table 10: Summary of the synthesized target compounds with preliminary characterization data.[1]

S/N	Compd code	Structure	MW	Exact mass	$[M+H]^+$ *m/z*	% Yield	% Purity	T_m (°C)	R_f	t_R (min)
1	**HB1-03**	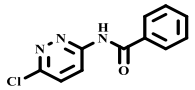	233.65	233.04	234.1	46.45	100	134-141	0.60	0.839
2	**HB2-12**	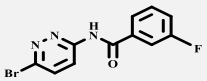	296.10	294.98	296.0	56.93	100	150-156	0.43	0.905
3	**HB2-13**	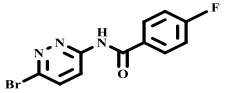	296.10	294.98	296.0	77.91	100	149-153	0.51	0.890
4	**HB2-14**	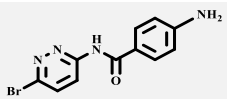	293.12	292.00	293.1	68.32	95.98	215-221	0.74	0.725
5	**HB3-05**	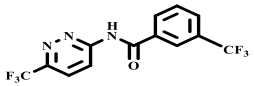	335.21	335.05	336.0	71.32	100	209-214	0.66	1.089
6	**HB4-02**	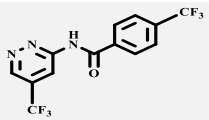	335.21	335.05	336.0	69.16	100	201-205	0.69	1.085
7	**HB3-02**	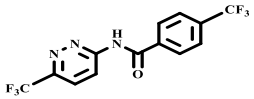	335.21	335.05	345.0	43.40	100	194-198	0.78	0.168
8	**HB2-03**	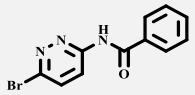	278.10	276.99	ND	ND	82.49	ND	ND	ND
9	**HB2-02**	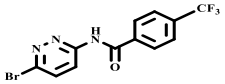	346.10	344.97	ND	ND	73.85	ND	ND	ND
10	**HB2-04**	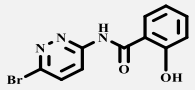	294.10	292.98	ND	ND	64.22	ND	ND	ND

Key: $[M+H]^+$ = pseudomolecular ion; T_m = melting point; *MW* = molecular weight; ND = not determined; R_f= retardation factor; t_R = retention time

4.3 Characterization of Target Compounds

4.3.1 Characterization of HB4-02

4.3.1.1 LC-MS Analysis

Figure 39 shows the mass spectrum for compound **HB4-02**.

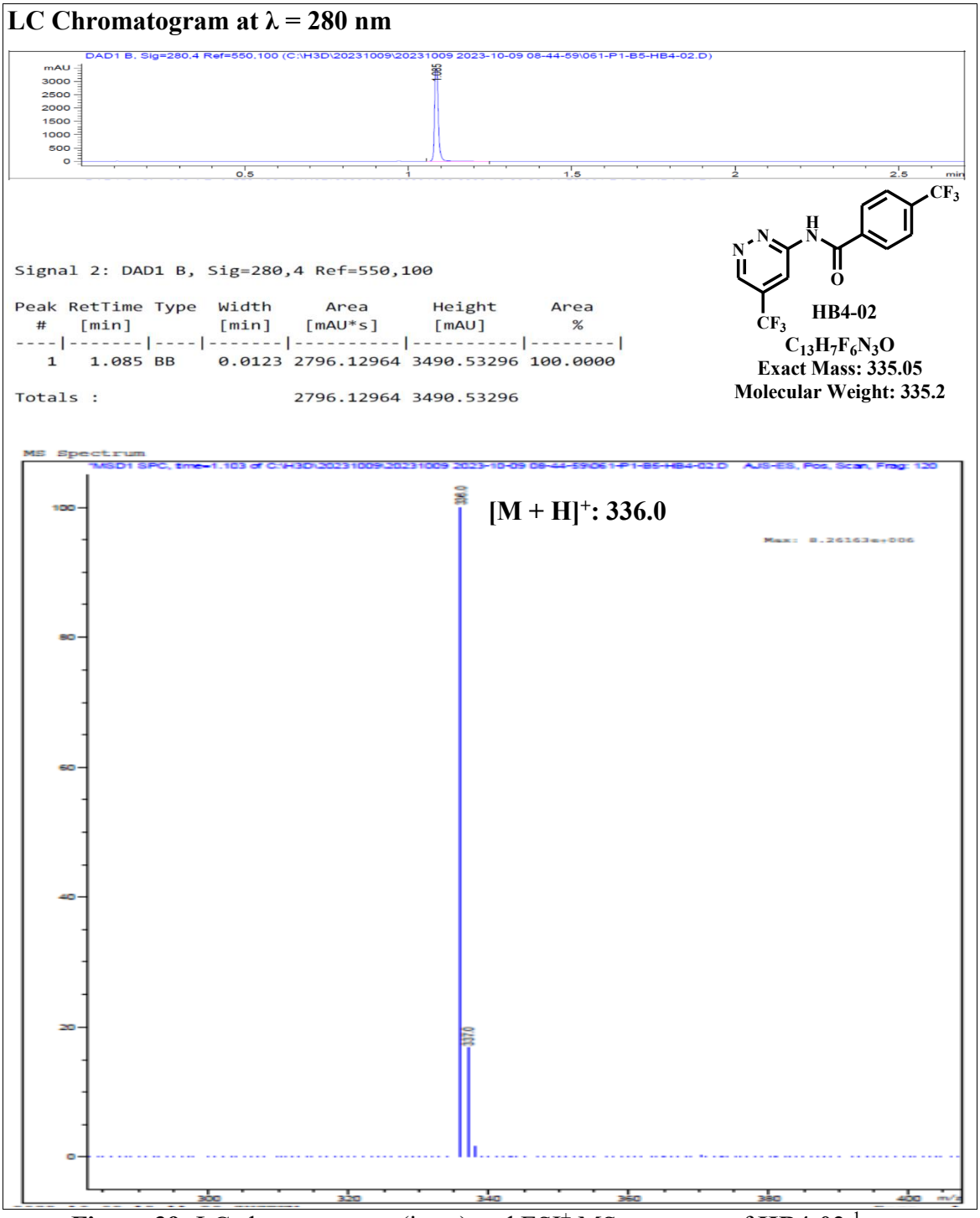

Figure 39: LC chromatogram (inset) and ESI$^+$ MS spectrum of **HB4-02.**[1]

Compound **HB4-02** was successfully synthesized as confirmed by the detection of its pseudomolecular ion ($[M+H]^+$ = 336.0) in the MS spectrum shown in Figure 39, consistent with a calculated exact mass of 335.05. The LC chromatogram acquired at λ = 280 nm showed that the compound had a retention time (t_R) of 1.085 min with a purity of 100%.

4.3.1.2 UV-Vis Analysis

In the UV-Vis spectrum (Figure 40), the wavelength of maximum absorption (λ_{max}) was observed at 330 nm. The experimental molar absorptivity (ε_{max}) was found to be 8,380.2 L mol^{-1} cm^{-1}, as calculated by the Beer-Lambert law (Equation 1).

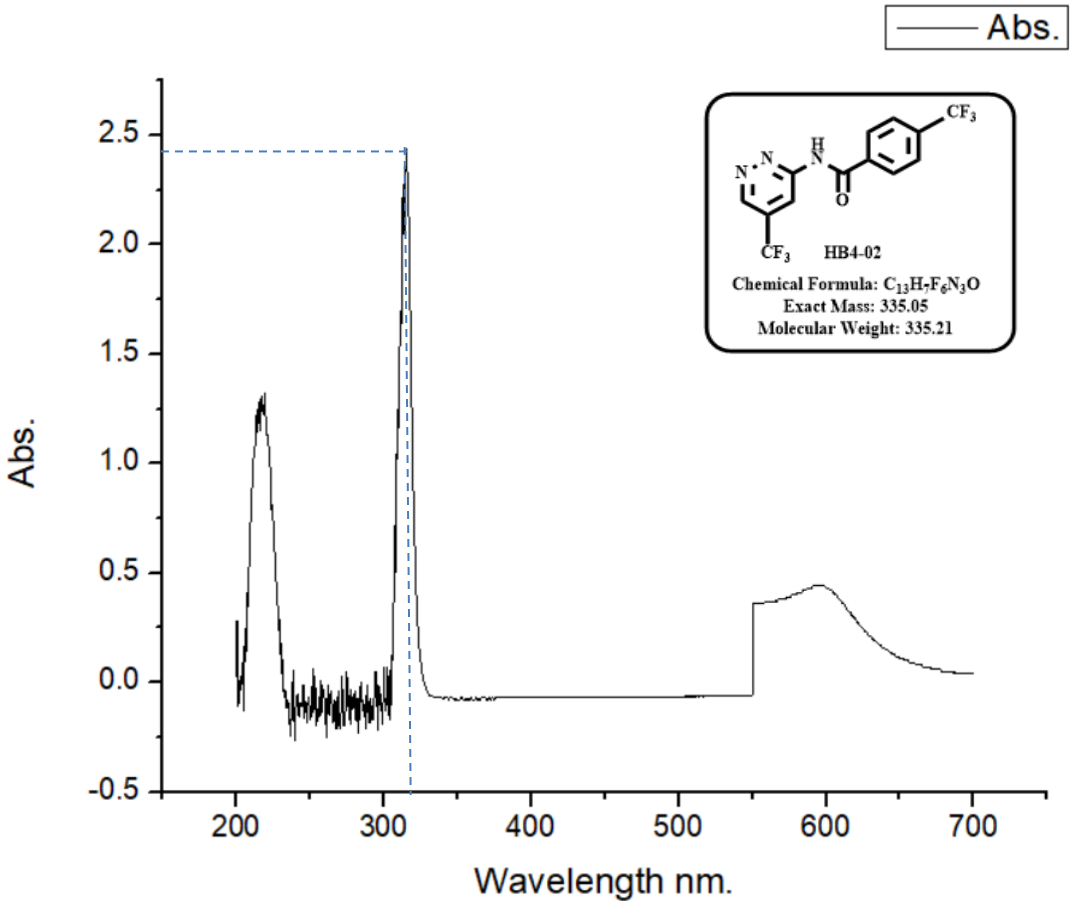

Figure 40: UV-Vis spectrum of **HB4-02** in MeOH.

4.3.1.3 IR Analysis

In the IR spectrum (Figure 41), the doublet N—H stretch observed at 3450 cm^{-1} consistent with a literature value of 3400 cm^{-1} and the in-plane N—H bend band at 1510 cm^{-1} (literature value = 1600 cm^{-1}) was evidence for the successful installation of the amide group (Table 11).[12]

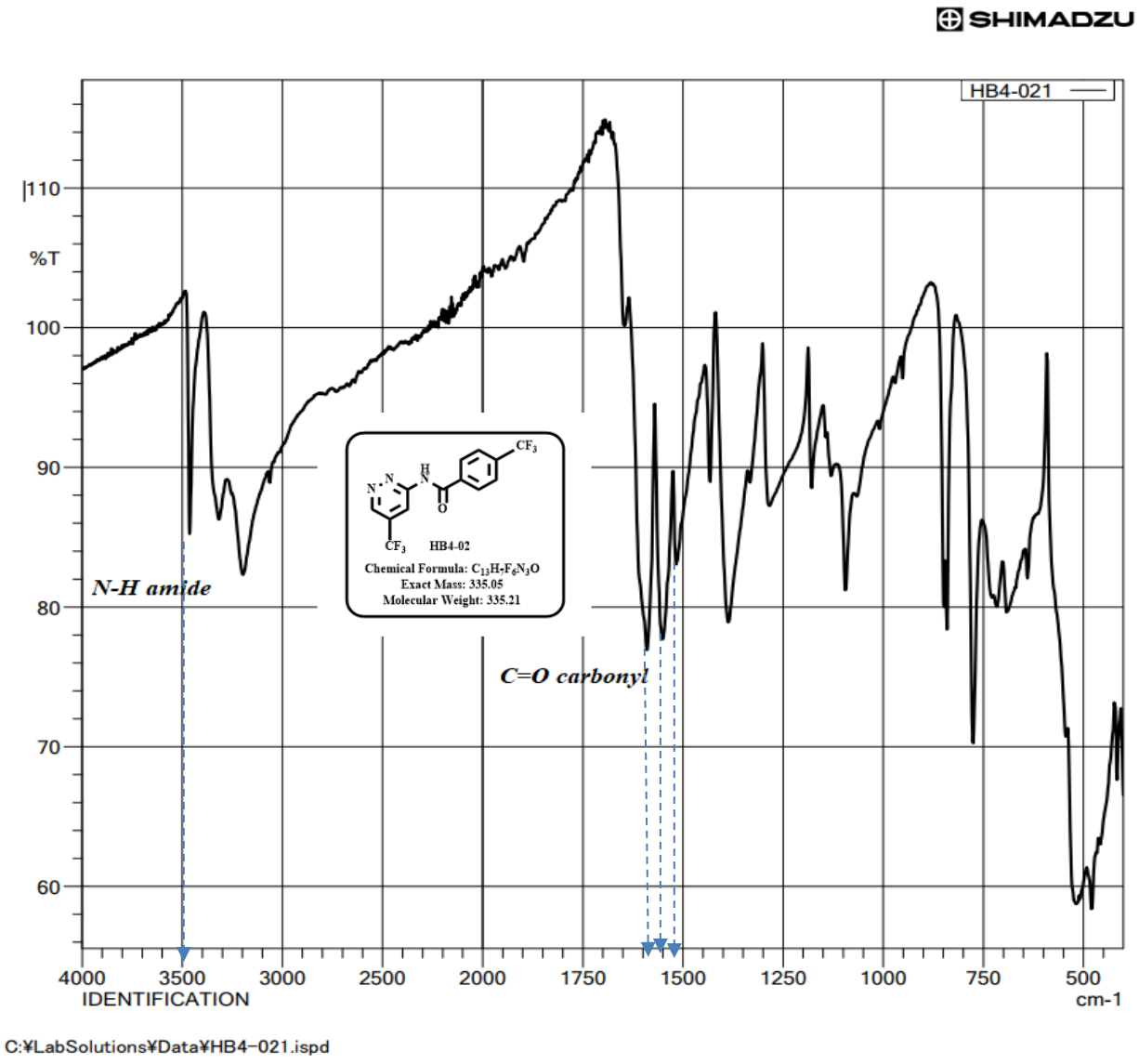

Figure 41: FT-IR spectrum of **HB4-02** using ATR (%T mode; 4 cm^{-1} resolution).

Table 11: Summary of FT-IR data for **HB4-02.**

Absorption band ($\tilde{\nu}$/cm^{-1})	Band description	Bond type	Functional group	Vibration type
3450	m, (s)	N-H	Amide	Stretch
3150	m, (br)	C-H		Stretch
1600	m, (s)	C=O	Amide	Stretch
1550	m, (s)	C=C	Aromatic	Stretch
1510	m, (s)	N-H	Amide	Bend

4.3.1.4 ^{1}H-NMR Analysis

The ^{1}H-NMR spectrum (Figure 42) omits two most prominent singlet peaks upfield with the tallest one at 2.51 ppm being for residual DMSO i.e. (CH_3)$_2$SO) within literature values of 2.5 - 2.54,[8–10] while that at 3.32 ppm corresponded to the H_2O impurity in DMSO-d_6 (around a literature value = 3.33 ppm)[9,11]. This was zoomed to clarify the unique analyte peaks as explained above.

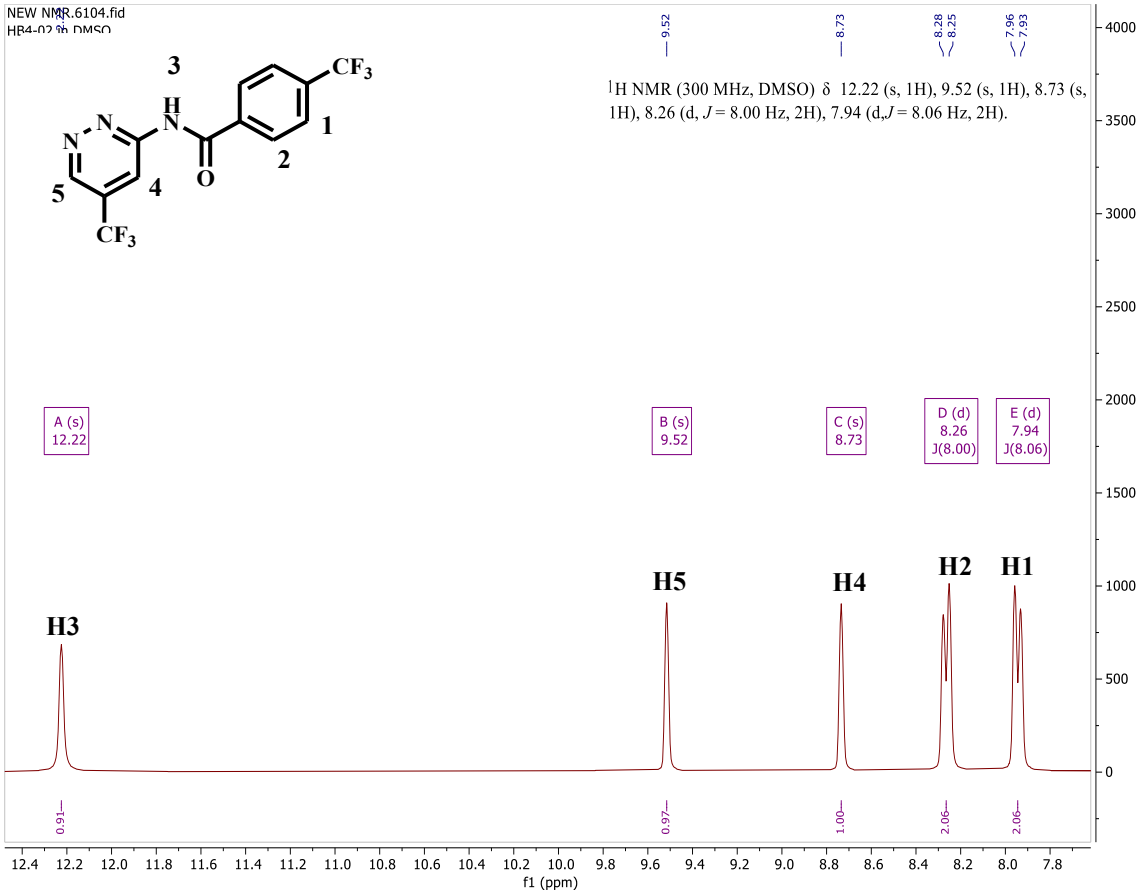

Figure 42: ^{1}H-NMR spectrum of **HB4-02** in DMSO-d_6 at 300 MHz.[1]

The rest of the peaks are shown and are for five (5) proton environments corresponding to a total of seven (7) protons (7H) present in the target compound. The most downfield singlet signal at δ = 12.22 ppm integrates for 1H (H^3) which represents the N*H* in the amide bond thereby confirming amide-bond formation. The singlet at δ = 9.52 ppm integrates for 1H correlating with H^5. Further upfield, the singlet at δ = 8.73 ppm, integrating for 1H correlates with H^4. The doublet at δ = 8.26 ppm integrates for 2Hs corresponding to H^2 within literature values of 6.2 - 8.4 ppm for phenyl

protons,[11] that experiences a short-range vicinal coupling to H^1 at $^3J_{H\text{-}H}$ = 8.00 Hz (literature J = 7.5 - 10 Hz for Ph protons).[21] The doublet at δ = 7.94 ppm integrating for 2H correlates with H^1 that experiences a short-range vicinal coupling to H^2 ($^3J_{H\text{-}H}$ = 8.06 Hz).[11,21] Peak H^3 corresponds to the most deshielded proton indicating connectivity to a highly electronegative atom (N).

4.3.1.5 ^{13}C-NMR Analysis

The peaks are for eleven chemically distinct carbon environments (11C, Figure 43).

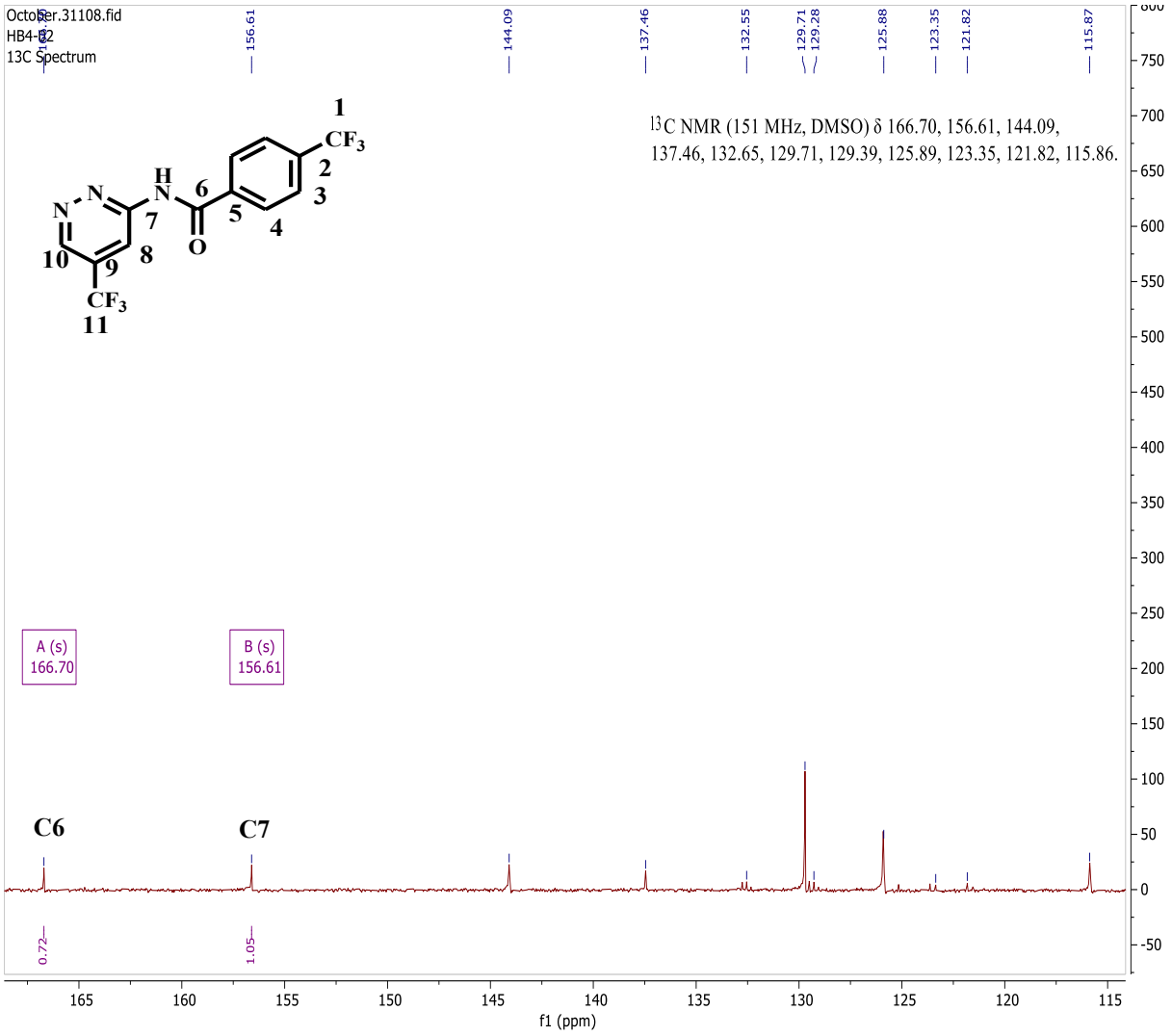

Figure 43: ^{13}C-NMR spectrum of **HB4-02** in DMSO-d_6 at 151 MHz.[1]

Although some signals could not be unambiguously assigned, the peak at δ = 166.70 ppm was attributed to the carbonyl carbon (C^6) within literature values of 150 - 180 ppm for carbonyl carbons.[21,22] Another one relatively upfield at δ = 156.61 ppm was associated with amidine carbon C^7 which is substantially deshielded by virtue of its aromaticity and connection to two nitrogens which are electronegative atoms.[23]

4.3.1.6 Identification of HB4-02 as 4-(Trifluoromethyl)-*N*-(5-(trifluoromethyl)pyridazin-3-yl)benzamide

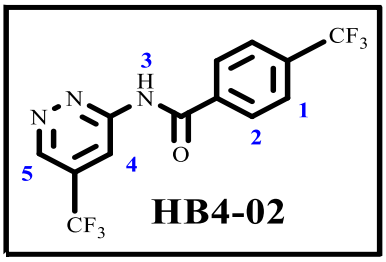

Obtained from 5-(trifluoromethyl)pyridazin-3-amine (0.202 g, 1.24 mmol, 1.0 eq) and 4-(trifluoromethyl)benzoic acid (0.284 g, 1.48 mmol, 1.2 eq). Purified by column chromatography (EtOAc:Hex 50:50) and crystallized in *n*-pentane/diethyl ether. Beige crystalline solid (0.287 g, 67.2%), R_f(EtOAc:Hex, 50:50) 0.69. ^{1}H-NMR (300 MHz, DMSO-d_6) δ_H 12.22 (s, 1H), 9.52 (s, 1H), 8.73 (s, 1H), 8.26 (d, J = 8.00 Hz, 2H), 7.94 (d, J = 8.06 Hz, 2H). ^{13}C-NMR (151 MHz, DMSO-d_6) δ_C 166.70, 156.61, 144.09, 137.46, 132.65, 129.71, 129.39, 125.89, 123.35, 121.82, 115.86; IR $\tilde{\nu}$ (ZnSe ATR cell)/cm^{-1} 3450 (N-H, amide), 3150 (C-H), 1600 (C=O, amide), 1550 (C=C, aromatic); UV-Vis (MeOH): $\lambda_{max}^{MeOH} = 330$ nm; $\varepsilon_{max}^{MeOH} = 8{,}380.2$ L mol^{-1} cm^{-1}; LC-MS (ESI$^+$): found m/z [M+H]$^+$ = 336.0, calculated exact mass = 335.05, purity = 100%, t_R = 1.085 min, m.p. = 201 – 205°C.

4.3.2 Characterization of HB2-14

4.3.2.1 LC-MS Analysis

Compound **HB2-14** was successfully synthesized as confirmed by the detection of its [M+H]$^+$ = 293.1 in the MS spectrum shown in Figure 44, consistent with a calculated exact mass of 292.00. The LC chromatogram acquired at λ = 280 nm showed that the compound had a t_R of 0.728 min with a purity of 100%.

Bromine-79 (^{79}Br) and ^{81}Br isotopes are known to be naturally abundant almost to the same extent (50.69% and 49.31% respectively). In this regard, the incorporation of a bromine-containing sub-structure into the target molecule was evident from the MS spectrum pattern observed in Figure 44 which is consistent with literature as the so called “bromine doublet”[6].

LC Chromatogram at λ = 280 nm

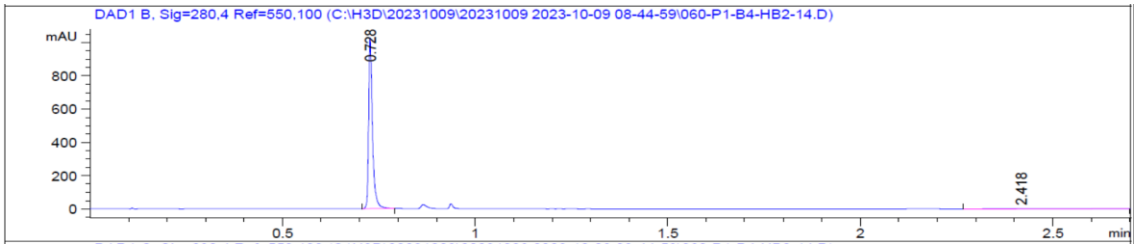

Signal 2: DAD1 B, Sig=280,4 Ref=550,100

Peak #	RetTime [min]	Type	Width [min]	Area [mAU*s]	Height [mAU]	Area %
1	0.728	BB	0.0105	703.09680	1023.53473	95.9792
2	2.418	BBA	0.1463	29.45453	2.39784	4.0208
Totals :				732.55133	1025.93256	

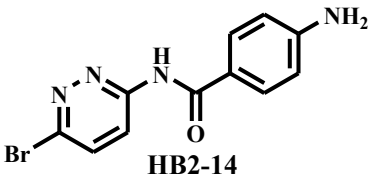

HB2-14

$C_{11}H_9BrN_4O$
Exact Mass: 292
Molecular Weight: 293.12

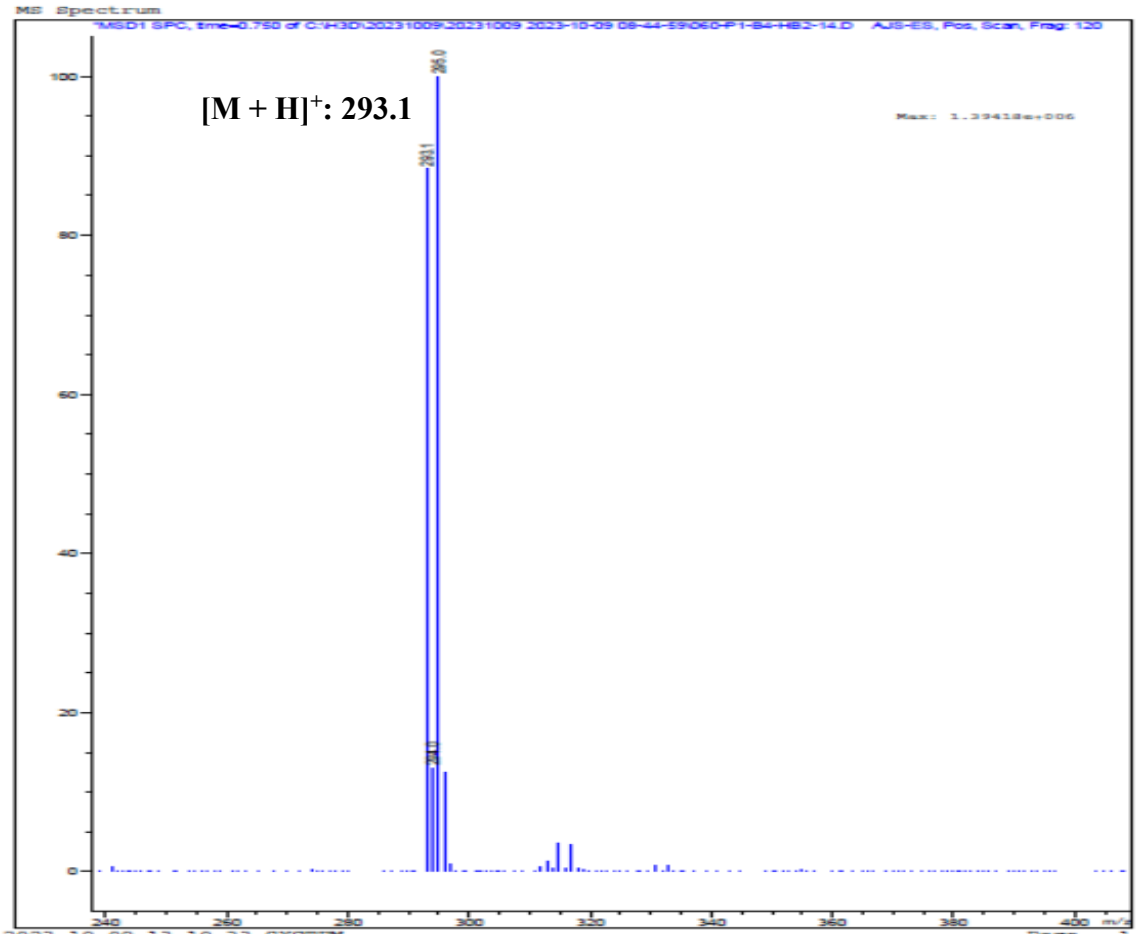

Figure 44: LC chromatogram (inset) and ESI$^+$ MS spectrum of **HB2-14**.[1]

4.3.2.2 UV-Vis Analysis

In the UV-Vis spectrum (Figure 45), the λ_{max} was observed at 330 nm. The experimental ε_{max} was found to be 11,134.4 L mol^{-1} cm^{-1}, as calculated by Equation 1.

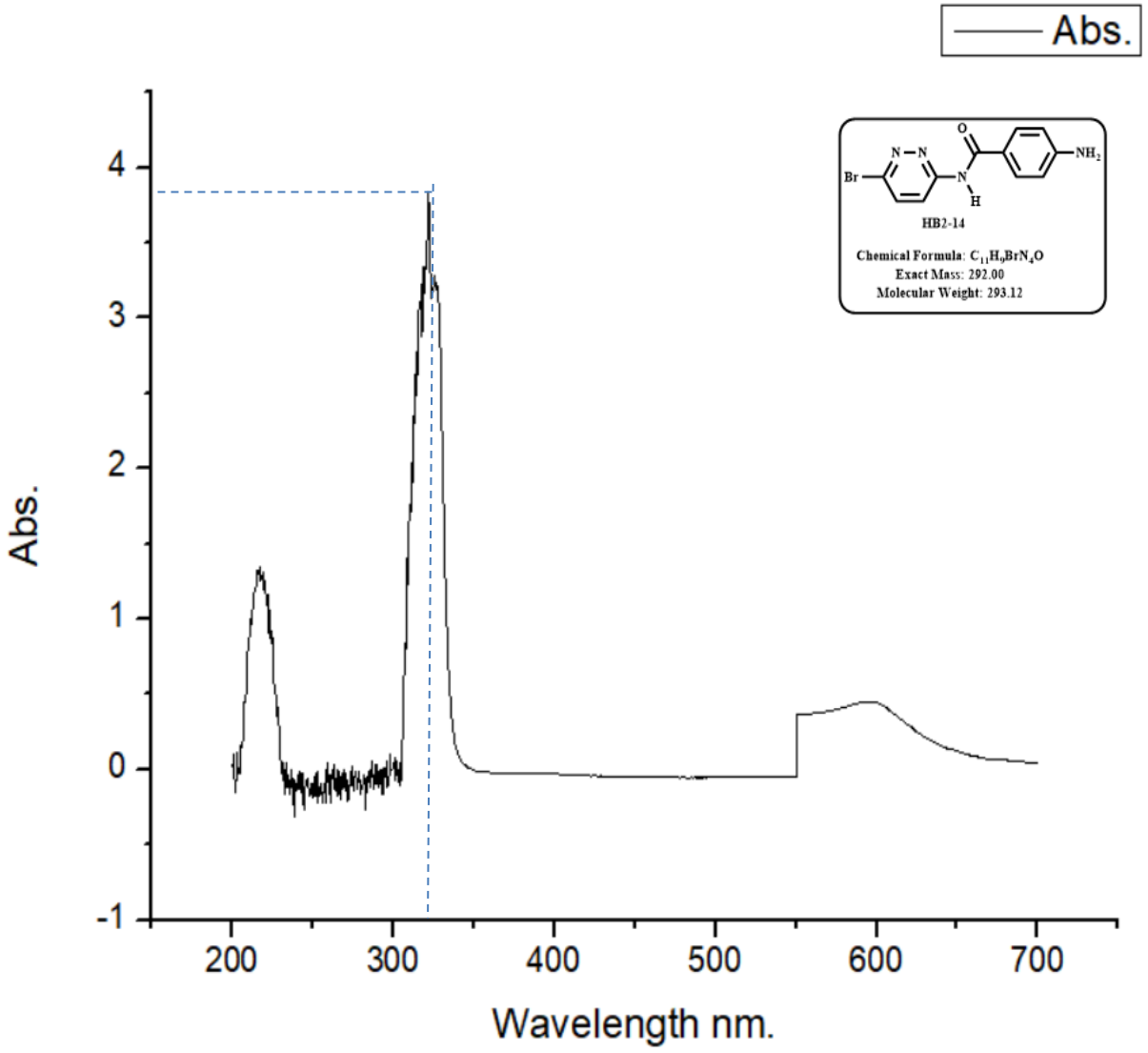

Figure 45: UV-Vis spectrum of **HB2-14** in MeOH.

4.3.2.3 IR Analysis

In the IR spectrum (Figure 46), most of the signals in the range 4000 - 3500 cm^{-1} are due to the water vapour in the air.[23] The doublet N—H stretch observed at 3480 cm^{-1} around a literature value of 3400 cm^{-1} and the in-plane N—H bend band at 1600 cm^{-1} (literature value = 1600 cm^{-1}) was evidence for the successful installation of the amide group (Table 12).[12]

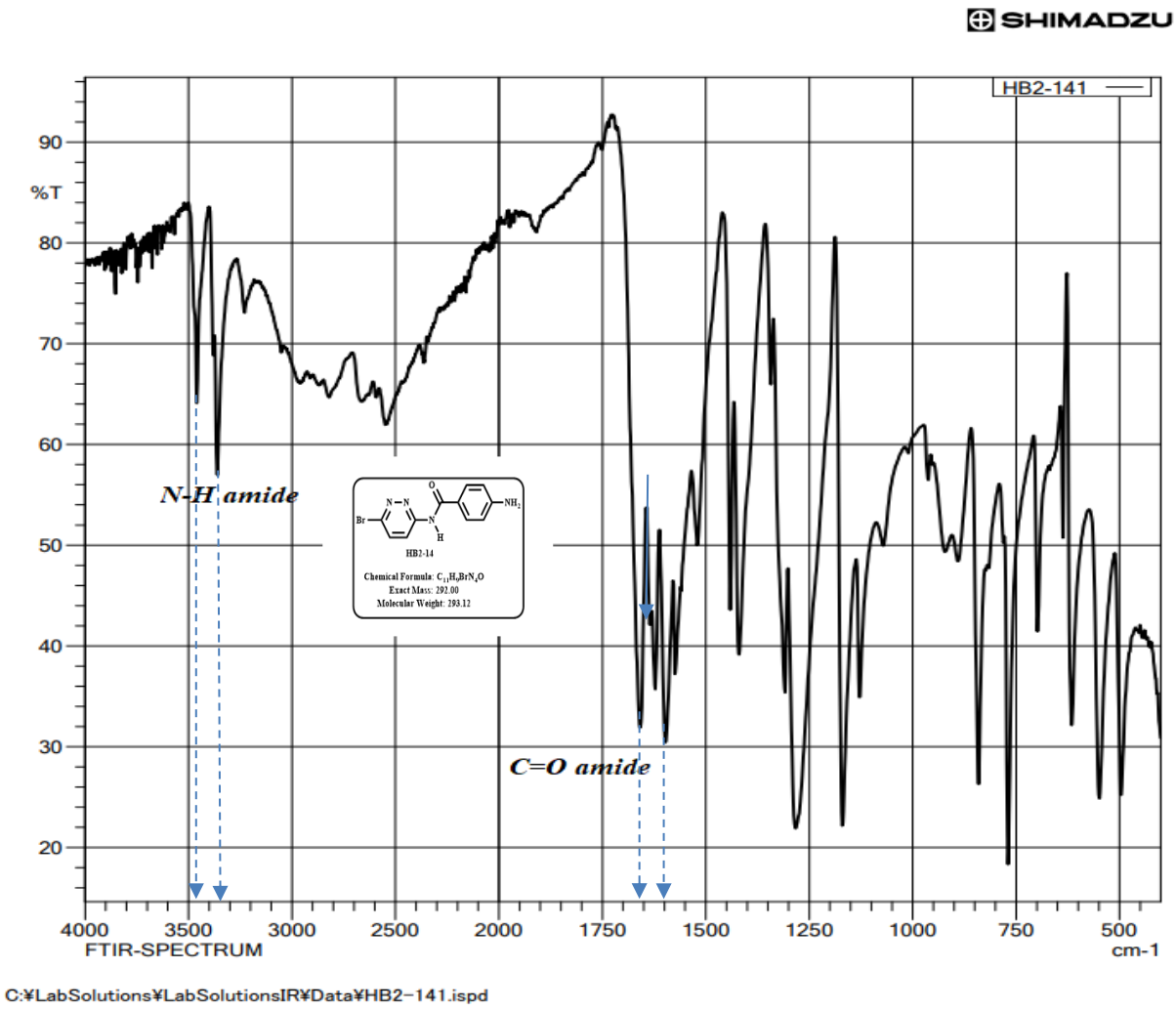

Figure 46: FT-IR spectrum of **HB2-14** using ZnSe ATR cell.

Table 12: Summary of FT-IR data for **HB2-14** using ZnSe ATR cell**.**

Absorption band ($\tilde{\nu}$/cm^{-1})	Band description	Bond type	Functional group	Vibration type
3480	m, (s)	N-H	Amide	Stretch
3350	m, (s)	C-H		Stretch
1650	s, (s)	C=O	Amide	Stretch
1650	s, (s)	C=C	Aromatic	Stretch
1600	s, (s)	N-H	Amide	Bend

4.3.2.4 ^{1}H-NMR Analysis

In the ^{1}H-NMR spectrum (Figure 47), the peaks shown are for six (6) signals are as assigned to a total of 9H present in the target compound.

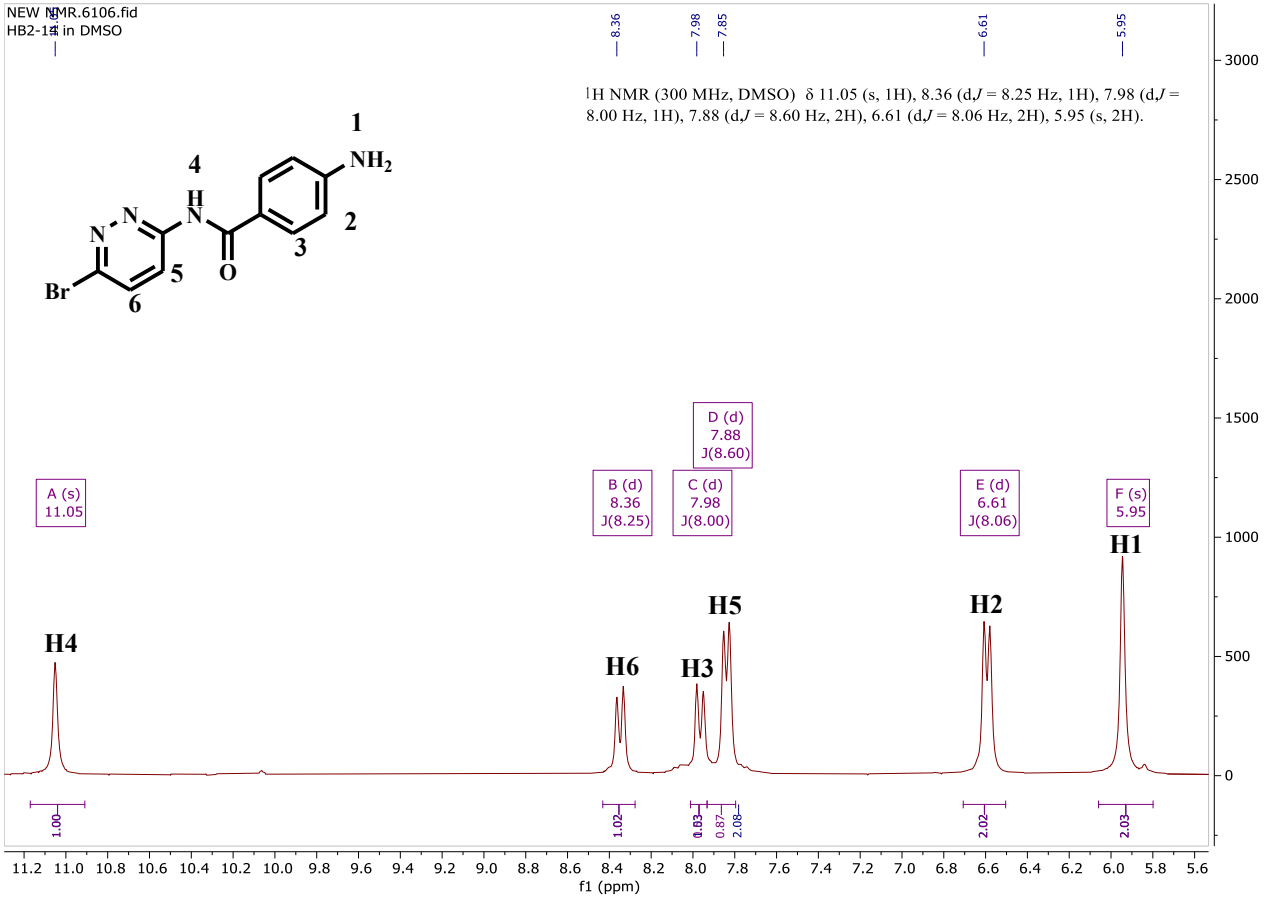

Figure 47: ^{1}H-NMR spectrum of **HB2-14** in DMSO-d_6 at 300 MHz.[1]

The most downfield singlet signal resonant at δ = 11.05 ppm integrating for 1H (H^4) confirms amide-bond formation being connected to a highly electronegative nitrogen (N*H*). The doublet at δ = 8.36 ppm integrating for 1H correlates with H^6 that experiences a short-range vicinal coupling to H^5 ($^{3}J_{H\text{-}H}$ = 8.25 Hz).[22] Further upfield, the doublet at δ = 7.98 ppm integrating for 1H correlates with H^3 that experiences a short-range vicinal coupling to H^2 ($^{3}J_{H\text{-}H}$ = 8.00 Hz).[22]. The doublet at δ = 7.88 ppm integrates for 2Hs corresponding to H^5 within literature values of 6.2 - 8.4 ppm for phenyl protons that experiences a short-range vicinal coupling to H^6 ($^{3}J_{H\text{-}H}$ = 8.25 Hz).[11,22] The doublet at δ = 6.61 ppm, integrating for 2Hs, correlates with H^2 that experiences a short-range

vicinal coupling to H^3 ($^3J_{H\text{-}H}$ = 8.06 Hz).[11,22] The singlet at δ = 5.95 ppm integrating for 2H correlates with H^1.

4.3.2.5 ^{13}C-NMR Analysis

The nine (9) peaks shown are representative of 9C environments as numbered (Figure 48), and a total of 11Cs present in the target compound.

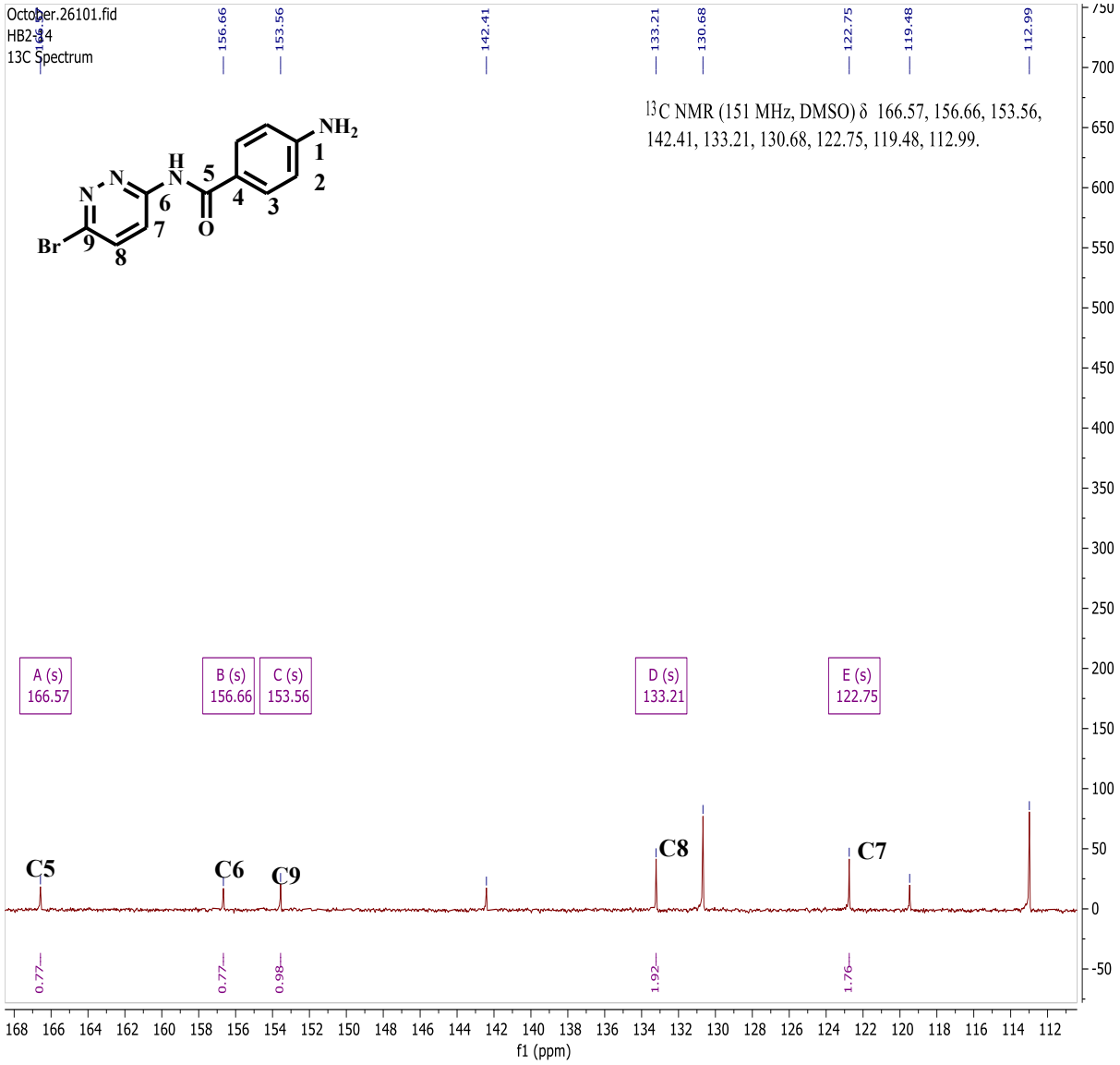

Figure 48: ^{13}C-NMR spectrum of **HB2-14** in DMSO-d_6 at 151 MHz.[1]

The presence of two diagnostic signals one at δ = 166.57 ppm i.e. most downfield attributed to the carbonyl carbon (C^5) within literature values of 150 - 180 ppm for carbonyl carbons.[21,22]

Another one relatively upfield at δ = 153.56 ppm, associated with the imine/*C*-Br carbon (C^9), correlating with literature values of 152.8 - 155.7 ppm for aryl halide carbons,[11,22] confirmed the synthesis of the target compound. Like for the preceding compound, the signal at 156.6 ppm can unambiguously be assigned to the amidine carbon C^6.[23] The signals at 133.21 ppm and 122.75 ppm can also be attributed to the aromatic carbons, C^8 and C^7, respectively. Being aromatic and non-quaternary, these carbons are expected to resonate as relatively intense signals compared to the quaternary carbons such as C^1, C^4, C^6 and C^9. As for the signals at 130.68 and 112.99 ppm, which are nearly twice as intense as those for C^8 and C^7, these can be assigned to 2Cs each.

4.3.2.6 Identification of HB2-14 as *N*-(6-bromopyridazin-3-yl)-4-aminobenzamide

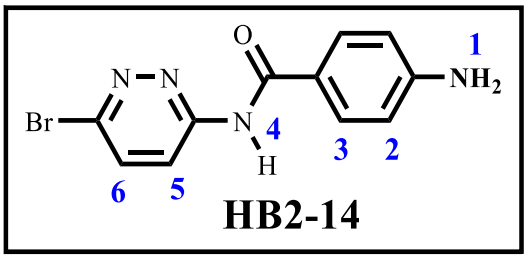

Obtained from 6-bromopyridazin-3-amine (0.213 g, 1.24 mmol, 1.0 eq) and 4-aminobenzoic acid (0.204 g, 1.49 mmol, 1.2 eq). Purified by column chromatography (EtOAc:Hex, 50:50) and crystallized in *n*-pentane/diethylether. White amorphous solid (0.248 g, 68.3%), R_f(EtOAc:Hex, 50:50) 0.74. ^{1}H-NMR (300 MHz, DMSO-d_6) δ_H 11.05 (s, 1H), 8.36 (d, J = 8.25 Hz, 1H), 7.98 (d, J = 8.00 Hz, 1H), 7.88 (d, J = 8.60 Hz, 2H), 6.61 (d, J = 8.06 Hz, 2H), 5.95 (s, 2H). ^{13}C-NMR (151 MHz, DMSO-d_6) δ_C 166.57, 156.66, 153.56, 142.41, 133.21, 130.68, 122.75, 119.48, 112.99; IR $\tilde{\nu}$ (ZnSe ATR cell)/cm^{-1} 3480 (N-H, amide), 3350 (C-H), 1650 (C=O, amide), 1600 (C=C, aromatic); UV-Vis (MeOH): $\lambda_{max}^{MeOH} = 330$ nm; $\varepsilon_{max}^{MeOH} = 11{,}134.4\ \text{L mol}^{-1}\ \text{cm}^{-1}$; LC-MS (ESI$^+$): found m/z $[M+H]^+$ = 293.1, calculated exact mass = 292.0, purity = 95.98%, t_R = 0.728 min, m.p. = 215 – 221°C.

4.3.3 Characterization of HB1-03

4.3.3.1 LC-MS Analysis

Compound **HB1-03** was successfully synthesized as confirmed by the detection of its $[M+H]^+$ = 234.1 in the MS spectrum shown in Figure 49, consistent with a calculated exact mass of 233.04. The LC chromatogram acquired at λ = 280 nm showed that the compound had a t_R of 0.839 min with a purity of 100%.

LC Chromatogram at λ = 280 nm

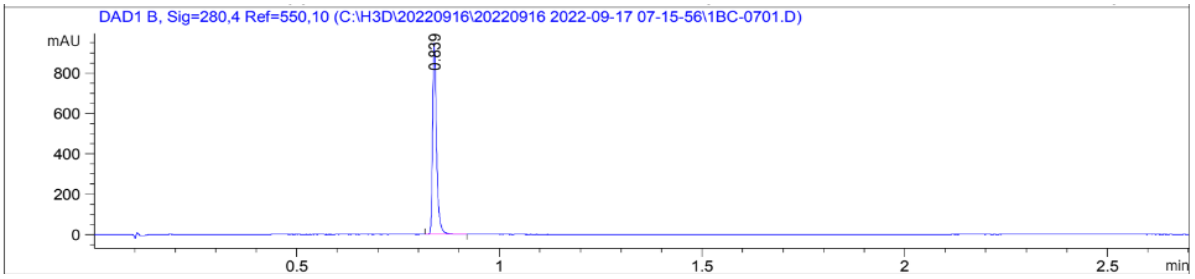

Signal 2: DAD1 B, Sig=280,4 Ref=550,10

Peak #	RetTime [min]	Type	Width [min]	Area [mAU*s]	Height [mAU]	Area %
1	0.839	BB	0.0102	625.23895	942.56158	100.0000
Totals :				625.23895	942.56158	

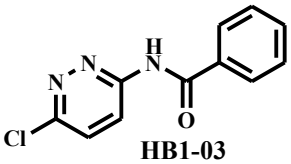

HB1-03

$C_{11}H_8ClN_3O$

Exact Mass: 233.04

Molecular Weight: 233.65

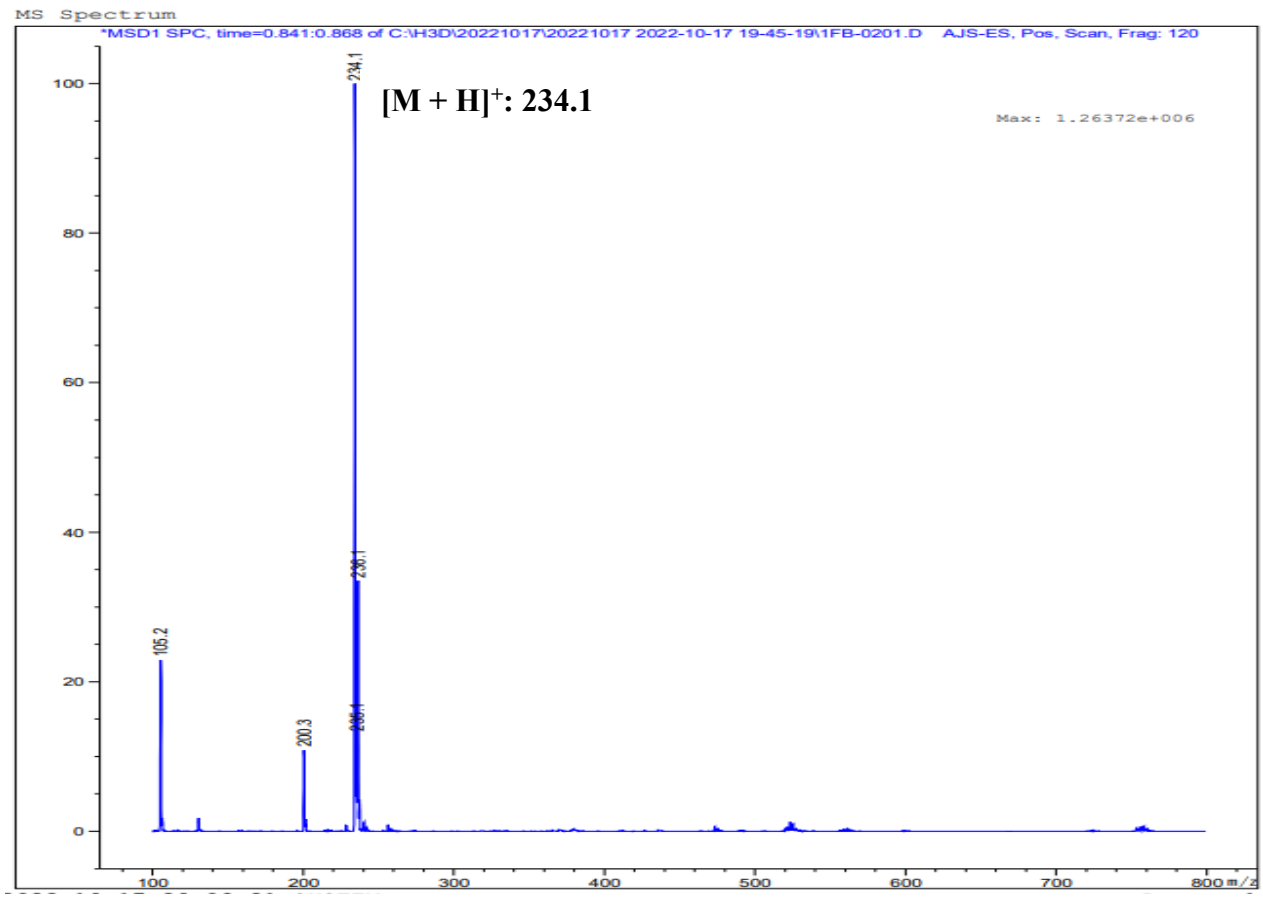

Figure 49: LC chromatogram (inset) and ESI^+ MS spectrum of **HB1-03**.[1]

4.3.3.2 UV-Vis Analysis

In the UV-Vis spectrum (Figure 50), the λ_{max} was observed at 225 nm. The experimental ε_{max} was found to be 3,271.2 L mol^{-1} cm^{-1}, as calculated by Equation 1.

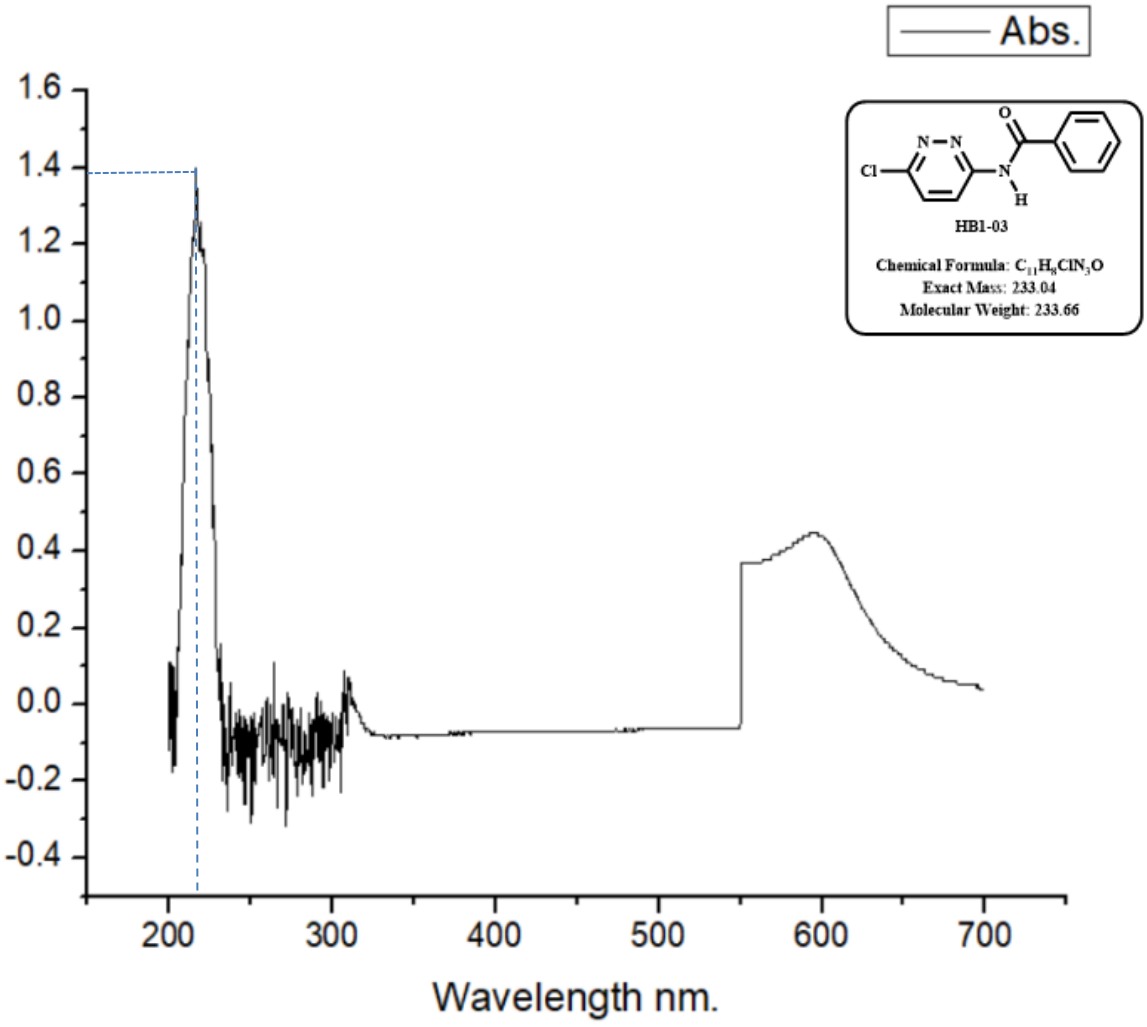

Figure 50: UV-Vis spectrum of **HB1-03** in MeOH.

4.3.3.3 IR Analysis

In the IR spectrum (Figure 51), most of the signals in the range 4000 - 3500 cm^{-1} are due to the water vapour in the air.[23] The doublet N—H stretch observed at 3100 cm^{-1} around a literature value of 3400 cm^{-1} and the in-plane N—H bend band at 1700 cm^{-1} (literature value = 1600 cm^{-1}) was evidence for the successful installation of the amide group (Table 13).[12]

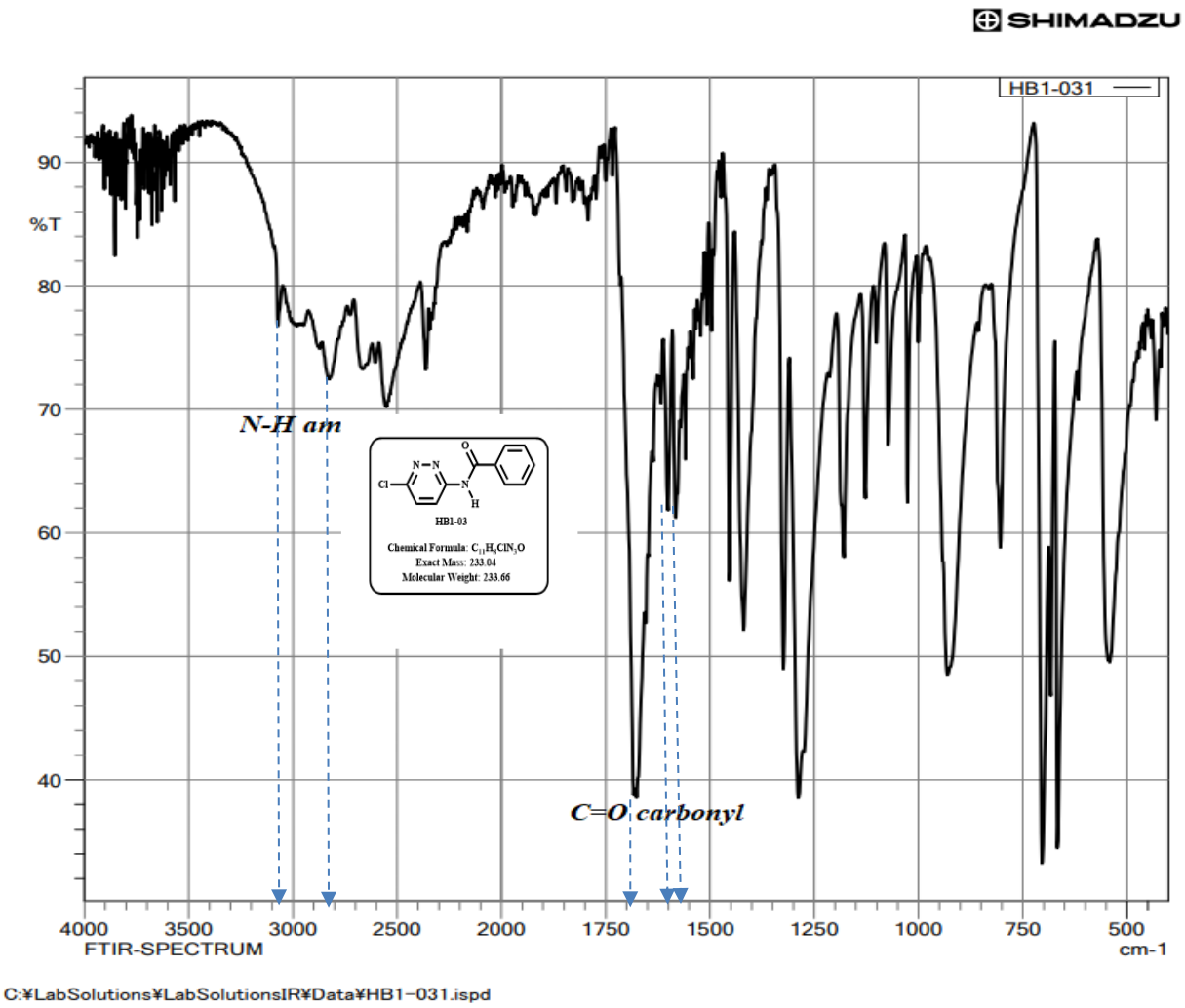

Figure 51: FT-IR spectrum of **HB1-03** using ZnSe ATR cell.

Table 13: Summary of FT-IR data for **HB1-03** using ZnSe ATR cell**.**

Absorption band ($\tilde{\nu}$/cm^{-1})	Band description	Bond type	Functional group	Vibration type
3100	w, (s)	N-H	Amide	Stretch
2800	w, (br)	C-H		Stretch
1620	s, (s)	C=O	Amide	Stretch
1600	m, (s)	N-H	Amide	Bend
1570	m, (s)	C=C	Aromatic	Stretch

4.3.3.4 ^{1}H-NMR Analysis

The ^{1}H-NMR spectrum (Figure 52) shows six (6) signals assigned to a total of 8H present in the target compound. The most downfield singlet signal at δ = 11.68 ppm integrating for 1H (H^4) confirms amide-bond formation (N*H*).[7]

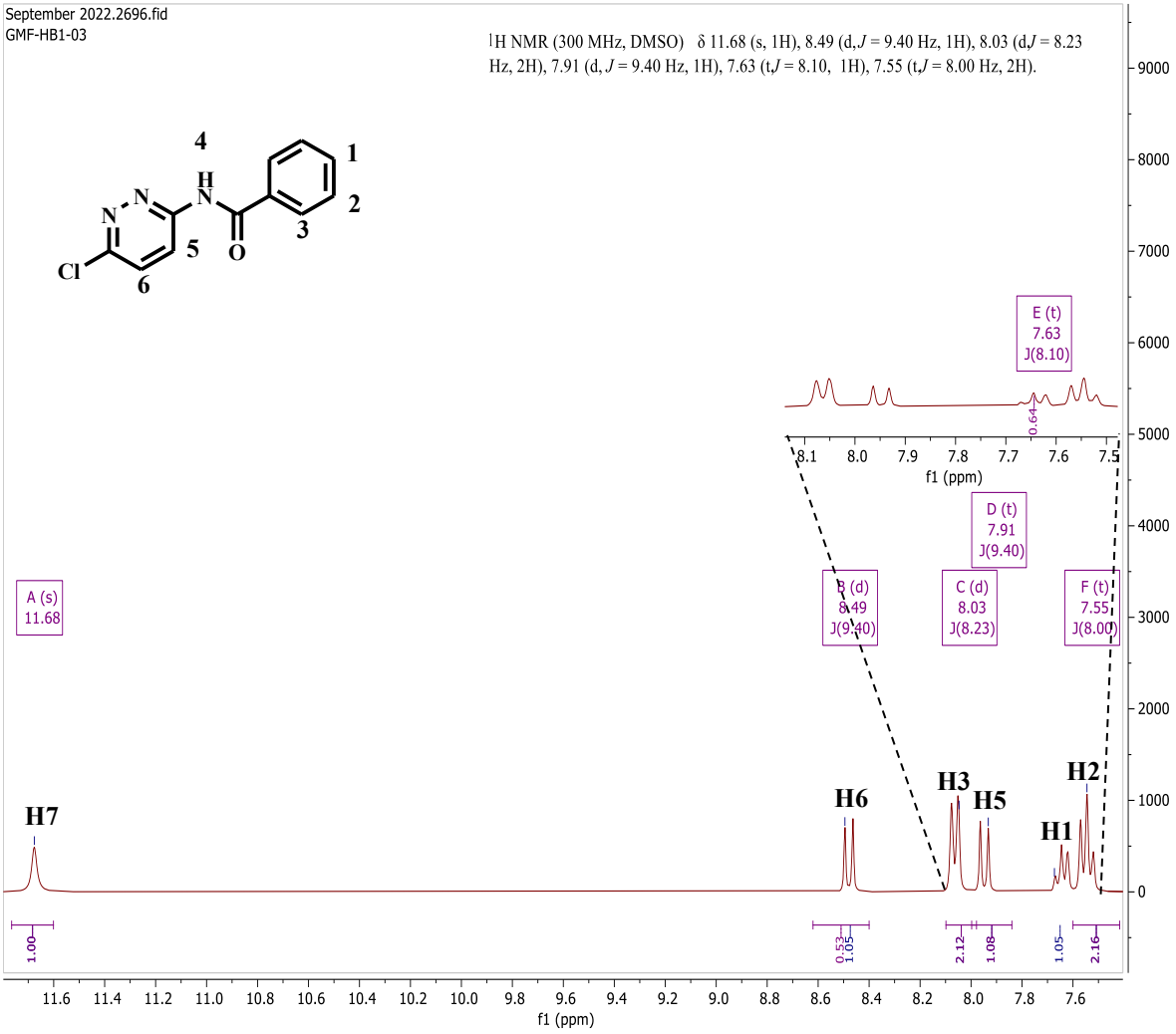

Figure 52: ^{1}H-NMR spectrum of **HB1-03** in DMSO-d_6 at 300 MHz.[1]

The doublet at δ = 8.49 ppm integrates for 1H corresponding to H^6 that experiences vicinal coupling ($^{3}J_{H\text{-}H}$ = 9.40 Hz) to H^5. Further upfield, the doublet at δ = 8.03 ppm integrating for 2H tallying with H^3 that experiences a short-range vicinal coupling to H^2 ($^{3}J_{H\text{-}H}$ = 8.23 Hz).[22] A triplet at δ = 7.91 ppm integrates for 1H corresponding to H^5 that experiences vicinal coupling ($^{3}J_{H\text{-}H}$) to H^6 (J = 9.40 Hz).[21]

Another triplet at δ = 7.63 ppm integrating for 1H was associated with H^1 within literature values of 6.2 - 8.4 ppm for phenyl protons that experiences a short-range vicinal coupling to H^2 ($^3J_{H\text{-}H}$ = 8.10 Hz).[11-22] Yet another triplet at δ = 7.55 ppm integrates for 2Hs corresponding to H^2 that experiences a short-range vicinal coupling to H^3 and H^1 ($^3J_{H\text{-}H}$ = 8.00 Hz).[11,22]

4.3.3.5 ^{13}C-NMR Analysis

The nine (9) peaks shown are representative of 9C environments (Figure 53), and a total of 11Cs present in the target compound.

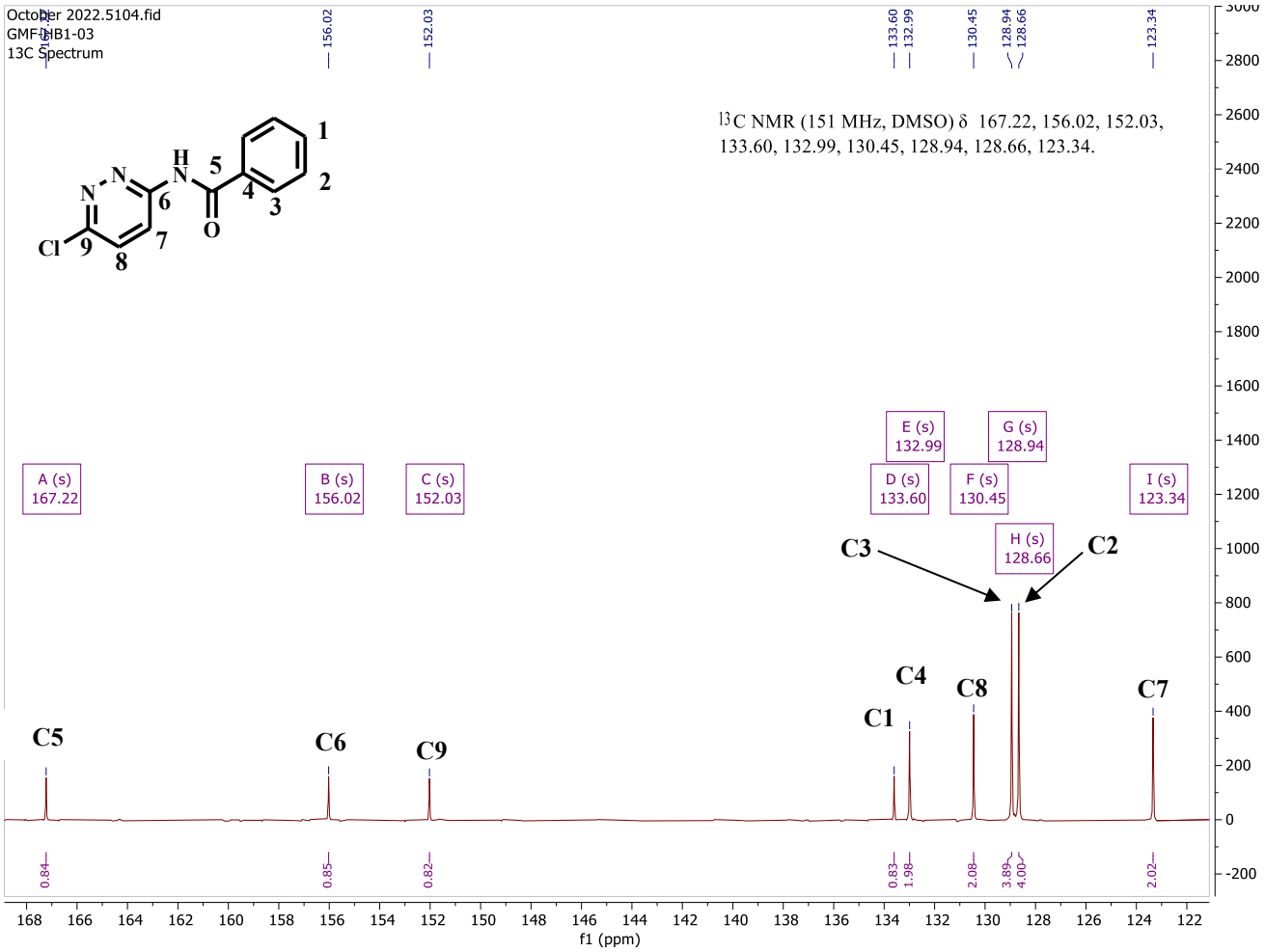

Figure 53: ^{13}C-NMR spectrum of **HB1-03** in DMSO-d_6 at 151 MHz.[1]

The presence of a diagnostic signal at δ = 167.22 ppm which is the most downfield was attributed to the carbonyl carbon (C^5) falling within literature values between 150 - 180 ppm for carbonyl carbons[21,22]. The other downfield signal at 156.02 ppm was attributed to the amidine carbon C^6, which is also relatively deshielded due to its attachment to two nitrogens.[23] Another signal at δ =

152.03 ppm was associated with the imine/ *C*-Cl carbon (C^9) within literature values of 152.8 - 155.7 ppm[11,22] for aryl halide carbons. The other less intense peak at 133.60 ppm arises from C^1 while those signals at 132.99 ppm, 130.45 ppm and 123.34 ppm were associated with C^4, C^8 and C^7, respectively. This assignment is reasonable because C^1 is the most deshielded amongst these three carbons – the deshielding effect arising from the resonance effect of the *para*-carbonyl functionality. On the other hand, C^7 is shielded by electron-enriching resonance effect of the *ortho*-amino while the effect is absent on carbon C^8. The signals at 128.94 ppm and 128.66 ppm, which are twice as intense as those for C^1, C^7 and C^8, were unambiguously assigned to C^3 and C^2, respectively.

4.3.3.6 Identification of HB1-03 as *N*-(6-chloropyridazin-3-yl)benzamide

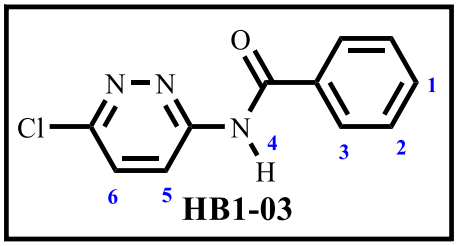

HB1-03

Obtained from 6-chloropyridazin-3-amine (0.314 g, 2.46 mmol, 1.0 eq) and benzoic acid (0.364 g, 2.96 mmol, 1.2 eq). Purified by column chromatography (EtOAc:Hex, 50:50) and crystallized in *n*-pentane/diethylether. White crystalline solid (0.267 g, 46.5%), R_f (EtOAc:Hex, 50:50) 0.60. ^{1}H-NMR (300 MHz, DMSO-d_6) δ_H 11.68 (s, 1H), 8.49 (d, J = 9.40 Hz, 1H), 8.03 (d, J = 8.23 Hz, 2H), 7.91 (d, J = 9.40 Hz, 1H), 7.63 (t, J = 8.10 Hz, 1H), 7.55 (t, J = 8.00 Hz, 2H). ^{13}C-NMR (151 MHz, DMSO-d_6) δ_C 167.22, 156.02, 152.03, 133.60, 132.99, 130.45, 128.94, 128.66, 123.34; IR $\tilde{\nu}$ (ZnSe ATR cell)/cm^{-1} 3100 (N-H, amide), 2800 (C-H), 1620 (C=O, amide), 1570 (C=C, aromatic); UV-Vis (MeOH): $\lambda_{max}^{MeOH} = 225$ nm; $\varepsilon_{max}^{MeOH} = 3{,}271.2$ L mol^{-1} cm^{-1}; LC-MS (ESI$^+$): found *m/z* $[M+H]^+$ = 234.1, calculated exact mass = 233.04, purity = 100%, t_R = 0.839 min, m.p. = 134 – 141 °C.

4.3.4 Characterization of HB2-13

4.3.4.1 LC-MS Analysis

Compound **HB2-13** was successfully synthesized as confirmed by the detection of its $[M+H]^+$ = 296.0 in the MS spectrum shown in Figure 54, consistent with a calculated exact mass of 294.98. The LC chromatogram acquired at λ = 280 nm showed that the compound had a t_R = 0.890 min with a purity of 100%.

LC Chromatogram at λ = 280 nm

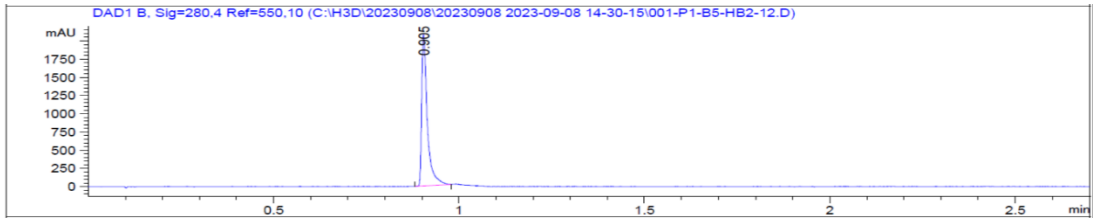

Signal 2: DAD1 B, Sig=280,4 Ref=550,10

Peak #	RetTime [min]	Type	Width [min]	Area [mAU*s]	Height [mAU]	Area %
1	0.905	BB	0.0165	2218.60864	2078.16187	100.0000
Totals :				2218.60864	2078.16187	

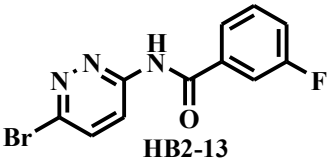

HB2-13
$C_{11}H_7BrFN_3O$
Exact Mass: 294.98
Molecular Weight: 296.1

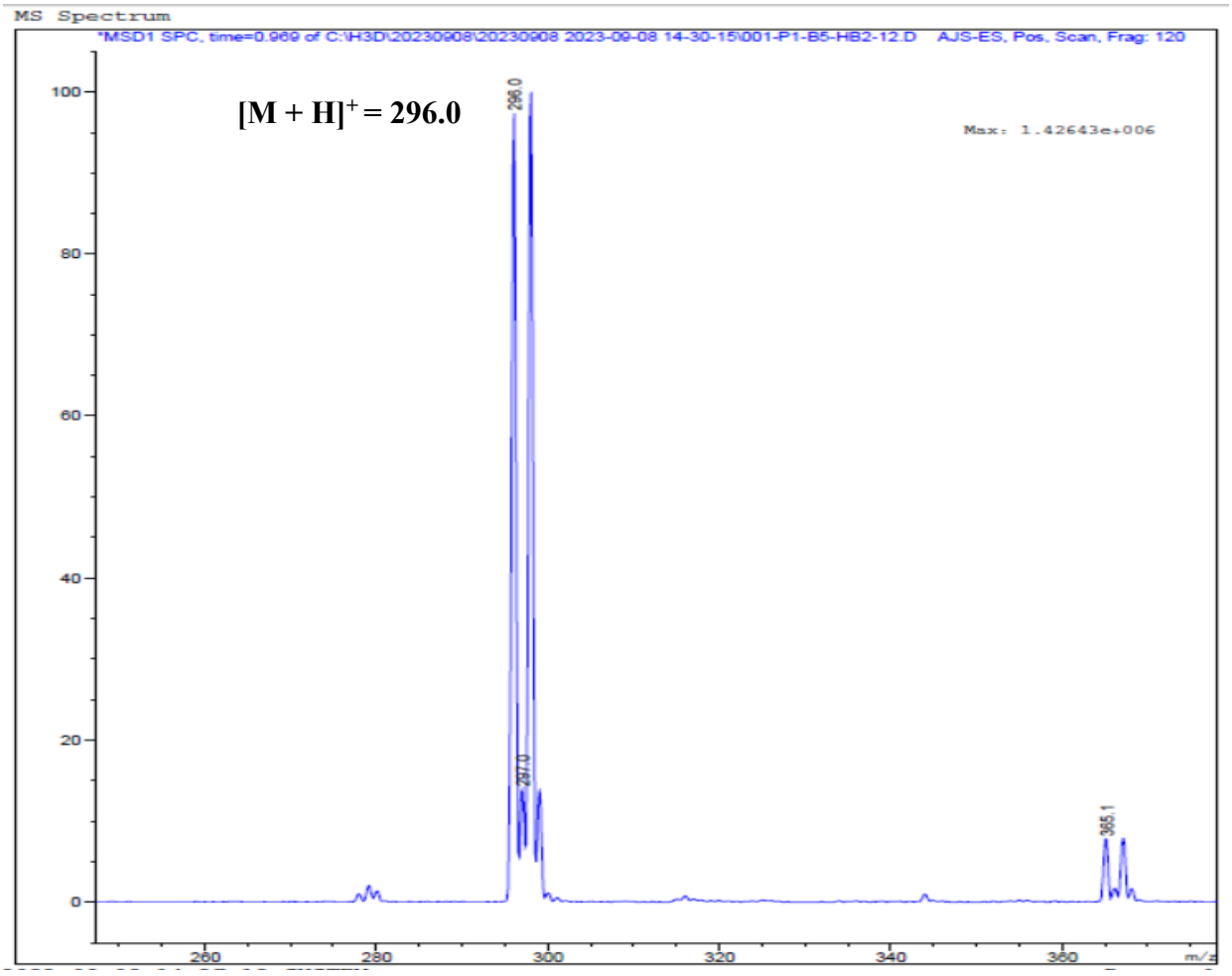

Figure 54: LC chromatogram (inset) and ESI$^+$ MS spectrum of **HB2-13**.[1]

As for **HB2-14** (*vide supra* subsection 4.3.2.1), the successful installation of a bromine-containing substructure was confirmed by a characteristic bromine pattern in the MS spectrum arising from an almost equal abundance of the two naturally occurring isotopes of bromine.[6]

4.3.4.2 UV-Vis Analysis

In the UV-Vis spectrum (Figure 55), the λ_{max} was observed at 225 nm. The experimental ε_{max} was found to be 4,145.4 L mol^{-1} cm^{-1}, as calculated by Equation 1.

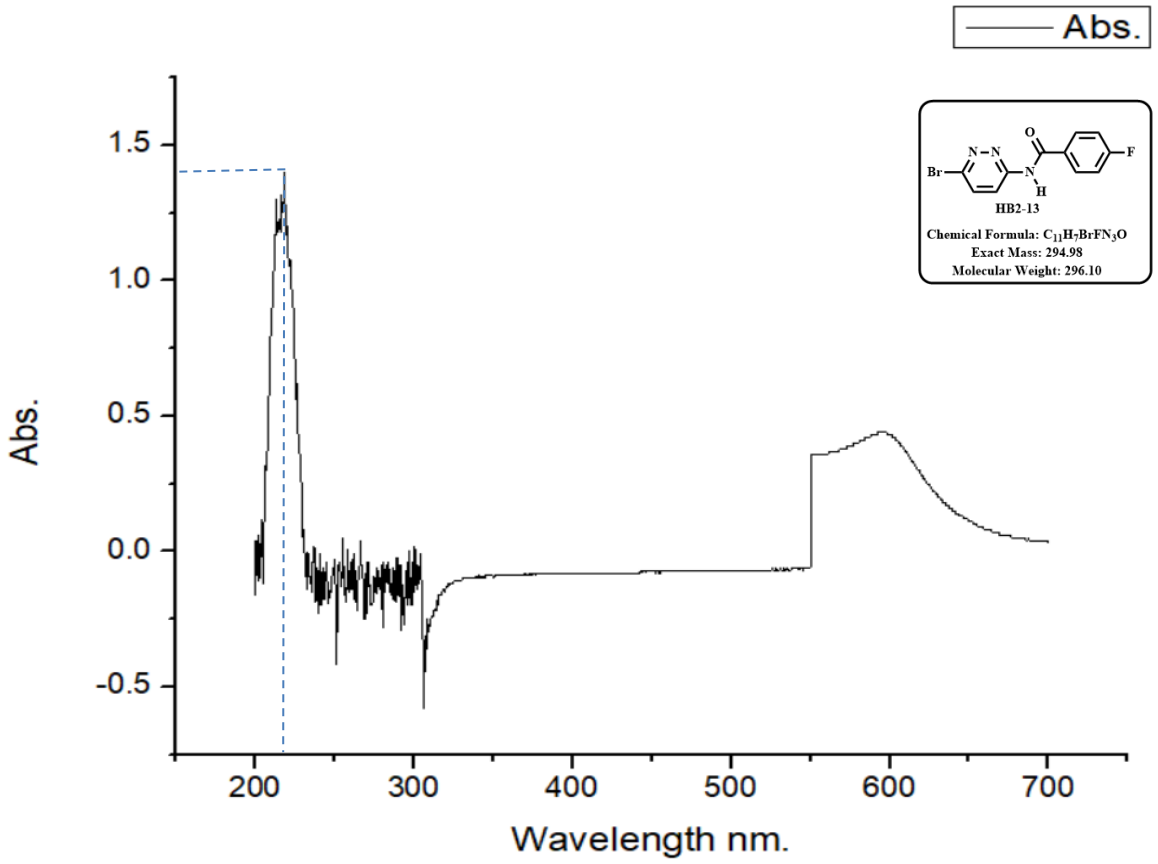

Figure 55: UV-Vis spectrum of **HB2-13** in MeOH.

4.3.4.3 IR Analysis

In the IR spectrum (Figure 56), the doublet N—H stretch observed at 3450 cm^{-1} around a literature value of 3400 cm^{-1} and the in-plane N—H bend band at 1520 cm^{-1} (literature value = 1600 cm^{-1}) was evidence for the successful installation of the amide group (Table 14).[12]

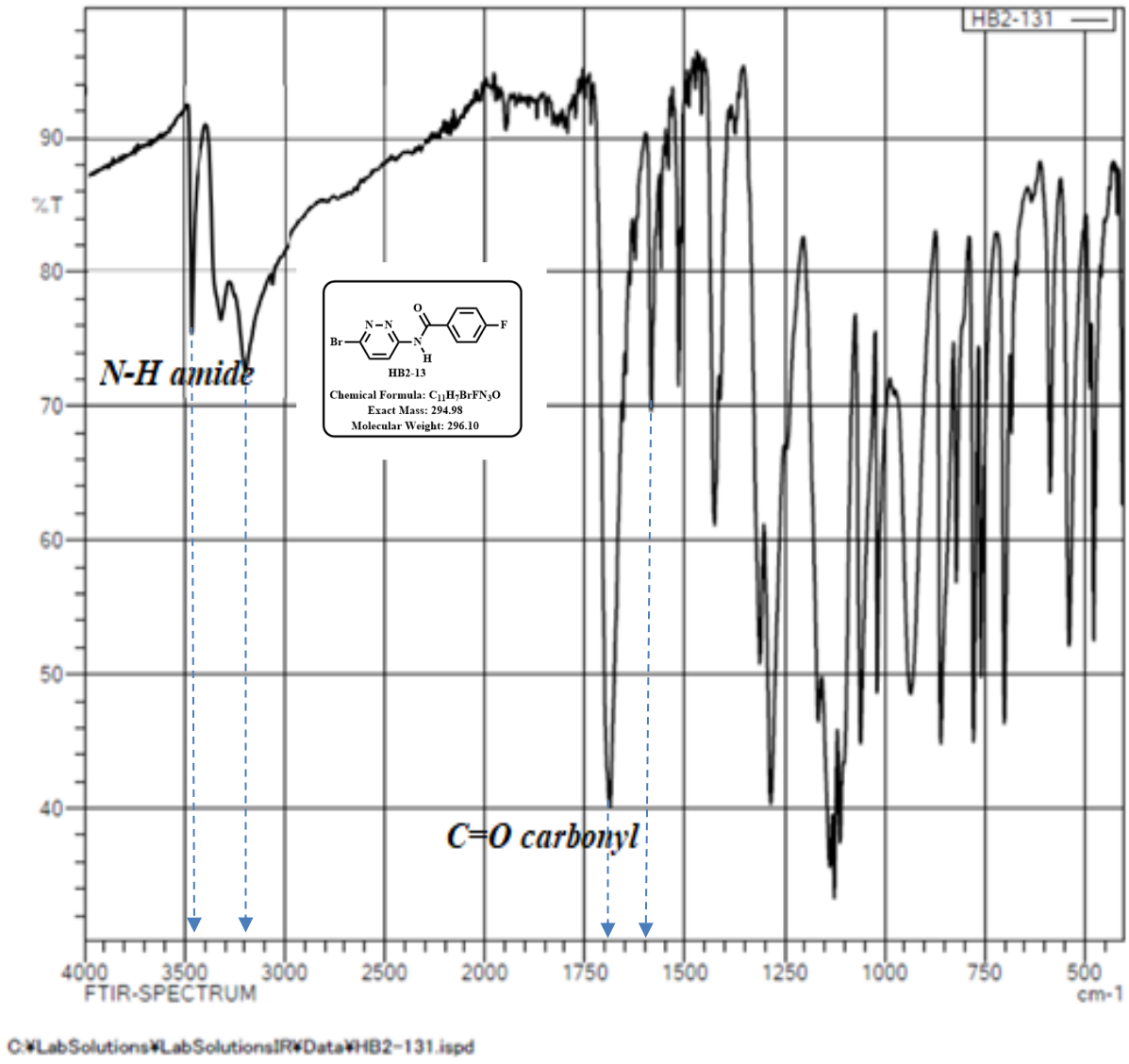

Figure 56: FT-IR spectrum of **HB2-13** using ZnSe ATR cell.

Table 14: Summary of FT-IR data for **HB2-13** using ZnSe ATR cell**.**

Absorption band ($\tilde{\nu}$/cm^{-1})	B band description	Bond type	Functional group	Vibration type
3450	m, (s), *d*	N-H	Amide	Stretch
3200	m, (br)	C-H		Stretch
1680	s, (s)	C=O	Amide	Stretch
1580	m, (s)	C=C	Aromatic	Stretch
1520	m, (s)	N-H	Amide	Bend

4.3.4.4 ^{1}H-NMR Analysis

The ^{1}H-NMR spectrum (Figure 57) shows five (5) signals assigned to a total of 7Hs present in the target compound.[7]

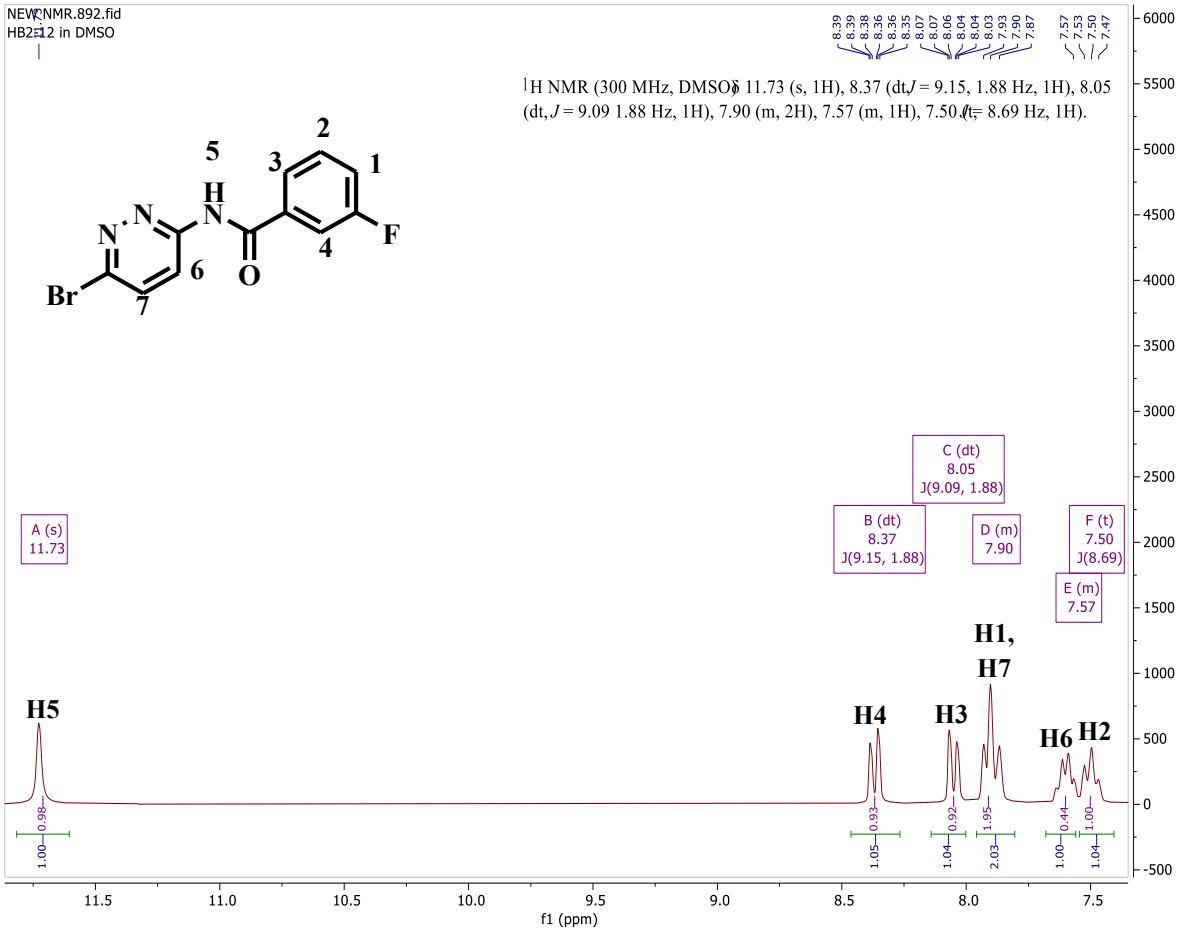

Figure 57: ^{1}H-NMR spectrum of **HB2-13** in DMSO-d_6 at 300 MHz.[1]

The most downfield singlet signal at δ = 11.73 ppm integrates for 1H (H^{5}) confirming amide-bond formation (N*H*). The doublet of triplets at δ = 8.37 ppm integrates for 1H correlating with H^{4} which experiences short-range vicinal coupling to H^{1} ($^{3}J_{\text{H-H}}$ = 9.15 Hz) and long-range coupling to H^{3} ($^{5}J_{\text{H-H}}$ = 1.88 Hz). Further upfield, the doublet of triplets at δ = 8.05 ppm integrating for 2H correlates with H^{3} within literature values between 6.2 - 8.5 ppm for phenyl protons,[11] that experiences short-range coupling to H^{2} ($^{3}J_{\text{H-H,}}$ = 9.09 Hz) and long-range coupling to F ($^{5}J_{\text{H-F,}}$ = 1.88 Hz).[22] The multiplet at δ = 7.90 ppm integrates for 1H corresponding to H^{1} and H^{7} that experiences short-range vicinal coupling to H^{2} ($^{3}J_{\text{H-H,}}$ = 9.53 Hz) and long-range coupling to H^{3} ($^{4}J_{\text{H-H,}}$ = 1.89 Hz).

The mutiplet at δ = 7.57 ppm integrating for 2H correlates with H^6 that experiences a short-range vicinal coupling to F ($^3J_{H\text{-}H}$ = 2.69 Hz) while the triplet at 7.50 ppm integrating for 1H correlated to H^2 which experiences short-range vicinal coupling to H^1 and H^3 ($^3J_{H\text{-}H}$ = 8.69 Hz).[22]

4.3.4.5 ^{13}C-NMR Analysis

The nine peaks shown are of 9C environments (Figure 58), and a total of 11Cs present in the target compound.

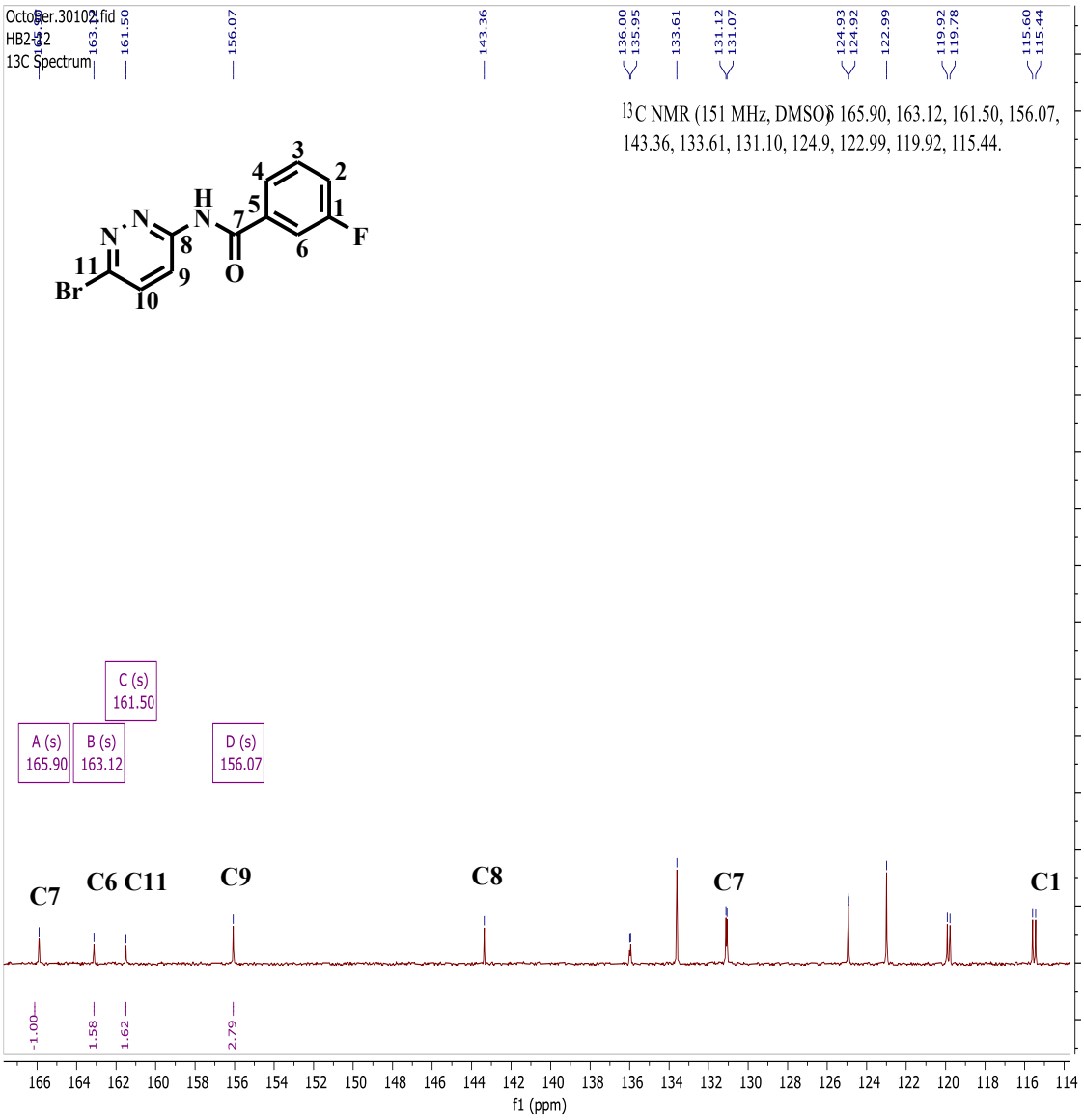

Figure 58: ^{13}C-NMR spectrum of **HB2-13** in DMSO-d_6 at 151 MHz.[1]

A diagnostic signal at δ = 165.90 ppm as the most downfield was attributed to the carbonyl carbon (C^7) which falls within literature values of 150 - 180 ppm for carbonyl carbons.[21,22] Another one further upfield at δ = 156.07 ppm was associated with the imine/ *C*-Br carbon (C^9) correlating with literature values of 152.8 - 155.7 ppm for aryl halide carbons.[11,22]

The relatively downfield peak at δ = 164.24 ppm is, most likely, due to the amidine carbon C^6, which is considerably deshielded by its attachment to two nitrogen atoms.[16] C^8 is more deshielded than C^7, the latter being shielded by the resonance effect from the ortho nitrogen. Therefore, the peak at δ = 143.20 ppm can be attributed to C^8 while C^7 is responsible for the peak at δ = 130.20 ppm. While the other signals may be much more challenging to accurately assign, the signal at δ = 115.83 ppm is a doublet which can be attributed to C^1 which couples to the fluorine atom.

4.3.4.6 Identification of HB2-13 as *N*-(6-bromopyridazin-3-yl)-4-fluorobenzamide

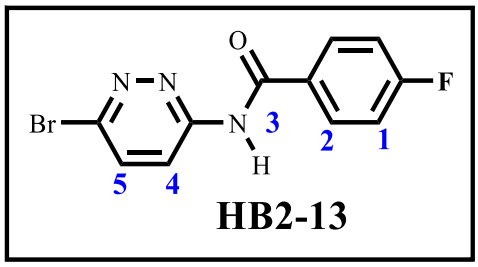

HB2-13

Obtained from 6-bromopyridazin-3-amine (0.213 g, 1.24 mmol, 1.0 eq) and 4-fluorobenzoic acid (0.208 g, 1.48 mmol, 1.2 eq). Purified by column chromatography (EtOAc:Hex, 50:50) and crystallized in *n*-pentane/diethylether. Beige crystalline solid (0.286 g, 77.91%), R_f (EtOAc:Hex, 50:50) 0.51. ^{1}H-NMR (300 MHz, DMSO-d_6) δ_H 11.68 (s, 1H), 8.37 (dt, J = 9.21, 2.00 Hz, 1H), 8.15 (m, 2H), 8.05 (dt, J = 9.53, 1.89 Hz, 1H), 7.39 (m, 2H). ^{13}C-NMR (151 MHz, DMSO-d_6) δ_C 165.90, 164.24, 156.20, 143.20, 133.55, 131.59, 130.20, 122.96, 115.83; IR $\tilde{\nu}$ (ZnSe/ATR cell)/cm^{-1} 3450 (N-H, amide), 3200 (C-H), 1680 (C=O, amide), 1580 (C=C, aromatic); UV-Vis (MeOH): λ_{max}^{MeOH} 225 nm; = $\varepsilon_{max}^{MeOH} = 4{,}145.4\ \mathrm{L\ mol^{-1}\ cm^{-1}}$; LC-MS (ESI$^+$): found *m/z* $[M+H]^+$ = 296.0, calculated exact mass = 294.98, purity = 100%, t_R = 0.890 min, m.p. = 149 – 153°C.

4.3.5 Characterization of HB3-05

4.3.5.1 LC-MS Analysis

Compound **HB3-05** was successfully synthesized as confirmed by the detection of its $[M+H]^+$ = 336.0 in the MS spectrum shown in Figure 59, consistent with a calculated exact mass of 335.05. The LC chromatogram acquired at λ = 280 nm showed that the compound had a t_R of 1.089 min with a purity of 100%.

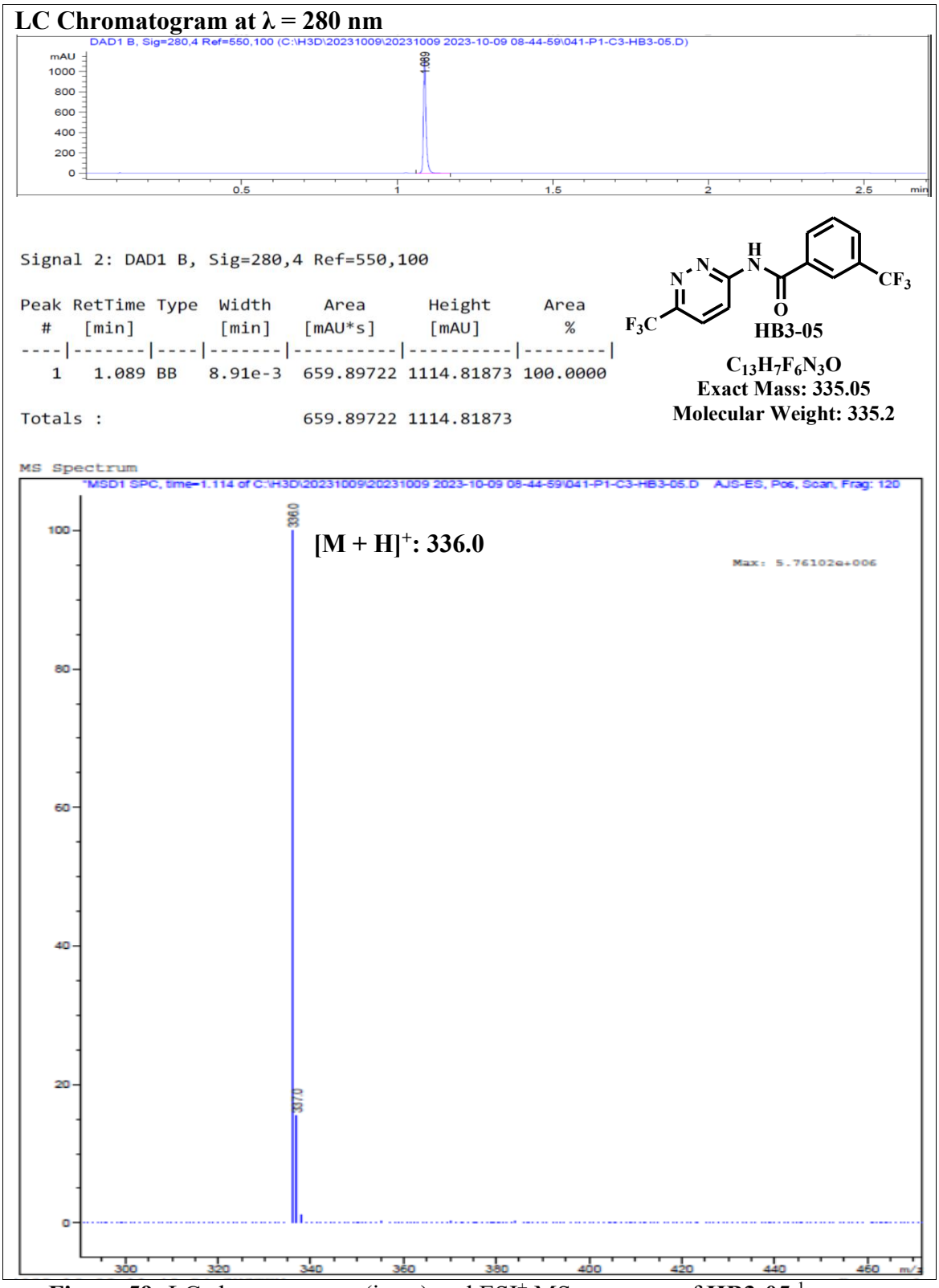

Figure 59: LC chromatogram (inset) and ESI$^+$ MS spectrum of **HB3-05**.[1]

4.3.5.2 UV-Vis Analysis

In the UV-Vis spectrum (Figure 60), the λ_{max} was observed at 330 nm. The experimental ε_{max} was found to be 11,732.3 L mol^{-1} cm^{-1}, as calculated by Equation 1.

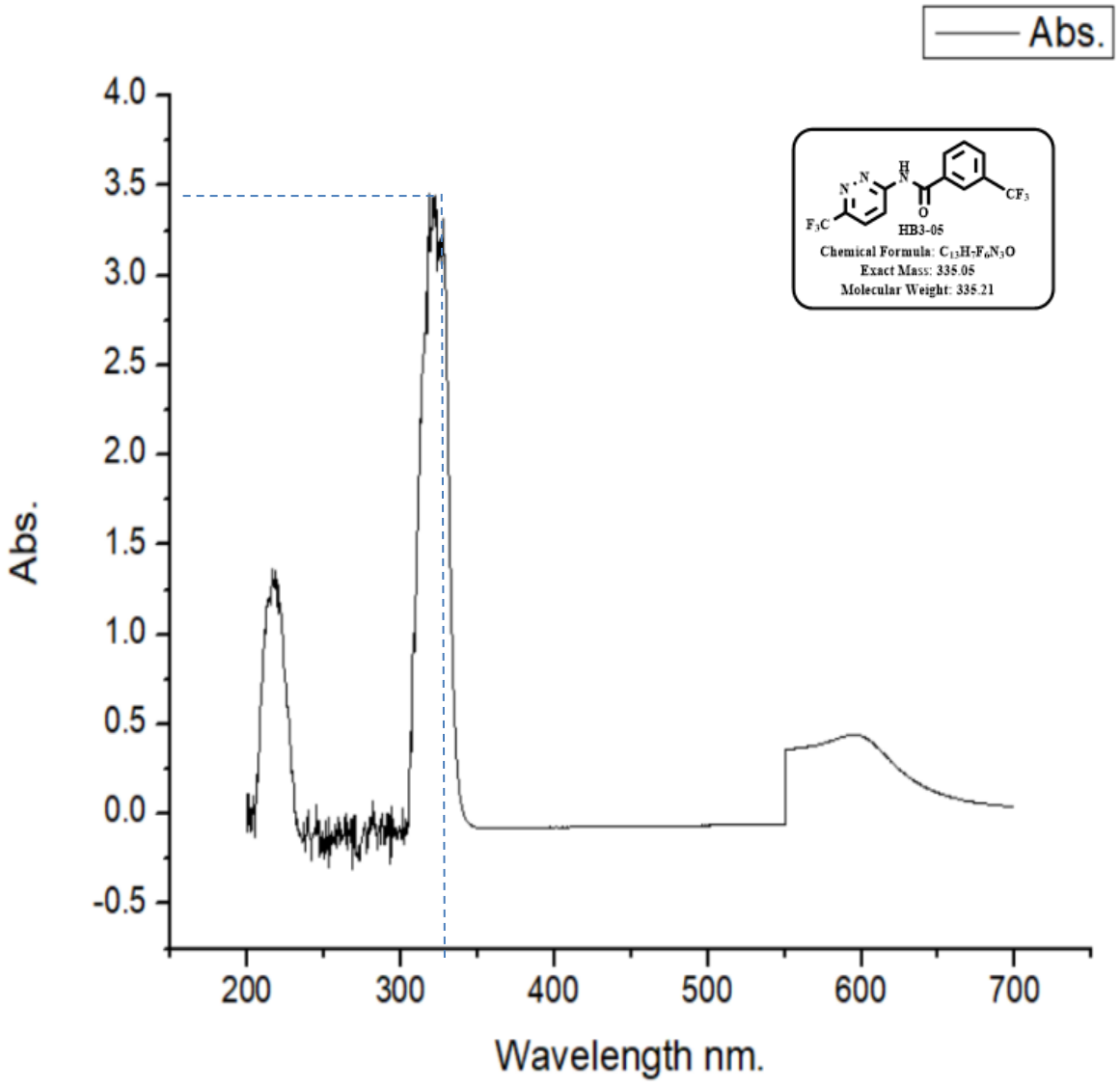

Figure 60: UV-Vis spectrum of **HB3-05** in MeOH.

4.3.5.3 IR Analysis

In the IR spectrum (Figure 61), the doublet N—H stretch observed at 3480 cm^{-1} around a literature value = 3400 cm^{-1} and the in-plane N—H bend band at 1500 cm^{-1} (literature value = 1600 cm^{-1}) was evidence for the successful installation of the amide group (Table 15).[12]

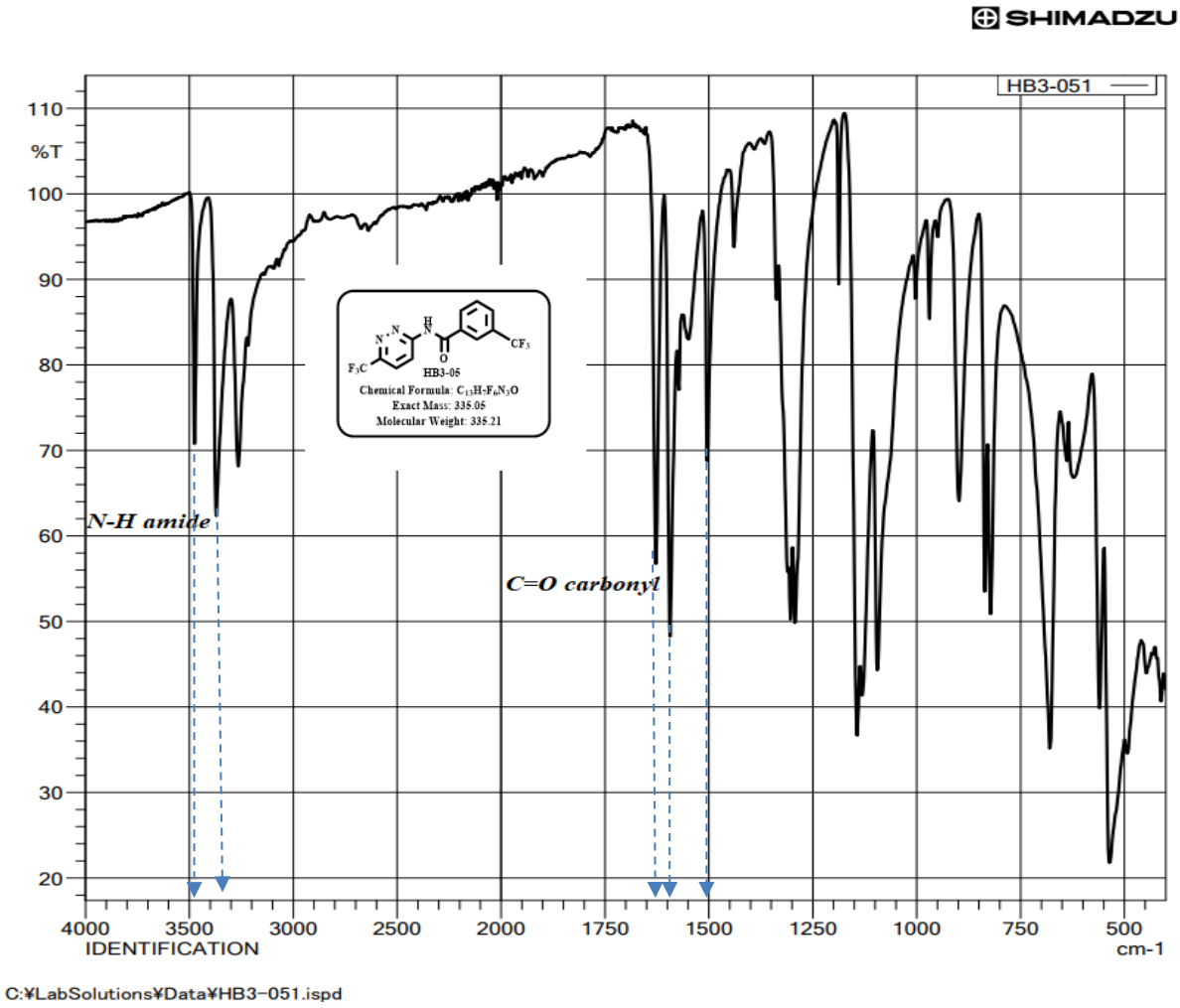

Figure 61: FT-IR spectrum of **HB3-05** using ZnSe ATR cell.

Table 15: Summary of FT-IR data for **HB3-05** using ZnSe ATR cell**.**

Absorption band ($\tilde{\nu}$/cm^{-1})	Band description	Bond type	Functional group	Vibration type
3480	m, (s), *d*	N-H	Amide	Stretch
3380	m, (s)	C-H		Stretch
1650	s, (s)	C=O	Amide	Stretch
1600	s, (s)	C=C	Aromatic	Stretch
1500	s, (s)	N-H	Amide	Bend

4.3.5.4 ^{1}H-NMR Analysis

The ^{1}H-NMR spectrum (Figure 62) shows five (5) signals assigned to a total of 7Hs present in the target compound.

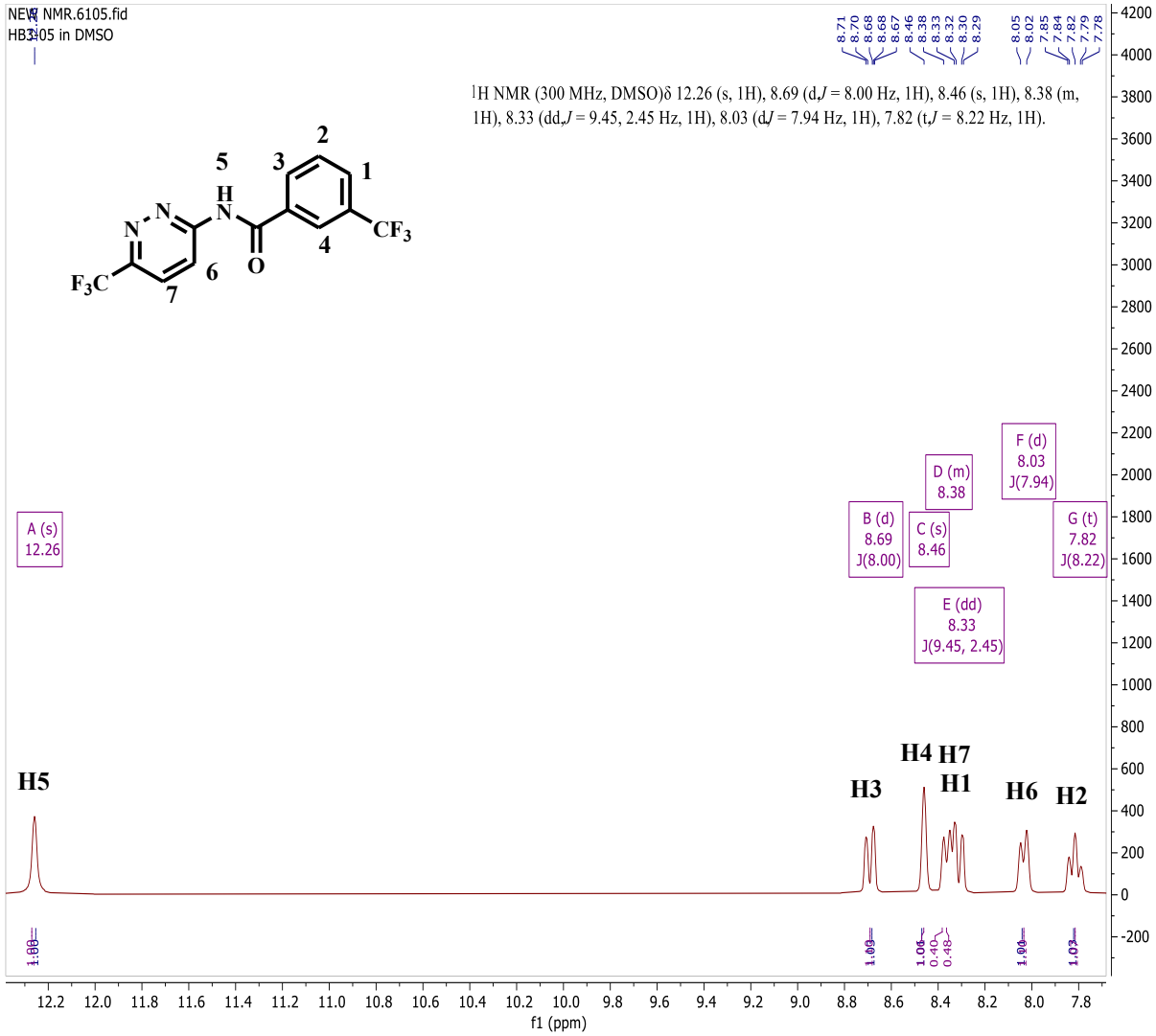

Figure 62: ^{1}H-NMR spectrum of **HB3-05** in DMSO-d_6 at 300 MHz.[1]

The most downfield singlet signal at δ = 12.26 ppm integrates for one proton (1H, H^5) confirming amide-bond formation (N*H*). The doublet at δ = 8.69 ppm integrates for one proton (1H) correlating with H^3 that experiences a short-range vicinal coupling to H^2 ($^{3}J_{H\text{-}H}$ = 8.00 Hz).[22] Further upfield, the singlet signal at δ = 8.46 ppm integrating for 1H correlates with H^4 within literature values 6.2 - 8.4 ppm for phenyl protons.[11]

The multiplet at δ = 8.38 ppm integrates for 1H corresponding to H^7. The doublet of doublets at δ = 8.33 ppm integrating for 1H correlates with H^1 that experiences a short-range vicinal coupling to H^2 ($^3J_{H\text{-}H,}$ = 9.45 Hz) with a literature value range of J = 7.5 - 10 Hz for phenyl protons and long-range coupling to F ($^4J_{H\text{-}F,}$ = 2.45 Hz).[11,21,22] The doublet at δ = 8.03 ppm integrating for 1H correlates with H^6 that experiences a short-range vicinal coupling to H^7 ($^3J_{H\text{-}H}$ = 7.94 Hz).[11] The triplet at δ = 7.82 ppm integrates for 1H correlating with H^2 that experiences a short-range vicinal coupling to H^1 and H^3 ($^3J_{H\text{-}H}$ = 8.22 Hz).[11,22]

4.3.5.5 ^{13}C-NMR Analysis

The peaks shown are representative of thirteen (13) chemically distinct carbon environments as numbered (Figure 63), and a total of thirteen (13) carbon atoms present in the target compound.

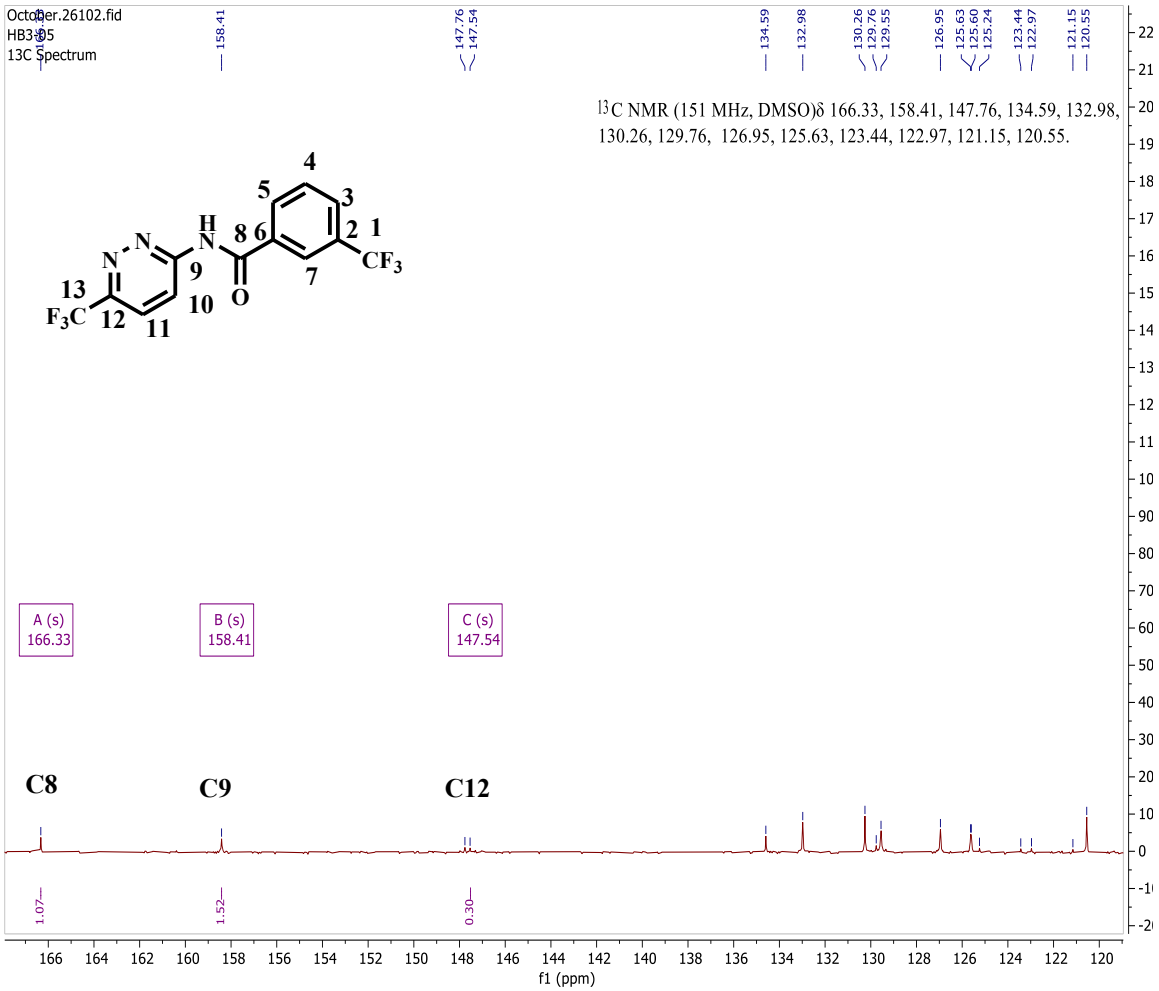

Figure 63: ^{13}C-NMR spectrum of **HB3-05** in DMSO-d_6 at 151 MHz.[1]

The presence of a diagnostic signal at δ = 166.33 ppm (most downfield), which was attributed to the carbonyl carbon (C^8) within literature values of 150 - 180 ppm for carbonyl carbons,[13,22] confirmed that the compound was successfully synthesized.

The signal at δ = 158.41 ppm was associated with the amidine carbon C^9 which is relatively deshielded for the same reasons given in the discussion of the NMR data for other compounds.[15] The imine carbon C^{12} accounted for the signal at δ = 147.54 ppm while the other signals cannot be assigned unambiguously in the absence of other advanced NMR techniques (section 5.4).

4.3.5.6 Identification of HB3-05 as 3-(Trifluoromethyl)-*N*-(6-(trifluoromethyl)pyridazin-3-yl)benzamide

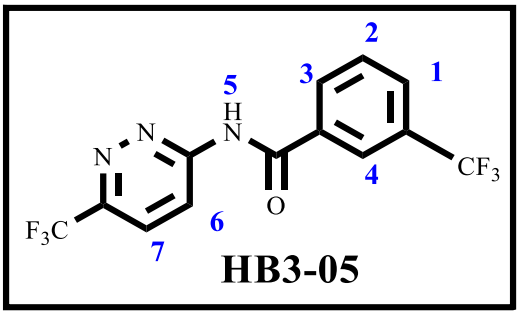

Obtained from 6-(trifluoromethyl)pyridazin-3-amine (0.202 g, 1.24 mmol, 1.0 eq) and 3-(trifluoromethyl)benzoic acid (0.284 g, 1.48 mmol, 1.2 eq). Purified by column chromatography (EtOAc:Hex, 50:50) and crystallized in *n*-pentane/diethyl ether. Brown amorphous solid (0.296 g, 71.3%), R_f (EtOAc:Hex, 50:50) 0.66. ^{1}H-NMR (300 MHz, DMSO-d_6) δ_H 12.26 (s, 1H), 8.69 (d, J = 8.00 Hz, 1H), 8.46 (s, 1H), 8.38 (m, 1H), 8.33 (dd, J = 9.45, 2.45 Hz, 1H), 8.03 (d, J = 7.94 Hz, 1H), 7.82 (t, J = 8.22 Hz, 1H). ^{13}C-NMR (151 MHz, DMSO-d_6) δ_C 166.33, 158.41, 147.76, 134.59, 132.98, 130.26, 129.76, 126.95, 125.63, 123.44, 122.97, 121.15, 120.55; IR $\tilde{\nu}$ (ZnSe ATR cell)/cm^{-1} 3480 (N-H, amide), 3380 (C-H), 1650 (C=O, amide), 1600 (C=C, aromatic); UV-Vis (MeOH): $\lambda_{max}^{MeOH} = 330$ nm; $\varepsilon_{max}^{MeOH} = 11{,}732.3\ \text{L mol}^{-1}\ \text{cm}^{-1}$; LC-MS (ESI$^+$): *m/z* $[M+H]^+$ = 336.0, calculated exact mass = 335.05, purity = 100%, t_R = 1.089 min, m.p. = 209 – 214°C.

4.3.6 Characterization of HB2-12

4.3.6.1 LC-MS Analysis

Compound **HB2-12** was successfully synthesized as confirmed by the detection of its $[M+H]^+$ = 296.0 in the MS spectrum shown in Figure 64, consistent with a calculated exact mass of 294.98. The LC chromatogram acquired at λ = 280 nm showed that the compound had a t_R of 0.905 min with a purity of 100%.

LC Chromatogram at λ = 280 nm

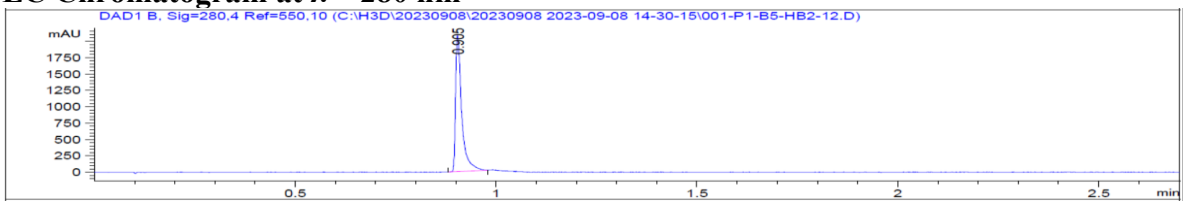

Signal 2: DAD1 B, Sig=280,4 Ref=550,10

Peak #	RetTime [min]	Type	Width [min]	Area [mAU*s]	Height [mAU]	Area %
1	0.905	BB	0.0165	2218.60864	2078.16187	100.0000
Totals :				2218.60864	2078.16187	

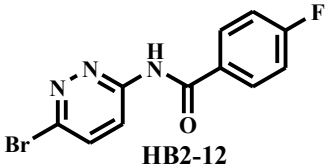

HB2-12
$C_{11}H_7BrFN_3O$
Exact Mass: 294.98
Molecular Weight: 296.1

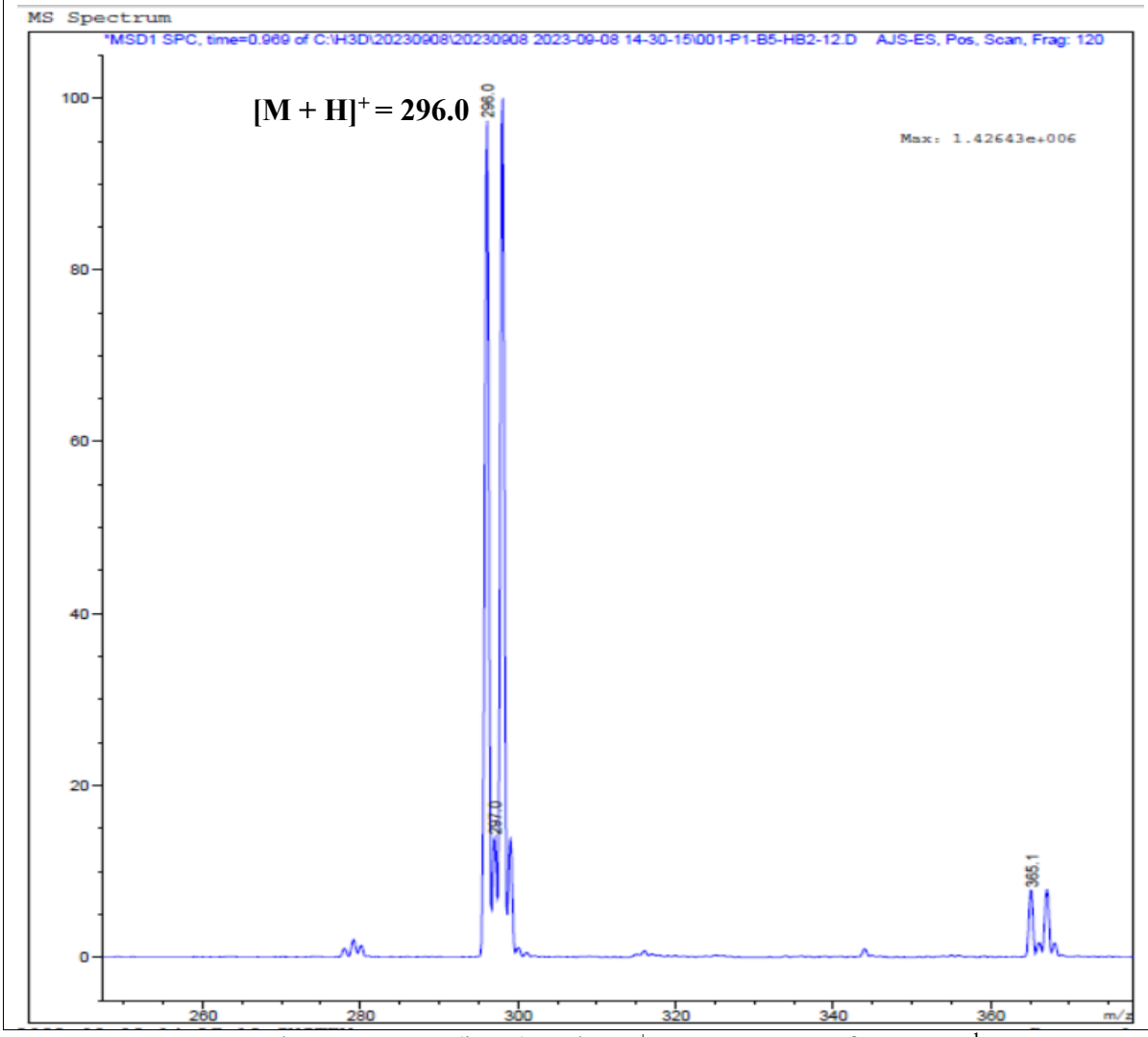

Figure 64: LC chromatogram (inset) and ESI$^+$ MS spectrum of **HB2-12**.[1]

As for **HB2-14** and **HB2-13** (*vide supra* subsection 4.3.2.1 and 4.3.2.1), the successful installation of a bromine-containing substructure was confirmed by a characteristic bromine pattern in the MS spectrum arising from an almost equal abundance of the two naturally occurring isotopes of bromine".[6]

4.3.6.2 UV-Vis Analysis

In the UV-Vis spectrum (Figure 65), the λ_{max} was observed at 225 nm. The experimental ε_{max} was found to be 4,145.4 L mol^{-1} cm^{-1}, as calculated by Equation 1.

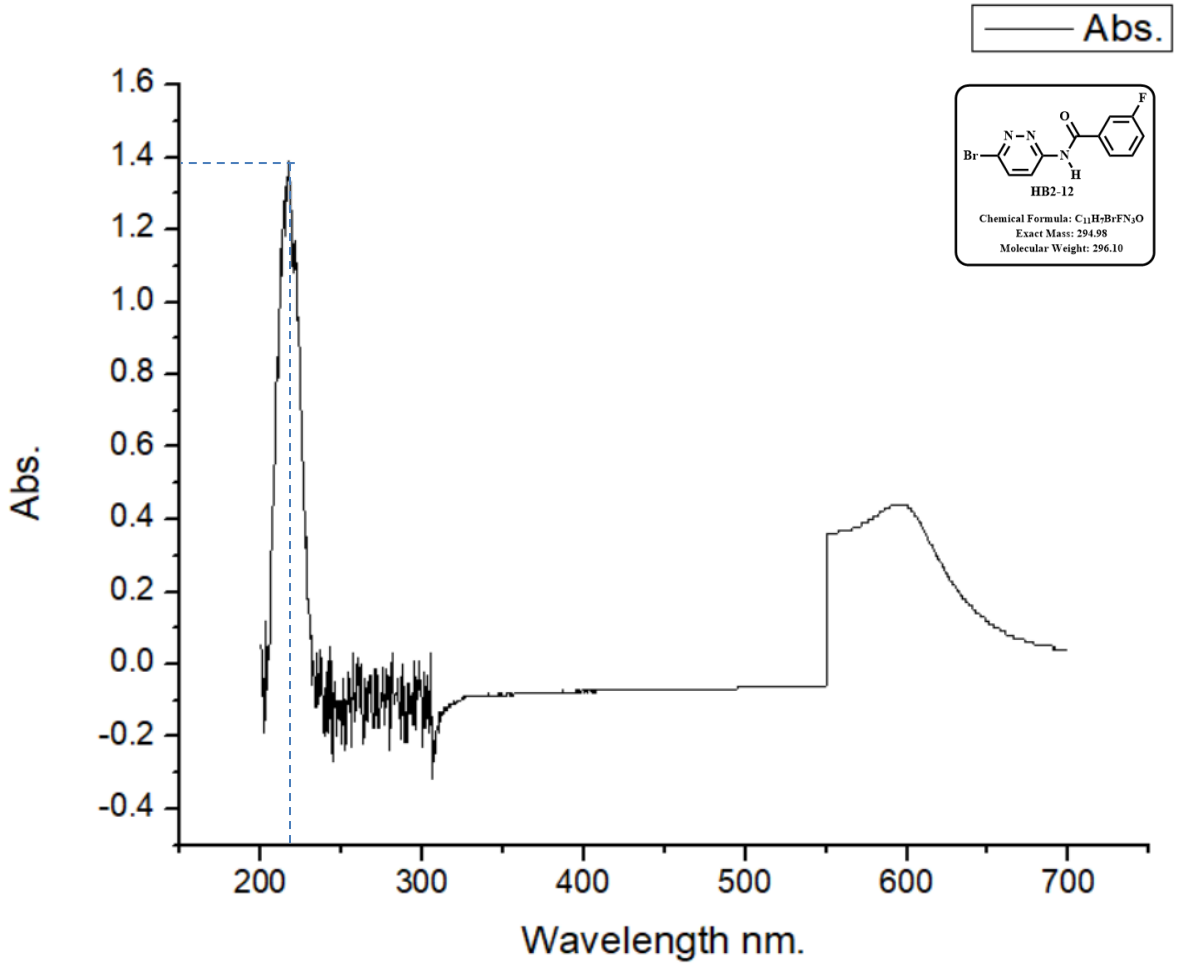

Figure 65: UV-Vis spectrum of **HB2-12** in MeOH.

4.3.6.3 IR Analysis

In the IR spectrum (Figure 66), the doublet N—H stretch observed at 3450 cm^{-1} around a literature value = 3400 cm^{-1} and the in-plane N—H bend band at 1600 cm^{-1} (literature value = 1600 cm^{-1}) was evidence for the successful installation of the amide group (Table 16).[12]

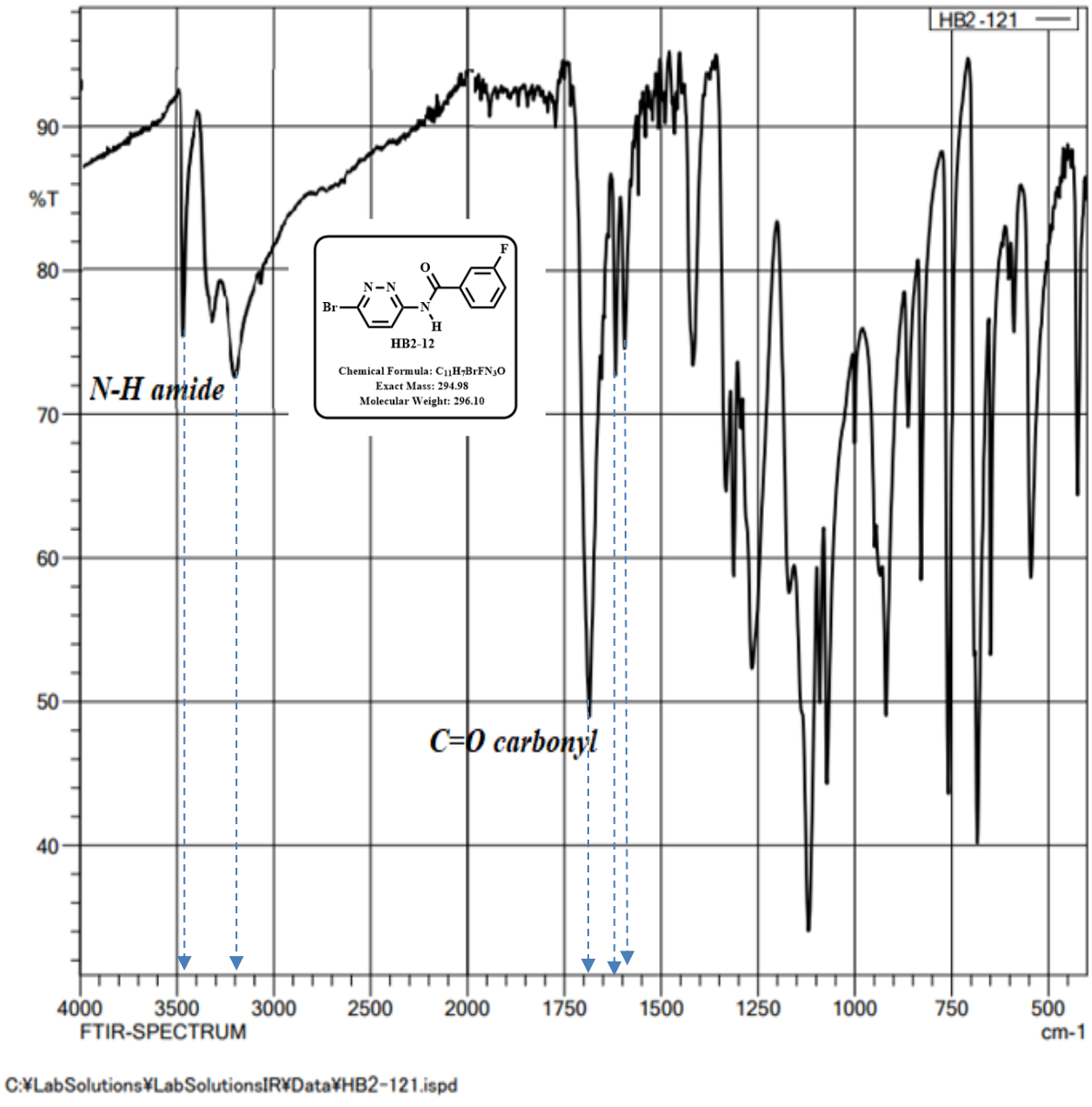

Figure 66: FT-IR spectrum of **HB2-12** using ZnSe ATR cell.

Table 16: Summary of FT-IR data for **HB2-12** using ZnSe ATR cell**.**

Absorption band ($\tilde{\nu}$/cm^{-1})	Band description	Bond type	Functional group	Vibration type
3450	m, (s), *d*	N-H	Amide	Stretch
3200	m, (br)	C-H		Stretch
1680	s, (s)	C=O	Amide	Stretch
1620	s, (s)	C=C	Aromatic	Stretch
1600	w (s)	N-H	Amide	Bend

4.3.6.4 ^{1}H-NMR Analysis

The ^{1}H-NMR spectrum (Figure 67) shows seven (7) signals assigned to 7H present in the target compound.

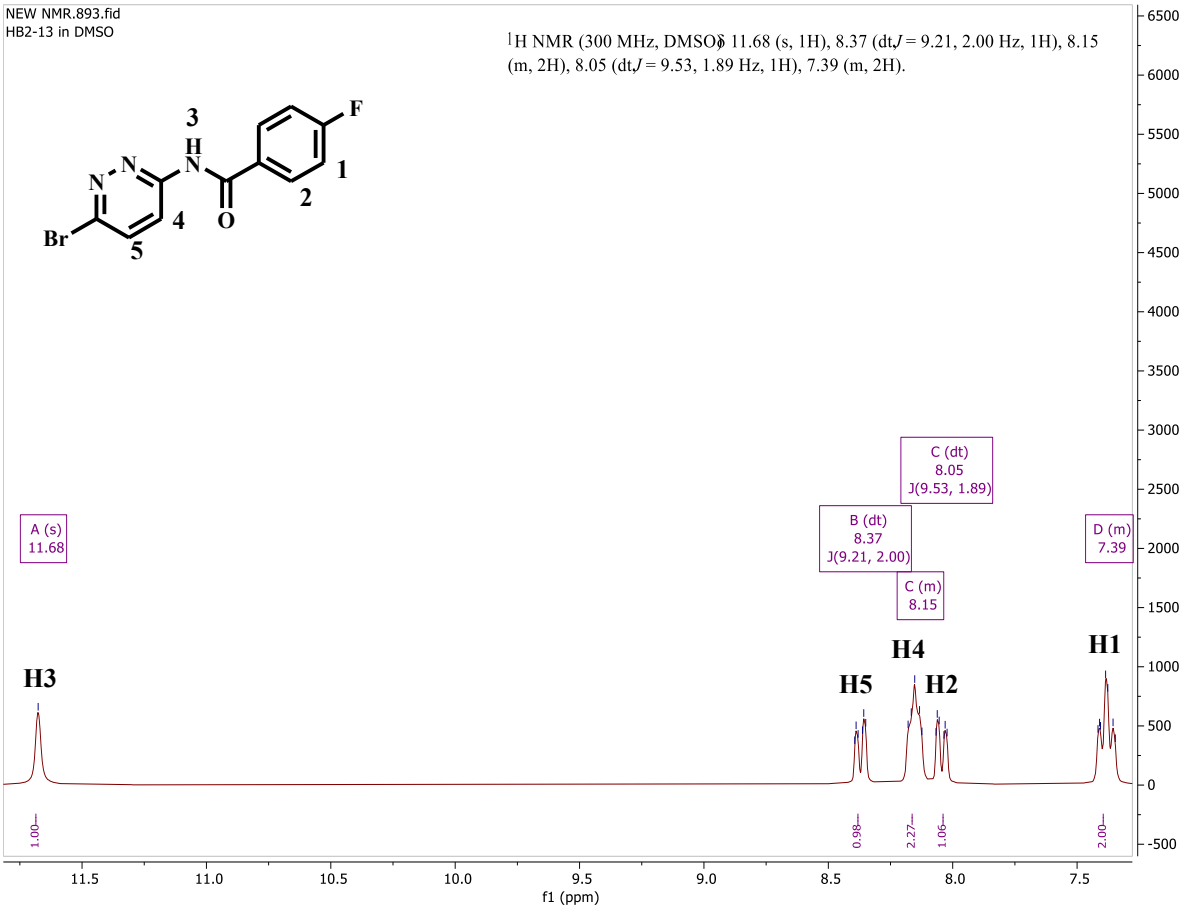

Figure 67: ^{1}H-NMR spectrum of **HB2-12** in DMSO-d_6 at 300 MHz.[1]

The most downfield singlet signal at δ = 11.68 ppm integrates for 1H (H^3) confirming amidation. In this compound, ^{1}H to ^{1}H coupling and ^{1}H to ^{19}F are both considered.[7] Upfield, the doublet of triplets at δ = 8.37 ppm integrating for 1H correlates with H^5 within literature values of 6.2 - 8.4 ppm for phenyl protons[11] that experiences vicinal coupling to F ($^3J_{H\text{-}H}$ = 9.21 Hz) within literature values of J = 7.5 - 10 Hz for phenyl protons[23] and long-range coupling to H^1 ($^4J_{H\text{-}F}$ = 2.00 Hz). Upfield, the doublet of multiplet at δ = 8.15 ppm integrating for 1H correlates with H^4. The doublet of triplets at 8.05 ppm integrating for 2H correlates with H^2 that experiences a short-range vicinal coupling to H^1 ($^3J_{H\text{-}H}$ = 9.53 Hz) and F ($^3J_{H\text{-}H}$ = 1.89 Hz).[22] The multiplet at 7.39 ppm integrating for 1H correlates with H^1.

4.3.6.5 ^{13}C-NMR Analysis

The peaks shown are for 11 chemically distinct C environments (Figure 68), and a total of 11C present in the target compound.

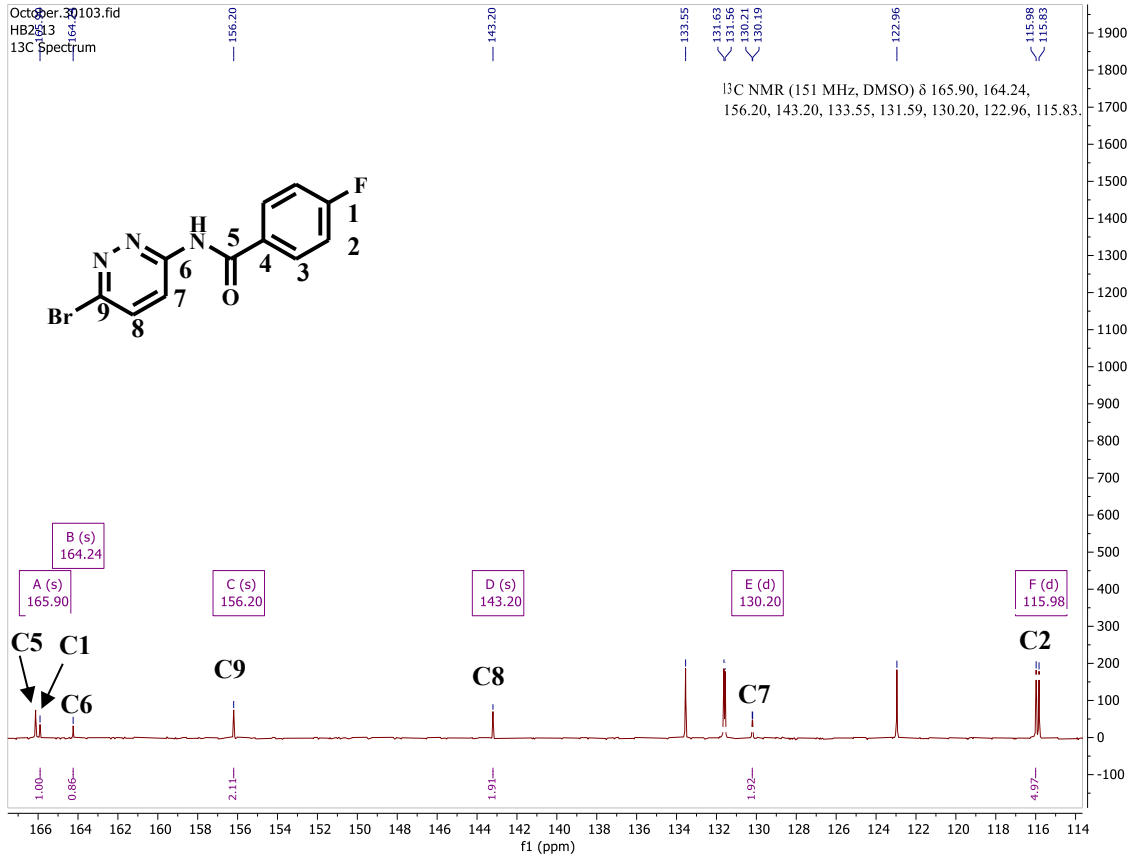

Figure 68: ^{13}C-NMR spectrum of **HB2-12** in DMSO-d_6 at 151 MHz.[1]

As was the case with previous compounds discussed (*vide supra*), the signal at δ = 165.90 ppm was attributed to the carbonyl carbon C^7 within literature values of 150 - 180 ppm for carbonyl carbons[13,14] confirming the successful synthesis of the target compound.

The amidine carbon C^8, which is common across all compounds, resonated at δ = 156.07 ppm while the new signal at δ = 163.12 ppm was associated with a new carbon environment, C^1, arising from the incorporation of a fluorine in the benzene ring.[13-15] The imine/ *C*-Br carbon C^{11}, also being relatively deshielded, resonated at δ = 161.50 ppm around literature values of 152.8 - 155.7 ppm for aryl halide carbons.[11,22]

4.3.6.6 Identification of HB2-12 as *N*-(6-bromopyridazin-3-yl)-3-fluorobenzamide

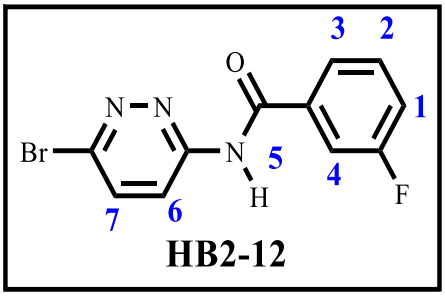

HB2-12

Obtained from 6-bromopyridazin-3-amine (0.213 g, 1.24 mmol, 1.0 eq) and 3-fluorobenzoic acid (0.208 g, 1.48 mmol, 1.2 eq). Purified by column chromatography (EtOAc:Hex, 50:50) and crystallized in *n*-pentane/diethylether. Light brown crystalline solid (0.209 g, 56.9%), R_f (EtOAc:Hex, 50:50) 0.43. ^{1}H-NMR (300 MHz, DMSO-d_6) δ_H 11.73 (s, 1H), 8.37 (dt, *J* = 9.15, 1.88 Hz, 1H), 8.05 (dt, *J* = 9.09, 1.88 Hz, 1H), 7.90 (m, 2H), 7.57 (m, 1H), 7.50 (t, *J* = 8.69 Hz, 1H). ^{13}C-NMR (151 MHz, DMSO-d_6) δ_C 165.90, 163.12, 161.50, 156.07, 143.36, 133.61, 131.10, 124.9, 122.99, 119.92, 115.44; IR $\tilde{\nu}$ (ZnSe ATR cell)/cm^{-1} 3450 (N-H, amide), 3200 (C-H), 1680 (C=O, amide), 1620 (C=C, aromatic); UV-Vis (MeOH): $\lambda_{max}^{MeOH} =$ 225 nm; $\varepsilon_{max}^{MeOH} = 4{,}145.4$ L mol^{-1} cm^{-1}; LC-MS (ESI$^+$): found *m/z* $[M+H]^+$ = 296.0, calculated exact mass = 294.98, purity = 100%, t_R = 0.905 min, m.p. = 150 – 156°C.

4.4 Characterization of Unwanted Products

HB3-02 appears to have been unsuccessful as can be judged by the absence of its corresponding pseudomolecular ion in the MS spectrum. Close scrutiny of the *m/z* ratio for the base peak in Figure 69 reveals that the recorded mass to change ratio is 345.0 which is less than the expected value (355.05) by 10 mass units which is too much to rationalize deprotonation. Since the method of ionization was soft, fragmentation would also not be a rational explanation.

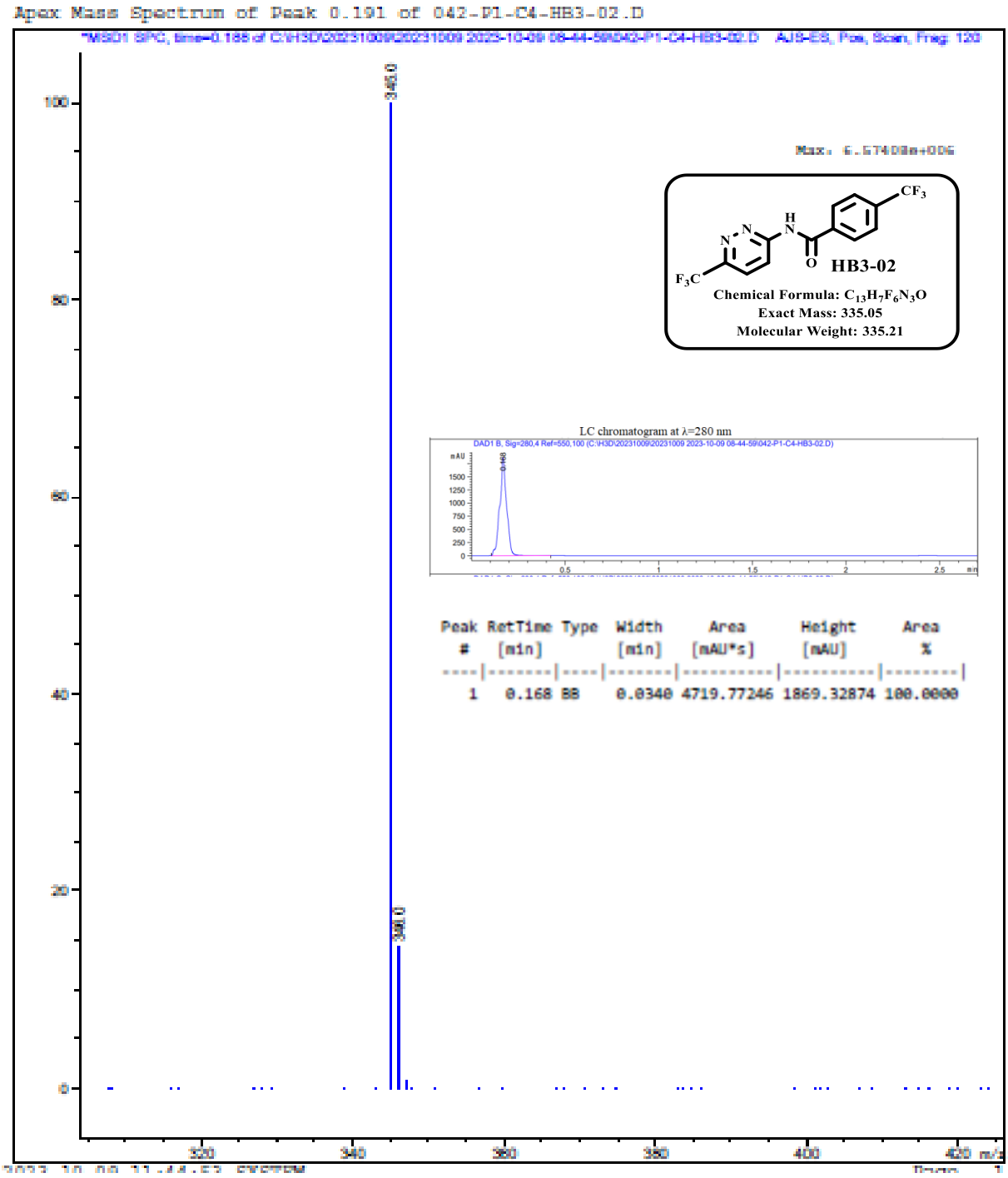

Figure 69: LC chromatogram (inset) and ESI$^+$ MS spectrum of **HB3-02.**

Close scrutiny of the *m/z* ratio for the base peak in Figure 69 and NMR spectra (Figure 71 and Figure 72) suggests that this unwanted product could correspond to the intermediate formed between the carboxylic acid and EDCI (exact mass = 345.166), as per mechanism in Figure 69 which is not complete as expected in Figure 38.

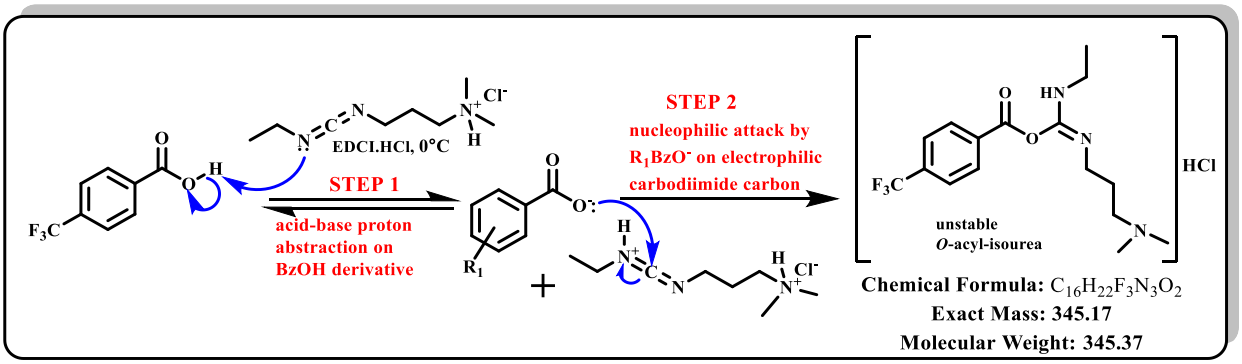

Figure 70: Incomplete mechanism showing formation of an unwanted *O*-acyl isourea product instead of **HB3-02.**

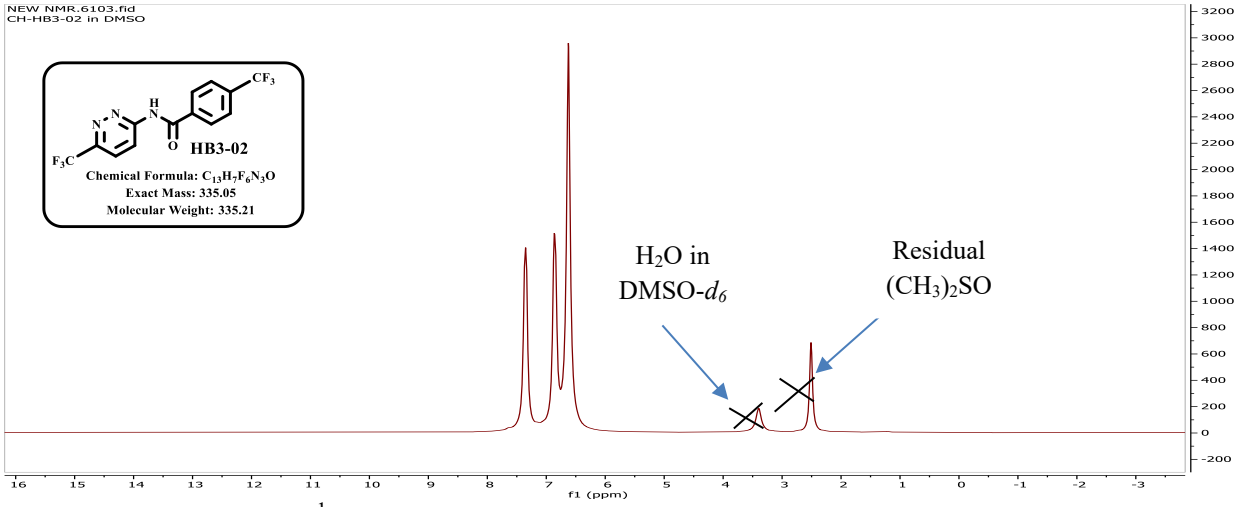

Figure 71: ^{1}H-NMR spectrum of **HB3-02** in DMSO-d_6 at 300 MHz.

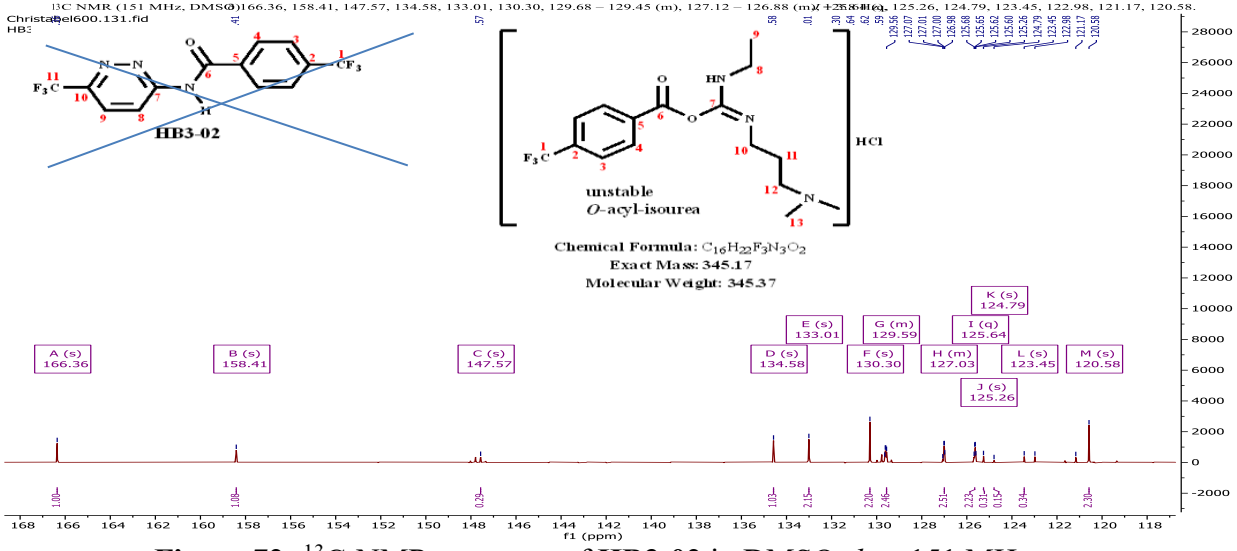

Figure 72: ^{13}C-NMR spectrum of **HB3-02** in DMSO-d_6 at 151 MHz.

The numbers of peaks in both NMR spectra (Figure 71 and Figure 72) are not consistent with the final product identified hence this could have been an *O*-acyl isourea intermediate (Figure 72) having 13 peaks in the ^{13}C-NMR spectrum accordingly, not the 11 peaks expected for **HB3-02**.

Reactions meant to furnish other target compounds coded as **HB2-03**, **HB2-02** and **HB2-04** appear to have been unsuccessful as judged from LC-MS experiments.

4.5 *In Vitro* Antischistosomal Assays

4.5.1 Severity Score Assays on Adult *S. mansoni*

The compounds synthesized in this research work were all inactive (severity score ≤1) albeit some revealed interesting structure-activity relationships with respect to the previously reported analogues (Table 17). In this regard, **HB4-02** was noteworthy. This compound is a closely related analogue of **MK1-11** with a very subtle difference – two carbons in the aniline portion of **MK1-11** being replaced by nitrogens (Table 5).[2] Although subtle, this change resulted in complete elimination of *in vitro* antischistosomal activity. This may suggest that the introduction of a pyridazine ring system is detrimental to activity.

Similarly, **HB3-05** is a closely related analogue of **AD-03** – the later compound was shown to exhibit substantial activity on adult worms *in vitro*. The almost complete elimination of activity which accompanies the replacement of two carbons on the aniline portion of **AD-03** with nitrogens to furnish **HB3-05** reveals the pyridazine ring system is unfavourable to activity.

The other four pyridazinic compounds in this study were equally inactive on adult worms suggesting the aniline-pyridazine replacement may not be tolerated which is not surprising as such molecular edits of this type can indeed either increase, reduce or even maintain activity (section 2.6).

Table 17 shows the phenotypic changes and severity scores of the target compounds assayed alongside **MK1-11**:[1]

Table 17: Phenotypic changes and severity scores for the effect of target compound exposure on adult *S. mansoni* at 5 µM.[1]

Compd code	Structure	Phenotypic changes*				Severity scores*			
		2 h	5 h	24 h	48 h	2 h	5 h	24 h	48 h
HB1-03	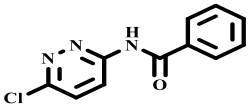	*S-Unc*				1	0	0	0
HB2-12	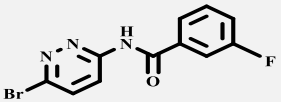	*S*				1	0	0	0
HB2-13	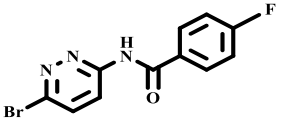					0	0	0	0
HB2-14	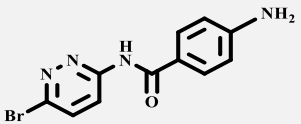					0	0	0	0
HB3-05	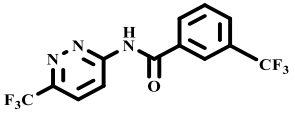	*S*	*S-Unc*			1	1	0	0
HB4-02	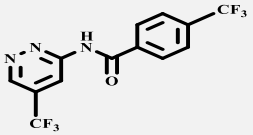					0	0	0	0
MK1-11[11]	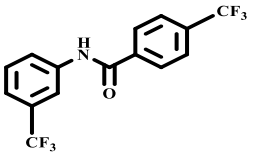	*S, on sides, slight shrunk*	*S, on sides, dark*	*Dying, deg, fat*	*Dying, deg, fat*	3	3	4	4

*Each compound was screened twice as a singleton and what is tabulated is representative data

[11] The data is very much similar to the initial findings[4]

4.5.2 Motility Assays on Adult *S. mansoni*

Table 18 shows the motility assays for adult *S. mansoni* worms on exposure to target compound **for HB1-03, HB2-12, HB2-13, HB2-14, HB3-05** and **HB4-02**, respectively, with reference to the negative control i.e. DMSO which, however, still shows inactivity for all the analogues.

Table 18: Motility assays of target compound exposure on adult *S. mansoni* at 5 μM*.

Compd code	Structure	% Mean motility							
		2 h		5 h		24 h		48 h	
		% Mean	SD	% Mean	SD	% Mean	SD	% Mean	SD
HB1-03	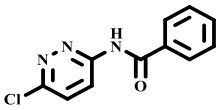	56.9	16.8	64.7	4.7	59.3	1.9	92.1	11.6
HB2-12	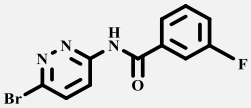	30.5	16.2	60.8	19.8	83.7	2.6	81.9	19.5
HB2-13	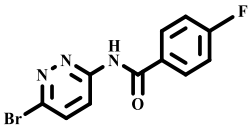	66.9	28.8	52.1	6.8	68.5	2.2	66.9	5.2
HB2-14	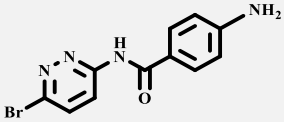	79.1	8.8	105.6	0.1	63.0	9.5	57.6	0.5
HB3-05	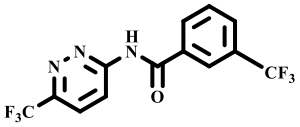	29.2	2.9	38.2	9.1	28.4	5.1	50.5	11.7
HB4-02	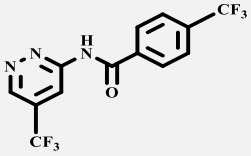	44.7	4.6	37.0	11.0	56.2	7.9	33.2	7.0

* To the nearest 1 decimal place

4.6 HEK293 Cytotoxicity: *In Silico* Predictions Vs *In Vitro* Assays

Although inactive on schistosome worms, comfortingly, they were experimentally found non-cytotoxic *in vitro* with 50% cytotoxic concentration (CC_{50}) values higher than the highest tested concentration of 20 μM with respect to the positive control i.e. bortezomib largely in accordance with Cyto-Safe™ *in silico* data on HEK293 (Table 19).[1,3] Compared to the previously reported compounds, **MK1-11**, which were the most active on schistosome worms, this new series appears less cytotoxic as **MK1-11** shows high cytotoxicity on HEK293 of a value of 8.46 ± 1.45 μM which

is comparable to the published value of 11.1 ± 0.2µM and moderate cytotoxicity on HepG2.[3,12] Even **HB4-02** which was predicted to be cytotoxic turned out to be non-cytotoxic empirically. This warrants further SAR expansion of the *N*-PdzBA-based compounds which may ultimately lead to a potent compound with a wide selectivity index value. HEK293 cells are an *in vitro* model that mimics cytotoxicity in human cells as a screen against cancerous side effects of the potential drug candidate.

Table 19: Experimental *in vitro* vs *in silico* cytotoxicity of on HEK293 cell line.[1,3]

Compd code	Structure	Expt HEK293 CC_{50} (µM)[1]	*In Silico* HEK293 Cytotox (Cyto-Safe™)(qualitative)
HB1-03	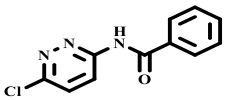	>20	Non-cytotoxic
HB2-12	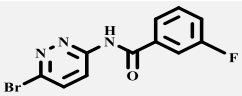	>20	Non-cytotoxic
HB2-13	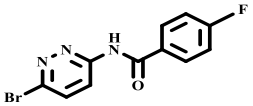	>20	Non-cytotoxic
HB2-14	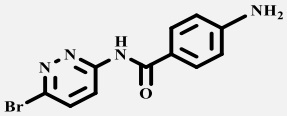	>20	Non-cytotoxic
HB3-05	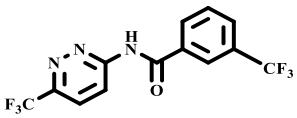	> 20	Non-cytotoxic
HB4-02	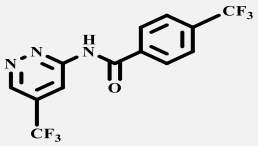	> 20	Cytotoxic
MK1-11	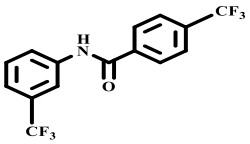	8.46 ± 1.45[13]	Cytotoxic

4.7 *In Silico* Physicochemical Property and SPR Evaluation

On *in silico* estimation of solubility using SwissADME™ AI/ML tool, the results are tabulated in Table 20, in comparison to **MK1-11** and **MMV687807**.

[12] Unpublished data

Table 20: *In silico* physicochemical properties (SwissADME™).[a]

Compd code	Structure	cLog*P*	*MW*	*RB*	*TPSA* (Å^2)	log*S**	*S** (µM)	log*S***	*S*** µM)
HB1-03	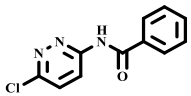	1.96	233.6	3	54.88	-2.89	1288	-2.75	1780
HB2-12	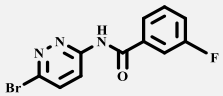	2.31	296.1	3	54.88	-3.35	446.7	-2.92	1200
HB2-13	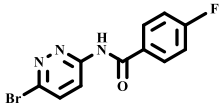	2.31	296.1	3	54.88	-3.35	446.7	-2.92	1200
HB2-14	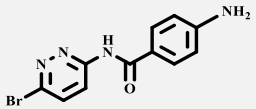	1.53	293.1	3	80.90	-2.84	1450	-2.66	2190
HB3-05	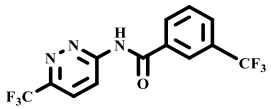	3.39	335.2	5	54.88	-3.75	177.8	-3.63	234.0
HB4-02	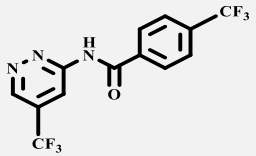	3.59	335.2	5	54.88	-3.73	186.2	-3.59	257.0
MK1-11	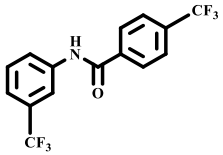	4.86	333.2	5	29.10	-5.18	6.607	-5.45	3.548
MMV687807	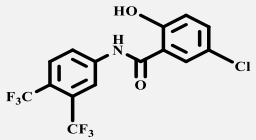	4.98	383.7	5	49.33	-5.91	1.230	-6.63	0.234

[a]Two criteria solubility: algorithmized *Delaney and **Ali GSE-style equations. **Key:** cLog*P* = calculated log*P*; Log*S* = logarithm of solubility; *MW* = molecular weight; *RB* = rotatable bonds; *S* = solubility; *TPSA* = topological polar surface area

From Table 20, **MMV687807** was estimated to be the least soluble followed by **MK1-11** (for each criterion). Both of them were unfavourably below the solubility 30 μM cut-off value, the latter compound having an experimental value of merely 13.3 μM[13]. The predicted properties show that the novel compounds reported in this research work are expected to possess improved solubilities (234-2190 μM) well into the millimolar range.

4.8 *In Silico* DMPK/ADME Property and SPR Evaluation

The activity of the *N*-PdzBA target compounds did not motivate the much more expensive DMPK experiments (unlike the *N*-PhBAs). However, *in silico* estimation using the BioSigLab PkCSM™ AI/ML tool, in comparison to **MK1-11** and **MMV687807** *in silico* and *in vitro* experimental values for the latter compound as elsewhere, gave the following results.

4.8.1 Absorption: Intestinal Absorption and Caco-2 Permeability

Table 21 shows the absorption data acquired *in silico* using PkCSM™.

Table 21: *In silico* intestinal absorption and Caco-2 permeability (PkCSM™).

Compd code	Structure	% Absorbed	logP_{app} (10^{-6} cm/s)
HB1-03	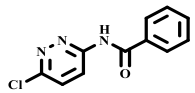	93.575	1.297
HB2-12	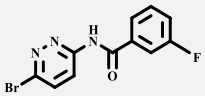	93.495	1.283
HB2-13	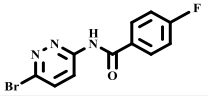	92.98	1.276
HB2-14	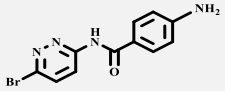	91.724	1.192
HB3-05	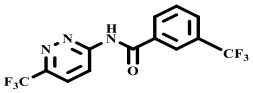	88.708	1.385
HB4-02	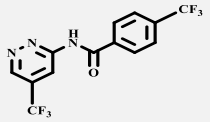	88.684	1.417
MK1-11	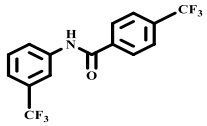	86.994	1.704
MMV 687807[26]	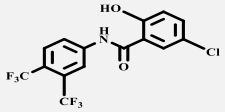	82.93	1.493

Key: Caco2 = colon carcinoma cell line 2 enterocyte; LogP_{app} = Log of apparent permeability

[13] Unpublished data

The higher estimated solubility (Table 20) of the *N*-PdzBAs target compounds compared to that of **MK1-11** etc. *N*-PhBAs would expectedly lead to higher intestinal absorption (Table 21) as demonstrated albeit *in silico*.

4.8.2 Distribution: V_{dss}, f_u, BBB- and CNS Permeability

Table 22 shows the distribution data acquired *in silico* using PkCSM™.

Table 22: *In silico* distribution (PkCSM™).

Compd code	Structure	V_{dss}, human (log L/kg)	f_u, human	Permeability	
				logP_{BBB}	logP_{CNS}
HB1-03	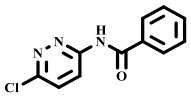	-0.234	0.256	0.155	-2.248
HB2-12	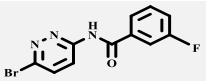	-0.277	0.251	0.12	-2.89
HB2-13	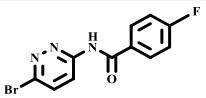	-0.3	0.274	0.26	-2.895
HB2-14	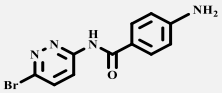	-0.249	0.389	-0.529	-2.932
HB3-05	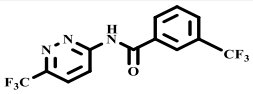	-0.501	0.154	0.129	-2.871
HB4-02	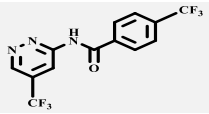	-0.606	0.131	0.033	-2.893
MK1-11	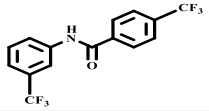	0.04	0.064	0.183	-0.642
MMV 687807	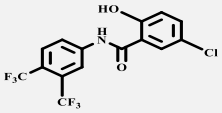	-0.232 IV=16.5[21]	0	0.152	-1.574

Key: BBB = blood-brain barrier; CNS = central nervous system; f_u = fraction unbound; LogP_{BBB} = logarithm of BBB permeability; LogP_{CNS} = logarithm of CNS permeability; V_{dss} = volume of distribution at steady state

According to the cLog*P* values in Table 20, **MK1-11** (cLog*P* = 4.86, Log*D* = 4.36) was more lipophilic than the pyridazinic compounds. Lipophilicity causes higher volumes of distribution due to partitioning into fatty tissues. Such compounds also have much higher permeability through the blood-brain barrier (BBB). Expectedly, compound **MK1-11** exhibited the highest predicted volume of distribution (0.04 Log L/kg) compared to the pyridazinic compounds reported herein. Furthermore, *in silico* predictions also show that it is likely to cross the BBB (LogP_{BBB} = 0.183) more readily compared to most of the new compounds.

4.8.3 Metabolism and Excretion: CYP Inhibition and *CL*

Table 23 shows the metabolic data acquired *in silico* using PkCSM™.

Table 23: *In silico* CYP inhibition (PkCSM™).

Compd code	Structure	CYP enzyme inhibition (Yes/No)			
		CYP1A2	CYP2C9	CYP2D6	CYP3A4
HB1-03	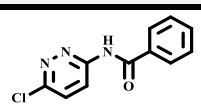	**Y**	**N**	**N**	**N**
HB2-12	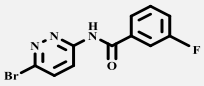	**Y**	**N**	**N**	**N**
HB2-13	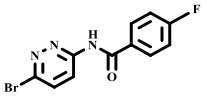	**Y**	**N**	**N**	**N**
HB2-14	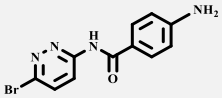	**N**	**N**	**N**	**N**
HB3-05	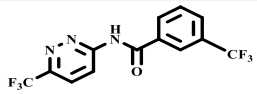	**Y**	**N**	**N**	**N**
HB4-02	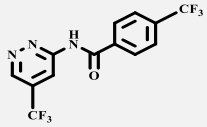	**Y**	**Y**	**N**	**N**
MK1-11	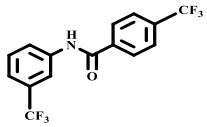	**Y**	**Y**	**N**	**N**
MMV687807	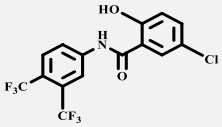	**Y**	**Y**	**N**	**N**
IC_{50} (μM)* [26]		>20	>20	>20	>40

*Note: fluorescence *CL* screening assay in human liver microsomes (HLM); **Key:** CYP = cytochrome P450

Drug-drug interactions are a major cause of drug toxicity and therapeutic failure.[27] To rule out the potential for such interaction, drug candidates are often tested on a panel of CYP enzymes to assess their risk of inhibiting or inducing these enzymes (section 2.6). In this regard, the compounds synthesized in this study were subjected to *in silico* prediction of their potential to inhibit CYPs. Comfortingly, all of them were predicted not to inhibit CYP3A4 and CYP2D6, the former being responsible for the metabolism of most drugs in clinical use and development including PZQ. While only **HB4-02** and **MK1-11** were predicted to inhibit CYP2C9, almost all the compounds were predicted to inhibit CYP1A2. However, it is anticipated that these

compounds may exhibit a safe drug-drug interaction profile considering that most drugs in clinical use/ development are metabolized by CYP3A4.[27]

Unlike for **MK1-11** and **MK-09** which underwent mouse liver microsome clearance (MLM *CL*) *in vivo* or **MMV687807** which underwent human liver microsome *CL* (Table 23), having shown unfavourably moderate to high clearance (Figure 16), no excretion assays were carried out nor simulated *in silico*. Such a phenomenon would lead to attrition of the potential drug which in turn would lead to loss of efficacy and a need for much higher doses.

4.9 References

(1) Dawoodjee, A. M.; Sichinga, J.; Banda, H.; Mbaya, S.; Funjika, E.; Mayoka, G.; Hikaambo, C.; Francisco, K. R.; Sun, Y. U.; Liu, L. J.; Caffrey, C. R.; Cheuka, P. M. Structure Activity Relationships of Antischistosomal *N*-Phenylbenzamides by Incorporation of Electron-withdrawing Functionalities. *Results Chem.* **2024**, *12*, 101890.

(2) Sichinga, J. Antischistosomal Structure-Activity Relationships of Nitrated *N*-Phenylbenzamide Derivatives. MSc Dissertation, University of Zambia, Lusaka, Zambia, **2023.**

(3) Kanyanta, M.; Lengwe, C.; Mambwe, D.; Francisco, K. R.; Liu, L. J.; Uli Sun, Y.; Amarasinghe, D. K.; Caffrey, C. R.; Cheuka, P. M. Activity of *N*-Phenylbenzamide Analogs against the Neglected Disease Pathogen, *Schistosoma mansoni*. *Bioorg. Med. Chem. Lett.* **2023**, *82*, 129164.

(4) Rich, D. H.; Singh, J. The Carbodiimide Method. In *Major Methods of Peptide Bond Formation*; Elsevier, **1979**; pp 241–261.

(5) Li, J. J.; Limberakis, C.; Pflum, D. A. *Modern Organic Synthesis in the Laboratory: A Collection of Standard Experimental Procedures*; Oxford University Press, **2007**.

(6) Pirrung, M. C. *The Synthetic Organic Chemist's Companion*; Wiley, **2007**.

(7) de Hoffmann, E.; Stroobant, V. *Mass Spectrometry: Principles and Applications*, 3rd ed.; Wiley, **2007**.

(8) Sharp, J. T.; Gosney, I.; Rowley, A. G. *Practical Organic Chemistry: A Student Handbook of Techniques*; Chapman, **1989**.

(9) Gottlieb, H. E.; Kotlyar, V.; Nudelman, A. NMR Shifts of Common Laboratory Solvents as Trace Impurities. *J. Org. Chem.* **1997**, *62* (21), 7512–7515.

(10) Silverstein, R. M.; Webster, F. X.; Kiemle, D. J. *Spectrometric Identification of Organic Compounds*, 7th ed.; Wiley, **2005**.

(11) Dean, J. R.; Jones, A. M.; Holmes, D.; Reed, R.; Weyers, J.; Jones, A. *Practical Skills in Chemistry*, 3rd ed.; Pearson, **2017**.

(12) Stuart, B. H. *Infrared Spectroscopy: Fundamentals and Applications*; Wiley, **2004**.

(13) Valeur, E.; Bradley, M. Amide Bond Formation: Beyond the Myth of Coupling Reagents. *Chem. Soc. Rev.* **2009**, *38* (2), 606–631.

(14) Montalbetti, C. A. G. N.; Falque, V. Amide Bond Formation and Peptide Coupling. *Tetrahedron*. **2005**, *61* (46), 10827–10852.

(15) Kurzer, F.; Douraghi-Zadeh, K.; Carraway, K. L.; Koshland, D. E.; Yavari, I.; Roberts, J. D. A New Mechanism Involving Cyclic Tautomers for the Reaction with Nucleophiles of the Water-Soluble Peptide Coupling Reagent 1-Ethyl-3-(3-(dimethy1amino)propyl)carbodiimide (EDC). *J. Am. Chem. Soc.* **1981**, *103* (2), 4689.

(16) Rebek, J.; Feitler, D. Mechanism of Carbodiimide Reaction. II. Peptide Synthesis on the Solid Phase. *J. Am. Chem. Soc.* **1974**, *96* (5), 1606–1607.

(17) Sheehan, C. A.; Cruickshank, P. A.; Boshart, G. L. A Convenient Synthesis of Water-soluble Carbodiimides. *J. Org. Chem*. **1961**, *26* (7), 2525–2528.

(18) Tenforde, T.; Fawwaza, N. A.; Freeman, N. K. Nuclear Magnetic Resonance and Infra-Red Studies on the Tautomerism of 1-Ethyl-3-(3'-dimethylaminopropyl)carbodiimide. *J. Org. Chem.* **1972**, *37* (21), 3372–3374.

(19) Yavari, I.; Roberts, J. D. Nitrogen-15 Nuclear Magnetic Resonance Spectroscopy. Carbodiimides. *J. Org. Chem.* **1978**, *43* (25), 4689–4693.

(20) Chan, L. C.; Cox, B. G. Kinetics of Amide Formation through Carbodiimide/ *N*-Hydroxybenzotriazole (HOBt) Couplings. *J. Org. Chem.* **2007**, *72* (23), 8863–8869.

(21) *CRC Handbook of Tables for Organic Compound Identification*, 3rd ed.; Rappoport, Z., Ed.; CRC Press, **1967**.

(22) Sykes, P. *A Guidebook to Mechanism in Organic Chemistry*, 6th ed.; Longman, **1986**.

(23) Shilov, S. *How Vacuum FTIR Simplifies Chemical Analysis*. Lab Manager. https://www.bigmaker.com/labx-media-group/How-Vacuum-FTIR-Simplifies-Chemical-Analysis/bmid=dd6e92ebfa80&bmid_type=member&bmid=dd6e92ebfa80 (accessed 2023-09-22).

(24) Clayden, J; Greeves, N.; Warren, S. *Organic Chemistry*, 2nd ed.; Oxford University Press, **2012**.

(25) Feitosa, F. L.; Cabral, V. F.; Sanches, I. H.; Silva-Mendonca, S.; Borba, J. V. V. B.; Braga, R. C.; Andrade, C. H. Cyto-Safe: A Machine Learning Tool for Early Identification of Cytotoxic Compounds in Drug Discovery. *J. Chem. Inf. Model*. **2024**, *64* (24), 9056–9062.

(26) Medicines for Malaria Venture. *MMV Pathogen Box Activity Biological Data SMILES Database.* Medicines for Malaria Venture, **2018**. https://www.mmv.org/sites/default/files/uploads/docs/mmv_open/Pathogen_Box_Activity_Biological_Data_Smiles.xlsx (accessed 2024-01-05).

(27) Zdesenko, G.; Mutapi, F. Drug Metabolism and Pharmacokinetics of Praziquantel: A Review of Variable Drug Exposure during Schistosomiasis Treatment in Human Hosts and Experimental Models. *PLoS Negl. Trop. Dis*. **2020**, *14* (9), e0008649.

CHAPTER 5

SUMMARIES, CONCLUSIONS, LIMITATIONS AND RECOMMENDATIONS

5.1 Chapter Overview

In this ultimate and epilogue chapter are to be found concise summaries, conclusions, limitations, recommendations including proposed structure-activity relationship (pSAR) explorations.

5.2 General Summary

In this research work, the design, synthesis and characterization of *N*-PdzBA derivatives were undertaken followed by profiling for antischistosomal activity on *S. mansoni* adult worms alongside cytotoxicity on the HEK293 cell line and also physicochemical properties experimentally and/or *in silico.*

The compounds synthesized in this research work were all inactive albeit some revealed interesting structure activity relationships with respect to the previously reported analogues. In this regard, **HB4-02** and **HB3-05** were noteworthy. These compounds are closely related analogues of **MK1-11** and **AD-03**, respectively, with a very subtle difference - two carbons in the aniline portion of **MK1-11** and **AD-03** being replaced by nitrogens.[1,2] Although subtle, these changes resulted in complete elimination of *in vitro* antischistosomal activity. The other four pyridazinic compounds were equally inactive on adult worms suggesting the aniline-pyridazine replacement may not be tolerated, as summarized in Figure 73.

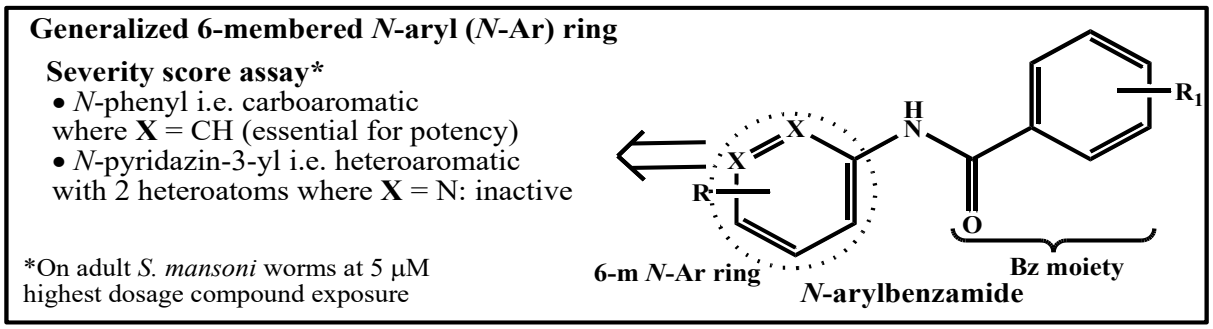

Figure 73: A graphical summary on SAR exploration on the **MMV687807** *N*-ArBA scaffold on adult *S. mansoni*.[1,2]

Although all the compounds were inactive on schistosome worms, they were non-cytotoxic *in vitro* on HEK293 with 50% cytotoxicity (CC_{50}) values higher than the highest tested concentration of 20 μM with respect to the positive control i.e. bortezomib mostly in accordance with *in silico* predictions. Compared to the previously reported compounds, **MK1-11** and **MK1-09** which were the most active on schistosome worms, this new series appears less cytotoxic *in vitro*.[1,2]

The cLog*P* data indicate that introducing heteroatoms into a phenyl ring leads to a reduction in the cLog*P* value as per theory which demonstrate a better solubility profile compared to the first generation compound **MK1-11**. **MMV687807** was estimated to be the least soluble followed by **MK1-11** both of them being unfavourably below the solubility 30 μM cut-off value.[1,2] The predicted properties show that the pyridazinic compounds are expected to possess improved solubilities (234-2190 μM) compared to the previously reported frontrunner analogue **MK1-11** which is a better developability profile and, therefore, the novel scaffold in them could undergo drug rescue against other disease indications namely as anti-COVID-19 and anti-Parkinson agents where the *N*-PdzBA scaffold has already shown activity as reported by other researcher elsewhere (section 2.7).[3,4]

In a nutshell, all the target compounds are Ro5-compliant and drug-like even by other drug-likeness parameters and have favourable other pharmacological properties as calculated *in silico*.

5.3 Conclusions

In conclusion, this MSc dissertation has reported the synthesis, *in vitro* antischistosomal, cytotoxicity and *in silico* physicochemical/ DMPK profiling of new *N*-PdzBA derivatives. Six *N*-PdzBA target compounds were synthesized by EDCI-mediated amide coupling to the required purity (≥ 95%) in moderate to high yields (43.40 – 77.91%). LC-MS was used to confirm purity and profile t_R as a drug physicochemical property while UV-Vis, IR, ^{1}H- and ^{13}C-NMR were used to characterize the target compounds comprehensively thereby adding vital reference spectro-analytical data about *N*-PdzBAs in literature which was scanty status quo. When tested on *S. mansoni* adult worms, the *N*-PdzBAs were generally inactive in terms of both the severity score assay (severity score ≤1) and the percentage motility assays (no significant reduction in motility) with **HB4-02** bearing the most conclusive SAR result to conclusively pin the pyridazine moiety to inactivity since its exact matched molecular pair analogue **MK1-11** was very potent.[1,2] This experimentally found inactivity while known to be

a possibility before is not predictable as explained in section 2.6.[5,6] Furthermore, the EC_{50} values could not be computed as the preliminary data at 5 μM did not motivate further activity tests. However, the *N*-PdzBAs experimentally showed lower cytotoxicity (CC_{50} > 20 μM), better estimated solubility (S_{aq} > 30 μM) and optimal hydrophobicity (cLog$P \leq 4$) versus **MK1-11** at 4.86 and **MMV687807** at 4.98.

5.4 Limitations

The major limitation was the lack of readily accessible suitable state-of-the-art instrumentation for characterization of the target compounds in our laboratory, university and nation at large. Consequently, for NMR analysis, some carbons could not be assigned because more advanced NMR techniques were not accessible since they were much more expensive namely: Distortionless Enhancement by Polarization Transfer (DEPT), Fluorine-19 (^{19}F-) NMR, Two-dimensional (2D) Correlation Spectroscopy (COSY), Incredible Natural Abundance Double Quantum Transfer Experiment (INADEQUATE), Nuclear Overhauser Effect Spectroscopy (NOESY), etc. as done elsewhere.[7,8]

5.5 Recommendations for Future Work

1. Antischistosomal assays on the trifluoromethylated target compounds **HB4-02** and **HB3-05** which are simply Pdz analogues to potent **MK1-11** and **AD-03** should be carried out on NTS immature parasites which is one of the immature stages on which PZQ is ineffective in the search for a multistage lead (Section 1.4).

2. Antischistosomal assays on all the *N*-PdzBA target compounds should be carried out on other schistosome species especially *S. haematobium* (which is even more prevalent in Zambia than *S. mansoni*; subsection 1.2.2) as the activity of any novel antischistosomal candidates on the former species (*S. haematobium*) must not necessarily be assumed from studies on the latter species (*S. mansoni*).[9,10]

3. Antischistosomal assays on all the *N*-PdzBA target compounds should be carried out on at 10 μM which is the range of the EC_{50} of PZQ (seeing that the cytotoxicity is very low) since this value is double that of the 5 μM at which this research work ended.[11,12]

4. Furthermore, additional *N*-PdzBA analogues, incorporating substituents from the second and fourth quadrants of the Craig plot (Figure 23), or an equivalent Topliss scheme could be explored.

5. The *N*-PdzBA could be tested against SARS-Cov2 (COVID19) where a 2022 study showed promising results.[3]

6. Figure 74 graphically outlines an antischistosomal pSAR exploration which could be undertaken in future.

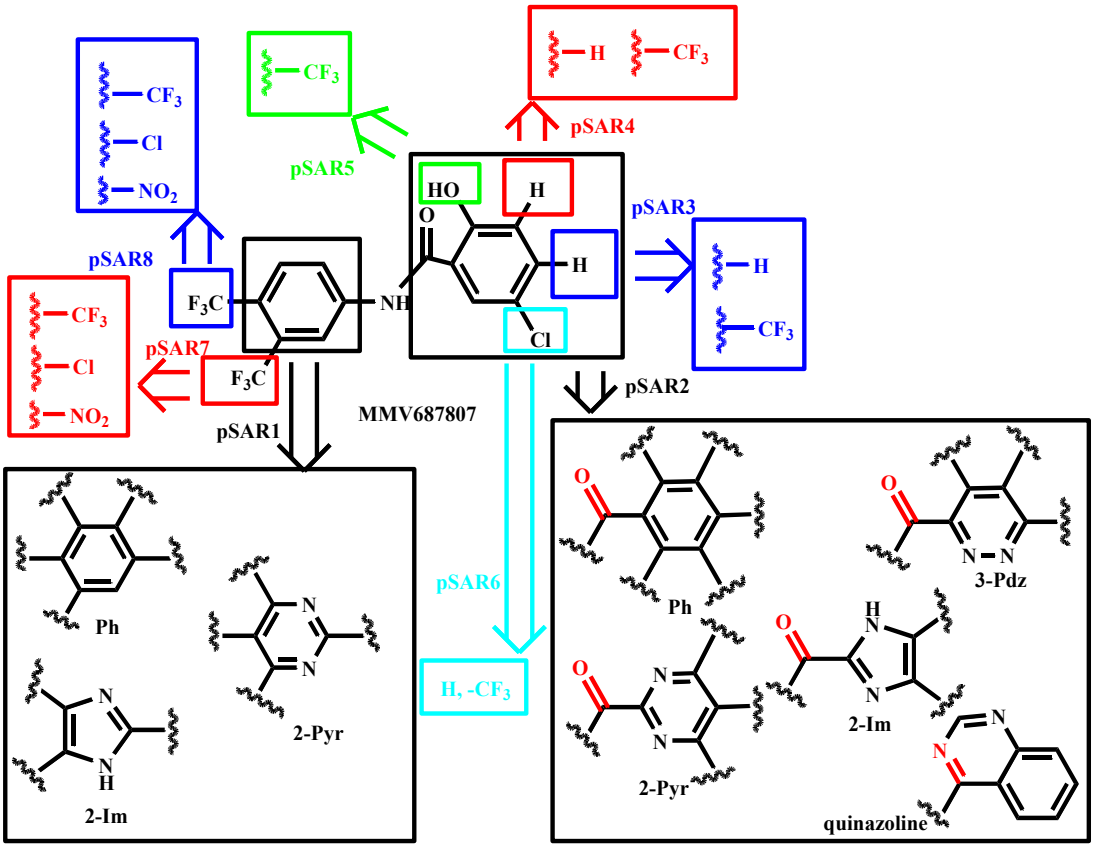

Figure 74: A graphical plan on proposed anti-SCH SAR (pSAR) exploration on **MMV687807.**

Note: pSAR2 3-Pdz (amide reversed) analogues are already known to be bioactive albeit against cancer. [13]

5.7 References

(1) Dawoodjee, A. M.; Sichinga, J.; Banda, H.; Mbaya, S.; Funjika, E.; Mayoka, G.; Hikaambo, C.; Francisco, K. R.; Sun, Y. U.; Liu, L. J.; Caffrey, C. R.; Cheuka, P. M. Structure Activity Relationships of Antischistosomal *N*-phenylbenzamides by Incorporation of Electron-withdrawing Functionalities. *Results Chem.* **2024**, *12*, 101890.

(2) Kanyanta, M.; Lengwe, C.; Mambwe, D.; Francisco, K. R.; Liu, L. J.; Uli Sun, Y.; Amarasinghe, D. K.; Caffrey, C. R.; Cheuka, P. M. Activity of *N*-Phenylbenzamide Analogs against the Neglected Disease Pathogen, *Schistosoma mansoni*. *Bioorg. Med. Chem. Lett.* **2023**, *82*, 129164.

(3) Sepay, N.; Chakrabarti, S.; Afzal, M.; Alarifi, A.; Mal, D. Identification of 4-Acrylamido-*N*-(Pyridazin-3yl)benzamide as Anti-COVID19 Compound: a DFTB, Molecular Docking, and Molecular Dynamics Study. *RSC Adv.* **2022**, *12* (37), 24178–24186.

(4) Ding, X.; Stasi, L. P.; Dai, X.; Long, K.; Peng, C.; Zhao, B.; Wang, H.; Sun, C.; Hu, H.; Wan, Z.; Jandu, K. S.; Philps, O. J.; Chen, Y.; Wang, L.; Liu, Q.; Edge, C.; Li, Y.; Dong, K.; Guan, X.; Tattersall, F. D.; Reith, A. D.; Ren, F. 5-Substituted-*N*-Pyridazinylbenzamides as Potent and Selective LRRK2 Inhibitors: Improved Brain Unbound Fraction Enables Efficacy. *Bioorg. Med. Chem. Lett.* **2019**, *29* (2), 212–215.

(5) Cuozzo, A.; Daina, A.; Perez, M. A. S.; Michielin, O.; Zoete, V. SwissBioisostere 2021: Updated Structural, Bioactivity and Physicochemical Data Delivered by a Reshaped Web Interface. *Nucleic Acids Res.* **2022**, *50* (D1), D1382–D1390.

(6) Patel, L.; Chandrasekhar, J.; Evarts, J.; Haran, A. C.; Ip, C.; Kaplan, J. A.; Kim, M.; Koditek, D.; Lad, L.; Lepist, E. I.; McGrath, M. E.; Novikov, N.; Perreault, S.; Puri, K. D.; Somoza, J. R.; Steiner, B. H.; Stevens, K. L.; Therrien, J.; Treiberg, J.; Villaseñor, A. G.; Yeung, A.; Phillips, G. 2,4,6-Triaminopyrimidine as a Novel Hinge Binder in a Series of PI3Kδ Selective Inhibitors. *J. Med. Chem.* **2016**, *59* (7), 3532–3548.

(7) Rebollar-Ramos, D.; Chen, S. N.; Lankin, D. C.; Ray, G. J.; Kleps, R. A.; Korhonen, S. P.; Lehtivarjo, J.; Pauli, G. F. Identification by HSQC and Quantification by qHNMR Innovate Pharmaceutical Amino Acid Analysis. *J. Pharm. Biomed. Anal*. **2024**, *251*, 116390.

(8) University of Cape Town. Powerful Spectrometer Takes Drug Discovery to New Level. *University News*. Cape Town November 20, **2014**. https://www.news.uct.ac.za/article/-2014-11-20-powerful-spectrometer-takes-drug-discovery-to-new-level (accessed 2023-08-17).

(9) Sichinga, J. Antischistosomal Structure-Activity Relationships of Nitrated *N*-Phenylbenzamide Derivatives. MSc Dissertation, University of Zambia, Lusaka, Zambia, **2023.**

(10) Cheuka, P. M. Drug Discovery and Target Identification against Schistosomiasis: A Reality Check on Progress and Future Prospects. *Curr. Top. Med. Chem.* **2021**, *22* (19), 1595–1610.

(11) Meister, I.; Ingram-Sieber, K.; Cowan, N.; Todd, M.; Robertson, M. N.; Meli, C., Patra, M.; Gasser, G.; Keiser, J. Activity of Praziquantel Enantiomers and Main Metabolites against *Schistosoma mansoni*. *Antimicrob. Agent. Chemother.* **2014**, *58* (9), 5466–5472.

(12) Patra, M.; Ingram, K.; Leonidova, A.; Pierroz, V.; Ferrari, S.; Robertson, M. N.; Todd, M. H.; Keiser, J.; Gasser, G. *In Vitro* Metabolic Profile and *In Vivo* Antischistosomal Activity Studies of (η(6)-Praziquantel)$Cr(CO)_3$ Derivatives. *J. Med. Chem.* **2013**, *56* (2), 9192–9198.

(13) Shan, B.; Hou, H.; Zhang, K.; Li, R.; Shen, C.; Chen, Z.; Xu, P.; Cui, R.; Su, Z.; Zhang, C.; Yang, R. Design, Synthesis, and Biological Evaluation of Bipyridazine Derivatives as Stimulator of Interferon Genes (STING) Receptor Agonists. *J. Med. Chem.* **2023**, *66* (5), 3327–47.

APPENDICES

Appendix A: Ethical Approval Letter

THE UNIVERSITY OF ZAMBIA
DIRECTORATE OF RESEARCH AND GRADUATE STUDIES

Great East Road Campus | P.O. Box 32379 | Lusaka10101 | Tel: +260-211-290 258/291 777
Fax: (+260)-211-290 258/253 952 | **E-mail**: director.drgs@unza.zm | Website: www.unza.zm

APPROVAL OF STUDY

IORG No. 0005376
NASRECREC IRB No. 00006465

19th September, 2023

REF NO. NASREC-2023- AUG – 013

Mr. Harrison Banda
The University of Zambia,
P.O. Box 32379,
LUSAKA.

Dear, Mr. Banda

RE: "SYNTHESIS AND ANTISCHISTOSOMAL STRUCTURE-ACTIVITY RELATIONSHIP PROFILING OF N-PYRIDAZIN-3-YLBENZAMIDES"

Reference is made to your protocol dated as captioned above. NASREC resolved to approve this study and your participation as Principal Investigator for a period of one year.

REVIEW TYPE	ORDINARY REVIEW	APPROVAL NO. NASREC-2023 AUG - 013
Approval and Expiry Date	Approval Date: 19th September, 2023	Expiry Date: 20th September, 2024
Protocol Version and Date	Version - Nil.	20th September, 2024
Information Sheet, Consent Forms and Dates	• English.	To be provided
Consent form ID and Date	Version - Nil	To be provided
Recruitment Materials	Nil	Nil
Other Study Documents	Questionnaire.	

Specific conditions will apply to this approval. As Principal Investigator it is your responsibility to ensure that the contents of this letter are adhered to. If these are not adhered to, the approval may be suspended. Should the study be suspended, study sponsors and other regulatory authorities will be informed.

CONDITIONS OF APPROVAL

- No participant may be involved in any study procedure prior to the study approval or after the expiration date.
- All unanticipated or Serious Adverse Events (SAEs) must be reported to NASREC within 5 days.
- All protocol modifications must be approved by NASREC prior to implementation unless they are intended to reduce risk (but must still be reported for approval). Modifications will include any change of investigator/s or site address.
- All protocol deviations must be reported to NASREC within 5 working days.
- All recruitment materials must be approved by NASREC prior to being used.
- Principal investigators are responsible for initiating Continuing Review proceedings. NASREC will only approve a study for a period of 12 months.
- It is the responsibility of the PI to renew his/her ethics approval through a renewal application to NASREC.
- Where the PI desires to extend the study after expiry of the study period, documents for study extension must be received by NASREC at least 30 days before the expiry date. This is for the purpose of facilitating the review process. Documents received within 30 days after expiry will be labelled "late submissions" and will incur a penalty fee of K500.00. No study shall be renewed whose documents are submitted for renewal 30 days after expiry of the certificate.
- Every 6 (six) months a progress report form supplied by The University of Zambia Natural and Applied Sciences Research Ethics Committee as an IRB must be filled in and submitted to us. There is a penalty of K500.00 for failure to submit the report.
- When closing a project, the PI is responsible for notifying, in writing or using the Research Ethics and Management Online (REMO),both NASREC
- and the National Health Research Authority (NHRA) when ethics certification is no longer required for a project.
- In order to close an approved study, a Closing Report must be submitted in writing or through the REMO system. A Closing Report should be filed when data collection has ended and the study team will no longer be using human participants or animals or secondary data or have any direct or indirect contact with the research participants or animals for the study.
- Filing a closing report (rather than just letting your approval lapse) is important as it assists NASREC in efficiently tracking and reporting on projects. Note that some funding agencies and sponsors require a notice of closure from the IRB which had approved the study and can only be generated after the Closing Report has been filed.

- A reprint of this letter shall be done at a fee.

- All protocol modifications must be approved by NASREC by way of an application for an amendment prior to implementation unless they are intended to reduce risk (but must still be reported for approval). Modifications will include any change of investigator/s or site address or methodology and methods. Many modifications entail minimal risk adjustments to a protocol and/or consent form and can be made on an Expedited basis (via the IRB Chair). Some examples are: format changes, correcting spelling errors, adding key personnel, minor changes to questionnaires, recruiting and changes, and so forth. Other, more substantive changes, especially those that may alter the risk-benefit ratio, may require Full Board review. In all cases, except where noted above regarding subject safety, any changes to any protocol document or procedure must first be approved by NASREC before they can be implemented.

Should you have any questions regarding anything indicated in this letter, please do not hesitate to get in touch with us at the above indicated address.

On behalf of NASREC, we would like to wish you all the success as you carry out your study.

Yours faithfully,

Dr. Musuku Kaonda

VICE-CHAIRPERSON
THE UNIVERSITY OF ZAMBIA NATURAL AND APPLIED SCIENCES RESEARCH ETHICS COMMITTEE - IRB

cc: Director, Directorate of Research and Graduate Studies
Assistant Director (Research), Directorate of Research and Graduate Studies
Assistant Registrar (Research), Directorate of Research and Graduate Studies

Appendix B: Collaborator Lab Shipment Documents

THE UNIVERSITY OF ZAMBIA
School of Natural Sciences
DEPARTMENT OF CHEMISTRY

P O Box 32379
Lusaka 10101, Zambia
E-mail: chemistry@unza.zm

Tel: 295436
Fax: (260-1-) 253952/254406
Telex: UNZA ZA 44370

31st August, 2022

TO WHOM IT MAY CONCERN

REF: SHIPMENT OF CHEMICAL COMPOUNDS FOR CHARACTERISATION

I wish to request your courier company to allow Mr. Harrison Banda, who is our MSc. In Chemistry Student, to ship his synthesized compounds for characterization at the University of Cape Town in South Africa.

The chemical compounds of thirteen (13) sample vials are all benzamide derivatives.

I wish to assure you that the said compounds, (13 vials in total, packed in 5 mg sample) are purely for academic purposes only and forms part of his proposed research. The compounds are also non-flammable, non-toxic and generally not dangerous to violate any of your courier regulations.

Your assistance will be appreciated.

Yours Sincerely,

Dr. E. Funjika

HEAD – DEPARTMENT OF CHEMISTRY

HEAD
DEPARTMENT OF CHEMISTRY
UNIVERSITY OF ZAMBIA
31 AUG 2022
P O BOX 32379
LUSAKA 10101

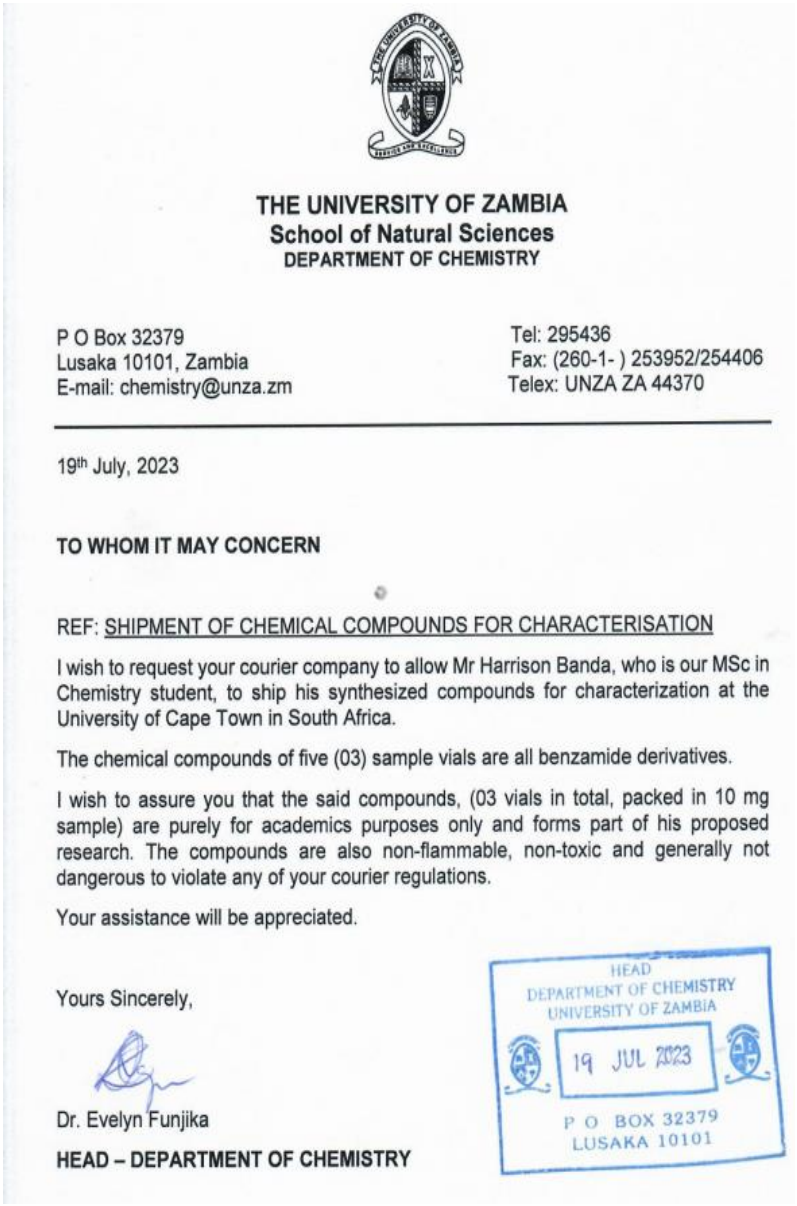

THE UNIVERSITY OF ZAMBIA
School of Natural Sciences
DEPARTMENT OF CHEMISTRY

P O Box 32379
Lusaka 10101, Zambia
E-mail: chemistry@unza.zm

Tel: 295436
Fax: (260-1-) 253952/254406
Telex: UNZA ZA 44370

19th July, 2023

TO WHOM IT MAY CONCERN

REF: SHIPMENT OF CHEMICAL COMPOUNDS FOR CHARACTERISATION

I wish to request your courier company to allow Mr Harrison Banda, who is our MSc in Chemistry student, to ship his synthesized compounds for characterization at the University of Cape Town in South Africa.

The chemical compounds of five (03) sample vials are all benzamide derivatives.

I wish to assure you that the said compounds, (03 vials in total, packed in 10 mg sample) are purely for academics purposes only and forms part of his proposed research. The compounds are also non-flammable, non-toxic and generally not dangerous to violate any of your courier regulations.

Your assistance will be appreciated.

Yours Sincerely,

Dr. Evelyn Funjika
HEAD – DEPARTMENT OF CHEMISTRY

HEAD
DEPARTMENT OF CHEMISTRY
UNIVERSITY OF ZAMBIA
19 JUL 2023
P O BOX 32379
LUSAKA 10101

Toxic Substance Control Act (TSCA) Certification

Date: October 23rd 2023
Waybill or reference number:

Check only one

Positive Certification

☐ I certify that all chemical substances in this shipment comply with all applicable rules or orders under TSCA and that I am not offering a chemical substance for entry in violation of TSCA or any applicable rule or order thereunder.

or

Negative Certification

☑ I certify that all chemicals in this shipment are not subject to TSCA.

Company name: Skaggs School of Pharmacy and Pharmaceutical Sciences
Company address: PSB Building, University of California San Diego, 9255 Pharmacy Lane, MC0657, La Jolla CA 92093, USA
Certifier name: Conor Caffrey
Certifier title: Professor
Certifier phone number: +1 858 534 5340
Certifier email address: ccaffrey@ucsd.edu
Certifier signature: Conor Caffrey
Digitally signed by Conor Caffrey
Date: 2023.10.20 08:11:04 -07'00'

Product description

1.	Package contain 6 small synthetic peptides which will be screened for antimicrobial activities in an academic research setting ONL
2.	Each peptide weighs 2-4 mgs. Peptides are not drugs or intended as drugs.
3.	Each peptide weighs 2-4 mgs. Peptides are not drugs or intended as drugs.
4.	Peptides are non hazardous, non-toxic and non-flammable.
5.	Total value is US$5.00.
6.	
7.	
8.	
9.	
10.	

If the certifier is unsure if their chemical substance is subject to TSCA compliance, contact the Environmental Protection Agency, TSCA Assistance Office at 1.202.554.1404 between 8:30 a.m. and 5:00 p.m.

Rev 1

Appendix C: Publications, Manuscripts, Conferences and Workshops

Journal Article Publications and Manuscripts in Press

1. Ameera M. Dawoodjee; John Sichinga; **Harrison Banda**; Steve Mbaya; Evelyn Funjika; Godfrey Mayoka; Christabel Hikaambo; Karol R. Francisco; Yujie Uli Sun; Lawrence J. Liu; Conor R. Caffrey; Peter Mubanga Cheuka. Structure Activity Relationships of Antischistosomal *N*-Phenylbenzamides by Incorporation of Electron-withdrawing Functionalities. *Results Chem.* **2024**, *12*, 101890. https://doi.org/10.1016/j.rechem.2024.101890 (Manuscript status: published).[14]

Results in Chemistry 12 (2024) 101890

Contents lists available at ScienceDirect

Results in Chemistry

journal homepage: www.sciencedirect.com/journal/results-in-chemistry

Structure activity relationships of antischistosomal *N*-phenylbenzamides by incorporation of electron-withdrawing functionalities

Ameera Mohammed Dawoodjee [a], John Sichinga [a], Harrison Banda [a], Steve Mbaya [a], Evelyn Funjika [a], Godfrey Mayoka [b], Christabel Hikaambo [c], Karol R. Francisco [d], Yujie Uli Sun [d], Lawrence J. Liu [d], Conor R. Caffrey [d,*], Peter Mubanga Cheuka [a,*]

[a] Department of Chemistry, School of Natural Sciences, University of Zambia, P.O. Box 32379, Lusaka, Zambia
[b] School of Pharmacy, Jomo Kenyatta University of Agriculture and Technology, P.O. Box 62 000 – 00200, Nairobi, Kenya
[c] Department of Chemistry, University of Cape Town, Rondebosch 7701, Cape Town, South Africa
[d] Center for Discovery and Innovation in Parasitic Diseases (CDIPD), Skaggs School of Pharmacy and Pharmaceutical Sciences, University of California San Diego, La Jolla, CA 92093, USA

2. **Harrison Banda**; Aberham Abere. Navigating the Challenge of Praziquantel Resistance in Schistosomiasis: Molecular Mechanisms and Future Directions. *Discover. Med.* **2025**. https://doi.org/10.1007/s44337-025-00293-x (Manuscript status: published).

Discover Medicine

Review

Determining the mechanisms of praziquantel resistance in schistosomiasis: insights and future directions

Harrison Banda[1] · Aberham Abere[2]

Received: 11 August 2024 / Accepted: 21 March 2025
Published online: 14 April 2025
© The Author(s) 2025 OPEN

[14] In this published journal article, *N*-PdzBAs are taken to be derivatives of *N*-PhBAs where the pyridazine moiety is incorporated as an example of electron-withdrawing groups (EWGs) hence the generalized title

3. Masebe Kanyanta; Ameera Mohammed Dawoodjee; Chilufya Lengwe; **Harrison Banda**; John Sichinga; Steve Mbaya; Godfrey Mayoka; Conor R. Caffrey; Lyn-Marie Birkholtz; Peter Mubanga Cheuka. Structure-Activity Relationship Studies of Antiplasmodial *N*-Phenylbenzamide and *N*-Pyridazin-3-ylbenzamide Analogues. *Bioorg. Med. Chem. Lett*. (Manuscript status: submitted on 17th November 2024).

4. **Harrison Banda**; Aberham Abere. Unveiling Schistosomiasis: A Review of Targeting Drug Resistance of Promoting Local Control in Sub-Saharan Africa. *J. Trop. Med.* (Manuscript status: submitted on 16th October 2024: ID 9935772).

International, National and University-wide Oral and Poster Conference Presentations and Their Published Abstracts

5. **Banda, H.**; Funjika, E.; Cheuka, P. M. (2025). Design, Synthesis, Antischistosomal and Physicochemical/ADMET Evaluation of *N*-Pyridazin-3-ylbenzamides by *In Silico* and *In Vitro* Approaches. **WCAIR/ UoD and University of Ghana, Drug Discovery Africa Conference 2025 (DDA25),** 12th – 14th March 2025. Theme: Medicinal and Computational Drug Discovery. Institute of Statistical, Social & Economic Research **(**ISSER) Conference Centre, University of Ghana & Erata Hotel, Legon, Accra, Ghana. (Oral and Poster.) https://d1ssu070pg2v9i.cloudfront.net/pex/wcair/2025/02/27202655/Drug-Discovery-Africa-Abstract-Book.pdf

6. **Banda, H.**; Funjika, E.; Cheuka, P. M. (2025). Synthesis, Antischistosomal Structure-Activity Relationship and Physicochemical/DMPK Profiling of *N*-Pyridazin-3-ylbenzamides by *In Silico* and *In Vitro* Approaches. **International Society for the Study of Xenobiotics (ISSX), ISSX Africa Workshop 2025 (ISSXA25),** 5th – 7th March 2025. Theme: Africa's Journey in Pharmacogenomics and DMPK: Exploring Progress and Potential. Indaba Hotel, Spa & Conference Centre, Sandton, Johannesburg, South Africa. (Poster; 1st author ISSX member.)

7. **Banda, H.**; Funjika, E.; Cheuka, P. M. (2024). Synthesis and Antischistosomal Structure-Activity Relationship Profiling of *N*-Pyridazin-3-ylbenzamides. **RSC Biological & Medicinal Chemistry Sector (BMCS), RSC-BMCS Postgraduate Symposium XVIII (BMCSPostGrad24),** 12th December 2024. Medical Sciences Teaching Centre, University of Oxford, Oxford, UK. (Oral and Poster.) https://cdn.eventsforce.net/files/ef-px6ci6a56tzs/website/295/fa0b8f6d-5364-45d7-b5c5-26f199b032ce/postgradute_symposium_handbook_2024.pdf

8. **Banda, H.**; Funjika, E.; Cheuka, P. M. (2024). Synthesis and Antischistosomal Structure-Activity Relationship Profiling of *N*-Pyridazin-3-ylbenzamides by *In Silico* and *In Vitro* Approaches. **ELRIG/ The Protein Society, Protein Sciences in Drug Discovery 2024 (PSDD24),** 18th – 19th November 2024. Francis Crick Auditorium, Hinxton Hall Conference Centre, Wellcome Genome Campus, Hinxton, Cambridge, UK. (Poster.)

9. **Banda, H.**; Funjika, E.; Cheuka, P. M. (2024). Synthesis and Antischistosomal Structure-Activity Relationship Profiling of *N*-Pyridazin-3-ylbenzamides. **RSC BMCS and Society for Chemical Industry (SCI) Fine Chemicals Group (FCG), 3rd RSC/SCI Symposium on New Therapeutics for Global Health (NTGH24),** 9th – 11th September 2024. Mitchell Hall, Cranfield University, Milton Keynes, UK. (Oral and Poster.) https://cdn.eventsforce.net/files/ef-px6ci6a56tzs/website/289/ae114bd3-1716-4ae5-9bba-a66de3372354/new_therapeutics_handbook_2024.pdf (accessed 2024-09-11)

10. **Banda, H.**; Funjika, E.; Cheuka, P. M. (2024). Synthesis and Antischistosomal Structure-Activity Relationship Profiling of *N*-Pyridazin-3-ylbenzamides. **Strengthening Health Professions in Zambia (SHEPIZ), 3rd SHEPIZ Annual Symposium,** 25th – 26th July 2024. Theme: Promoting Healthcare Using One Health Approach in Higher Education and Research in Zambia. Sub-theme: Therapeutic Approaches: From Indigenous Knowledge System to Precision Medicine. Mulungushi International Conference Centre (MICC), Lusaka, Zambia. (Oral.)

11. **Banda, H.**; Funjika, E.; Cheuka, P. M. (2024). Synthesis and Antischistosomal Structure-Activity Relationship Profiling of *N*-Pyridazin-3-ylbenzamides. **H3D Foundation at UCT, 5th H3D Symposium,** 21st – 24th May 2024. Theme: Imaging Treatments for Drug Resistant Infections of Bacterial and Mycobacterial Origin. Sub-theme: Neglected Tropical Diseases. Radisson Blu Mosi-Oa-Tunya Resort, Livingstone, Zambia. (Oral and Poster.)

12. **Banda, H.**; Funjika, E.; Cheuka, P. M. (2023). Synthesis and Antischistosomal Structure-Activity Relationship Profiling of *N*-Pyridazin-3-ylbenzamides. **University of Zambia Postgraduate Students Association (UNZAPOGRASA), 2023 UNZAPOGRASA Research Symposium**. Theme: Research and Innovation; the Wheels of Development, 5th – 6th October 2023. QT Lodge, Chilanga, Zambia. (Oral; 1st Prize.)

Workshops on the Sidelines of Conferences, Symposia and Colloquia

(a) WCAIR/UoD and UG (12th March 2025). Foundations of Computational Generative Drug Design of Small Molecules: Constructions, Scorings, and Search Workshop. DDA25, 12th – 14th March 2025. Ghana-Korea Information Access Centre, Balme Library, University of Ghana, Legon, Accra, Ghana.

(b) ISSX (5th March 2025). Pharmacometrics Africa Workshop/Short Course: Leveraging Pharmacometrics to Improve Therapeutics in Africa – An Introduction to Pharmacokinetic Modelling and Simulation. ISSXA25, 5th – 7th March 2025. The Indaba Hotel, Spa & Conference Centre, Sandton, Johannesburg, RSA.

(c) RSC Centre for Information & Computer Applications Group (CICAG) (16th September 2024). Artificial Intelligence (AI) in Chemistry. RSC CICAG/ BMCS, 7th RSC-CICAG/RSC-BMCS AI in Chemistry Meeting (AIChem24), 16th – 18th September 2024. Wolfson Hall, Churchill College, University of Cambridge, Cambridge, UK. https://cdn.eventsforce.net/files/ef-px6ci6a56tzs/website/278/5da0c9b4-d054-4e84-8c10-3afd60f127d7/final_ai_in_chemistry_2024_handbook.pdf

(d) UNZA Directorate of Research, Innovation and Development, DRID (formerly Directorate of Research and Graduate Studies, DRGS) (10th – 12th June 2024). Advanced Research Methodology. UNZAPOGRASA, Research Methodology Seminar, 10th – 12th June 2024. Confucius Institute, UNZA, Lusaka, Zambia.

(e) Ersilia Open-Source Initiative (EOSI) (24th May 2024). AI Tools in Antimicrobial Drug Discovery. H3D, 5th H3D Symposium, 21st – 24th May 2024. Radisson Blu Mosi-Oa-Tunya Resort, Livingstone, Zambia.

(f) International Federation of Pharmaceutical Manufacturers and Associations (IFPMA) and H3D (27th November 2023). Powerful, Locally Driven Partnerships for Health Innovation

in Africa: How H3D and Its Foundation Are Breaking Barriers in Innovation. Africa CDC, 3rd Conference on Public Health in Africa, 27th – 30th November 2023. MICC, Lusaka, Zambia.

Scanned Certificates

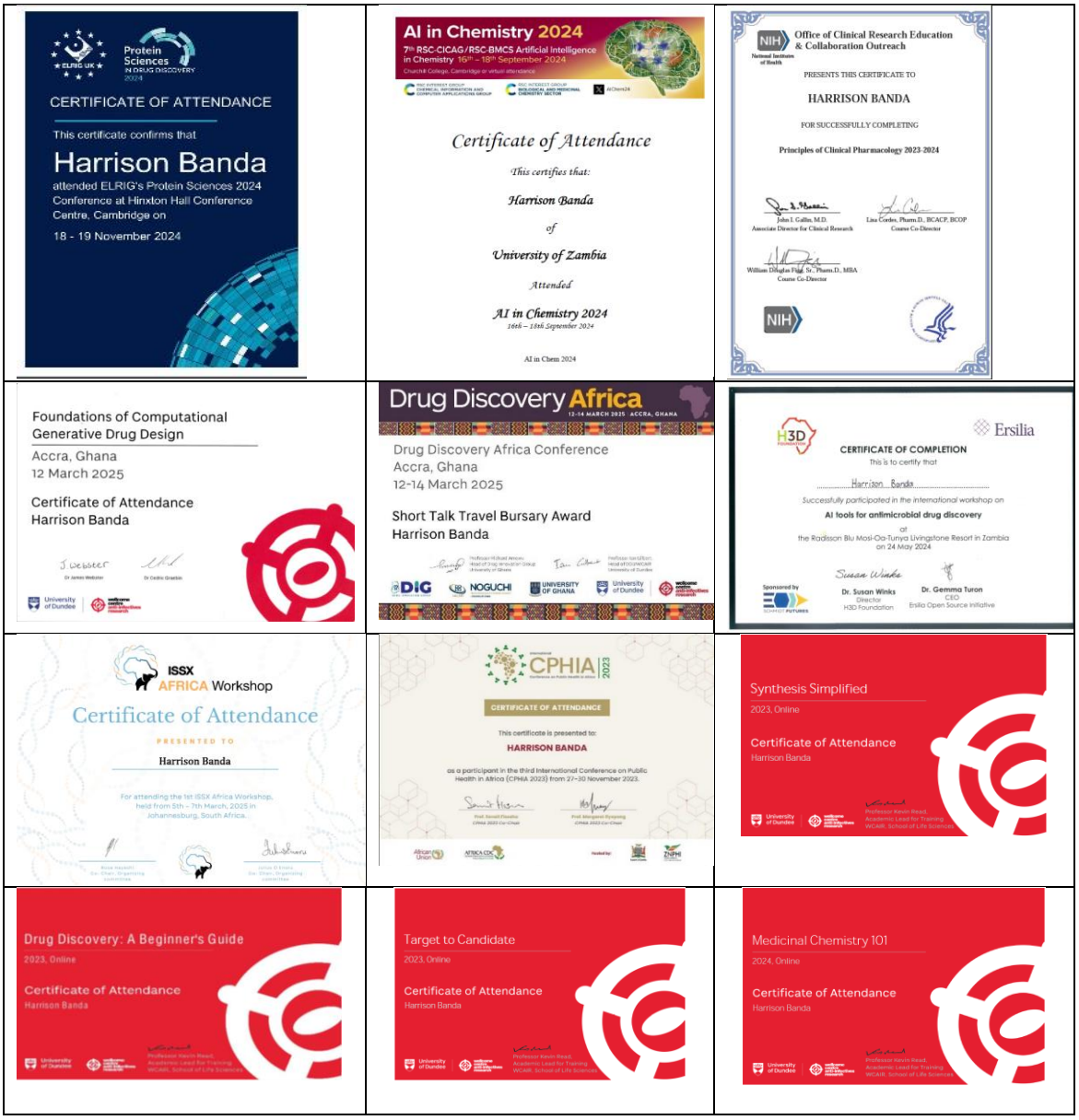

Online Accessible Certificates

1. H3D, UCT, RSA: https://www.coursera.org/account/accomplishments/verify/5FHYWCSKWSY7?utm_product=course
2. University of California San Diego (UCSD), San Diego, USA (3 courses): https://www.coursera.org/account/accomplishments/specialization/D4CE2E78T6HA
3. Novartis and Davidson College, Davidson, NC, USA (6 courses): https://www.coursera.org/account/accomplishments/specialization/BFB82G3PZPH1
4. Davidson College, Davidson, NC, USA: https://courses.edx.org/certificates/bdf4a71e5f6043e9b691a7415dbc8c80
5. American Chemical Society membership: https://credentials.acs.org/76261410-5803-4498-8ae0-13dedbfe2483#acc.Tq2Na3EI

Photo Gallery at In-person Conferences

Figure 75: Photo gallery at in-person conferences.

Legend: 1st Row: Ghana: Accra DDAC25; RSA: Jo'burg with ISSA Chairperson Dr Rose Hayeshi; with Ameera Dawoodjee at ISSXA25; **2nd Row**: UK: Cambridge PSDD24; AIChem24, Univ of Cambridge; Cranfield Univ NTGH24 with Prof Mark Gardner; with Prof Richard Amewu; **3rd Row**: with Dr Mary Sheldon; Lusaka: SHEPIZ24; Livingstone: getting certificate from Prof Ian Gilbert; with Kelly Chisanga and Dr Mwila Mulubwa at H3D24; H3D24; **4th Row**: Lusaka: MICC with Prof Kelly Chibale at CPHIA23; With DNDi at CPHIA23; With END at CPHIA2; **5th Row**: Chilanga: At UNZAPOGRASA23 prize-giving ceremony; 1st Prize medal; NS Seminar; IH CSZ NSCME19with Chilufya Lengwe, K. Chisanga, Blessings Mwansa and Masebe Kanyanta.